

**Analysis of Pyomelanins:  
Biologically derived conjugated polymers**

**Hanaa Ahmed Galeb**



**This dissertation is submitted for the degree of Doctor of Philosophy**

**Department of Chemistry**

**January 2023**

*In Dedication to my Parents.*

## Declaration

This thesis has not been submitted in support of an application for another degree at this or any other university. It is the result of my own work and includes nothing that is the outcome of work done in collaboration except where specifically indicated. Many of the ideas in this thesis were the product of discussion with my supervisor Dr. John G. Hardy.

Excerpts of this thesis have been published in the following conference manuscripts and academic publications:

- Galeb H.A, Wilkinson EL, Stowell AF, Lin H, Murphy ST, Martin-Hirsch PL, Mort RL, Taylor AM, Hardy JG. Melanins as sustainable resources for advanced biotechnological applications. *Global challenges*. 2021 Feb;5(2):2000102.
- Galeb H.A, Lamantia A, Robson A, König K, Eichhorn J, Baldock SJ, Ashton MD, Baum JV, Mort RL, Robinson BJ, Schacher FH. The Polymerization of Homogentisic Acid In Vitro as a Model for Pyomelanin Formation. *Macromolecular Chemistry and Physics*. 2022 Mar;223(6):2100489.
- Galeb H.A, Eichhorn J, Harley S, Robson AJ, Martocq L, Nicholson SJ, Ashton MD, Abdelmohsen HA, Pelit E, Baldock SJ, Halcovitch NR. Phenolic Polymers as Model Melanins. *Macromolecular Chemistry and Physics*. 2023 May 31:2300025.

Hanaa Ahmed Galeb

Lancaster University

# **Analysis of Pyomelanins: Biologically-derived conjugated polymers**

**Hanaa Ahmed Galeb**

January 2023

## **Overview**

Melanins are an important class of biopolymers that are widespread in nature and have diverse origins, chemical compositions and functions in nature. Their physicochemical properties make them interesting for application in materials science for a range of medical and technical applications. Phenolic monomers are common building blocks of melanins (observed in allomelanin, eumelanin, neuromelanin, pheomelanin and pyomelanin), and are known to play important roles in intermolecular/material interactions which underpin their biological roles and potential technical/medical applications.

Alkaptonuria is a rare metabolic disorder that results in the accumulation of homogentisic acid (HGA) in the body which results in dark urine and/or blue/black discoloration of bodily tissues due to the formation of pyomelanin (a complex polymer mostly constituted of polymerised HGA). Alkaptonuria is relatively understudied and the focus of this thesis was to investigate pyomelanin formation/deposition using a variety of analytical techniques which may enhance our understanding of the deposition of pyomelanin *in vivo*. The thesis includes data from microscopic, spectroscopic and other techniques to offer insights into the physicochemical properties of pyomelanin and variants thereof, observing interesting correlations between the functional groups on the monomers constituting the polymers and their properties (e.g., pendant groups acting as dopants for their electrical properties).

The introduction chapter of this thesis has been published as a review article, with results obtained from this research contributing to two research papers in print and two further research papers imminent for submission.

## **Acknowledgements**

Praise be to Allah, first and foremost, for His great gifts. Praise be to Allah who helped me and gave me the strength and power for completing this thesis.

I would like to acknowledge and express my sincere gratitude to my supervisor, Dr John Hardy, for his support and continuous guidance throughout my doctoral research journey.

My thanks also extend to Prof Adam Taylor, Dr. Jemma Kerns, Dr. Nathan Halcovitch, Dr. Sara Baldock, Dr. Victor Chechik, Dr. Benjamin Robinson, Dr. Koen Vercruysse, Dr. Alexander Robson, Dr. Jane Stockmann and Sam Harley. I am extremely grateful to my loving parents; to my father, who loved me unconditionally, and my mother, who showered me with her blessings and prayers, and gave me the strength to keep going.

My deepest and warmest thanks go to my husband, Fouzi. Without his love, understanding, and encouragement at every single step of this long journey, I could not have reached this point. Fouzi, thank you for believing in me; without you, this would still be a dream. Last but by no means least, I would like to express my gratitude to my children, Ahmed, Abdulrahman, Abdulmohsen, and Jumanah, for all their support, patience, love, and sacrifices over the years it took to complete this thesis.

My special thanks are extended to my brothers and sisters for believing in me and supporting all my endeavours in this major accomplishment.

I am also grateful to the government of Saudi Arabia and King Abdulaziz University for providing me with financial support during my studies at Lancaster University.

My thanks go to my friends and colleagues for sharing the challenges and providing support when needed. Additionally, I am grateful to everyone who directly or indirectly provided me with help and support.



## Contents

|          |  |           |
|----------|--|-----------|
| <b>1</b> | <b>Introductory Chapter .....</b>                            | <b>1</b>  |
| 1.1      | <b>Introduction .....</b>                                    | <b>1</b>  |
| 1.2      | <b>Analysis of Melanins.....</b>                             | <b>8</b>  |
| 1.2.1    | High Performance Liquid Chromatography (HPLC).....           | 12        |
| 1.2.2    | Gel Permeation Chromatography (GPC).....                     | 13        |
| 1.2.3    | Mass Spectrometry (MS).....                                  | 14        |
| 1.2.4    | Nuclear Magnetic Resonance (NMR) Spectroscopy .....          | 16        |
| 1.2.5    | Electron Paramagnetic Resonance (EPR) Spectroscopy .....     | 17        |
| 1.2.6    | Infrared Spectroscopy (IR) .....                             | 18        |
| 1.2.7    | Raman Spectroscopy .....                                     | 18        |
| 1.2.8    | Ultraviolet-visible (UV-Vis) Spectroscopy .....              | 20        |
| 1.2.9    | X-ray Photoelectron Spectroscopy (XPS) .....                 | 20        |
| 1.2.10   | Scattering and Diffraction.....                              | 21        |
| 1.2.11   | Thermal Characterization.....                                | 23        |
| 1.2.12   | Electrical Characterization.....                             | 24        |
| 1.2.13   | Visual and Microscopic Characterization .....                | 25        |
| 1.2.14   | Scanning Electron Microscopy (SEM) .....                     | 28        |
| 1.2.15   | Transmission Electron Microscopy (TEM) .....                 | 29        |
| 1.2.16   | Scanning Probe Microscopy (SPM).....                         | 30        |
| 1.3      | <b>Mechanism of polymerization to form HGA.....</b>          | <b>31</b> |
| 1.4      | <b>Conclusion .....</b>                                      | <b>33</b> |
| 1.5      | <b>Aim and objectives.....</b>                               | <b>34</b> |
| <b>2</b> | <b>Experimental Technique Chapter .....</b>                  | <b>36</b> |
| 2.1      | <b>Instrumental techniques for pyomelanin analysis .....</b> | <b>36</b> |

|        |   |    |
|--------|---|----|
| 2.1.1  | UV-Vis Spectroscopy .....                               | 36 |
| 2.1.2  | Fourier-transform Infrared (FTIR) Spectroscopy .....    | 37 |
| 2.1.3  | Nuclear Magnetic Resonance (NMR) Spectroscopy .....     | 39 |
| 2.1.4  | Solid State NMR (ssNMR) .....                           | 40 |
| 2.1.5  | X-ray Photoelectron Spectroscopy (XPS) .....            | 41 |
| 2.1.6  | Size Exclusion Chromatography (SEC) .....               | 43 |
| 2.1.7  | Dynamic Light Scattering (DLS).....                     | 44 |
| 2.1.8  | Scanning Electron Microscopy (SEM) .....                | 45 |
| 2.1.9  | Energy Dispersive X-ray (EDX) Spectroscopy .....        | 46 |
| 2.1.10 | Transmission Electron Microscopy (TEM) .....            | 47 |
| 2.1.11 | Electron Paramagnetic Resonance (EPR) Spectroscopy..... | 48 |
| 2.1.12 | Cyclic Voltammetry (CV).....                            | 49 |
| 2.1.13 | Conductive-probe atomic force microscopy (C-AFM).....   | 51 |
| 2.1.14 | X-ray diffraction (XRD) .....                           | 52 |
| 2.1.15 | Scanning electrochemical microscopy (SECM) .....        | 53 |
| 2.1.16 | Zeta potential .....                                    | 54 |

|            |   |           |
|------------|---|-----------|
| <b>3</b>   | <b>The Polymerisation of Homogentisic Acid In Vitro as a Model for<br/>Pyomelanin Formation .....</b> | <b>57</b> |
| <b>3.1</b> | <b>Introduction .....</b>   | <b>58</b> |
| <b>3.2</b> | <b>Experimental Section .....</b>   | <b>61</b> |
| 3.2.1      | Polymerisation of HGA (Lower Concentration of HGA–No Enzyme Control).....                             | 61        |
| 3.2.2      | Polymerisation of HGA (Lower Concentration of HGA in the Presence of Enzymes).....                    | 61        |
| 3.2.3      | Polymerisation of HGA (Higher Concentration of HGA–No Enzyme Control).....                            | 62        |
| 3.2.4      | Polymerisation of HGA (Higher Concentration of HGA in the Presence of Enzymes) ..                     | 62        |
| <b>3.3</b> | <b>Results and Discussion .....</b>   | <b>63</b> |
| <b>3.4</b> | <b>Conclusion .....</b>   | <b>76</b> |

|          |  |            |
|----------|--|------------|
| <b>4</b> | <b>Analysis of phenolic polymers as model melanins .....</b> | <b>77</b>  |
| 4.1      | <b>Introduction .....</b>                                    | <b>78</b>  |
| 4.2      | <b>Experimental Section .....</b>                            | <b>78</b>  |
| 4.2.1    | Synthesis of melanins .....                                  | 78         |
| 4.3      | <b>Results and Discussion .....</b>                          | <b>79</b>  |
| 4.4      | <b>Conclusion .....</b>                                      | <b>92</b>  |
| <b>5</b> | <b>Analysis of melanin-ECM interactions .....</b>            | <b>93</b>  |
| 5.1      | <b>Introduction .....</b>                                    | <b>94</b>  |
| 5.2      | <b>Experimental Section .....</b>                            | <b>95</b>  |
| 5.2.1    | Preparation of polyDOPA-CSA: .....                           | 95         |
| 5.2.2    | Preparation of polyDOPA-CSC:.....                            | 95         |
| 5.2.3    | Preparation of polyDOPA-CSA-CSC:.....                        | 96         |
| 5.2.4    | Preparation of polyHGA-CSA:.....                             | 96         |
| 5.2.5    | Preparation of polyHGA-CSC:.....                             | 97         |
| 5.2.6    | Preparation of polyHGA-CSA-CSC:.....                         | 97         |
| 5.3      | <b>Results and Discussion .....</b>                          | <b>98</b>  |
| 5.4      | <b>Conclusion .....</b>                                      | <b>110</b> |
| <b>6</b> | <b>Pyomelanin-ECM interactions .....</b>                     | <b>111</b> |
| 6.1      | <b>Introduction .....</b>                                    | <b>112</b> |
| 6.2      | <b>Experimental Section .....</b>                            | <b>113</b> |
| 6.2.1    | Preparation of samples: .....                                | 113        |
| 6.2.2    | Raman Spectroscopy: .....                                    | 113        |
| 6.3      | <b>Results and Discussion .....</b>                          | <b>114</b> |
| 6.4      | <b>Conclusion .....</b>                                      | <b>124</b> |

|          |   |            |
|----------|---|------------|
| <b>7</b> | <b>Conclusion &amp; Future Work .....</b> | <b>125</b> |
| 7.1      | Conclusion .....                          | 125        |
| 7.2      | Future work .....                         | 126        |
| <b>8</b> | <b>Appendices .....</b>                   | <b>160</b> |
| 8.1      | Appendix .....                            | 160        |
| 8.2      | Appendix .....                            | 190        |
| 8.3      | Appendix .....                            | 198        |
| 8.4      | Appendix .....                            | 203        |

## List of Tables

|  |     |
|--|-----|
| TABLE 1.1: BIOTECHNOLOGY TYPES. ....   | 7   |
| TABLE 1.2 ANALYTICAL TECHNIQUES APPLIED TO MELANINS.....   | 8   |
| TABLE A.1.1: SUMMARY OF XPS DATA (C 1S AND O 1S) FOR HGA. ....   | 170 |
| TABLE A.1.2: SUMMARY OF XPS DATA (C 1S AND O 1S) FOR POLYHGA (NO ENZYME CONTROL).....                      | 171 |
| TABLE A.1.3: SUMMARY OF XPS DATA (C 1S AND O 1S) FOR POLYHGA FORMED IN THE PRESENCE OF<br>TYROSINASE. .... | 172 |
| TABLE A.1.4: SUMMARY OF XPS DATA (C 1S AND O 1S) FOR POLYHGA FORMED IN THE PRESENCE OF<br>LACCASE.....     | 173 |
| TABLE A.1.5: SUMMARY OF XPS DATA (C 1S AND O 1S) FOR POLYHGA FORMED IN THE PRESENCE OF<br>PEROXIDASE. .... | 174 |

## List of Figures

|   |    |
|---|----|
| FIGURE 1.1: EYE CATCHING EXAMPLES OF COLOUR IN NATURE (INCLUDING MELANIN-DERIVED COLOURS).<br>.....   | 2  |
| FIGURE 1.2: EXAMPLES OF NATURALLY OCCURRING PIGMENT .....   | 3  |
| FIGURE 1.3: COMMON BIOSYNTHETIC PATHWAYS FOR MELANINS.....  | 4  |
| FIGURE 1.4: THE THREE-STEP, FOUR-LEVEL HIERARCHICAL BUILD-UP MECHANISM OF NATURAL AND<br>BIOMIMETIC EUMELANIN, BASED ON THE STATE OF LITERATURE.....  | 6  |
| FIGURE 1.5: A BRIEF TIMELINE OF MELANIN-BASED ELECTRONICS RESEARCH. ....  | 25 |
| FIGURE 1.6: A POSTULATED SCHEME FOR THE FORMATION OF OCHRONOTIC PIGMENT IN ALKAPTONURIA.<br>.....   | 32 |
| FIGURE 3.1: THE CHEMICAL STRUCTURES OF HOMOGENITISIC ACID (HGA) AND BENZOQUINONE ACETIC<br>ACID (BQA).....  | 59 |
| FIGURE 3.2: SCHEMATIC OF THE POLYMERIZATION OF HOMOGENITISIC ACID (HGA) TO FORM PYOMELANIN.<br>.....  | 60 |
| FIGURE 3.3: UV–VIS SPECTRA OF HGA REACTION MIXTURES AFTER 6 WEEKS AT EITHER PH 5.0 OR 7.4, IN<br>THE ABSENCE OF ENZYME (CONTROL) OR PRESENCE OF ENZYME (LACCASE (LACC), PEROXIDASE<br>(HRP), TYROSINASE (TYR)).....   | 65 |
| FIGURE 3.4: XPS C 1S CORE LINE SPECTRA: A) HGA; B) POLYHGA (NO ENZYME CONTROL AT PH 5.0); C)<br>POLYHGA (NO ENZYME CONTROL AT PH 7.4); D) POLYHGA (FORMED IN THE PRESENCE OF<br>TYROSINASE AT PH 5.0); E) POLYHGA (FORMED IN THE PRESENCE OF TYROSINASE AT PH 7.4); F)<br>POLYHGA (FORMED IN THE PRESENCE OF LACCASE AT PH 5.0); G) POLYHGA (FORMED IN THE<br>PRESENCE OF LACCASE AT PH 7.4); H) POLYHGA AT PH 5.0); AND I) POLYHGA (FORMED IN THE<br>PRESENCE OF PEROXIDASE AT PH 7.4). .... | 67 |
| FIGURE 3.5: XPS O 1S CORE LINE SPECTRA A) HGA; B) POLYHGA (NO ENZYME CONTROL AT PH 5.0); C)<br>POLYHGA (NO ENZYME CONTROL AT PH 7.4); D) POLYHGA (FORMED IN THE PRESENCE OF<br>TYROSINASE AT PH 5.0); E) POLYHGA (FORMED IN THE PRESENCE OF TYROSINASE AT PH 7.4); F)<br>POLYHGA (FORMED IN THE PRESENCE OF LACCASE AT PH 5.0); G) POLYHGA (FORMED IN THE   |    |

|  |    |
|--|----|
| PRESENCE OF LACCASE AT pH 7.4); H) POLYHGA (FORMED IN THE PRESENCE OF PEROXIDASE AT pH 5.0); AND I) POLYHGA (FORMED IN THE PRESENCE OF PEROXIDASE AT pH 7.4). .....  | 68 |
| FIGURE 3.6: FTIR SPECTRA OF DIALYZED POLYHGA ISOLATED AFTER 6 WEEKS OF REACTION AT pH 5.0 AND pH 7.4, GENERATED IN THE ABSENCE OF ENZYME (NO ENZYME CONTROL) OR PRESENCE OF ENZYME (LACCASE (LACC), PEROXIDASE (HRP), AND TYROSINASE (TYR)). .....   | 70 |
| FIGURE 3.7: BAND EPR SPECTRA OF POLYHGA SAMPLES GENERATED AT pH 7.4 IN THE ABSENCE OF ENZYMES (BLACK), OR PRESENCE OF LACCASE (BLUE), PEROXIDASE (RED), OR TYROSINASE (GREEN). .....   | 72 |
| FIGURE 3.8: EXPERIMENTAL EPR SPECTRUM OF POLYHGA GENERATED IN THE PRESENCE OF PEROXIDASE SAMPLE (BLACK) AND SIMULATION (RED). THE SIMULATION INCLUDED A BROAD C-CENTERED COMPONENT ( $G = 2.0034$ , VOIGTIAN LINE SHAPE WITH PEAK-TO-PEAK WIDTH 4.2 G, 97.8%) AND A SHARPER SEMIQUINONE RADICAL ( $G = 2.004$ , GAUSSIAN LINE SHAPE WITH PEAK-TO-PEAK WIDTH 2.2 G, 2.2%). .....  | 72 |
| FIGURE 3.9: CONDUCTIVE TIP AFM DATA FOR POLYHGAS. COMPARISON OF THE CONDUCTANCE HISTOGRAMS FOR POLYHGAS GENERATED IN THE PRESENCE OF LACCASE (LACC) AT pH 7.4, OR PEROXIDASE (HRP) AT pH 7.4 OR 5.0, RESPECTIVELY. ....  | 75 |
| FIGURE 4.1: A SCHEMATIC OF THE POLYMERIZATION OF CAT, DOPA OR HGA TO FORM MODEL MELANINS IS IMPORTANT TO NOTE THAT NATURAL MELANINS MAY CONTAIN OTHER MONOMERS DEPENDING ON THE CONDITIONS UNDER WHICH THEY ARE FORMED IN VIVO, AND THE POLYMERS DEPICTED ARE THEREFORE SIMPLIFIED VERSION OF MELANINS, POLYCAT, POLYDOPA OR POLYHGA, RESPECTIVELY (DEPICTED ABOVE), THAT ARE STUDIED HEREIN. ....   | 80 |
| FIGURE 4.2: UV-VIS SPECTRA OF THE POLYMERS STUDIED HEREIN. (0.0026 MG/ML). ....  | 81 |
| FIGURE 4.3: X-RAY PHOTOELECTRON SPECTROSCOPY (XPS) SPECTRA. A) POLYCAT-HS C 1s CORE LINE SPECTRA. B) POLYCAT-HS O 1s CORE LINE SPECTRA. C) POLYCAT-LS C 1s CORE LINE SPECTRA. D) POLYCAT-LS O 1s CORE LINE SPECTRA. E) POLYDOPA-HS C 1s CORE LINE SPECTRA. F) POLYDOPA-HS O 1s CORE LINE SPECTRA. G) POLYDOPA-LS C 1s CORE LINE SPECTRA. H) POLYDOPA-LS O 1s CORE LINE SPECTRA. I) POLYHGA-HS C 1s CORE LINE SPECTRA. J) POLYHGA-HS O 1s CORE LINE SPECTRA. .... | 83 |
| FIGURE 4.4: TRANSMISSION ELECTRON MICROSCOPY (TEM) AND SCANNING ELECTRON MICROSCOPY (SEM) IMAGES OF SAMPLES STUDIED HEREIN. A) POLYCAT-HS TEM. B) POLYCAT-HS SEM   |    |

|  |     |
|--|-----|
| (SCALE BAR REPRESENTS 10 $\mu\text{M}$ ). C) POLYCAT-LS TEM. D) POLYCAT-LS SEM (SCALE BAR REPRESENTS 10 $\mu\text{M}$ ). E) POLYDOPA-HS TEM. F) POLYDOPA-HS SEM (SCALE BAR REPRESENTS 1 $\mu\text{M}$ ). G) POLYDOPA-LS TEM. H) POLYDOPA-LS SEM (SCALE BAR REPRESENTS 1 $\mu\text{M}$ ). I) POLYHGA-HS TEM. J) POLYHGA-HS SEM (SCALE BAR REPRESENTS 1 $\mu\text{M}$ ).....   | 86  |
| FIGURE 4.5: FOURIER-TRANSFORM INFRARED (FTIR) SPECTRA OF MONOMERS AND POLYMERS. A) CATECHOL (CAT), POLYCAT-HS, AND POLYCAT-LS. B) LEVODOPA (DOPA), POLYDOPA-HS, AND POLYDOPA-LS. C) HOMOGENITISIC ACID (HGA) AND POLYHGA-HS.....   | 87  |
| FIGURE 4.6: -BAND ELECTRON PARAMAGNETIC RESONANCE (EPR) SPECTRA OF POLYMERS STUDIED HEREIN.....  | 88  |
| FIGURE 4.7: EXPERIMENTAL ELECTRON PARAMAGNETIC RESONANCE (EPR) SPECTRUM OF POLYCAT-HS (BLACK) AND SIMULATION (RED). THE SIMULATION INCLUDED A BROAD C-CENTERED COMPONENT ( $G = 2.0033$ , 41.6%) AND A SHARPER SEMIQUINONE RADICAL ( $G = 2.0048$ , 58.4%). .....  | 89  |
| FIGURE 4.8: CONDUCTANCE DATA FOR POLYMERS STUDIED HEREIN. A) POLYCAT-HS I-V CURVES. B) POLYCAT-HS CONDUCTANCE HISTOGRAM. C) POLYCAT-LS I-V CURVES. D) POLYCAT-LS CONDUCTANCE HISTOGRAM. E) POLYDOPA-HS I-V CURVES. F) POLYDOPA-HS CONDUCTANCE HISTOGRAM. G) POLYDOPA-LS I-V CURVES. H) POLYDOPA-LS CONDUCTANCE HISTOGRAM. I) POLYHGA-HS I-V CURVES. J) POLYHGA-HS CONDUCTANCE HISTOGRAM. DATA COURTESY OF SAM..... | 91  |
| FIGURE 5.1: STRUCTURES OF THE MODEL MELANINS (POLYDOPA AND POLYHGA, RESPECTIVELY) AND CHONDROITIN SULFATE DERIVATIVES (CSA AND CSC, RESPECTIVELY), THAT ARE STUDIED HEREIN. ....   | 98  |
| FIGURE 5.2: UV-VIS SPECTRA OF THE POLYMERS STUDIED HEREIN (0.0208MG/ML .....   | 99  |
| FIGURE 5.3: TEM. A) POLYDOPA-CSA. B) POLYDOPA-CSC. C) POLYHGA-CSA. D) POLYHGA-CSC. E) POLYDOPA-CSA-CSC. F) POLYHGA-CSA-CSC.....  | 100 |
| FIGURE 5.4: XPS SPECTRA (C 1s CORE LINE SPECTRA). A) CSA. B) CSC. C) POLYDOPA-CSA. D) POLYDOPA-CSC. E) POLYDOPA-CSA-CSC. F) POLYHGA-CSA. G) POLYHGA-CSC. H) POLYHGA-CSA-CSC. ....  | 102 |

|  |     |
|--|-----|
| FIGURE 5.5: XPS SPECTRA (O 1S CORE LINE SPECTRA). A) CSA. B) CSC. C) POLYDOPA-CSA. D) POLYDOPA-CSC. E) POLYDOPA-CSA-CSC. F) POLYHGA-CSA. G) POLYHGA-CSC. H) POLYHGA-CSA-CSC. ....  | 103 |
| FIGURE 5.6: FTIR SPECTRA OF MONOMERS AND POLYMERS STUDIED HEREIN. ....   | 105 |
| FIGURE 5.7: <sup>13</sup> C ssNMR SPECTRA OF THE MATERIALS STUDIED HEREIN. ....  | 107 |
| FIGURE 5.8: I-V MEASUREMENTS FOR MATERIALS STUDIED HEREIN. A) DOPA. B) HGA. C) CSA. D) CSC. E) POLYDOPA-CSA. F) POLYDOPA-CSC. G) POLYDOPA-CSA-CSC. H) POLYHGA-CSA. I) POLYHGA-CSC. J) POLYHGA-CSA-CSC. DATA COURTESY OF SAM. ....  | 109 |
| FIGURE 6.1: SCHEMATIC OF THE POLYMERIZATION OF HOMOGENITISIC ACID (HGA) TO FORM POLYHGA, A SIMPLIFIED MODEL OF PYOMELANIN STUDIED HEREIN. IT IS IMPORTANT TO NOTE THAT NATURAL PYOMELANIN SAMPLES MAY CONTAIN OTHER MONOMERS DEPENDING ON THE CONDITIONS UNDER WHICH THEY ARE FORMED IN VIVO. ....   | 114 |
| FIGURE 6.2: RAMAN SPECTRA OF TENDONS STUDIED HEREIN. A) TURKEY TENDON ALONG THE LENGTH (UNTREATED). B) DISTAL SECTION OF TENDON. C) PROXIMAL OF TENDON. D) MID-POINT SECTION OF TENDON. ....   | 116 |
| FIGURE 6.3: FTIR SPECTRA OF TENDONS STUDIED HEREIN. A) PROXIMAL SECTION OF TENDON. B) MID-POINT OF TENDON. C) DISTAL SECTION OF TENDON. ....   | 118 |
| FIGURE 6.4: SEM. A) PROXIMAL SECTION OF TENDON (CONTROL). B) PROXIMAL SECTION OF TENDON (LOW [HGA]). C) PROXIMAL SECTION OF TENDON (HIGH [HGA]). D) MID-POINT SECTION OF TENDON (CONTROL). E) MID-POINT SECTION OF TENDON (LOW [HGA]). F) MID-POINT SECTION OF TENDON (HIGH [HGA]). G) DISTAL SECTION OF TENDON (CONTROL). H) DISTAL SECTION OF TENDON (LOW [HGA]). I) DISTAL SECTION OF TENDON (HIGH [HGA]). .... | 119 |
| FIGURE 6.5: SECM. A) PROXIMAL SECTION OF TENDON (CONTROL). B) PROXIMAL SECTION OF TENDON LOW [HGA]). C) PROXIMAL SECTION OF TENDON (HIGH [HGA]) ....   | 121 |
| FIGURE 6.6: SECM. A) MID SECTION OF TENDON (CONTROL). B) MID SECTION OF TENDON LOW [HGA]). C) MID SECTION OF TENDON (HIGH [HGA]) ....  | 122 |
| FIGURE 6.7: SECM. A) DISTAL SECTION OF TENDON (CONTROL). B) DISTAL SECTION OF TENDON LOW [HGA]). C) DISTAL SECTION OF TENDON (HIGH [HGA]) ....   | 123 |

|  |     |
|--|-----|
| FIGURE A.1.1: PHOTOGRAPHS OF REACTION MIXTURES. IN EACH CASE FROM LEFT TO RIGHT: NO ENZYME CONTROL, WITH PEROXIDASE, WITH LACCASE, WITH TYROSINASE. A) AFTER 24 HOURS AT PH 5. B) AFTER 24 HOURS AT PH 7.4. C) AFTER 6 WEEKS AT PH 5. D) AFTER 6 WEEKS AT PH 7.4. ....   | 160 |
| FIGURE A.1.2: UV-VIS SPECTRA OF REACTION MIXTURES OVER A PERIOD OF 24 HOURS AT PH 7.4. A) NO ENZYME CONTROL. B) WITH PEROXIDASE. C) WITH LACCASE. D) WITH TYROSINASE. E AND F) AVERAGE PEAK INTENSITY OVER 24 HOURS AT 248 AND 290 NM, RESPECTIVELY: NO ENZYME CONTROL (BLACK LINE), WITH PEROXIDASE (RED LINE), WITH LACCASE (BLUE LINE), WITH TYROSINASE (GREEN LINE). FOR THE NO ENZYME CONTROL, REACTION IN THE PRESENCE OF LACCASE OR TYROSINASE, THE PEAK INTENSITY AT 290 NM CHARACTERISTIC OF HGA DECREASES IN INTENSITY OVER 24 HOURS, AND THE PEAK INTENSITY AT 248 NM CHARACTERISTIC OF BQA INCREASES IN INTENSITY; BY COMPARISON FOR THE REACTION IN THE PRESENCE OF PEROXIDASE THE OXIDATION OF HGA TO BQA IS VERY FAST, AS IS THE ONSET OF POLYMERIZATION (BROAD BAND ABSORPTION > 300 NM). .... | 161 |
| FIGURE A.1.3: <sup>1</sup> H NMR OF HGA IN D <sub>2</sub> O. ....  | 162 |
| FIGURE A.1.4: <sup>1</sup> H NMR OF POLYHGA IN D <sub>2</sub> O (NO ENZYME CONTROL AT PH 5.0); INCLUDES TRACE OF ACETONE. ....   | 163 |
| FIGURE A.1.5: <sup>1</sup> H NMR OF POLYHGA IN D <sub>2</sub> O (NO ENZYME CONTROL AT PH 7.4). ....  | 163 |
| FIGURE A.1.6: <sup>1</sup> H NMR OF POLYHGA IN D <sub>2</sub> O (FORMED IN THE PRESENCE OF TYROSINASE AT PH 5.0). ....   | 164 |
| FIGURE A.1.7: <sup>1</sup> H NMR OF POLYHGA IN D <sub>2</sub> O (FORMED IN THE PRESENCE OF TYROSINASE AT PH 7.4). ....   | 164 |
| FIGURE A.1.8: <sup>1</sup> H NMR OF POLYHGA IN D <sub>2</sub> O (FORMED IN THE PRESENCE OF LACCASE AT PH 5.0). ....  | 165 |
| FIGURE A.1.9: <sup>1</sup> H NMR OF POLYHGA IN D <sub>2</sub> O (FORMED IN THE PRESENCE OF LACCASE AT PH 7.4). ....  | 165 |
| FIGURE A.1.10: <sup>1</sup> H NMR OF POLYHGA IN D <sub>2</sub> O (FORMED IN THE PRESENCE OF PEROXIDASE AT PH 5.0). ....  | 166 |
| FIGURE A.1.11: <sup>1</sup> H NMR OF POLYHGA IN D <sub>2</sub> O (FORMED IN THE PRESENCE OF PEROXIDASE AT PH 7.4). ....  | 166 |
| FIGURE A.1.12: XPS WIDE SCANS: A) HGA; B) POLYHGA (NO ENZYME CONTROL AT PH 5.0); C) POLYHGA (NO ENZYME CONTROL AT PH 7.4); D) POLYHGA (FORMED IN THE PRESENCE OF TYROSINASE AT PH 5.0); E) POLYHGA (FORMED IN THE PRESENCE OF TYROSINASE AT PH 7.4); F) POLYHGA (FORMED IN THE PRESENCE OF LACCASE AT PH 5.0); G) POLYHGA (FORMED IN THE   |     |

|   |     |
|---|-----|
| PRESENCE OF LACCASE AT PH 7.4); H) POLYHGA (FORMED IN THE PRESENCE OFEROXIDASE AT PH 5.0); I) POLYHGA (FORMED IN THE PRESENCE OF PEROXIDASE AT PH 7.4).....   | 167 |
| FIGURE A.1.13: XPS C 1S CORE LINE SPECTRA: A) HGA; B) POLYHGA (NO ENZYME CONTROL AT PH 5.0); C) POLYHGA (NO ENZYME CONTROL AT PH 7.4); D) POLYHGA (FORMED IN THE PRESENCE OF TYROSINASE AT PH 5.0); E) POLYHGA (FORMED IN THE PRESENCE OF TYROSINASE AT PH 7.4); F) POLYHGA (FORMED IN THE PRESENCE OF LACCASE AT PH 5.0); G) POLYHGA (FORMED IN THE PRESENCE OF LACCASE AT PH 7.4); H) POLYHGA (FORMED IN THE PRESENCE OF PEROXIDASE AT PH 5.0); I) POLYHGA (FORMED IN THE PRESENCE OF PEROXIDASE AT PH 7.4).....          | 168 |
| FIGURE A.1.14: XPS O 1S CORE LINE SPECTRA: A) HGA; B) POLYHGA (NO ENZYME CONTROL AT PH 5.0); C) POLYHGA (NO ENZYME CONTROL AT PH 7.4); D) POLYHGA (FORMED IN THE PRESENCE OF TYROSINASE AT PH 5.0); E) POLYHGA (FORMED IN THE PRESENCE OF TYROSINASE AT PH 7.4); F) POLYHGA (FORMED IN THE PRESENCE OF LACCASE AT PH 5.0); G) POLYHGA (FORMED IN THE PRESENCE OF LACCASE AT PH 7.4); H) POLYHGA (FORMED IN THE PRESENCE OF PEROXIDASE AT PH 5.0); I) POLYHGA (FORMED IN THE PRESENCE OF PEROXIDASE AT PH 7.4).....          | 169 |
| FIGURE A.1.15: SEC DATA FOR VARIOUS SAMPLES. A) BLANK CONTROL. B) POLYHGA (NO ENZYME CONTROL AT PH 5.0). C) POLYHGA (NO ENZYME CONTROL AT PH 7.4). D) POLYHGA (FORMED IN THE PRESENCE OF TYROSINASE AT PH 5.0). E) POLYHGA (FORMED IN THE PRESENCE OF TYROSINASE AT PH 7.4). F) POLYHGA (FORMED IN THE PRESENCE OF LACCASE AT PH 5.0). G) POLYHGA (FORMED IN THE PRESENCE OF LACCASE AT PH 7.4). H) POLYHGA (FORMED IN THE PRESENCE OF PEROXIDASE AT PH 5.0). I) POLYHGA (FORMED IN THE PRESENCE OF PEROXIDASE AT PH 7.4).. | 175 |
| FIGURE A.1.16: SEM AND EDX DATA FOR POLYHGA (NO ENZYME CONTROL AT PH 5.0). A) SEM-EDX LAYERED IMAGE (SCALE BAR REPRESENTS 25 MM). B) EDX SPECTRUM.....  | 175 |
| FIGURE A.1.17: SEM AND EDX DATA FOR POLYHGA (NO ENZYME CONTROL AT PH 7.4). A) SEM-EDX LAYERED IMAGE (SCALE BAR REPRESENTS 25 MM). B) EDX SPECTRUM.....  | 176 |
| FIGURE A.1.18: SEM AND EDX DATA FOR POLYHGA FORMED IN THE PRESENCE OF TYROSINASE AT PH 5.0. ....  | 176 |
| FIGURE A.1.19: SEM AND EDX DATA FOR POLYHGA FORMED IN THE PRESENCE OF TYROSINASE AT PH 7.4. ....  | 177 |
| FIGURE A.1 20: SEM AND EDX DATA FOR POLYHGA FORMED IN THE PRESENCE OF LACCASE AT PH 5.0. ....   | 177 |

|   |     |
|---|-----|
| FIGURE A.1.21: SEM AND EDX DATA FOR POLYHGA FORMED IN THE PRESENCE OF LACCASE AT PH 7.4.    |     |
| A) SEM-EDX LAYERED IMAGE (SCALE BAR REPRESENTS 25 MM). B) EDX SPECTRUM. ....                | 177 |
| FIGURE A.1.22: SEM AND EDX DATA FOR POLYHGA FORMED IN THE PRESENCE OF PEROXIDASE AT PH5.0.  |     |
| A) SEM-EDX LAYERED IMAGE (SCALE BAR REPRESENTS 25 MM). B) EDX SPECTRUM. ....                | 178 |
| FIGURE A.1.23: SEM AND EDX DATA FOR POLYHGA FORMED IN THE PRESENCE OF PEROXIDASE AT PH7.4.  |     |
| A) SEM-EDX LAYERED IMAGE (SCALE BAR REPRESENTS 25 MM). B) EDX SPECTRUM. ....                | 178 |
| FIGURE A.1.24: HIGH MAGNIFICATION SEM IMAGES. A) POLYHGA, NO ENZYME CONTROL AT PH 7.4       |     |
| (SCALE BAR REPRESENTS 100 NM). B) POLYHGA FORMED IN THE PRESENCE OF TYROSINASE AT PH        |     |
| 7.4 (SCALE BAR REPRESENTS 100 NM). C) POLYHGA FORMED IN THE PRESENCE OF LACCASE AT PH       |     |
| 7.4 (SCALE BAR REPRESENTS 100 NM). D) POLYHGA FORMED IN THE PRESENCE OF PEROXIDASE AT       |     |
| PH 7.4 (SCALE BAR REPRESENTS 1 MM). FIGURE A.1.26. EXPERIMENTAL EPR SPECTRUM OF             |     |
| POLYHGA GENERATED IN THE ABSENCE OF ENZYMES AT PH 7.4, (BLACK) AND SIMULATION (RED).        |     |
| THE SIMULATION INCLUDED A BROAD C-CENTERED COMPONENT ( $G = 2.0034$ , VOIGTIAN LINE SHAPE   |     |
| WITH PEAK-TO-PEAK WIDTH 4.3 G, 93.8%) AND A SHARPER SEMIQUINONE RADICAL ( $G = 2.0039$ ,    |     |
| GAUSSIAN LINE SHAPE WITH PEAK-TO-PEAK WIDTH 2.7 G, 6.2%). ....                              | 179 |
| FIGURE A.1.25: FTIR SPECTRA OF DIALYZED POLYHGA ISOLATED AFTER 6 WEEKS OF REACTION AT PH    |     |
| 5.0 AND PH 7.4, GENERATED IN THE ABSENCE OF ENZYME (NO ENZYME CONTROL) OR PRESENCE OF       |     |
| ENZYME (LACCASE [LACC], PEROXIDASE [HRP], TYROSINASE [TYR]). ....                           | 180 |
| FIGURE A.1.26: EXPERIMENTAL EPR SPECTRUM OF POLYHGA GENERATED IN THE ABSENCE OF ENZYMES     |     |
| AT PH 7.4, (BLACK) AND SIMULATION (RED). THE SIMULATION INCLUDED A BROAD C-CENTERED         |     |
| COMPONENT ( $G = 2.0034$ , VOIGTIAN LINE SHAPE WITH PEAK-TO-PEAK WIDTH 4.3 G, 93.8%) AND A  |     |
| SHARPER SEMIQUINONE RADICAL ( $G = 2.0039$ , GAUSSIAN LINE SHAPE WITH PEAK-TO-PEAK WIDTH    |     |
| 2.7 G, 6.2%). ....  | 181 |
| FIGURE A.1.27: EXPERIMENTAL EPR SPECTRUM OF POLYHGA GENERATED IN THE PRESENCE OF LACCASE    |     |
| AT PH 7.4, SAMPLE (BLACK) AND SIMULATION (RED). THE SIMULATION INCLUDED A BROAD C-          |     |
| CENTERED COMPONENT ( $G = 2.0034$ , VOIGTIAN LINE SHAPE WITH PEAK-TO-PEAK WIDTH 4.5 G,      |     |
| 95.2%) AND A SHARPER SEMIQUINONE RADICAL ( $G = 2.0039$ , GAUSSIAN LINE SHAPE WITH PEAK-TO- |     |
| PEAK WIDTH 2.7 G, 4.8%). ....   | 181 |

|  |     |
|--|-----|
| FIGURE A.1.28: EXPERIMENTAL EPR SPECTRUM OF POLYHGA GENERATED IN THE PRESENCE OF TYROSINASE AT PH 7.4, SAMPLE (BLACK) AND SIMULATION (RED). THE SIMULATION INCLUDED A BROAD C-CENTERED COMPONENT ( $G = 2.0036$ , VOIGTIAN LINE SHAPE WITH PEAK-TO-PEAK WIDTH 4.4 G, 96.1%) AND A SHARPER SEMIQUINONE RADICAL ( $G = 2.0039$ , GAUSSIAN LINE SHAPE WITH PEAK-TO-PEAK WIDTH 3.0 G, 3.9%).   | 182 |
| FIGURE A.1.29: CYCLIC VOLTAMMOGRAMS OF POLYHGAS. A) POLYHGA (PREPARED IN THE PRESENCE OF TYROSINASE AT PH 5.0) AT PH 5.0. B) POLYHGA (PREPARED IN THE PRESENCE OF TYROSINASE AT PH 7.4) AT PH 7.4. C) POLYHGA (PREPARED IN THE PRESENCE OF LACCASE AT PH 5.0) AT PH 5.0. D) POLYHGA (PREPARED IN THE PRESENCE OF LACCASE AT PH 7.4) AT PH 7.4. E) POLYHGA (PREPARED IN THE PRESENCE OF PEROXIDASE AT PH 5.0) AT PH 5.0. F) POLYHGA (PREPARED IN THE PRESENCE OF PEROXIDASE AT PH 7.4) AT PH 7.4. | 183 |
| FIGURE A.1.30: CONDUCTIVE PROBE AFM SETUP.   | 184 |
| FIGURE A.1.31: I-V CURVES FOR THE POLYHGA GENERATED IN THE PRESENCE OF TYROSINASE AT PH 5.0. DATA COURTESY OF ANGELO.  | 185 |
| FIGURE A.1.32: I-V CURVES FOR THE POLYHGA GENERATED IN THE PRESENCE OF TYROSINASE AT PH 7.4  | 186 |
| FIGURE A.1.33: I-V CURVES FOR THE POLYHGA GENERATED IN THE PRESENCE OF LACCASE (LACC) AT PH 5.0.   | 187 |
| FIGURE A.1.34: I-V CURVE FOR THE POLYHGA GENERATED IN THE PRESENCE OF LACCASE (LACC) AT PH 7.4.  | 187 |
| FIGURE A.1.35: I-V CURVE FOR THE POLYHGA GENERATED IN THE PRESENCE OF PEROXIDASE (HRP) AT PH 5.0.  | 188 |
| FIGURE A.1.36: I-V CURVE FOR THE POLYHGA GENERATED IN THE PRESENCE OF PEROXIDASE (HRP) AT PH 7.4.  | 188 |
| FIGURE A.1.37: COMPARISON OF LOG G COUNTER MAPS FOR THE POLYHGAS GENERATED IN THE PRESENCE OF LACCASE (LACC) AT PH 7.4, OR PEROXIDASE (HRP) AT PH 7.4 OR 5.0, RESPECTIVELY.  | 189 |

|   |     |
|---|-----|
| FIGURE A.2.1: <sup>1</sup> H NMR OF CAT (RED, INCLUDES TRACE OF ACETONE), POLYCAT-HS (BLUE) AND POLYCAT-LS (GREEN) IN D <sub>2</sub> O. ....  | 190 |
| FIGURE A.2.2: <sup>1</sup> H NMR OF L-DOPA (RED), POLYLDOPA-HS (BLUE) AND POLYLDOPA-LS (GREEN) IN D <sub>2</sub> O. ....  | 190 |
| FIGURE A.2.3: <sup>1</sup> H NMR OF HGA (RED) AND POLYHGA-HS (BLUE) IN D <sub>2</sub> O. ....   | 191 |
| FIGURE A.2.4: XPS SPECTRA. A) POLYCAT-HS WIDE SCAN. B) POLYCAT-LS WIDE SCAN. C) POLYDOPA-HS WIDE SCAN. D) POLYDOPA-LS WIDE SCAN. E) POLYHGA-HS WIDE SCAN. ....  | 192 |
| FIGURE A.2.5: X-RAY DIFFRACTOGRAMS OF SAMPLES STUDIED HEREIN. ....  | 193 |
| FIGURE A.2.6: FTIR SPECTRA OF MONOMERS AND POLYMERS. A) CAT, POLYCAT-HS AND POLYCAT-LS. B) DOPA, POLYDOPA-HS AND POLYDOPA-LS. C) HGA AND POLYHGA-HS. ....   | 194 |
| FIGURE A.2.7: CYCLIC VOLTAMMOGRAMS OF MONOMERS AND POLYMERS STUDIED HEREIN. A) CAT pH 5. B) CAT pH 7.4. C) POLYCAT-HS pH 5. D) POLYCAT-HS pH 7.4. E) POLYCAT-LS pH 5. F) POLYCAT-LS pH 7.4. ....                      | 195 |
| FIGURE A.2.8: CYCLIC VOLTAMMOGRAMS OF MONOMERS AND POLYMERS STUDIED HEREIN. A) DOPA pH 5. B) DOPA pH 7.4. C) POLYDOPA-HS pH 5. D) POLYDOPA-HS pH 7.4. E) POLYDOPA-LS pH 5. F) POLYDOPA-LS pH 7.4. ....                | 196 |
| FIGURE A.2.9: CYCLIC VOLTAMMOGRAMS OF MONOMERS AND POLYMERS STUDIED HEREIN. A) HGA pH 5. B) HGA pH 7.4. C) POLYHGA-HS pH 5. D) POLYHGA-HS pH 7.4. ....  | 197 |
| FIGURE A.3.1: X-RAY DIFFRACTOGRAMS OF SAMPLES STUDIED HEREIN. ....  | 198 |
| FIGURE A.3.2: FTIR SPECTRA OF MONOMERS AND POLYMERS STUDIED HEREIN (FULL SPECTRUM). ....  | 198 |
| FIGURE A.3.3: CYCLIC VOLTAMMOGRAMS OF MONOMERS. A) DOPA pH 5. B) DOPA pH 7.4. C) HGA pH 5. D) HGA pH 7.4. E) CSA pH 5. F) CSA pH 7.4. G) CSC pH 5. H) CSC pH 7. ....  | 199 |
| FIGURE A.3.4: CYCLIC VOLTAMMOGRAMS OF POLYMERS STUDIED HEREIN. A) POLYDOPA-CSA pH 5. B) POLYDOPA-CSA pH 7.4. C) POLYDOPA-CSC pH 5. D) POLYDOPA-CSC pH 7.4. E) POLYDOPA-CSA-CSC pH 5. F) POLYDOPA-CSA-CSC pH 7.4. .... | 200 |

FIGURE A.3.5: CYCLIC VOLTAMMOGRAMS OF POLYMERS STUDIED HEREIN. A) POLYHGA-CSA pH 5. B) POLYHGA-CSA pH 7.4. C) POLYHGA-CSC pH 5. D) POLYHGA-CSC pH 7.4. E) POLYHGA-CSA-CSC pH 5. F) POLYHGA-CSA-CSC pH 7.4. ....201

FIGURE A.3.6: SET UP FOR ELECTRONIC MEASUREMENT.....202

FIGURE A.4.1: X-RAY DIFFRACTOGRAMS OF SAMPLES STUDIED HEREIN. A) PROXIMAL SECTION OF TENDON. B) MID-POINT OF TENDON. C) DISTAL SECTION OF TENDON. .... 203

FIGURE A.4.2: FTIR SPECTRA OF TENDONS STUDIED HEREIN. A) PROXIMAL SECTION OF TENDON. B) MID-POINT OF TENDON. C) DISTAL SECTION OF TENDON..... 204

## Abbreviations and Acronyms

| <b>Abbreviation</b> | <b>Definition</b>                        |
|---------------------|--|
| AAS                 | Atomic Absorption Spectroscopy           |
| AES                 | Atomic Emission Spectroscopy             |
| AFM                 | Atomic Force Microscopy                  |
| AKU                 | Alkaptonuria                             |
| BQA                 | Benzoquinoneacetic acid                  |
| C-AFM               | Conductive probe atomic force microscopy |
| CAT                 | Catechol (1,2-dihydroxybenzene)          |
| CSA                 | Chondroitin sulfate A                    |
| CSC                 | Chondroitin sulfate C                    |
| CV                  | Cyclic voltammetry                       |
| DHI                 | Dihydroxyindole                          |
| DHICA               | 5,6-dihydroxyindole-2-carboxylic acid    |
| DLS                 | Dynamic light scattering                 |
| DOPA                | Levodopa                                 |

|            |  |
|------------|--|
| DSC        | Differential scanning calorimetry                              |
| ECM        | Extracellular matrix   |
| EDX/EDS    | Energy dispersive X-ray spectroscopy                           |
| EIS        | Electrochemical impedance spectroscopy                         |
| EPR/ESR    | Electron Paramagnetic Resonance                                |
| ESR        | Electron Spin Resonance Spectroscopy                           |
| FTIR       | Fourier transform infrared spectroscopy                        |
| GPC/SEC    | Gel Permeation Chromatography or Size Exclusion Chromatography |
| HGA        | Homogentisic acid  |
| HPLC       | High Performance Liquid Chromatography                         |
| HRP        | Horseradish peroxidase   |
| LACC       | Laccase  |
| MS         | Mass Spectrometry  |
| NMR        | Nuclear Magnetic Resonance Spectroscopy                        |
| OCT        | Optical coherence tomography                                   |
| polyCAT-HS | Poly catechol- High solubility                                 |
| polyCAT-LS | Poly catechol- Low solubility                                  |

|             |   |
|-------------|---|
| polyDOPA-HS | Poly levodopa -high solubility                      |
| polyDOPA-LS | Poly levodopa- low solubility                       |
| polyHGA-HS  | Poly Homogentisic acid -high solubility             |
| SAXS        | Small angle X-ray scattering                        |
| SECM        | Scanning electrochemical microscopy                 |
| SEM         | Scanning Electron Microscopy                        |
| SFDS        | Spatial frequency domain spectroscopy               |
| SLS         | Static light scattering                             |
| SPM         | Scanning Probe Microscopy                           |
| ssNMR       | Solid state nuclear magnetic resonance spectroscopy |
| STM         | Scanning Tunneling Microscopy                       |
| TEM         | Transmission Electron Microscopy                    |
| TGA         | Thermogravimetric analysis                          |
| TYR         | Tyrosinase  |
| UV-Vis      | Ultraviolet-visible Spectroscopy                    |
| WAXS        | Wide angle X-ray scattering                         |

|     |                                  |
|-----|----------------------------------|
| XPS | X-ray Photoelectron Spectroscopy |
| XRD | X-ray diffraction                |
| XRF | X-ray Fluorescence Spectroscopy  |



# 1 Introductory Chapter

## Overview

Melanins are a class of biopolymers that are widespread in nature and have diverse origins, chemical compositions, and functions. Their chemical, electrical, optical, and paramagnetic properties offer opportunities for applications in materials science, particularly for medical and technical uses. This chapter focuses on the application of analytical techniques to study melanins in multidisciplinary contexts with a view to their use for advanced biotechnological applications.

## 1.1 Introduction

The color a light source has is dependent on the wavelengths of light mixed together. Perception of color is dependent on the species observing an object <sup>1,2</sup>, and the color of an object is dependent on the parts of the spectrum visible to the species that are not absorbed (e.g. by dyes, pigments, etc.) and reflected/scattered/transmitted, and/or interference effects <sup>3-8</sup>. Colorants (dyes and pigments) impart color to a material; dyes are molecular species, whereas pigments are particulates (and their color tends to be more stable than dyes [i.e. less likely to bleach]) <sup>9</sup>. Dyes and pigments absorb light in specific wavelength ranges due to their system of conjugated bonds in their structure (i.e. chromophore) and are responsible for some of the colors we and other species observe, as exemplified by the dark spots in seashells<sup>10-12</sup>, and birds feathers <sup>13</sup> (shown in **Figure 1.1**).

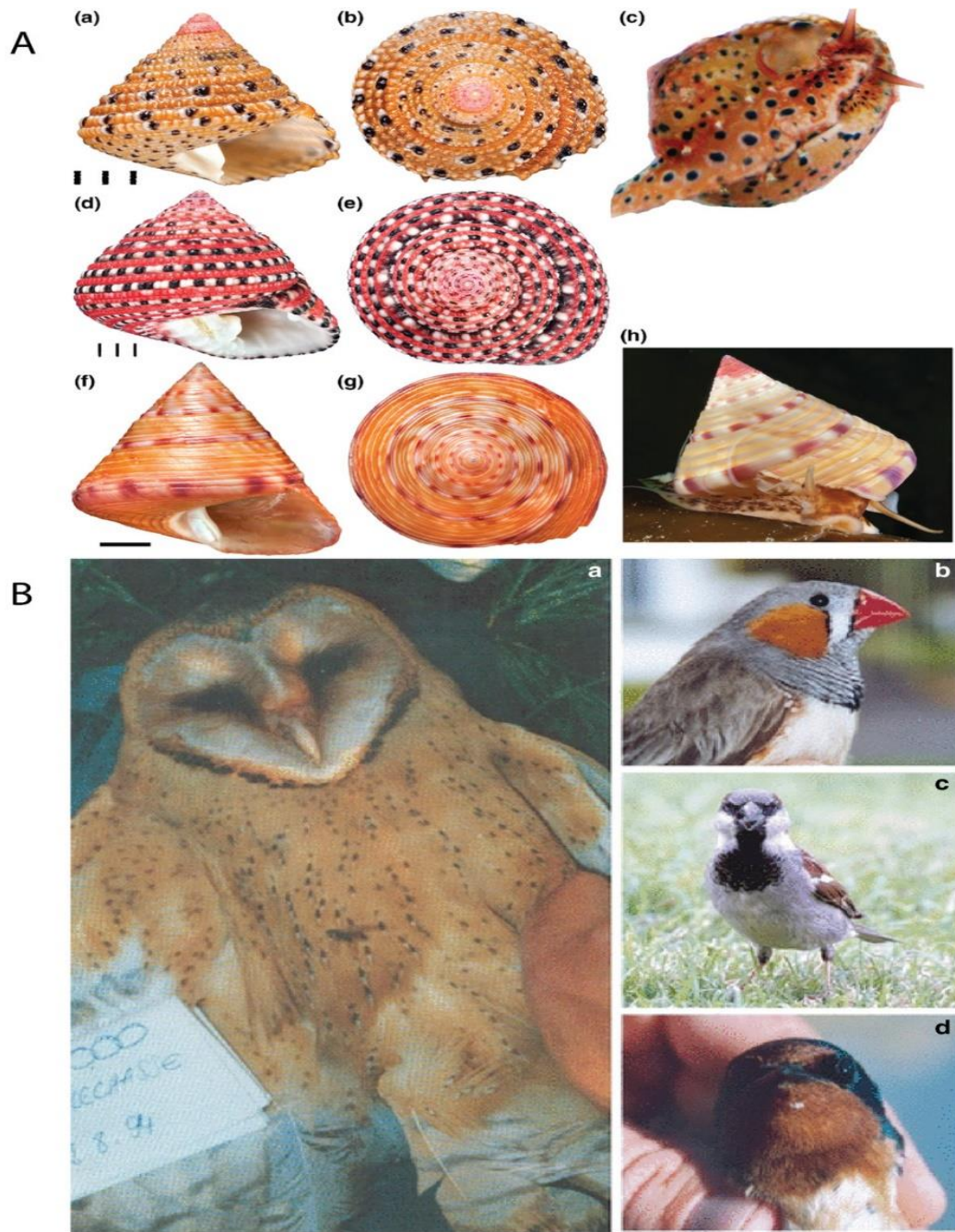


Figure 1.1: Eye catching examples of colour in nature (including melanin-derived colours).

A) Photographs of colorful seashells. (a–c) *Clanculus margaritarius* C. (a, b) Two views of a shell of *Clanculus margaritarius* C (specimen #2). Note that this specimen is subadult. (c) Colored foot of a live animal. Note that the color and pattern are the same as found on the shell. (d, e) Two views of a *Clanculus pharaonius* shell (specimen #4). (f–h) *Calliostoma zizyphinum*. (f, g) Two views of a shell of *Calliostoma zizyphinum* (specimen #2). (h) Living animal showing foot color (not the same specimen). Note that the foot color and pattern in this species do not match the shell. Scale bars for *Clanculus* spp are in mm. Scale bar for *Calliostoma* is 1 cm. Reproduced with permission 20. Copyright 2017, Wiley. B) Color photos showing the melanin based ornamental traits in four species that have been well-studied in the context of metals, amino acids, and hormones. (A) Black breast spotting and chestnut breast coloring in a barn owl, © Alex Roulin. (B) Black breast striping and patch in a male zebra finch, © Kevin McGraw. (C) Black throat badge of male house sparrow, © Janine Russell. (D) Brown forehead and throat plumage in a barn swallow, © Kevin McGraw. Reproduced with permission. Copyright 2008, Wiley

Naturally occurring pigments (known as biochromes), are synthesized and accumulated in, or excreted from, living organisms (animals [Humans], bacteria [*Escherichia coli*] and plants [chestnut (*Castanea mollissima*) and oat (*Avena sativa*)]). They can be classified into six major groups as N-heterocyclic derivatives (e.g. betalains [such as betanin] and eumelanins), O-heterocyclic derivatives (e.g. anthocynins [such as rosinidin] and other flavonoid pigments); quinones (e.g. derivatives of anthraquinone [such as 9,10-anthraquinone], benzoquinone, naphthoquinone, etc.); tetrapyrroles (e.g. porphyrin derivatives such as chlorophyll and heme); tetraterpenoid derivatives (e.g. carotenoids [such as  $\beta$ -carotene] and iridoids); and “miscellaneous” (e.g. lipofuscins [such as *N*-retinylidene-*N*-retinyl-ethanolamine] and fungal pigments<sup>14-16</sup>) see (Figure 1.2).

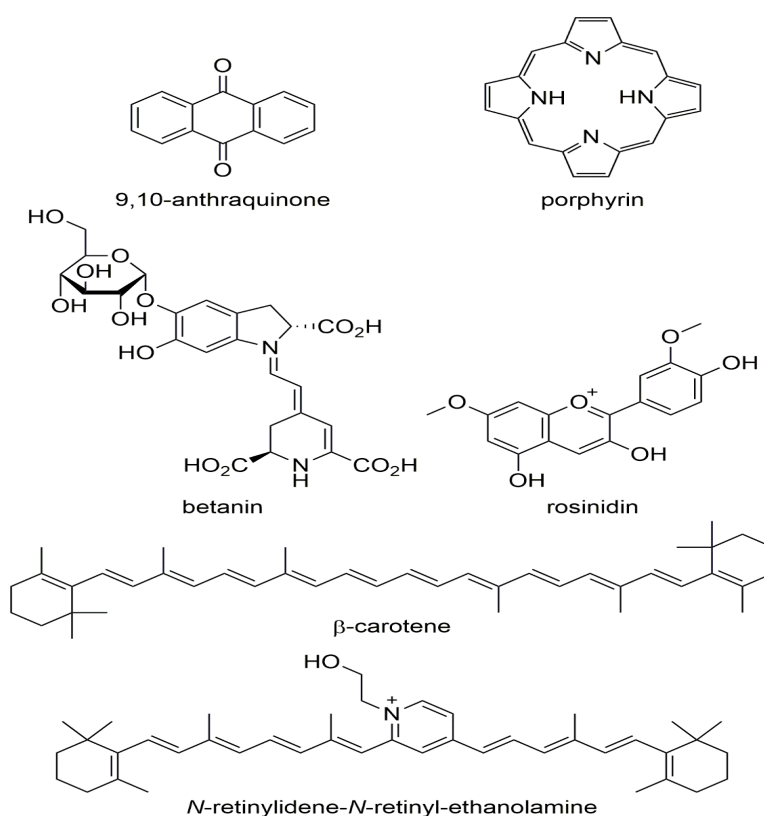


Figure 1.2: Examples of naturally occurring pigments.

Melanins are a class of biopolymers with diverse origins and chemical compositions, which are widespread in nature, and the focus of this chapter (representative structures are shown in **Figure 1.3**). While the name melanin was initially applied to black pigments, it has subsequently been used to describe pigments of colors from black/brown eumelanins<sup>17</sup> to red/yellow pheomelanins<sup>18,19</sup>, all of which play a role in skin pigmentation<sup>20</sup>, in combination with carotenoids, haemoglobin, etc.<sup>17,21</sup>. Melanins have a variety of functions in nature (from photoprotection to photosensitization<sup>20,22</sup>, antioxidant defense and metal/drug binding)<sup>23-26</sup> which reflect a unique combination of chemical, electrical, optical and paramagnetic properties<sup>27-30</sup>, and their properties have resulted in their application in materials science for a range of historical<sup>31</sup>, medical and technical applications<sup>30,32-36</sup>.

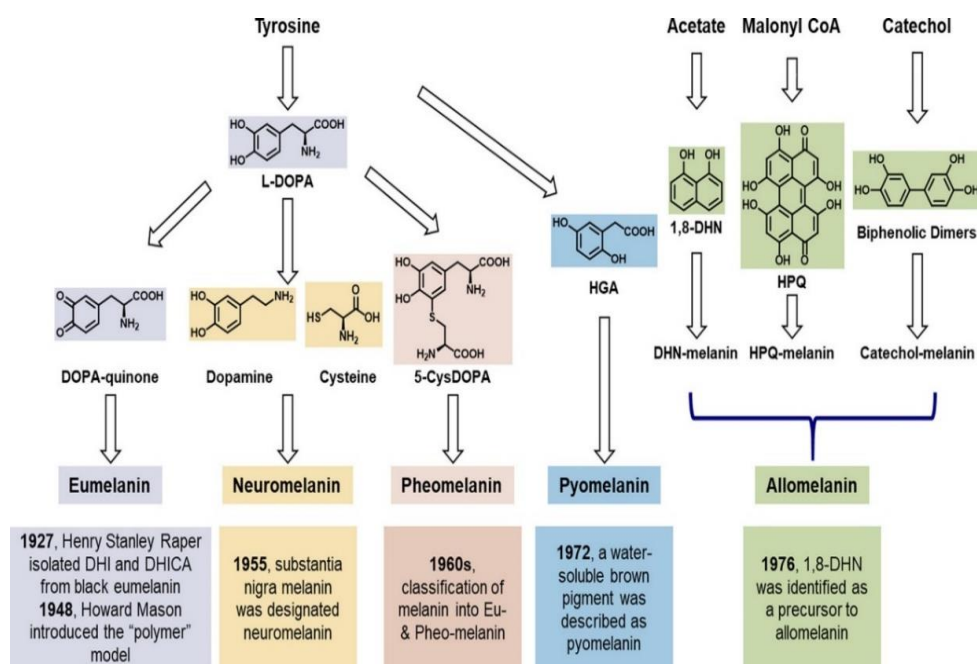


Figure 1.3: Common biosynthetic pathways for melanins. Reproduced with permission<sup>38</sup>. Copyright 2021, American Chemical Society.

Melanin production is typically an oxidative process involving reactive oxygen species occurring *in vivo*, often also involving enzymes such as oxidases (e.g. phenolases that catalyze the oxidation of phenol derivatives [eumelanins and pheomelanins are produced within melanocytes by a complex biosynthetic pathway involving the tyrosinase-catalyzed oxidation of tyrosine]) followed by uncontrolled polymerization of the oxidized intermediates (often involving a reactive quinone intermediate prone to reactions with amine and hydroxyl groups and capable of undergoing reversible redox reactions)<sup>19</sup>. In contrast to the production of polynucleic acids (e.g. DNA, RNA) and proteins, melanin production does not involve “templates” and therefore the compositions and sequences of “monomers” in the backbone of the melanins is random (albeit clearly influenced by the feedstocks available, organism/tissue and other conditions); however, eumelanins are rich in L-dopa<sup>37</sup>, pheomelanin is rich in 5-cys-dopa<sup>37</sup>, neuromelanins are rich in 5,6-dihydroxyindole<sup>38,39</sup>, catechol melanins are rich in catecholic monomers<sup>40,41</sup>, insect melanin is rich in *N*-acetyl-dopamine<sup>42,43</sup>, pyromelanin is rich in homogentisic acid (HGA), and allomelanins are rich in 1,8-dihydroxynaphthalene (DHN)<sup>19,44</sup>, see **(Figure 1.3)**. Oligomeric species (e.g. trichochromes occurring in hair<sup>45</sup> tend to have relatively low molecular weights and are soluble; by comparison, the polymerisation of melanins<sup>46</sup> yields species with higher molecular weights and the formation of insoluble pigment particles. The generation of these insoluble pigment particles<sup>47</sup> is proposed to proceed via a nucleation and growth mechanism **(Figure 1.4)** as detailed in an excellent review by Strube and coworkers<sup>48</sup>. Melanins are produced by a variety of life forms including bacteria<sup>49,50</sup>, and eukarya (e.g. fungi<sup>45,51-53</sup> plants<sup>54,55</sup>, animals<sup>37,56,57</sup>, and humans<sup>58</sup>), and play a role in photoprotection or in the case of some fungi the conversion of radiation into chemical

energy for growth, opening up the potential for them to play a critical role for life in extreme environments on Earth and perhaps elsewhere in the universe <sup>59-68</sup>.

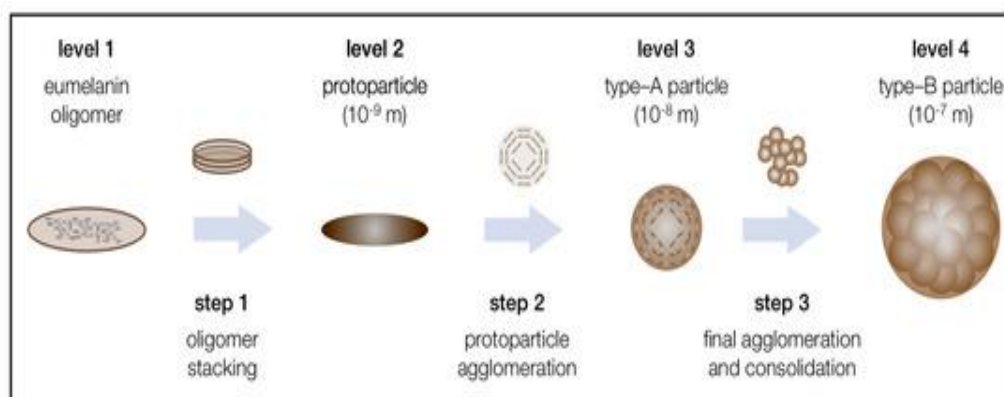


Figure 1.4: The three-step, four-level hierarchical build-up mechanism of natural and biomimetic eumelanin, based on the state of literature Reproduced with permission <sup>48</sup>. Copyright 2017, MDPI.

A multitude of reviews on melanins exist, covering various aspects of their biochemistry, functions and applications <sup>37, 46, 57, 69-80</sup>. This chapter focuses on the application of analytical techniques to study melanins in multidisciplinary contexts with a view to their use as sustainable resources for advanced biotechnological applications. The scope of the literature (thousands of papers) prevents this from being comprehensive in coverage, however it covers a wide variety of analytical techniques applied to melanins, highlighting a few examples of the insights drawn from analysis of melanins <sup>81</sup> and their precursors produced by bacteria and eukarya (including laboratory-based scientists and engineers). It should be of interest to researchers from multidisciplinary backgrounds seeking an overview of techniques used to study this class of biomolecules with a view to their novel biotechnological applications <sup>82, 83</sup>, which are classified in a color-coded fashion that encompasses broad areas of use (Table 1.1) <sup>84</sup>.

Table 1.1: Biotechnology types.

| Biotechnology Classification | Scope   |
|------------------------------|---|
| Blue biotechnology           | Marine/Sea: use of marine/sea resources to create products and industrial applications <sup>85-87</sup> .   |
| Brown biotechnology          | Management of Arid Lands and Deserts: innovation/creation of biotechnologies to enable/manage agriculture in arid lands and deserts <sup>88</sup> .   |
| Dark biotechnology           | Defense: biotechnology related to bioterrorism, biological weapons and biowarfare (e.g. microorganisms and toxins to cause diseases/death in humans, livestock and crops) <sup>89,90</sup> .  |
| Gold biotechnology           | Computational/Bioinformatics: in silico biotechnology for the development and production of products (e.g. compound identification and toxicity/function screening) <sup>84</sup> .   |
| Grey biotechnology           | Environmental Applications: biotechnologies focused on the maintenance of biodiversity and the remediation of pollutants <sup>88</sup> .  |
| Green biotechnology          | Agricultural: use of agricultural processes (e.g. transgenic plants) to produce feedstocks/materials <sup>88</sup> .  |
| Purple/violet biotechnology  | Ethics/Law/Philosophy: issues surrounding biotechnology <sup>88, 91, 92</sup> .   |
| Red biotechnology            | Medical Technology: biotechnology for medical, pharmaceutical and health applications <sup>88, 91, 92</sup> .   |
| White biotechnology          | Industrial Biotechnology: biotechnology applied to industrial processes (e.g. enzyme mediated synthesis, synthetic/engineering biology) for the development & production/processing of valuable chemicals and materials <sup>88</sup> . |

Yellow biotechnology      Food & Insect: biotechnology used to produce food, or biotechnology to control/use insects <sup>88</sup>.

---

## 1.2 Analysis of Melanins

Melanins produced by organisms have been separated and analysed by various methods <sup>93-96</sup>, enabling their subsequent application for fundamental and applied science, technology, engineering and medicine. This section of the review summarizes the techniques used to study melanins (**Table 1.2**) which underpins their biotechnological applications in various industry sectors.

*Table 1.2 Analytical techniques applied to melanins.*

| Analytical Technique.  | Practical application to melanins and materials containing melanins.  |
|--|---|
| High Performance Liquid Chromatography (HPLC)                              | HPLC has been shown to be particularly useful in the analysis of low molecular weight melanin precursors <sup>97-100</sup> .  |
| Gel Permeation Chromatography (GPC) or Size Exclusion Chromatography (SEC) | GPC/SEC has been shown to be particularly useful in the analysis of high molecular weight melanins (and the conversion of the low molecular weight species to high molecular weight melanins) <sup>101, 102</sup> .   |
| Mass Spectrometry (MS)   | MS measures the mass-to-charge ratios of ionized species (molecules or fragments thereof) which are correlated to their molecular weights via time of flight (TOF) measurements. Low molecular weight species analysed by techniques such as ESI or high molecular weight species by MALDI <sup>103-106</sup> . |

|   |  |
|---|--|
| Nuclear Magnetic Resonance (NMR) Spectroscopy                                       | NMR spectroscopy provides information about the chemical environments of spin active nuclei in materials, and therefore the chemical structure of melanins and their precursors (and potentially metal ions bound to such species) using either solution state or solid state NMR depending on the solubility of the samples <sup>107, 108</sup> .                                       |
| Electron Paramagnetic Resonance (EPR) or Electron Spin Resonance (ESR) Spectroscopy | EPR/ESR spectroscopy can be used to detect and identify free radicals and paramagnetic centres (e.g. organic radicals, metals etc.). Melanins display paramagnetic character due to free radicals in their structures (e.g. semiquinone free radicals) which absorb microwaves under magnetic fields yielding spectra characteristic of the radical species present <sup>109-111</sup> . |
| Atomic Absorption Spectroscopy (AAS) and Atomic Emission Spectroscopy (AES)         | AAS and AES measure the light absorbed/emitted by samples in the gaseous state (typically metal ions) and have been used to quantify the metal content of various melanins/materials <sup>108, 112</sup> .   |
| Chemiluminescence Spectroscopy  | Chemiluminescence spectroscopy enables measurement of light emitted as a result of a chemical reaction, and has been used to study the excited species formed through oxidative reactions (e.g. oxidized linoleic acid with melanin) <sup>113, 114</sup> .   |
| Fluorescence Spectroscopy   | Fluorescence spectroscopy most often measures light emission from samples with electrons that have been excited, however, it is also possible to measure absorption for cases involving single/pairs of fluorophores, and has been used to study autofluorescence of melanin-containing materials, metabolic activity of melanin-producing species, etc <sup>113, 115</sup> .            |
| Infrared Spectroscopy   | Fourier transform infrared (FTIR) spectroscopy relies on spectral differences for IR transmission (passing through samples), absorbance or reflection, where these differences enable functional group identification in melanins based on the energies of specific vibrational mode <sup>115, 116</sup> .   |
| Mössbauer Spectroscopy  | Mössbauer spectroscopy probes the properties of specific isotopic nuclei in different atomic environments by analyzing the resonant absorption of gamma rays, potentially interesting for the analysis of the interactions of metal ions with melanins <sup>117</sup> .  |

|  |   |
|--|---|
| Phosphorescence Spectroscopy                 | Phosphorescence spectroscopy enables measurement of light emitted relatively slowly from a molecule, and can be used to study singlet oxygen phosphorescence (e.g. during the photobleaching of melanosomes) <sup>113</sup> .   |
| Photoacoustic Spectroscopy                   | Photoacoustic spectroscopy records the sound waves emitted by materials that absorb radiation, and can be used to study the melanin content of a variety of biological materials, and moreover for drug delivery and theranostic applications <sup>118</sup> .                      |
| Photothermal Spectroscopy                    | Photothermal spectroscopy enables measurement of heat evolved on absorption of radiation which has been applied to study melanins from various sources (e.g. synthetic melanins, the melanin content of skin) <sup>119</sup> .  |
| Pump-Probe Spectroscopy                      | Pump-probe spectroscopy (and variants thereof) has been used to examine the primary photodynamics of melanins, and is useful for mapping the distribution of melanin in pigmented tissues and moreover enabling early diagnosis of melanoma <sup>120, 121</sup> .                   |
| Raman Spectroscopy                           | Raman spectroscopy relies on the inelastic scattering of monochromatic light to study the vibrational/rotational modes of molecules, and can be used to analyse bond/chromophore connectivity in melanins <sup>108, 118, 122</sup> .  |
| Terahertz Time-Domain Spectroscopy (THz-TDS) | THz-TDS is an efficient technique for the coherent generation and detection of broadband THz radiation for studying material response at THz frequencies, with exciting results for diagnostic imaging of cancers/melanomas during surgeries to assist removal <sup>123-125</sup> . |
| Ultraviolet-visible (UV-Vis) Spectroscopy    | UV-Vis spectroscopy (in either absorption or reflectance modes) is routinely employed in the study of melanins (e.g. bond conjugation and connectivity) <sup>115</sup> .  |
| X-ray Fluorescence (XRF) Spectroscopy        | XRF is often used for elemental/chemical analysis (e.g. assessing the concentrations of metal ions which are known to play important roles in oxidative damage of tissues containing melanins) <sup>108</sup> .   |

|   |   |
|---|---|
| X-ray Photoelectron Spectroscopy (XPS)  | XPS offers insight into chemical composition (formula) and the chemical/electronic state of the elements in melanin-containing materials <sup>108, 118</sup> .  |
| Scattering and Diffraction              | A variety of scattering and diffraction techniques (e.g. turbidimetry, nephelometry, SLS, DLS, XRD, SAXS, WAXS) enable elucidation of molecular weights of melanins, or the crystallinity and microstructure of melanin-containing materials/species <sup>126-135</sup> .   |
| Thermal Characterization                | A variety of calorimetric methods exist for monitoring heat flow to study molecules in the solution and solid phase (e.g. calorimetry, TGA, DSC), thereby enabling elucidation of various processes including melanin formation kinetics, melanin processability and stability in various environments which are important when incorporating them in materials for various applications <sup>136-140</sup> . |
| Electrical Characterization             | Electrochemical characterisation of materials are useful in light of their interesting properties. Studies of reduction/oxidation processes and electron transfer using cyclic voltammetry (CV), electrochemical impedance spectroscopy (EIS) and dielectric spectroscopy enable the rational investigation of the protonic and electronic contributions <sup>141, 142</sup> .                                |
| Visual and Microscopic Characterization | Photography offers a simple method of capturing evidence of color over a large scale (mm to km), consequently, photographs provide a useful initial starting point in studies of phenomena, including coloration of melanin-containing materials/species <sup>143, 144</sup> .  |
| Scanning Electron Microscopy (SEM)      | SEM is used to analyse particle size distributions and elemental compositions when used in combination with energy dispersive X-ray spectroscopy (EDX/EDS) <sup>140, 145, 146</sup> .   |
| Transmission Electron Microscopy (TEM)  | TEM is used to analyse particle size distributions and elemental compositions when used in combination with energy dispersive X-ray spectroscopy (EDX/EDS) <sup>140, 145, 146</sup> .   |

|                           |   |
|---------------------------|---|
| Scanning Probe Microscopy | SPM (e.g. profilometry, STM, AFM, etc.) uses various probes to analyse the surface of samples enabling examination of a multitude of properties of melanin-containing materials/species (e.g. electronics, mechanics, spectroscopy, etc.) <sup>147, 148</sup> .   |
| Computational Studies     | Chemoinformatic studies, such as atomistic simulations are used to study the structure of melanins and melanin-containing materials; and bioinformatic studies are used to examine functional and structural genomics, transcriptomics, proteomics, metabolomics, glycomics, lipidomics, etc. <sup>135, 149-155</sup> . |

---

### 1.2.1 High Performance Liquid Chromatography (HPLC)

Chromatography enables the separation of low molecular weight species based on differences in their interactions with the adsorbent material (typically a column packed with silica, optionally derivatised with species including alkyl chains), causing different elution times for the different components enabling their separation and subsequent identification and quantification<sup>97-100</sup>. HPLC has been shown to be particularly useful in the analysis of low molecular weight melanin precursors because of its ability to separate different species from complex chemical mixtures<sup>156</sup>, a few examples of which are highlighted. HPLC has been used to study the generation of homogentisic acid (from tyrosine and phenylalanine) and its excretion, auto-oxidation and self-polymerization to form melanin for a variety of bacteria, including *Bacillus thuringiensis*<sup>157</sup>, *Burkholderia cenocepacia*<sup>158</sup>, *Escherichia coli*<sup>159</sup>, *Shewanella algae*<sup>160</sup>, *Shewanella colwelliana*<sup>161</sup>, *Vibrio cholerae*<sup>161</sup>, *Rubrivivax benzoatilyticus* JA2<sup>162</sup>, to name a few. Biosynthetic pathways under various conditions (e.g. anaerobic/aerobic conditions) can be studied, offering insight into the utilization of L-phenylalanine as source of nitrogen under

anaerobic/aerobic conditions but not as a carbon source as reviewed <sup>163</sup>, identification of key metabolites (e.g. L-tyrosine, 4-hydroxyphenylpyruvic acid, homogentisic acid), and enzyme activities leading to homogentisate accumulation and pyomelanin production <sup>162</sup>. HPLC has been used in the analysis of fungal melanin production by studying fungal melanin intermediates and related metabolites <sup>164</sup>. In a fascinating study, HPLC enabled the elucidation of the effect gamma radiation on the growth of melanised fungi (*Cryptococcus neoformans*, *Cryptococcus sphaerospermum* and *Wangiella dermatitidis*), demonstrating that they use the melanin they produce to convert gamma radiation into chemical energy for growth (i.e. that the fungi are radiotrophic, and grow faster when exposed to radiation; with clear potential for grey biotechnology applications) <sup>68</sup>. HPLC has been used as a semi-quantitative method of HGA quantitation in the urine of patients with Alkaptonuria (AKU), offering opportunities for its use as a quick diagnostic tool for AKU <sup>165</sup>, the effects of medications (e.g. antioxidants such as ascorbic acid) on AKU patients <sup>166</sup>, for the detection of persons heterozygous for deficiency of homogentisic acid oxidase (i.e. red biotechnology) <sup>167</sup>. HPLC has also been used to analyse melanin degradation products from patients with melanoma <sup>168</sup> and oligomeric species (trichochromes) from hair (i.e. red biotechnology) <sup>169</sup>.

### **1.2.2 Gel Permeation Chromatography (GPC)**

GPC (also known as Size Exclusion Chromatography SEC) is an analytical technique that separates polymers by size (as a function of their elution from columns filled with a porous gel) <sup>101, 102</sup>. GPC has been shown to be particularly useful in the analysis of high molecular weight melanins (and the conversion of the low molecular weight

species to high molecular weight melanins), a few examples of which are highlighted. From a fundamental science perspective, GPC has been used to study the oxidation of monomers into melanins in the presence/absence of other species. GPC has been employed in studies demonstrating that: the polymerisation of HGA to be enhanced at higher pH <sup>170</sup>; the H<sub>2</sub>O<sub>2</sub> mediated oxidation of phenolics (e.g. L-DOPA) can yield light- or dark-colored pigments depending on the oxidizing potential of the environment <sup>171</sup>; <sup>172</sup>; the presence of anionic polysaccharides during the polymerisation of catecholamine precursors (including dopamine, epinephrine and norepinephrine) resulted in the generation of larger melanin particles <sup>173</sup>. With a view to more applied research, GPC has been used to follow melanin production via a white biotechnology approach <sup>174-178</sup>, employing mutant strains of *Alcaligenes eutrophus* to transform tyrosine into p-hydroxyphenylacetic acid, which is then converted to HGA, which subsequently polymerises to form pyomelanin <sup>179</sup>. GPC has also been used to characterise processes inhibiting melanogenesis in mouse melanoma cells *in vitro* and in brown guinea pigs *in vivo* <sup>180</sup>, and moreover, the eumelanin produced by fungi (*Auricularia auricula*) that was subsequently used as a hepatoprotective antioxidant to treat mice with acute alcoholic liver injury (i.e. red biotechnology) <sup>181</sup>.

### **1.2.3 Mass Spectrometry (MS)**

MS measures the mass-to-charge ratios of ionized species (molecules or fragments thereof) which are correlated to their molecular weights via time of flight (TOF) measurements <sup>103-106</sup>. The most common ionisation methods are atmospheric pressure chemical ionisation (APCI), chemical ionisation (CI), electron impact (EI), electrospray

ionisation (ESI), fast atom bombardment (FAB), field desorption / field ionisation (FD/FI), matrix assisted laser desorption ionisation (MALDI) and thermospray ionisation (TSP); and the optimal ionisation method is sample dependent. Various forms of MS have been used for the analysis of melanins and their precursors, a few examples of which are highlighted. In humans, urine of patients with alkaptonuria becomes dark due to the oxidation of homogentisic acid (HGA) to benzoquinone acetic acid (BQA), which is a common means of diagnosis and the reason it is often known as black urine disease. A variety of different mass spectrometry techniques have been applied for the analysis of HGA and oxidation products thereof in samples of patient's bodily fluids including EI-MS <sup>182</sup>, gas chromatography coupled to MS (GC-MS) <sup>183, 184</sup>, liquid chromatography coupled to MS (LC/TOF-MS in ESI mode) <sup>185</sup>, which also enables studies of the binding of HGA and BQA to amyloids <sup>186</sup>, which can potentially offer insight into the natural melanin formation process <sup>187, 188</sup>, and give insight into potential therapeutic opportunities for removing the damaging pigment in this condition. More advanced MS setups have facilitated various studies, including LC–tandem mass spectrometry (LC–MS/MS in ESI mode) to quantify tyrosine and HGA in clinical trial samples to determine the efficacy and response to nitisinone in the treatment of AKU <sup>189</sup>, mixtures of homovanillic acid, vanillylmandelic acid, orotic acid and HGA <sup>190</sup>, LC-QTOF-MS was used to evaluate the effect of nitisinone on the urinary metabolome of patients and mice with AKU <sup>191</sup>, and the products of polymerisation of tyrosine and HGA have been studied by MALDI-TOF <sup>17, 192</sup>; all of which serve to highlight the importance of MS techniques to study melanins for red biotechnology applications. An elegant study demonstrated the use of TOF-secondary ion MS (TOF-SIMS) for MS imaging of melanin-containing fossil samples <sup>193, 194</sup>. The presence of the 1,8-dihydroxynaphthalene (DHN)-melanin (characterised by a variety of techniques

including MALDI-TOF) produced by the fungal banana pathogen *Mycosphaerella fijiensis* in banana leaves naturally infected with black Sigatoka disease was positively correlated to the disease stage (i.e. green/yellow biotechnology). Importantly, it was demonstrated that the melanin acted as a light-activated phytotoxin that functions by the generation of singlet oxygen that damages the plant tissues <sup>44</sup>, thereby highlighting the importance of such natural melanins for both green and dark biotechnologies.

#### **1.2.4 Nuclear Magnetic Resonance (NMR) Spectroscopy**

NMR spectroscopy provides information about the chemical environments of spin active nuclei in materials <sup>107, 108</sup>. The choice of solution state or solid state NMR experiments is chosen based on the solubility of the melanins, with the possibility to use solution state NMR for precursors of melanins <sup>185, 195</sup>, melanin-metal ion interactions <sup>196</sup>, or indeed soluble melanins produced by yeast (e.g. *Yarrowia lipolytica* <sup>197</sup>), or human derived neuromelanin <sup>198, 199</sup>, whereas solid state NMR was necessary for the melanins produced by bacteria (*Rubrivivax benzoatilyticus* JA2 <sup>162</sup>), yeast (*Cryptococcus neoformans* <sup>200</sup>), cuttlefish (*Sepia officinalis* <sup>196, 201</sup>), human hair <sup>201, 202</sup> and moreover for samples derived from human alkaptonuric joint tissues where spectral linewidths from strongly pigmented ochronotic tissue were considerably increased relative to non-pigmented control indicating a marked increase in the level of molecular disorder in the collagen supported by electron microscope images (i.e. red biotechnology) <sup>203</sup>.

### 1.2.5 Electron Paramagnetic Resonance (EPR) Spectroscopy

Electron paramagnetic resonance (EPR) or electron spin resonance (ESR) spectroscopy can be used to detect and identify free radicals and paramagnetic centres (e.g. organic radicals, metals etc.)<sup>109-111</sup>. Melanins display paramagnetic character due to free radicals in their structures (e.g. semiquinone free radicals) which absorb microwaves under magnetic fields yielding spectra characteristic of the radical species present. EPR/ESR spectroscopy is therefore a potent method of studying melanins, with reports of its use for fundamental biochemistry studies (e.g. melanin type<sup>202, 204-207</sup>, effect of pH<sup>208-210</sup>), characterising melanins from different species including bacteria (*Rubrivivax benzoatilyticus* JA2<sup>162</sup>, *Vibrio natriegens*<sup>211</sup>, *Streptomyces cyaneofuscatus*<sup>212</sup>), yeast (*Cryptococcus neoformans*<sup>200</sup>), mushrooms (*Inonotus hispidus*<sup>213</sup>), black soldier flies (*Hermetia illucens*<sup>214, 215</sup>), squid (*Loligo opalescens*<sup>205</sup>), cuttlefish (*Sepia officinalis*<sup>216</sup>) and cephalopod ink sacs from the Jurassic era<sup>217</sup>. Ionizing irradiation changes the EPR/ESR signals of fungal melanins due to changes in the electronic structure of the melanins, which informed a fascinating study of melanized fungal cells (*Wangiella dermatitidis*, *Cryptococcus Neoformans* and *Cladosporium Sphaerospermum*) which displayed increased growth relative to non-melanized cells after exposure to ionizing radiation<sup>68</sup>. EPR/ESR can contribute to fundamental neuroscience by enhancing our understanding of the role of melanin and iron in the pathogenesis of oxidative damage in neuromelanin found in the substantia nigra<sup>218</sup>, and moreover photoaging of eyes (i.e. red biotechnology)<sup>219, 220</sup>. EPR/ESR also have significant potential for the analysis of hair and skin<sup>220, 221</sup>, as discussed as highlighted in an excellent review<sup>222</sup>.

### 1.2.6 Infrared Spectroscopy (IR)

Infrared spectroscopy<sup>115, 116</sup>, often Fourier transform infrared (FTIR) spectroscopy relies on spectral differences for IR transmission (passing through samples), absorbance or reflection, where these differences enable functional group identification based on the energies of specific vibrational modes. FTIR is a very popular method of characterising melanins due to its simplicity, availability and broad applicability, and has been used to characterise synthetic melanins (formed with a variety of monomers including dopamine<sup>223, 224</sup>, 5-S-cysteinyldopa<sup>225</sup>, 1,8-dihydroxynaphthalene<sup>226</sup>, and homogentisic acid<sup>227</sup>; and optionally the presence of additives such as anionic polysaccharides<sup>173</sup> to mimic the biological milieu) and natural melanins from bacteria (e.g. *Pseudomonas sp.*<sup>228</sup>, *Pseudomonas stutzeri*<sup>229</sup>, *Streptomyces cyaneofuscatus*<sup>212</sup>), fungi (e.g. *Inonotus hispidus*<sup>213</sup>, *Lasiodiplodia theobromae*<sup>230</sup>, *Yarrowia lipolytica*<sup>231</sup>), cuttlefish (*Sepia officinalis*<sup>96, 232, 233</sup>) and humans (e.g. kidney and prostate stones<sup>234</sup>, Egyptian mummies from 1500 B.C.<sup>235</sup>).

### 1.2.7 Raman Spectroscopy

Raman spectroscopy<sup>108, 118, 122</sup> relies on the inelastic scattering of monochromatic light to study the vibrational/rotational modes of molecules, and is well suited to the characterisation of a variety of biological materials<sup>236</sup>. Raman spectroscopy and variants thereof have been used to analyse bond/chromophore connectivity in eumelanin<sup>237</sup>, cuttlefish melanins used as pigments in works of art<sup>238</sup>, to quantify the proportions of the constituent monomers (DHI and DHICA) in eumelanins in bird feathers<sup>239</sup>, and the molecular vibrations of pheomelanins in bird feathers have been demonstrated to be associated with reactive oxygen species production in the

mitochondria of melanocytes and systemic oxidative stress and damage, potentially linking pheomelanin synthesis to human melanoma risk <sup>240</sup>. A combination of HPLC, Raman and computational studies demonstrated that the vibrational properties of melanins play a more significant role in the colour of bird feathers than concentration-based effects <sup>241</sup>; moreover, a combination of Raman data and computational data demonstrate that the black colour of hairs and other parts of spiders is due to eumelanin, rather than the previously suggested ommochrome Ommin A <sup>242</sup>, thereby highlighting the potential of gold biotechnology approaches for fundamental biological studies. Raman spectroscopic analysis of the fungal melanins produced by *Neocatenulostroma* genus sustained by the colonisation of gypsum in the Atacama desert (one of the driest regions of earth) <sup>243</sup> highlights the importance of fundamental analytical studies of melanins for both brown and grey biotechnologies. The presence of eumelanins and pheomelanins in human skin offer a potentially useful clinical method for non-invasively investigating the eyes <sup>244, 245</sup> or the skin <sup>246</sup>. Indeed, the use of Raman spectroscopy to identify melanin within cells or tissues <sup>246-249</sup> is becoming more routine in biomedical fields as it is emerging that differences between normal and cancer cells can be detected <sup>250-253</sup> and as a tool to predict cancer cells response to various therapies <sup>250</sup> potentially allowing patients to receive specific treatments more likely to work for them as current treatment regimes are standardized with patients following on from one failed therapy to another based on the therapies generalised success rate; thereby highlighting the importance of fundamental analytical studies of melanins for red biotechnologies.

### 1.2.8 Ultraviolet-visible (UV-Vis) Spectroscopy

Ultraviolet-visible (UV-Vis) spectroscopy <sup>115</sup> (in either absorption or reflectance modes) is routinely employed in the study of melanins (e.g. alkaptonuria-derived pyromelanins) and is useful for fundamental biochemistry <sup>170, 172, 173, 254</sup>, diagnostic testing <sup>17, 185, 255, 256</sup> and archaeology (e.g. Egyptian mummies <sup>235</sup>). UV-Vis can be used to follow melanin production by bacteria (e.g. *Alcaligenes eutrophus* <sup>179</sup>, *Pseudomonas sp.* <sup>228</sup>, *Rubrivivax benzoatilyticus* <sup>162</sup>, *Streptomyces cyaneofuscatus* <sup>212</sup>), and mushrooms (*Inonotus hispidus* <sup>213</sup>), which is potentially useful for the production of melanins via a white biotechnology approach <sup>174-178</sup>. The melanins produced by *Yarrowia lipolytica* yeast sequester heavy metal ions due to the presence of the metal chelating phenolics (L-tyrosine or L-DOPA) incorporated during its synthesis, enabling the subsequent generation of metallic nanostructures, of which, silver nanostructures were shown to displayed antifungal activity towards *Aspergillus sp.*, offering potential as antifungal additives in various materials <sup>231</sup>.

### 1.2.9 X-ray Photoelectron Spectroscopy (XPS)

XPS involves irradiating samples with X-rays and measuring the kinetic energy and number of electrons emitted, yielding spectra that offer insight into chemical composition (formula) and the chemical/electronic state of the elements <sup>108, 118</sup>. XPS has been applied for a variety of different melanins and reasons, showing the presence of eumelanin in cephalopod ink sacs from the Jurassic era (>160M years ago), highlighting the potential for fundamental science offering information to archaeological studies <sup>217</sup> and in combination with computational studies for technological applications <sup>195</sup>. XPS can be used to characterize and analyse the metal ion interactions with melanins, for

example metal binding by melanins produced by *Pseudomonas stutzeri*<sup>229</sup>, highlighting the potential of such natural melanins for environmental remediation and thereby both blue and grey biotechnologies. XPS has been used to study the discoloration of a model Rattan crop (*Daemonorops margaritae*) which is cultivated on a large scale in Southeast Asia, however, discoloration diminishes its economic value, and this was shown to be primarily due to the melanins produced by fungi that grow on the rattan (in this case by XPS analysis of rattan inoculated with *Lasiodiplodia theobromae*)<sup>230</sup>, which is important for green biotechnology supported economies.

#### **1.2.10 Scattering and Diffraction**

A variety of scattering and diffraction techniques enable elucidation of the crystallinity and microstructure of materials<sup>126-135</sup>, a few examples of which will be highlighted. Turbidimetry and nephelometry are routinely used to assess growth curves of bacteria/yeast which are of potential importance for the production of melanins via a white biotechnology approach<sup>257-261</sup>. Static light scattering (SLS) observes the average scattering intensity of a solution/suspension over a period of time, whereas dynamic light scattering (DLS) observes fluctuations of the scattered light over very short periods of time, offering insights into molecular weights of polymers and particle sizes (typically nanometer scale and upwards). Light scattering has been used to study synthetic melanins (e.g. polydopamine<sup>262, 263</sup>), naturally occurring melanins in bacteria (*Vibrio natriegens*<sup>211</sup>), yeast (*Cryptococcus neoformans*<sup>200</sup>), fungi (*Aspergillus oryzae*<sup>264</sup>), mushrooms (*Inonotus hispidus*<sup>213</sup>), cuttlefish (*Sepia officinalis*<sup>263</sup>), and can be used to study the health of eyes for patients with various conditions (e.g. for patients with pigmentary dispersion glaucoma<sup>265</sup>).

X-ray diffraction (XRD) studies enable elucidation of the crystallinity of materials (e.g. identification/quantitation of specific phases, and/or orientation) and is suited to well-ordered crystalline materials. Melanins tend to be non-crystalline amorphous solids due to the irregular nature of their monomer composition, consequently XRD patterns of melanins are typically broad peaks that can be relatively uninformative, exemplified by melanins produced by bacteria (e.g. *Bacillus safensis*<sup>266</sup>, *Klebsiella* sp. GSK<sup>267</sup>, *Rubrivivax benzoatilyticus* JA2<sup>162</sup>, *Pseudomonas stutzeri*<sup>268</sup>), yeast (*Cryptococcus neoformans*, *Aspergillus niger*, *Wangiella dermatitides* and *Coprinus comatus*<sup>269</sup>), frogs (*Rana esculenta* L<sup>270</sup>), cuttlefish (*Sepia officinalis*<sup>271</sup>), and humans<sup>272, 273</sup>.

X-ray scattering studies enable elucidation of the crystallinity of materials (e.g. identification/quantitation of specific phases, orientation of phases, and electron density) and is suited to non-/semi-crystalline materials. X-ray scattering studies are classified as either small angle X-ray scattering (SAXS) or wide angle X-ray scattering (WAXS) depending on the distance from the sample to the detector (for WAXS the sample to detector distance is shorter and therefore diffraction maxima at larger angles are observed)<sup>274</sup>. SAXS and WAXS offer insight into the assembly of the polymer chains in a variety of melanins, which is useful from a fundamental perspective with synthetic melanins, particularly when studying the melanin assembly process from individual chains to stacks of the chains (3.4 Å spacing), that assemble into 6- to 10-nm-sized melanin protomolecules (interacting via solvophobic and hydrogen bonding interactions)<sup>275-277</sup>; or indeed, the potential role of metal ions on the assembly process<sup>278</sup>. A combination of SAXS and WAXS (SWAXS) has also been used to interrogate composites incorporating melanin and synthetic polymers<sup>279</sup>, and SAXS has also been used to study natural composites (hair) revealing subtle differences in the hair of

humans without/with the pigmentation disorder Alopecia Areata, with notably smaller melanin particles in the hair of patients with Alopecia Areata<sup>280</sup>. Small angle neutron scattering (SANS) is complementary to SAXS because neutrons interact with atomic nuclei, whereas X-rays interact with electron clouds, consequently neutrons penetrate matter more deeply. SANS has been used to investigate synthetic melanins based on tyrosine and the potential role of metal ions on the melanin assembly process<sup>278</sup>, or DHI<sup>281</sup> and the potential role of biomolecules in the DHI-derived pigment assembly process (i.e. red biotechnology)<sup>282</sup>.

### **1.2.11 Thermal Characterization**

A variety of calorimetric methods exist for monitoring heat flow to study molecules in the solution and solid phase, thereby enabling elucidation of various processes<sup>136-140</sup>. Isothermal microcalorimetry of solutions/suspensions of melanins has been used to study synthetic melanin formation kinetics (e.g. tyrosine conversion to L-dopa then melanin catalyzed by tyrosinase<sup>283</sup>), and the interaction of melanins with biomolecules (e.g. DNA<sup>284</sup>) or metal ions<sup>285</sup>. Thermogravimetric analysis (TGA) and differential scanning calorimetry (DSC) are popular methods of analysing polymer-based materials in the solid state. TGA records differences in the mass of substances as a function of temperature or time (highlighting processes including phase transitions, absorption, desorption, chemisorptions, decomposition, etc.), whereas DSC examines how a sample's heat capacity (Cp) is changed by temperature (e.g. during transitions including melting, glass transitions, phase changes, etc.), and such data can be correlated with data obtained from scattering and diffraction experiments. The information obtained from TGA and DSC offers insight into polymer processability and stability in various environments which are important when incorporating them in materials for various

applications. TGA has been used to study melanins produced by bacteria (e.g. *Klebsiella* sp. GSK<sup>267</sup>), fungi<sup>286</sup>, garlic<sup>287</sup>, cuttlefish (*Sepia officinalis*<sup>287, 288</sup>), banana peel and bovine eyes<sup>289</sup>; and DSC has been used to study melanins produced by bacteria (e.g. *Pseudomonas* sp.<sup>290</sup>), fungi<sup>291</sup>, and cuttlefish (*Sepia officinalis*<sup>292</sup>). A study of healthy or alkaptanuric cartilage tissues used TGA and DSC to demonstrate that the total water content in healthy cartilage was higher than in AKU cartilage, that the percentage of freezable water was higher in AKU compared to healthy cartilage, and accordingly, non-freezable water was lower in AKU compared to the control; a significant difference was observed in the heat capacity of samples, with healthy tissue showing capacity value fivefold higher higher (owing to differences in water content after melanin binding in the diseased state) . Together, the data suggests that the presence of ochronosis affects the physicochemical, thermal and mechanical properties of the cartilage which will affect cartilage degradation (i.e. red biotechnology)<sup>293</sup>.

### **1.2.12 Electrical Characterization**

Electrical characterisation of melanins and materials containing melanins is useful in light of their potential applications<sup>141, 142</sup>. Studies of reduction/oxidation processes and electron transfer using cyclic voltammetry are particularly useful for melanins, with fundamental studies on melanins formed chemically from single monomers (e.g. L-DOPA<sup>294</sup>, dihydroxyindole (DHI)<sup>295</sup>, 3,4-dihydroxyphenylacetic acid<sup>296</sup>, HGA<sup>297, 298</sup>, 1,8-dihydroxynaphthalene<sup>226</sup>), combinations of DHI and 5,6-dihydroxyindole-2-carboxylic acid (DHICA)<sup>299-301</sup>, and natural melanins from bacteria (e.g. *Shewanella oneidensis* MR-1<sup>192</sup>, *Pseudomonas aeruginosa*<sup>302</sup>), plants (including fungi: basidial fungi<sup>303</sup>, *Cryptococcus neoformans*<sup>304</sup> and *Nigella sativa*<sup>305</sup>), cuttlefish (*Sepia*

*officinalis*<sup>300</sup>), and human hair-derived pheomelanins<sup>306</sup>. Electrochemical impedance spectroscopy and dielectric spectroscopy enabled the rational investigation of the protonic and electronic contributions, suggesting melanins are protonic conductors<sup>307-309</sup>, which is important because the electrical properties of melanins<sup>310-315</sup> underpin their potential technical and medical applications<sup>316-318</sup>, and it is noteworthy that the potential for melanins in electronics has seen an explosion of interest (see **Figure 1.5**).

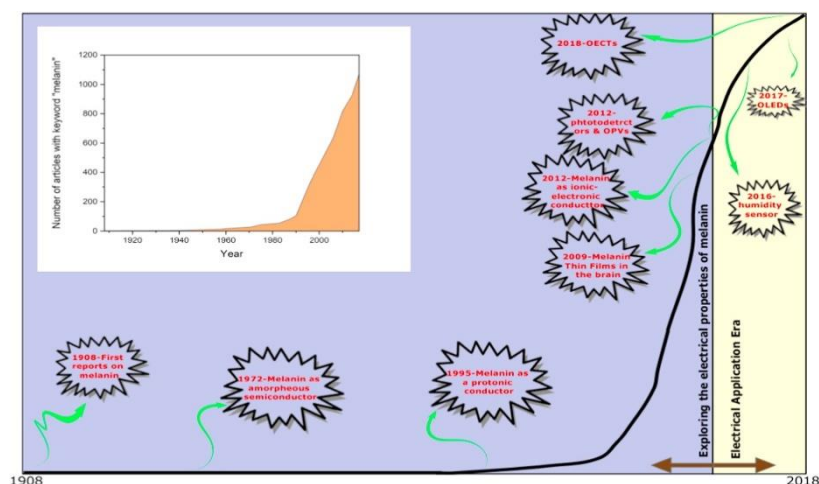


Figure 1.5: A brief timeline of melanin-based electronics research. The black line represents the number of publications with the keyword "melanin" and key milestones in melanin-based electronics research. Reproduced with permission<sup>319</sup>. Copyright 2018, Elsevier B. V

### 1.2.13 Visual and Microscopic Characterization

A variety of visual and microscopic techniques can be employed to study melanins and materials containing melanins<sup>143, 144</sup>. Photography offers a simple method of capturing evidence of color over a large scale (mm to km), consequently, photographs provide a useful initial starting point in studies of phenomena, including architectural coloration<sup>60</sup>, birds plumage<sup>320</sup>, and medical case reports of gross anatomical observations of the discoloration of tissues for patients with alkaptonuria or their production of darkly colored urine<sup>321-325</sup>. However, photographs do not normally differentiate the source of

coloration (pigmentation, reflection, scattering, transmission, and/or interference effects<sup>320, 326-328</sup>) motivating the application of high-resolution microscopy potentially combined with another analytical technique (e.g. scanning electron microscopy and energy dispersive X-ray spectroscopy). An exception to this utilises recent advances in digital camera technologies (potentially with smart phones) that enable hyperspectral imaging which facilitates characterisation of melanins<sup>329</sup>, and points towards some potentially very exciting developments in affordable personalised medicine that are aligned with the UN's sustainable development goals (specifically goal 3, good health and well-being, due to the prevalence of smart phones worldwide). Other techniques that also exploit the visible portion of the electromagnetic spectrum include reflectance colorimetry/spectrophotometry<sup>330-333</sup>, diffuse reflectance spectroscopy<sup>334</sup> and emission spectroscopy<sup>335, 336</sup>, where melanin concentration on skin can be quantified via colour systems such as RGB and CIELAB.

Histological studies of the microscopic anatomy of cells and tissues (of samples of *in vitro*, *ex vivo* and *in vivo* studies) can be obtained using various forms of microscopy (optical, electron, scanning probe, etc.). The use of microscopy and stains to enhance pigmentation to the naked eye is important as clinically, in connective tissue disorders such as AKU, by the time the deposition of melanin like polymers in tissues occurs and is visible to the naked eye the structural and biochemical integrity of the tissue is gone. Enhancing the pigmentation process through chemical reaction *in vitro*<sup>337, 338</sup> gives a greater indication of the origin of the pigmentation processes both intracellularly and extracellularly and represents the time at which most therapeutic interventions should be targeted. A variety of techniques have been applied to analyse samples *ex vivo* including: optical microscopy bone/cartilage of AKU patients<sup>339, 340</sup>; two photon

microscopy has been used to examine melanin from cuttlefish (*Sepia officinalis*<sup>341</sup>); two photon fluorescence TPF microscopy<sup>293</sup> has been used to study slices of healthy and unhealthy tissues (cartilage) of humans with alkaptonuria, observing differences in extracellular matrix density in cartilage with alkaptonuria compared with healthy cartilage; fluorescence microscopy has been used to investigate the autofluorescence properties of histologic sections of mouse eyes<sup>342</sup>; apertureless scanning near-field optical microscopy (capable of generating images with resolution better than the diffraction limit<sup>343</sup>) and confocal laser scanning microscopy data has been applied to analyse the distribution of melanins within zebrafish retinal tissues<sup>344</sup>.

Studies *in vivo* can employ optical coherence tomography (OCT) which uses low-coherence light to capture micrometer-resolution images within optical scattering media (and variations of OCT). It is possible to visualize melanin in skin<sup>345</sup> and the retinal pigment epithelium via photoacoustic tomography<sup>346-348</sup>, photothermal OCT<sup>349</sup>, or polarization sensitive OCT<sup>350-352</sup> if the concentration of melanin is sufficiently high, and an elegant study utilized hyperspectral OCT<sup>353</sup> for the visualization of tissues containing significantly lower concentrations of melanin<sup>354</sup>. It should be noted that optical methods including OCT are prone to scattering by different colorant, material compositions/structure thus leading to limited penetration depth (typically 100  $\mu\text{m}$  – 1 mm)<sup>355, 356</sup>. The optical properties of the skin can also be quantified macroscopically using spatial frequency domain spectroscopy (SFDS, which is based on diffuse optical spectroscopy) *in vivo*. In SFDS, tissues are illuminated with structured projections from a spatial light modulator, such as a digital micro-mirror device. By exploiting appropriate models of light propagation over visible to near-infrared wavelengths, tissue absorption and scattering coefficients and chromophore concentrations can be determined *in-vivo*<sup>357-359</sup>. Furthermore, by combining it with techniques such as

multiphoton microscopy, it is possible to obtain detailed microscopic structural information at the cellular spatial resolution thus allowing the upper dermis to be imaged. It can further provide quantitative information on the epidermis and dermis, extending the penetration depth up to ca. 5 mm<sup>357-359</sup>. Complementary computational studies of light-tissue interaction have been used to assess melanin concentration/distributions in various organisms/tissues<sup>360-367</sup> and potentially adverse effects of such irradiation<sup>368-371</sup>, offering insight into both fundamental and applied biomedical studies (i.e. red biotechnology).

#### **1.2.14 Scanning Electron Microscopy (SEM)**

SEM uses a beam of electrons to illuminate samples and creates images from measurements of electrons that are reflected or back scattered off the surface of the sample, enabling analysis of particle size distributions and elemental compositions when used in combination with energy dispersive X-ray spectroscopy (EDX/EDS)<sup>140, 145, 146</sup>. SEM and optionally EDX/EDS has been applied to study synthetic melanins<sup>29, 226</sup>, and melanins produced by a variety of species, including: bacteria (*Pseudomonas* sp.<sup>228</sup>, *Pseudomonas stutzeri*<sup>229</sup>, *Rubrivivax benzoatilyticus*<sup>162</sup>); yeast (*Yarrowia lipolytica*<sup>231</sup>); fungi (*Aspergillus fumigatus*<sup>372</sup>, *Inonotus hispidus*<sup>213</sup>, *Mycosphaerella fijiensis*<sup>44</sup>, *Armillaria cepistipes*<sup>286</sup>); cuttlefish (*Sepia officinalis*<sup>373</sup>); zebrafish<sup>374</sup>, melanosomes isolated from human hair<sup>280, 375</sup>) and from bovine/fish eyes<sup>376, 377</sup>; the cartilage of AKU patients<sup>293, 339-341</sup>, and neuromelanin in the substantia nigra of human brain tissue<sup>378</sup>; typically observing nanometer scale particles that have aggregated to form larger particles with sizes between tens to hundreds of micrometers.

SEMs equipped with EDX/EDS has been used to quantify the elemental composition of various melanins/materials including: C and S in fossils<sup>377</sup>; C, Ca, Cu and O in melanins produced by bacteria (e.g. *Pseudomonas sp.*<sup>228</sup>, *Myxococcus xanthus* and *Sinorhizobium meliloti*<sup>379</sup>); C, K, N, Na, O, S in melanins produced by various strains of fungi<sup>286</sup>; C, Ca, Cl, K, Mg, N, Na, O and S in melanins produced by cuttlefish (*Sepia officinalis*<sup>373</sup>); C, Cu, Fe, N, Na, O, S and Zn in melanins sourced from human hair<sup>280, 375, 380</sup>, and healthy/diseased tissues (including aortic valves, bones, brain and cartilage containing C, O, N, S, Na, and Ca<sup>378, 381-383</sup>).

### **1.2.15 Transmission Electron Microscopy (TEM)**

TEM uses a beam of electrons to illuminate samples and creates images from measurements of electrons that pass through very thin specimens (and contrast in images caused by differences in electron densities within different regions of the samples)<sup>140, 145, 146</sup>. TEM has been used to examine melanins and materials containing melanins from a variety of sources including: synthetic melanins (based on DHICA/DHI<sup>384</sup>, L-DOPA<sup>231</sup>, 1,8-dihydroxynaphthalene<sup>226</sup>); bacteria (*Pseudomonas maltophilia*<sup>284</sup>, *Pseudomonas stutzeri*<sup>229</sup>, *Vibrio natriegens*<sup>211</sup>), yeast (*Cryptococcus neoformans*<sup>200</sup>), fungi (*Aspergillus fumigatus*<sup>372</sup>, *Gaeumannomyces graminis var. graminis*<sup>385</sup>), human bone osteosarcoma cell lines *in vitro*<sup>337</sup> and human tissues *ex vivo* (e.g. aortic valves<sup>381</sup>, bone<sup>382, 386</sup>, cartilage<sup>203, 387</sup>); and TEM equipped with EDX/EDS has been used to quantify the elemental composition of Al, C, Ca, Cl, Cu, Fe, O, P, Si and Zn in human melanosomes in the eye *ex vivo*<sup>388</sup>.

### 1.2.16 Scanning Probe Microscopy (SPM)

SPM uses various probes to analyse the surface of samples enabling examination of a multitude of properties<sup>147, 148</sup>. The simplest form of SPM is contact profilometry that has been used to analyse the nanometer scale features of films of synthetic melanins (e.g. based on DHI<sup>389</sup> and other monomers<sup>390, 391</sup>). Scanning tunneling microscopy (STM) is a form of scanning probe microscopy<sup>392</sup> capable of generating high resolution images (down to the Å scale) based on quantum tunneling of electrons between the surface and the STM tip. STM has been employed to analyse synthetic melanins (e.g. based on tyrosine<sup>393-395</sup>, DHI<sup>311, 396, 397</sup>, DHICA<sup>310</sup>, DHI and DHICA<sup>312</sup>), and cuttlefish melanins (*Sepia officinalis*<sup>398, 399</sup>), often in combination with computational studies.

Atomic force microscopy (AFM)<sup>400</sup> is a form of scanning probe microscopy capable of generating high resolution images (down to the Å scale) using tips with various functionalities. AFM studies typically show melanin particle aggregates (ca. 100-200 nm) of smaller particles (ca. 1-10 nm) that either assemble into larger particles in natural samples, or are deposited as thin films on substrates for more applied studies. AFM has been used to analyse melanins from a variety of sources including: synthetic melanins (e.g. based on L-DOPA<sup>401-405</sup>, DHI<sup>224, 406</sup>, DHICA<sup>407</sup>, DHI and DHICA<sup>408</sup>, dihydroxynaphthalene (DHN<sup>409</sup>)); *Nigella sativa*<sup>305</sup>; fungi (*Aspergillus fumigatus*<sup>372</sup>); cuttlefish (*Sepia officinalis*<sup>398, 410, 411</sup>), various other cephalopods species (*Sepia esculenta*, *Sepia 30haraon*, *Sepia 30haraonic*, *Sepiella japonica*, *Euprymna berryi*, and *Uroteuthis (Photololigo) edulis*<sup>412</sup>); feathers of black fish crows (*Corvus ossifragus*) and iridescent wild turkeys (*Melleagris gallopavo*)<sup>411</sup>, black human hair<sup>411</sup>, human neuromelanin<sup>378</sup>, and human eye melanosomes<sup>219, 413</sup>. Such studies have also enabled

the elucidation of features such as the shape and size of melanosomes (e.g. in black hair are ellipsoidal eumelanosomes, whereas those in red hair are mainly spherical pheomelanosomes<sup>414</sup>), and the presence of cosmetic residues on the surface of hair<sup>415</sup>. Force-indentation measurements have revealed different mechanical properties of retinal pigment epithelium melanosomes isolated from human donors that may be related to the presence of thin deposits of lipofuscin on the surface of the melanosomes<sup>416</sup>, electrostatic force microscopy and conductive-AFM were used to spatially resolve the electrical properties of synthetic melanins (e.g. based on L-DOPA<sup>408,417</sup>), cuttlefish (*Sepia officinalis*<sup>399</sup>) and magnetic force microscopy has been used to examine the magnetic properties of melanin-Fe<sub>3</sub>O<sub>4</sub> nanoparticles<sup>397</sup>.

### **1.3 Mechanism of polymerization to form HGA**

It is worth noting that the mechanism of pyomelanin formation is similar to other melanins, with an enzymatically-controlled phase (the enzyme is commonly a phenolase, see also an excellent review of C-C bond formation by enzymatic oxidation from Guengerich and Yoshimoto<sup>418</sup> followed by a second phase where the oxidized intermediates polymerise in an uncontrolled fashion<sup>19,419</sup>. Homogentisic acid (HGA) is an Intermediary product in the metabolism of the amino acids, phenylalanine and tyrosine<sup>73</sup>. Deficiency of the enzyme homogentisic acid oxidase (HGO) due to an “inherited error of metabolism” has been found in Alkaptonuria patients from birth<sup>420</sup>. This situation leads to excess HGA<sup>73,420</sup> which is auto-oxidized to form pyomelanin (urine)<sup>73</sup> and polymerized (body)<sup>420,421</sup> forming a blackish coloured melanin-like pigment<sup>17</sup> of connective tissues such as cartilage, skin, and tendon. The distribution and affinity of HGA for such tissues, numerous chemical reactions and the formation of

intermediate metabolites are among the biochemical mechanism and reactions leading to pigmented polymer<sup>420</sup>. Alkaptonuria (AKU) has been linked with terms such as black bone disease and ochronosis (yellow colouration), implying a process with varied effects unlike normal pigmentation<sup>17</sup>. However, AKU pigment is still poorly studied, with over 40-year-old knowledge needing updating as pigmentation is considered as the basis for morbidity of the condition. Zannoni et al. (1969) implied that HGA polyphenol oxidase (HGAPO) contained in connective tissues can catalyze the oxidation and polymerization of HGA to “ochronotic-lik” pigment (**Figure 1.6**). This followed their earlier postulation of benzoquinoneacetic acid (BQA), a substrate of HGAPO as a probable intermediate in the biochemical pathway for the pigment formation.

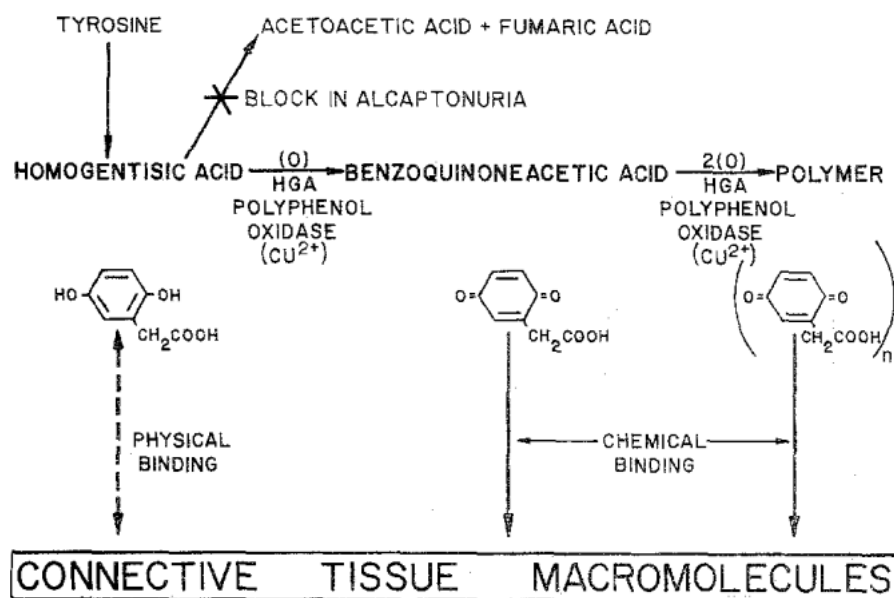


Figure 1.6: A postulated scheme for the formation of ochronotic pigment in alkaptonuria. (Reproduced with permission Copyright © 1969 Published by Elsevier B.V.)

Homogentisic acid is a phenolic acid and Ghoul and Chebil (2012) described oxidoreductive enzymes as having the ability to transform phenols into polymer products via oxidative coupling reactions by self-coupling or cross-coupling with other molecules. The authors further described a four-step oxidative polymerization of phenols as fundamentally a polycondensation reaction<sup>422</sup>. Many natural polymers including mammalian pigments result from oxidative coupling<sup>179</sup>. Such coupling reactions usually give a complex mix of products including dimers, oligomers and sometimes polymers<sup>179</sup>. The four steps are: the formation of phenoxy radicals; the phenoxy radicals forming dimers by recombination; a probable electron-transfer reaction leading to the formation of oligomer radicals; and the formation of higher molecular weight oligomers by recombination.

## **1.4 Conclusion**

As highlighted throughout the chapter, melanins are a class of biopolymers with diverse origins, chemical compositions and functions that are widespread in nature. Their abundance, chemical/electrical/optical/paramagnetic properties offer them significant potential for application in materials science and engineering for a multitude of technical and biomedical applications. This chapter offers an overview of the analytical techniques commonly used to study melanins from various sources including agriculture, fermentation, insects, marine sources, etc. which potentially involve a spectrum of biotechnologies (blue, brown, grey, green, white or yellow). The analytical techniques can be used in a variety of disciplinary contexts for multidisciplinary, interdisciplinary and transdisciplinary research and development, recognizing that

melanins have significant potential for use as sustainable resources for advanced biotechnological applications (e.g. red biotechnology, biomedical applications).

## **1.5 Aim and objectives**

Melanins are an important class of biopolymers that are widespread in nature and have diverse origins, chemical compositions and functions in nature. Their chemical, electrical, optical and paramagnetic properties make them interesting for application in materials science for a range of medical and technical applications. Alkaptonuria is a rare metabolic disorder that results in the accumulation of homogentisic acid (HGA) in the body which results in dark urine and/or blue/black discoloration of bodily tissues due to the formation of pyomelanin (a complex polymer mostly constituted of polymerised HGA).

The aim of this study to investigate pyomelanin formation/deposition using a variety of analytical techniques which may enhance our understanding of the deposition of pyomelanin in vivo.

Objective 1) Review the literature describing the application of analytical techniques to study melanins.

Objective 2) Analysis of the polymerisation of homogentisic acid (HGA) in vitro. Understand if the (bio)chemical environment (e.g., pH and enzymes) plays a role in the polymerisation of HGA, as this will play a role in where AKU deposits are formed in the body (e.g. answering the question “Is one enzyme better at polymerizing HGA?”, “Does pH affect the ability of the enzyme to polymerise the HGA?”) – see chapter 3.

Objective 3) Analysis of the polymerisation of similar phenols (catechol and levodopa) in vitro. Understand if the (bio)chemical environment (e.g., monomers available) plays a role in the structure of the melanins formed, and their properties – see chapter 4.

Objective 4) Analysis of the polymerisation of HGA in the presence of components of the extracellular matrix (ECM) in vitro. Understand if the (bio)chemical environment (e.g., ECM available – exemplified with chondroitin sulfate A and C) may play a role in the structure of the melanins formed, and their properties – see chapter 5.

Objective 5) Analysis of the polymerisation of HGA in the presence of cells in vitro. Understand if the (bio)chemical environment (e.g., cells, exemplified with a turkey tendon model) may play a role in the structure of the melanins formed, and their properties – see chapter 6.

# 2 Experimental Technique Chapter

## Overview

In this chapter, the techniques used to characterize the materials in Chapters 3, 4, 5 and 6 are discussed. The techniques applied to study the melanins in this study include IR, UV-VIS and NMR which are used to provide information about the molecular structure and properties of the materials analysed (vibrations of functional groups, electronic structure and organisation of atoms within the molecule, respectively). Scanning electron microscopy and energy dispersive X-ray spectroscopy (SEM/EDX) and transmission electron microscopy (TEM) were used to gain an insight into the morphology, particle size, form, and elemental composition of these materials. Electrochemical studies such as cyclic voltammetry, conductive probe atomic force microscopy (C-AFM) and scanning electrochemical microscopy (SECM) were employed to investigate reduction/oxidation processes and the conductivity of the materials.

## 2.1 Instrumental techniques for pyomelanin analysis

### 2.1.1 UV-Vis Spectroscopy

**Theory:** Ultraviolet-visible spectroscopy or ultraviolet-visible spectrophotometry (UV-Vis or UV/Vis) concerns the absorption spectroscopy or reflectance spectroscopy in a section of the ultraviolet (between 190-380 nm) and the whole, adjacent visible (between 380-750 nm) spectral regions. The technique measures the absorption of light

across these spectral wavelengths through a liquid containing a sample. Some molecules can absorb wavelengths of UV-Vis light, and the functional group is known as a chromophore. Generally, the higher the amount of UV-Vis chromophore detected, the higher the concentration of that compound. Ultraviolet and visible radiation interacts with matter which causes electronic transitions from the ground state to a higher energy state. In either absorption or reflectance mode, UV-Vis spectroscopy has been routinely employed in the study of melanin (e.g., assessing bond conjugation and connectivity)<sup>423</sup>. The absorption of spectra produced from samples at given wavelengths can be directly related to the sample concentration using the Beer Lambert law <sup>424</sup> which is the underlying principle of UV-Vis spectroscopy. A steady light source is necessary when using this method that can emit light over a range of wavelengths. Quartz sample holders are essential for UV investigation due to their transparency to most of UV light normal glass, plastics and solvent can act as a filter and absorb UV light <sup>425</sup>. There has been a significant increase in the number of publications reporting measurable tissue spectroscopy data in the UV-Vis wavelength range<sup>426</sup> as the method is commonly used for the measurement of chemical compounds <sup>427</sup>. UV-Vis is a cheap, easy, and non-destructive technique which allows sample recovery.

**Practice:** Spectra were recorded in UV Quartz cuvettes (Standard Cell with PTFE Stopper, manufactured in UV Quartz (195 nm to 2.5  $\mu\text{m}$ ); path length = 10 mm, inside width = 10 mm, volume = 3.5 mL); on an Agilent Technologies Cary 60 UV-vis supplied by Thermo Fisher Scientific in Heysham, UK.

### 2.1.2 Fourier-transform Infrared (FTIR) Spectroscopy

**Theory:** Fourier transform infrared (FTIR) spectroscopy employs a mathematical

process (Fourier transform) to interpret the raw data (interferogram) into the real spectrum<sup>428, 429</sup> which is recorded between 4000 and 400  $\text{cm}^{-1}$ <sup>430</sup>. The technique which has been accessible to researchers since the 1970s uses the complete source spectrum in contrast to the individual wavelengths produced by grating and/or prism systems employed in conventional IR spectroscopy<sup>431</sup>. Fourier transform infrared spectrometers offer accuracy, sensitivity, and speed, previously unattainable with wavelength dispersive spectrometers as the spectrum of a Fourier transform spectrometer can be produced in a shorter time than that given by a conventional spectrometer<sup>432</sup>. Generally, FTIR is used to examine the functional group present in the given compound<sup>433</sup>. The method comprises the absorption, emission, reflection, or photoacoustic spectrum attained by Fourier transform of an optical interferogram<sup>432</sup> and has been employed as the major technique for determining the infrared (IR) absorption and emission spectra of most materials<sup>434</sup>. The concurrent analysis of numerous frequency components in a single operation is the underlying strength of FTIR spectroscopy. The major benefits of the FTIR method and dispersive spectroscopy techniques is that nearly all compounds display distinctive absorption/emission, consequently, they can be analysed both qualitatively and quantitatively<sup>435</sup>. Variations in the distinctive pattern of absorption bands clearly show a modification in the material composition. The technique is useful in characterizing and identifying unknown materials, detecting contaminants in a material, discovering additives, and identifying decomposition and oxidation<sup>436</sup>. The conventional IR spectrometers are not very useful for far IR region from 20-400  $\text{cm}^{-1}$ <sup>432</sup> due to the weak sources and lower detector sensitivity<sup>432</sup>. Fourier transform infrared spectroscopy is a non-destructive and rapid method requiring minimum sample preparation.<sup>435</sup>

**Practice:** All spectra were recorded using an Agilent Technologies Cary 630 FTIR instrument (Agilent Technologies Ltd., Cheadle, UK) at a resolution of  $1\text{ cm}^{-1}$  and was an average of 16 scans.

### 2.1.3 Nuclear Magnetic Resonance (NMR) Spectroscopy

**Theory:** Nuclear magnetic resonance (NMR) spectroscopy is a non-destructive and non-invasive analytical chemistry method<sup>437</sup> employed in quality control and research for determining the molecular structure as well as the content and purity of a sample<sup>438</sup>. The technique “uses radiofrequency waves to reveal information about magnetic nuclei”<sup>439</sup>. The magnetic field generates an energy transfer from lower to higher energy levels which matches with a signal that is detected as the corresponding nucleus’s NMR spectrum<sup>440</sup>. Based on the accessibility of versatile measurement and analysis schemes and the detailed understanding of the underlying spin physics, the method has had an important impact on an extensive range of disciplines including condensed matter physics, medicine, most branches of chemistry, and structural biology over the past decades<sup>441</sup>. Nuclear magnetic resonance spectroscopy can quantitatively determine molecular parameters such as atomic ratios, chemical shifts, coupling constants, and spin multiplicity that can be used to elucidate the structure of known compounds, as well as an unknown structure<sup>442</sup>. Bothwell and Griffin<sup>439</sup> reported that NMR varies from other methods of spectroscopy in three significant ways: first, the technique considers how the nuclei of a precise, user-chosen, chemical element are spread amongst the molecules of a sample, giving NMR a wider range of targets than most other spectroscopic methods; second, the signals generated by NMR are sensitive to the local environment of the nuclei under scrutiny, providing a means for probing the chemical and physical surrounding of an atom and which can reveal more information

about a given sample than most spectroscopic methods; third, NMR is less damaging and more highly penetrating than other forms of spectroscopy.

**Practice:**  $^1\text{H}$  NMR (400 MHz) spectra were recorded using a Bruker AVANCE III 400 NMR spectrometer using residual solvent as internal standards in deuterated solvents ( $\text{D}_2\text{O}$ )<sup>443</sup>. Chemical shift ( $\delta$ ) values were recorded in parts per million (ppm)<sup>444</sup>.

#### 2.1.4 Solid State NMR (ssNMR)

**Theory:** Solid state nuclear magnetic resonance (ssNMR) spectroscopy is a vital analytical tool which is employed to determine the chemical composition, dynamic properties, and local structure of solids<sup>445, 446</sup> and semi-solids<sup>446</sup>. It is an atomic-level method<sup>446</sup> as well as a very specialized area of spectroscopy<sup>447</sup> employed in biology, chemistry, materials science and physics to examine numerous material systems including biomolecules, glasses as well as other amorphous and disordered solids, organic and inorganic crystals, and polymers, impacting research<sup>152</sup>. It is a powerful probe of the molecular-level electronic, geometric, and magnetic setting around a target nucleus<sup>448</sup>, needing the employment of special methods to overcome basic issues in the analysis of solid samples<sup>447, 449</sup>. The oscillatory response of nuclei having non-zero spins in a magnetic field to resonant excitation by radiofrequency (RF) irradiation defines NMR<sup>446</sup>. The Zeeman interaction between such external magnetic fields and the nuclear spins is the fundamental principle of ssNMR, thus enabling the detection of most of the periodic table elements as they have at least one isotope with non-zero nuclear spin<sup>450</sup>. Cross polarisation (CP) and magic-angle spinning (MAS) are employed to decrease or remove the line broadening observed in ssNMR to enable the attainment

of high-resolution NMR spectra from solid state samples <sup>447</sup>. The major disadvantages of ssNMR are its complexity (often with experimental methods and data analysis), long experimental times, and high cost <sup>451</sup>. In addition, a strong user expertise is needed as the technique is non-routine, and the experimental protocol and data analysis to be used often have to be developed on a case-by-case basis <sup>451</sup>. Regardless, ssNMR is a very flexible and non-destructive method, allowing the attainment of dynamic and structural data on wide space and time ranges <sup>451</sup>. The technique also has the possibility to examine complex heterogeneous systems at the maximum probable resolution in a comprehensive way <sup>452</sup>. However, it lacks resolution compared to solution NMR <sup>453</sup>.

**Practice:** A Bruker AVANCE III HD 700 WB was used to record <sup>13</sup>C NMR spectra via crosspolarization/magic angle spinning. Chemical shift ( $\delta$ ) values were recorded in parts per million (ppm).

### 2.1.5 X-ray Photoelectron Spectroscopy (XPS)

**Theory:** X-ray photoelectron spectroscopy (XPS) or electron spectroscopy is the study of the distribution of energy of the electrons released from X-ray illuminated compounds <sup>454</sup>. The kinetic energy of emitted electrons is determined when x-rays bombard the material surface <sup>455</sup>. Generally, XPS probes to a depth of 10 nm, but the sample must be evacuated prior to analysis <sup>456</sup> due to the technique being carried out usually under ultra-high vacuum which may not reflect the real condition of elements <sup>457</sup>. X-ray photoelectron spectroscopy is generally used to examine the chemical composition at the surfaces of solids in analytical laboratories <sup>458</sup>. By determining the binding energies of the core electrons of molecular systems, XPS has also been used

successfully to study the structure of molecules<sup>423, 459</sup>. The capacity of the method to assign chemical states to the detected atoms upon exploration of the first few atomic layers has shown XPS to be a powerful tool for chemical analysis. Quantification using the technique is based on Einstein's assumption based on the photoelectric effect in 1905 that the energy needed to remove the electron from the material was subtracted from the energy of the incident photon to give the kinetic energy of the ejected electron<sup>460</sup>. All electrons including those at the core and the valence levels can be examined in principle and in this regard, XPS is different from ultraviolet photoelectron spectroscopy in which only the valence electrons can be investigated<sup>454</sup>. The two main features of this method that makes it powerful as an analytical technique are its capacity to reveal information on the chemical state from the elements in the sample and its surface sensitivity<sup>455</sup>. Excluding helium and hydrogen, all elements can be detected.

**Practice:** A Kratos Analytical Axis Supra X-ray photoelectron spectrometer with a monochromatic Al K $\alpha$  source (1.487 keV) was used to analyse surface chemical composition.<sup>461, 462</sup> Powdered samples were mounted using carbon tape in a well-shaped holder. An internal flood gun was applied for neutralizing charging effects. Wide-scan and core-line spectra were recorded at pass energies of 160 and 20 eV and step sizes of 1 and 0.1 eV, respectively. Samples were measured in triplicate at an emission angle of 0° (relative to the surface normal), a power of 225 W (15 kV  $\times$  15 mA), and an analysis area of 700  $\times$  300  $\mu$ m. Data were quantified and processed by CasaXPS (ver.2.3.23PR 1.0, Casa Software Ltd.) using linear baseline correction. All spectra were adjusted for charge compensation effects by offsetting the binding energy relative to the C-C component of the C 1s spectrum at 285.0 eV.

### 2.1.6 Size Exclusion Chromatography (SEC)

**Theory:** Size exclusion chromatography (SEC) is a separation method controlled by entropy in which molecules are separated based on size or hydrodynamic molecular volume <sup>463</sup>. The technique comprises gel filtration chromatography (GFC) or gel filtration which is the chromatographic separation of biological macromolecules (biopolymers) with the employment of firm inorganic packing particles or porous gels, while gel permeation chromatography (GPC) is an analogous procedure of separation for synthetic macromolecules <sup>464</sup>. Generally, SEC is a liquid column chromatographic technique in which a sample solution is passed through a column filled with porous packing and is moved along the column by aqueous solvent if GFC or organic solvent if GPC <sup>465</sup>. With suitable column calibration or using molecular-weight-sensitive detectors like mass spectrometry, or light scattering, the averages of the statistical molecular weight, and the molecular weight distribution can be readily attained <sup>463</sup>. Thus, SEC is the foremost efficient, and fastest method for determining these characteristics of biopolymers and synthetic polymers <sup>466</sup>. The separation of ions and small molecules from large molecules, obtaining natural allergens as well as the determination of the molecular masses and/or molecular mass distributions and sizes for macromolecules of natural and synthetic origins are included amongst the major functions of SEC <sup>467</sup>. Size separation is preferably attained by differential pore permeation. The pore volume, which is effectively accessible, is less for a large molecule than for a small one, thus rendering larger molecules to be eluted from the column earlier with cognizance of their shorter retention times in the pores of the packing than smaller ones <sup>464</sup>. Size exclusion chromatography technique is easy to operate, fast and relatively cheap <sup>468</sup>. However, its major limitation is that it is poorly reproducible regarding molar mass analysis because of challenges in obtaining a pure

size-exclusion separation for numerous reasons such as concentration effects, preferential interactions, and secondary exclusion <sup>466</sup>.

**Practice:** Aqueous SEC was measured on a Jasco system equipped with a DG-2080-53 degasser, PU-980 pump, and an RI-2031 Plus refractive index detector (Jasco Deutschland Labor-und Datentechnik GmbH, Groß-Umstadt, Germany) with 0.1 m Na<sub>2</sub>HPO<sub>4</sub>/0.05% NaN<sub>3</sub> pH 9 as an eluent and at a flow rate of 1 mL min<sup>-1</sup> on a column set of PSS SUPREMA 1000 and 30 Å (10 µm) at 30 °C (PSS, Mainz, Germany). Polyethyleneoxide (PEO) was used for calibration.

### 2.1.7 Dynamic Light Scattering (DLS)

**Theory:** Measurement of light scattering from matter is a useful method with applications in various scientific disciplines where, depending on the detector and source of light, certain properties of molecules can be investigated <sup>469</sup>. Dynamic light scattering (DLS), otherwise referred to as photon correlation spectroscopy (PCS) or quasi-elastic light scattering, is a very powerful method for examining a wide range of phenomena including the dynamic conduct of fluids near critical points, laminar flows <sup>470</sup>, and the diffusion characteristics of macromolecules in solution <sup>469</sup>. The diffusion coefficient and the hydrodynamic radii determined from it depend on the shape and size of macromolecules. The technique determines the time-dependent fluctuations in the scattering intensity resulting from particles undergoing random Brownian motion <sup>471</sup>. There exists a correlation between the Brownian motion of particles and their hydrodynamic diameter <sup>466</sup> as such motion of macromolecules is dependent on their size, temperature, and solvent viscosity. Thus, information on the precise temperature

is vital for DLS determinations since the solvent viscosity is dependent on the temperature<sup>469</sup>. DLS measurements employ a helium–neon laser as a light source using scattering right angle of 90 degrees or back angle of 173 degrees as the detector position to incident light<sup>472</sup>. Data obtained by DLS are generally confirmed by another size characterisation method such as transmission electron microscopy (TEM), where you would expect to observe differences in sample sizes because DLS samples are solvated whereas TEM samples are analysed under vacuum<sup>472</sup>. DLS is a fast, non-invasive, and sensitive technique which can be used under an extensive variety of solvent conditions<sup>473</sup>.

**Practice:** DLS measurements were performed using an ALV laser CGS3 Goniometer equipped with a 633 nm HeNe laser (ALV GmbH, Langen, Germany) at 25 °C and at a detection angle of 90°. The CONTIN analysis of the obtained correlation functions was performed using the ALV 7002 FAST Correlator Software.

### **2.1.8 Scanning Electron Microscopy (SEM)**

**Theory:** Scanning electron microscopy (SEM) is a broadly used and versatile surface analytical method<sup>474</sup> as it enables the investigation of the chemical composition, crystal structure, electrical behaviour (surface charging), and surface topography of approximately the top 1 µm of numerous materials in modern science due to its better resolution, ease of sample observation, greater depth of focus, and higher magnification over optical microscopy<sup>475</sup>. Sample preparation time is very short using SEM method compared to transmission electron microscopy<sup>475</sup> and its analysis is quite easy as most samples only need to be conductive<sup>476</sup>. However, a gold coating is essential for characterizing non-conductive biomolecules due to the absence of enough signals for

clear imaging<sup>433</sup>. A beam of electrons is aimed onto the specimen which interacts with the atoms of the sample to release low-energy secondary electrons from the surface which are important for imaging and thus the morphology of the sample with the SEM approach<sup>477</sup>. Scanning electron microscopy is a cheap, easy to use, non-destructive, and rapid approach to surface analysis, and is applied extensively in various fields including biology, chemistry, and geology<sup>474</sup>.

**Practice:** Prior to imaging, the samples were sputter-coated with a 10 nm layer of gold. The structures were observed using either a JEOL JSM-6390L V operating at 15 kV or a JEOL JSM 7800F scanning electron microscope (JEOL, Welwyn Garden City, UK) operating at 10–15 kV.

### **2.1.9 Energy Dispersive X-ray (EDX) Spectroscopy**

**Theory:** Energy dispersive X-ray spectroscopy (EDX), also known as energy-dispersive X-ray analysis or energy-dispersive X-ray microanalysis<sup>478</sup> is a standard method suitable for characterizing and quantifying elemental compositions in a material<sup>479</sup>. Together with electron energy-loss spectroscopy (EELS), which determines the kinetic energy variation of incident electrons after inelastic interactions with a sample, EDX which detects the signature X-ray signals produced in a sample constitute the two major spectroscopic methods of analytical electron microscopy (AEM)<sup>480</sup>. Both EDX and EELS have the capacity for elemental identification of elements comprising atoms with prominent spectral structures<sup>481</sup>. The EDX analysis can be employed to measure the elemental composition of separate points or to map out the lateral dispersion of elements from the imaged region<sup>482</sup>. Thus, EDX can be employed for qualitative analysis as

described and quantitative analysis in which the relative abundance of the identified elements are evaluated <sup>483</sup>. In quantitative analysis, a specific element's concentration in a sample is determined by the peak intensities. By determining the energies of the emitted X-rays from the area being excited by an electron beam in qualitative analysis, the elements contained in the sample can be determined <sup>484</sup> as the energies and intensities are correlated to the atomic number of the emitting element <sup>485</sup>. Energy dispersive x-ray spectroscopy is a non-destructive and relatively simple method <sup>485</sup> usually employed as a hyphenated system with transmission electron microscopy (TEM), scanning electron microscopy (SEM) or scanning transmission electron microscopy (STEM) <sup>482</sup>.

**Practice:** For qualitative EDX analysis, the samples were sputter-coated with a layer of gold (60 s, 20 mA,  $8 \times 10^{-2}$  mBar,  $\approx 5$  nm) using a Quorum Q150RES sputter coater (Quorum Technologies Ltd.) and then investigated using a field-emission SEM JEOL JSM 7800F with an EDX system (X-Max50, Oxford Instruments, Abingdon, UK) at 10 mm working distance and 10 kV voltage mounted on a brass JEOL holder with 25 mm carbon tables (G3348N, Agar Scientific, Stansted, UK). Three measurements were performed per sample and average results were presented.

#### **2.1.10 Transmission Electron Microscopy (TEM)**

**Theory:** Transmission electron microscopy (TEM) is a quantitative technique used to determine the distribution, shape, and size of a sample <sup>486</sup>. The method has developed as a foundation of characterisation in chemistry, materials science, medicine, and physics since its inception about 100 years ago <sup>487</sup>. Although it functions on a different principle than scanning electronic microscopy (SEM), it can give similar information

<sup>488</sup> as for example, TEM can also be used for a greater resolution (0.0001  $\mu\text{m}$ ), approximately one to two orders of magnitude higher than SEM <sup>489</sup>. Transmission electron microscopy can be operated at diverse electron energies like 100 keV which is frequently used for conventional TEM and 1 MeV for high-resolution imaging <sup>490</sup>. Thus, the method, with its analytical capabilities and numerous imaging modes serves as an essential tool for chemical and structural characterisation even at the nanoscale for all sample types <sup>491</sup>. Limitations of conventional TEM techniques include complex and time-consuming sample preparation process, inability to visualize living specimens, presenting two-dimensional images <sup>492</sup>, and a need for high vacuum <sup>486</sup>.

**Practice:** For TEM analysis copper grids were rendered hydrophilic by Ar plasma cleaning for 30 s (Diener Electronics). 10  $\mu\text{L}$  of the respective sample solution were applied to the grid and excess sample was blotted with a filter paper. TEM images were acquired with a 200 kV FEI Tecnai G2 20 equipped with a 4k x 4k Eagle HS CCD and a 1k x 1k Olympus MegaView camera for overview images.

### **2.1.11 Electron Paramagnetic Resonance (EPR) Spectroscopy**

**Theory:** Electron paramagnetic resonance (EPR) spectroscopy, otherwise known as electron spin resonance (ESR), and infrequently electron magnetic resonance (EMR) is used for the detection of paramagnetic species which includes any atom, complex, or molecule having at least one unpaired electron <sup>493</sup>. The fundamental concepts of the method are like those of nuclear magnetic resonance (NMR) spectroscopy, but it is the electron spins and not those of the atomic nuclei that are excited <sup>494</sup>. However, NMR is less sensitive and restricted to the radio frequency range with its experiments carried

out at higher temperature <sup>494</sup>, and generally for diamagnetic species <sup>495</sup>. The technique is based on the resonant absorption of microwave radiation by paramagnetic species when positioned in a strong magnetic field <sup>496</sup>. With cognizance that an electron can occur in two spin states of unequal energies in the presence of a magnetic field, shifts between these states can be induced by the absorption of electromagnetic radiation having equal energy to their energy variance, which can be found in the microwave region of the electromagnetic spectrum <sup>497</sup>. The technique allows the examination of species even in micromolar or lower concentrations due its high sensitivity <sup>498</sup> and can also characterize structural features within 0.5 to 5 nm range in systems deficient of long-range order <sup>499</sup>. Thus, EPR offers good structural contrast even in complex materials. The method is precise, non-destructive, non-invasive, and very sensitive analytical method <sup>500</sup> which is frequently limited by instrument availability <sup>501</sup>.

**Practice:** Room-temperature EPR spectra of polyHGA powders were recorded at X-band on a JEOL X320 spectrometer using 0.1 mW microwave power and 1 G modulation width (100 kHz modulation frequency). The *g* values were determined by using a Mn<sup>2+</sup> marker.

### 2.1.12 Cyclic Voltammetry (CV)

**Theory:** Cyclic voltammetry (CV) is widely employed in electroanalytical chemistry to measure redox properties of molecules in solution <sup>502</sup>. Even though the approach is one of the more complex electrochemical methods, CV is very regularly used due to its provision of a wealth of experimental data and insights into both the kinetic and thermodynamic specifics of numerous chemical systems <sup>503</sup>. The kinetic details which are usually offered in combination with simulation software will normally include varying the scan rate and other settings as well as studying how distinctive features such

as the peak currents and peak potentials alter because of these variations<sup>504</sup>. Analytical measurement with CV is usually carried out in an electrochemical cell comprising a working electrode, counter electrode, and reference electrode with a liquid solution or solid membrane as the electrolyte in the cell<sup>505</sup>. The potential of the working electrode in the system being investigated is determined with respect to the reference electrode, while the potential is scanned back and forth between predefined lower and upper limits, and the current passing between the working electrode and the counter electrode being recorded at the same time<sup>506</sup>. The downward peak indicates the reduction of the active species in the solution, and the upward peak indicates the species' oxidation<sup>506</sup>. The resulting voltammogram of the CV approach relays data as a function of an energy scan just like with the conventional spectrum<sup>507</sup>, with the information provided being plotted as current (A) versus potential (V)<sup>508</sup> or current (A) (vertical axis) versus potential (V) or time (s) as the potential varies linearly with time<sup>507</sup>. The potential variation is known as the scan rate or sweep rate (v), while the range of the working potential is referred to as the operating potential or potential window<sup>508</sup>.

**Practice:** Voltammetry was carried out using an EmStat 3+ potentiostat with PSTrace 4.7 software (PalmSens Houten, Netherlands) at ambient temperature. The cell was comprised of a three-electrode system with an Ag/AgCl reference electrode, a gold counter electrode, and a glassy carbon working electrode (GCE). The GCE was coated with a film prepared by drying 10  $\mu$ L of a suspension of polyHGA (1 mg) in Nafion perfluorinated resin solution (10  $\mu$ L of a 5 wt% mixture of lower aliphatic alcohols and water, containing 45% water; from Sigma-Aldrich, Gillingham, UK) overnight in a fume hood at room temperature. Buffer (pH 5 or 7.4, described above) was used as the

electrolyte, with a scan rate of  $0.01 \text{ V s}^{-1}$  between  $-1$  and  $1 \text{ V}$ .

### **2.1.13 Conductive-probe atomic force microscopy (C-AFM)**

**Theory:** Conductive atomic force microscopy (C-AFM) is included amongst the scanning probe microscopy (SPM) techniques and has been extensively employed to examine the local electromagnetic, molecular, or physical features on a microscopic scale <sup>509</sup>. The CP-AFM setup needs a well-characterized conductive tip <sup>510</sup> to enable its secondary imaging mode that can produce high spatial resolution imaging <sup>509</sup> and to allow the determination of electronic structures at the nanometer level as a result of the accuracy and stability of making an electronic contact using the tip <sup>511</sup>. Current flows through the conducting material-coated tip and the conducting sample when the tip-surface is positioned at voltage difference which thus enables the device to employ electrical current to construct the surface outline of the sample <sup>512</sup>. By determining and recording current between the conductive tip and the substrate in contact mode, the technique can probe the electronic characteristics of samples and map the current in a wide range from  $1 \text{ pA}$  to  $10 \text{ mA}$  with immediate collection of topographic data <sup>509</sup>. Multiple fields including chemical, electric, force, and optical fields can be combined with C-AFM method to show the local multifield coupling phenomenon <sup>509</sup>. Conductive atomic force microscopy technique assures accurate, non-destructive, and quick analysis <sup>509</sup>.

**Practice:** A triangular bias voltage was applied on the AFM stage in electric contact with the samples. A Pt-coated AFM probe acted as a drain for the electric current. The electric signal collected by the conductive probe was fed into an  $I/V$  converter with a low-noise filter built in. Output current and bias voltage were recorded by an AFM

controller in real time. Multiple  $I$ - $V$  traces were recorded and processed to extract the electrical conductance, which is an intrinsic property of the samples under investigation. The setup is depicted in **(Figure A.1.30 Appendices)**.

#### **2.1.14 X-ray diffraction (XRD)**

**Theory:** X-ray diffraction (XRD, elastic scattering) spectroscopy is an X-ray scattering technique which has been extensively used for determining the chemical composition, crystal structure, and electronic structure of materials <sup>513</sup>. Although the method is a bulk-sensitive analytical technique, it can be employed to offer data that are relevant to surface variations in appropriate circumstances <sup>514</sup> and is normally employed for long-range order crystalline material <sup>472</sup>. The working principle of XRD is based on the reflection of parallel X-ray beam incidence on a crystal plane of the sample that is to be characterized <sup>472</sup>. The rays are diffracted in a pattern that is determined by the arrangement, location, and size of the crystal constituents <sup>515</sup>. This pattern is a basic physical property of the material which completely elucidates and identifies its structure <sup>516</sup>. The output from the XRD instrument is usually called a diffractogram which is a plot of intensity of scattered rays on the y-axis versus a function of the scanning angle on the x-axis <sup>517</sup>. X-ray diffraction is a non-destructive technique <sup>518</sup> but can be time-consuming, may need a large sample size and has a low intensity of diffracted X-rays especially for low atomic number material <sup>472</sup>.

**Practice:** XRD patterns were recorded using a Rigaku SmartLab powder diffractometer with a  $2\theta$  scattering range of 10 to 90° and a resolution of 0.1°.

### 2.1.15 Scanning electrochemical microscopy (SECM)

**Theory:** Scanning electrochemical microscopy (SECM) is a method in which the current that flows via an ultramicroelectrode (UME) tip of 10  $\mu\text{m}$  diameter or less near a conductive, semiconductive, or insulating substrate dipped in solution is employed to characterize processes and structural features at the substrate<sup>519</sup> as the tip is moved on or close to the surface<sup>520</sup>. The technique can probe the transfers of electrons, ions, or molecules, as well as other reactions at air-liquid, liquid-liquid, and liquid-solid interfaces<sup>521</sup>. Scanning electrochemical microscopy generates chemical and topographic data in the z direction for probed surfaces, or in the x-y directions for surface imaging<sup>522</sup> which is based on the interaction of the substrate with a species electro-produced at the tip<sup>520</sup>. Detection of the variations in tip position or some other tip variable allows for images formation with the method as the tip is moved on or near to a surface<sup>520</sup>. In SECM, the tip and the substrate are constituents of an electrochemical cell which also comprise auxiliary and reference electrodes<sup>519, 520</sup>. The substrate may also function as the second working electrode<sup>521</sup>. Scanning electrochemical microscopy has been employed in biological systems to examine enzyme activity and for the assessment of the electrocatalytic activities of various materials including oxygen-reduction reactions<sup>523</sup>. An extensive variety of experimental systems and substrates can be characterized with the application of a range of operational modes<sup>524</sup> including the cyclic voltametric, feedback<sup>519</sup>, generation/collection, potentiometric, and redox competition (or shielding) modes<sup>521</sup>. Normalisation of SECM data enables the comparison between measurements carried out using diverse probe dimensions<sup>524</sup>. The SECM technique comprises a “feedback” procedure as a vital feature<sup>520</sup>. The direction of the current feedback shows the form of the substrate surface as electrically

conducting or insulating, while the signal magnitude provides an insight into the distance of the tip from the substrate, or otherwise, an insight into the species turnover rate at the substrate<sup>520</sup>. The accurate positioning abilities allows for the high spatial<sup>521</sup> and temporal resolution of SECM when quantifying material flux from a surface<sup>524</sup>. This serves as a major strength of the technique over other electrochemical methods using UMEs<sup>521</sup> leading to its application in a variety of fields<sup>524</sup>. Available resolution with SECM is limited by the curvature of the tip and its distance from the substrate<sup>520</sup>.

**Practice:** Scanning electrochemical microscopy (SECM) measurements were carried out using a custom build SECM setup. A CH Instruments potentiostat (Model#6059) was used for controlling the DC potential and recording the current, while a NanoMax 3-axis positioning system equipped with closed-loop piezo stepper motors controlled by a BSC-203 motion controller (Thorlabs) was employed for sample positioning. SECM imaging was performed in feedback mode using ferrocenemethanol (FcMeOH), as redox mediator, in a two-electrode configuration with the potential biased between a 7  $\mu\text{m}$  diameter carbon fiber ultramicroelectrode (UME) biased to oxidize FcMeOH versus a Ag wire counter/quasi-reference electrode. A constant UME tip height of 1  $\mu\text{m}$  was maintained throughout as confirmed via probe approach curves (data not shown). UME fabrication has been described previously

#### **2.1.16 Zeta potential**

**Theory:** The zeta ( $\zeta$ ) potential or electrokinetic potential is the electrostatic potential at the electrokinetic slip plane randomly separating the liquid medium in an immobile layer at the solid surface from most of the solution<sup>525</sup> and is also the reflection of the

surface charges <sup>526</sup>. This potential which also signifies a feature of the electrical properties of the gaseous/liquid interface <sup>527</sup>, is a basic parameter in models of electrical double layers and their related characteristics such as electrode capacitance and electroosmosis <sup>528</sup>. Zeta potential is an excellent indicator of the degree of the electrostatic repulsive interaction between particles and is generally employed to envisage and control dispersion stability <sup>529</sup>. Numerous techniques identified for measuring  $\zeta$ -potential include colloid vibration potential, electroacoustic sonic amplitude, electro-osmosis, electrophoresis, sedimentation potential, and streaming potential <sup>530</sup>. The most applicable of the techniques are the electrophoretic determinations which are quick <sup>530</sup>, give dependable results <sup>531</sup>, and allow calculations of the  $\zeta$ -potential from the dispersed particles' mobility, as well as the streaming potential measurements, which enable the  $\zeta$ -potential to be obtained from the pressure dependency of the potential difference between two sides of a porous plug <sup>525</sup>. In the simplest terms,  $\zeta$ -potential is directly proportional to the electrophoretic mobility <sup>529</sup>, and its extent is a pointer to the dispersion stability against aggregation <sup>532</sup> which occur because of existing van der Waals attractive forces <sup>533</sup>. Although determinations with the  $\zeta$ -potential method are easy, simple, and reproducible, there exists an insufficient grasp of the operating principles, data interpretation, and sample preparation <sup>534</sup> which constitute the various issues that pose difficulty in constantly determining and integrating the potential <sup>532</sup>. Zeta potential is pH dependent, thus, the sample pH should be determined before and after  $\zeta$ -potential readings <sup>535</sup> which are recorded in millivolts (mV) <sup>536</sup>. The concentration of any additives, ionic strength, and temperature affect the zeta potential <sup>537</sup>. Therefore, the  $\zeta$ -potential value should be given with its standard deviation and the number of runs as well as the composition of the dispersion medium, pH, sample concentration, and the temperature of the measurement as a minimum <sup>535</sup>.

Additional data which should be provided include the dielectric constant, dispersing medium viscosity, Henry function estimation used, instrument make and model, type of zeta cell employed, and the voltage applied<sup>535</sup>. Zeta-potential values over  $\pm 30$  mV are taken as discreetly stable against aggregation because of charge stabilisation<sup>533</sup>, while values in the range of  $-10 < 0 < 10$  mV are considered as neutral<sup>535</sup>. Zeta potential is applicable in numerous scientific fields including agriculture, chemistry, chemical engineering, medicine, materials science, and pharmaceuticals<sup>536</sup>. Although zeta potential determinations regularly need large samples, it is a non-destructive technique, and the sample can be recovered after the analysis<sup>538</sup>.

**Practice:** Zeta-potentials were measured on a ZetaSizer Nano ZS from (Malvern Instruments, Malvern, UK) *via* M3-PALS technique with a laser beam at 633 nm. The detection angle was 13°. All measurements were performed in three consecutive runs and the values obtained averaged

# **3 The Polymerisation of Homogentisic Acid In Vitro as a Model for Pyomelanin Formation**

## **Overview**

Melanins are a class of biopolymers that are widespread in nature, with diverse origins, compositions, and functions, and their chemical and optoelectronic properties render them potentially useful for application in materials science for various biotechnological applications. For patients with alkaptonuria, the accumulation of homogentisic acid (HGA) in their bodies is associated with the concomitant deposition of pyomelanin, which is a pigment that contains significant amounts of polymerised HGA (polyHGA) in the bodily tissues of the patients. The polymerisation of HGA under various different conditions in vitro is investigated using a selection of different analytical chemistry techniques to understand if there may be a correlation between the conditions and pigment deposition in vivo, and their potential for application as green/sustainable and components of electronic devices.

### 3.1 Introduction

Melanins are a class of biopolymers with diverse origins, compositions, and colors, from black /brown eumelanins<sup>539</sup> to red/yellow pheomelanins,<sup>18, 19</sup> all of which are present in the skin/hair.<sup>20</sup> Melanins fulfill a variety of roles in nature (including photoprotection to photosensitisation,<sup>20, 22</sup> antioxidant defense and metal/drug binding),<sup>23, 26</sup> which reflect their combination of chemical, electrical, optical and paramagnetic properties.<sup>27, 540</sup> Such properties facilitate their application in materials science for a range of medical and technical applications.<sup>32, 540</sup>

Melanin production is an oxidative process involving reactive oxygen species and enzymes followed by uncontrolled polymerisation of the oxidized intermediates.<sup>19</sup> In contrast to the production of polynucleic acids (e.g., DNA and RNA) and proteins, melanin production does not involve “templates” and, therefore, the compositions, connectivity, and sequences of “monomers” in the backbone of the melanins are random (albeit clearly influenced by the feedstocks available, organism/tissue, and other conditions). Various melanins exist, each of which is rich in certain monomers: eumelanins (L-dopa),<sup>541</sup> pheomelanin (5-cys-dopa),<sup>541</sup> neuromelanins (5,6-dihydroxyindole),<sup>38, 39</sup> catechol melanins (catecholic monomers),<sup>40, 41</sup> insect melanin (*N*-acetyl-dopamine),<sup>42, 542</sup> allomelanins (1,8-dihydroxynaphthalene),<sup>19, 543</sup> and pyromelanin (homogentisic acid (HGA) and potentially a benzoquinone derivative (benzoquinone acetic acid, BQA<sup>544</sup>); **Figure 3.1**).<sup>73</sup> The polymerisation of melanins<sup>46</sup> yields species with high molecular weights and often the formation of insoluble pigment<sup>47</sup> (the formation of which is proposed to proceed via a nucleation and growth mechanism),<sup>545</sup> and the structures, properties, and applications of natural and synthetic melanins have been reviewed.<sup>46, 423, 541, 546-551</sup>

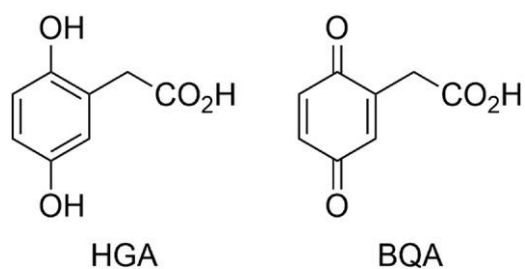


Figure 3.1: The chemical structures of homogentisic acid (HGA) and benzoquinone acetic acid (BQA).

Pyomelanins and ochronotic pigment formation can be driven enzymatically or indeed via autopolymerisation in the presence of oxygen in a variety of prokaryotic/eukaryotic species. Eukaryotic organisms contain a variety of enzymes in varying concentrations in different intracellular/extracellular environments, and therefore studies to understand the polymerisation of HGA in various conditions may offer insight into the deposition of pyomelanin pigmentation in various tissues (of importance for diseases like alkaptonuria). In the case of an extremely rare disorder termed black urine disease or alkaptonuria, a mutation in the enzyme homogentisate 1,2-dioxygenase (HGD), results in the inability to metabolise the amino acids phenylalanine and tyrosine which leads to an accumulation of HGA in the body. A consequence of this being the discolouration of the urine and parts of the body to a darker colour, along with a range of other illnesses and symptoms that present over time.

Here we report the results of an investigation of the polymerisation of HGA to form polyHGA (a simplified version of pyomelanin, **(Figure 3.2)** in the absence or presence of enzymes (a laccase (LACC),<sup>552</sup> peroxidase (horseradish peroxidase (HRP)), or tyrosinase (TYR)) at either pH 5.0 or 7.4. A selection of different analytical techniques was applied to study the resultant pyomelanins, including UV–vis spectroscopy, nuclear

magnetic resonance (NMR) spectroscopy, X-ray photoelectron spectroscopy (XPS), size exclusion chromatography (SEC), dynamic light scattering (DLS), scanning electron microscopy (SEM), energy-dispersive X-ray (EDX) spectroscopy, Fourier-transform infrared (FTIR) spectroscopy, electron paramagnetic resonance (EPR) spectroscopy, cyclic voltammetry (CV), and conductive probe atomic force microscopy (C-AFM). Condition-dependent polyHGA formation was observed, which offers insight into real-world observations of pyomelanin pigment deposition inside specific tissues in the body (e.g., observed by eye or histological studies),<sup>170, 203, 387, 553</sup> and moreover, highlights their potential for optimisation for utilisation in electronic devices.<sup>423</sup>

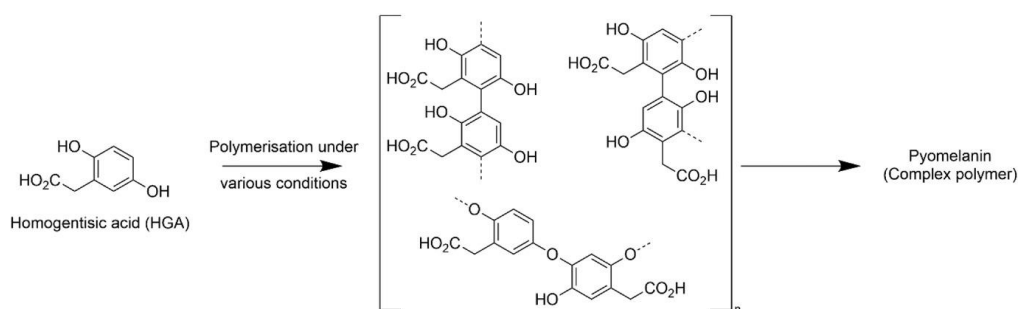


Figure 3.2: schematic of the polymerization of homogentisic acid (HGA) to form pyomelanin. It is important to note that pyomelanin may contain other monomers depending on the conditions under which they are formed in vivo, and a simplified version of pyomelanin, polyHGA (depicted above), is studied herein.

## **3.2 Experimental Section**

### **3.2.1 Polymerisation of HGA (Lower Concentration of HGA–No Enzyme Control)**

HGA was dissolved in buffer (at a concentration of HGA of  $10.4 \text{ mg mL}^{-1}$ ) at room temperature in the presence of air. The buffers were either sodium acetate (0.1 M, pH 5) or phosphate-buffered saline (0.1 M, pH 7.4) and if necessary, after the addition of HGA the pH was corrected by addition of 1 M NaOH or HCl. Samples were isolated at specific points in time before/after dialysis (molecular weight cutoff of 3.5 kDa) against water (4 L), refreshing the water every few hours for 5 days. The dialyzed mixtures were lyophilized (freeze dryer from Labconco Corporation), supplied by Thermo Fisher Scientific in Heysham, UK. Samples were stored in a freezer until analysed.

### **3.2.2 Polymerisation of HGA (Lower Concentration of HGA in the Presence of Enzymes)**

HGA was dissolved in buffer (at a concentration of 0.052 g HGA in 5 mL of buffer solution, i.e., concentration of HGA of  $10.4 \text{ mg mL}^{-1}$ ) at room temperature in the presence of air. The buffers were either sodium acetate (0.1 M, pH 5) or phosphate-buffered saline (0.1 M, pH 7.4) and, if necessary, after the addition of HGA the pH was corrected by addition of 1 M NaOH or HCl. Enzymatic polymerisation reactions were initiated by addition of 85 units of enzyme chosen from HRP (the unit used when defining or describing enzymes is either the unit U or IU internationally, with this unit alluding to the catalytic activity of an enzyme. 1 U  $\mu\text{mol}/\text{min}$  is used to define how much one micromole of substrate is catalysed by a given enzyme within a one-minute period in a specific experimental setting or condition) supplied by Alfa Aesar (Thermo

Fisher Scientific) in Heysham, UK, *Agaricus bisporus* LACC and mushroom TYR. Hydrogen peroxide (30%, 50  $\mu$ L) was added. Samples were isolated at specific points in time before/after dialysis (molecular weight cutoff of 3.5 kDa) against water (4 L), refreshing the water every few hours for 5 days. The dialyzed mixtures were lyophilized (freeze dryer from Labconco Corporation), supplied by Thermo Fisher Scientific in Heysham, UK. Samples were stored in a freezer until analysed.

### **3.2.3 Polymerisation of HGA (Higher Concentration of HGA–No Enzyme Control)**

HGA was dissolved in buffer (at a concentration of 0.168 g HGA in 5 mL of buffer solution, i.e., concentration of HGA of 33.6 mg mL<sup>-1</sup>) at room temperature in the presence of air. The buffers were either sodium acetate (0.1 M, pH 5) or phosphate-buffered saline (0.1 M, pH 7.4) and, if necessary, after the addition of HGA the pH was corrected by addition of 1 M NaOH or HCl. Samples were isolated at specific points in time before/after dialysis (molecular weight cutoff of 3.5 kDa) against water (4 L), refreshing the water every few hours for 5 days. The dialyzed mixtures were lyophilized (freeze dryer from Labconco Corporation), supplied by Thermo Fisher Scientific in Heysham, UK. Samples were stored in a freezer until analysed.

### **3.2.4 Polymerisation of HGA (Higher Concentration of HGA in the Presence of Enzymes)**

HGA was dissolved in buffer (at a concentration of 0.168 g HGA in 5 mL of buffer solution, i.e., concentration of HGA of 33.6 mg mL<sup>-1</sup>) at room temperature in the presence of air. The buffers were either sodium acetate (0.1 M, pH 5) or phosphate-

buffered saline (0.1 M, pH 7.4) and, if necessary, after the addition of HGA the pH was corrected by addition of 1 M NaOH or HCl. Enzymatic polymerisation reactions were initiated by addition of 170 units of enzyme chosen from HRP (supplied by Alfa Aesar (Thermo Fisher Scientific) in Heysham, UK), *Agaricus bisporus* LACC and mushroom TYR. Hydrogen peroxide (30%, 50  $\mu$ L) was added. Samples were isolated at specific points in time before/after dialysis (molecular weight cutoff of 3.5 kDa) against water (4 L), refreshing the water every few hours for 5 days. The dialyzed mixtures were lyophilized (freeze dryer from Labconco Corporation), supplied by Thermo Fisher Scientific in Heysham, UK. Samples were stored in a freezer until analysed.

### 3.3 Results and Discussion

The product of the polymerisation of HGA (**Figure 3.1**) was studied in the absence (control) or presence of enzymes (a laccase,<sup>170, 203, 387, 552-554</sup> peroxidase, or tyrosinase) at either pH 5 or 7.4 with a view to understand the potential role of enzymes and pH on the formation of ochronotic pigment (**Figure 3.2**).

There were discernible differences in the color of the reaction mixtures within hours (with solutions at pH 5 somewhat lighter in color than those at pH 7.4), and the reaction mixtures proceeded to become significantly darker over a period of weeks, which is characteristic of pyomelanins (**Figure A.1.1, Appendices**). The addition of tyrosinase to HGA when compared to the control experiment in the absence of tyrosinase showed discernible differences in the UV–vis spectra (**Figure A.1.2, Appendices**), with the appearance of a second peak at 250 nm due to the oxidation of HGA to BQA (in addition to the characteristic peak of HGA at 290 nm),<sup>555</sup> which was more pronounced for experiments carried out at pH 7.4 than at pH 5.

UV-vis spectra were recorded over 24 h using a concentration of HGA of  $10.4 \text{ mg mL}^{-1}$  to avoid complications with precipitate formation and light scattering/precipitation complicating UV-vis spectra recording and/or interpretation over the period of the experiment. UV-vis spectra showed that using a laccase or peroxidase produced significantly more polyHGA than tyrosinase or the no-enzyme control, with polyHGA production being condition dependent, with peroxidase  $\geq$  laccase  $>$  tyrosinase  $\approx$  no enzyme control (**Figure A.1.2, Appendices**). It is important to note that each enzyme works best at a specific optimal pH value (In general the optimal pH for tyrosinase is 6 to 7.5), and deviations in pH from the optimal may result in a decrease in activity due to alterations in the shape of the enzyme's active site, and the subtle differences in the pH dependence of the UV-vis spectra are in line with the literature (laccases,<sup>556</sup> peroxidases,<sup>557, 558</sup> tyrosinases,<sup>559</sup> and HGA autopolymerisation at high pH values<sup>170, 203, 387, 553-555</sup> (albeit outside the physiologically relevant pH range for humans))<sup>560</sup> and are also suggestive of various oxidation states of the monomeric units constituting the backbone of the polyHGAs.

The corresponding percentage yields of the polyHGA precipitate isolated by lyophilisation after 5 days of reaction using a concentration of HGA of  $10.4 \text{ mg mL}^{-1}$ , followed by dialysis (molecular weight cutoff of 3.5 kDa) showed a similar trend: peroxidase  $\geq$  laccase  $>$  tyrosinase  $\approx$  no enzyme control (percentage yields of  $11 \pm 2\%$ ,  $11 \pm 8\%$ ,  $7 \pm 2\%$ , and  $6 \pm 2\%$ , respectively, at pH 5;  $21 \pm 4\%$ ,  $7 \pm 3\%$ ,  $5 \pm 1\%$ , and  $5 \pm 2\%$ , respectively, at pH 7.4). To produce sufficient melanin for analysis via other techniques, experiments were carried out under analogous conditions with the concentration of HGA of  $33.6 \text{ mg mL}^{-1}$  for longer periods of time (6 weeks) yielding

polyHGA showing a broadband absorption typical of melanins (**Figure 3.3; Figure A.1.1, Appendices**).

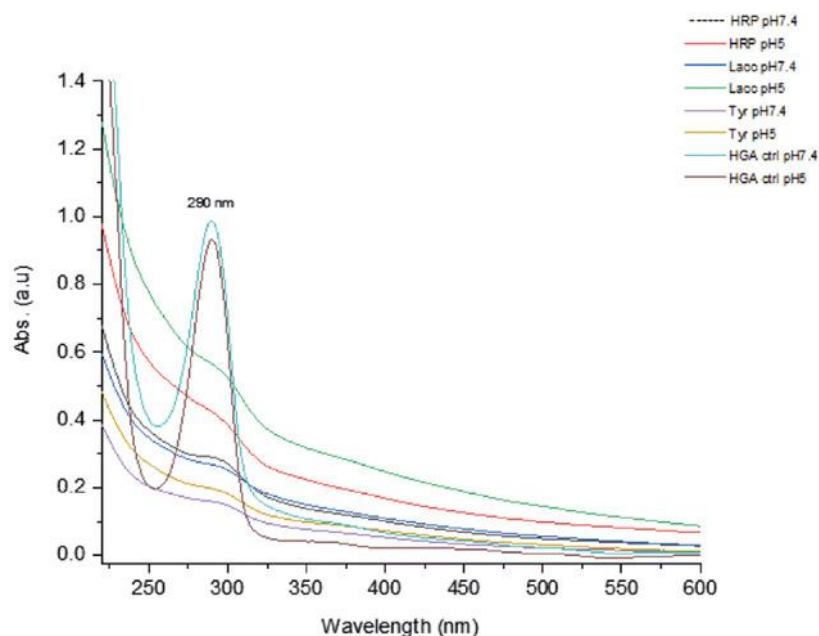


Figure 3.3: UV-vis spectra of HGA reaction mixtures after 6 weeks at either pH 5.0 or 7.4, in the absence of enzyme (control) or presence of enzyme (laccase (LACC), peroxidase (HRP), tyrosinase (TYR)). Spectra for BQA found in appendix

While the  $^1\text{H}$  NMR spectra recorded in  $\text{D}_2\text{O}$  of HGA show characteristically sharp peaks for the three aromatic protons and two alkyl protons ( $\text{Ar-CH}_2\text{-CO}_2\text{H}$ ) on HGA (**Figure A.1.3, Appendices**), after polymerisation for 6 weeks the  $^1\text{H}$  NMR spectrum for the polyHGA (no enzyme control at pH 5) is sharp indicative of relatively little polymerisation in line with the mass isolated (**Figures A.1.4, Appendices**), whereas the  $^1\text{H}$  NMR spectra for the other polyHGAs typically have broad lines suggesting the polymers have high molecular weights and/or aggregation of the oligomers/polymers, which is the characteristic of melanins (**Figures A.1.5-A1.11, Appendices**). In principle, it may be possible to estimate the ratio of Ar-Ar/C-C bonds to Ar-O-Ar/C-O-C bonds from the ratio of aromatic:alkyl protons, with a ratio of 2:3 alkyl:aromatic

protons indicative of no/minimal reaction (e.g., HGA control and no enzyme control at pH 5) or formation of Ar-O-Ar/C-O-C bonds, and deviation from that ratio indicative of formation of a greater proportion of Ar-Ar/C-C bonds, which is suggested by our data. It is noteworthy that our data are in line with solid-state NMR studies of monomer connectivity in pyromelanins,<sup>554</sup> and studies of pH dependence of polymerisation of phenolic compounds suggest the preference for C-C bond formation instead of C-O-C bond formation at the pH values employed in this study with various enzymes (cognizant of the fact that enzymes function best at a specific optimal pH value at which the shape of the enzyme's active site is optimal for function with specific substrates);<sup>422, 561-563</sup> furthermore, polymers connected via C-O-C bonds are expected to have lower electrical conductivity than polymers connected via C-C bonds akin to graphene derivatives.<sup>564</sup>

XPS data (**Figures 3.4 and 3.5; Figures A.1.12-A.1.14 and Tables A.1.1-A.1.5, Appendices**) confirmed that the HGA and polyHGAs were predominantly composed of C and O (with traces of N (residual enzyme), Na/Cl (residual buffer), and Si (substrate)). The C 1s spectra confirmed the presence of C-C, C-O, C=O, O-C=O, and  $\pi$ - $\pi$  bonds; and the O 1s spectra confirmed the presence of C=O and C-O bonds, and a Na KLL Auger peak, which overlaps the O 1s envelope at 536 eV. There were no clear trends in the data to determine the connectivity of the polyHGA backbone<sup>565</sup> (e.g., ratio of Ar-Ar/C-C bonds to Ar-O-Ar/C-O-C bonds normalized against the peak for O-C=O; (**Tables A.1.1-A.1.5, Appendices**), and the varying levels of C=O bonds (plausibly due to both carboxylic acids and quinones) are suggestive of differing oxidation states for the monomers incorporated in the backbone of the polyHGAs.

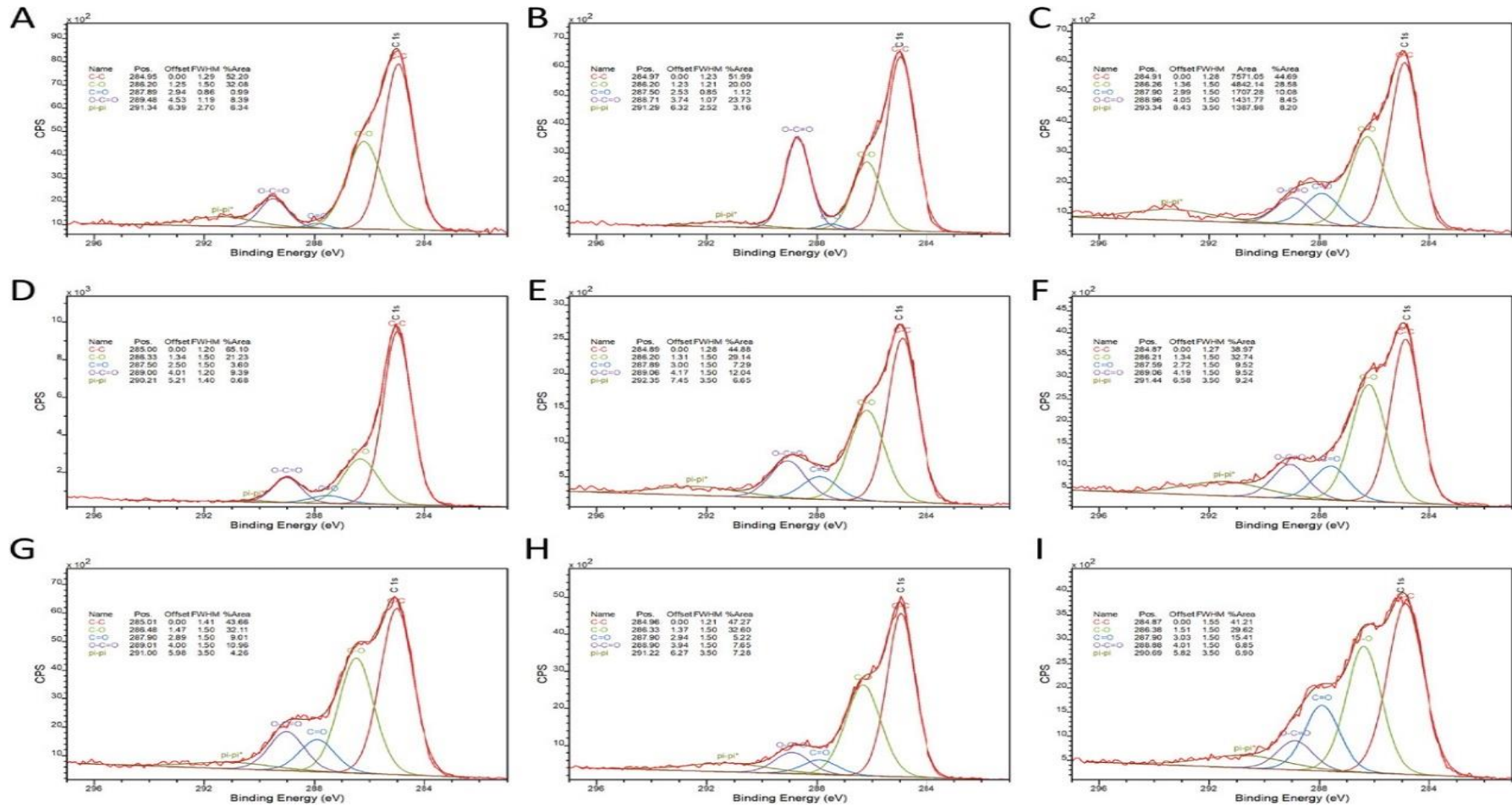


Figure 3.4: XPS C 1s core line spectra: A) HGA; B) polyHGA (no enzyme control at pH 5.0); C) polyHGA (no enzyme control at pH 7.4); D) polyHGA (formed in the presence of tyrosinase at pH 5.0); E) polyHGA (formed in the presence of tyrosinase at pH 7.4); F) polyHGA (formed in the presence of laccase at pH 5.0); G) polyHGA (formed in the presence of laccase at pH 7.4); H) polyHGA at pH 5.0; and I) polyHGA (formed in the presence of peroxidase at pH 7.4).

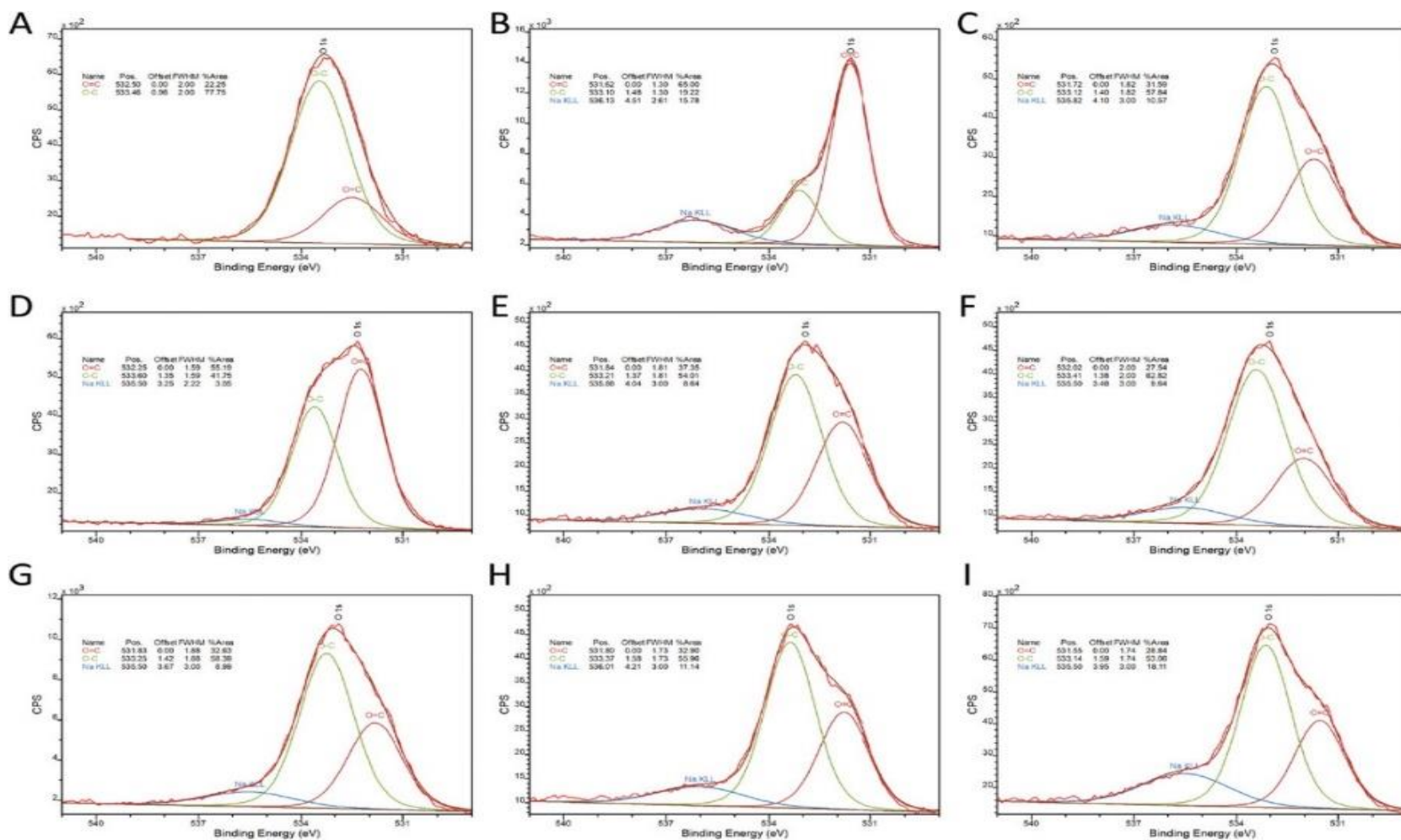


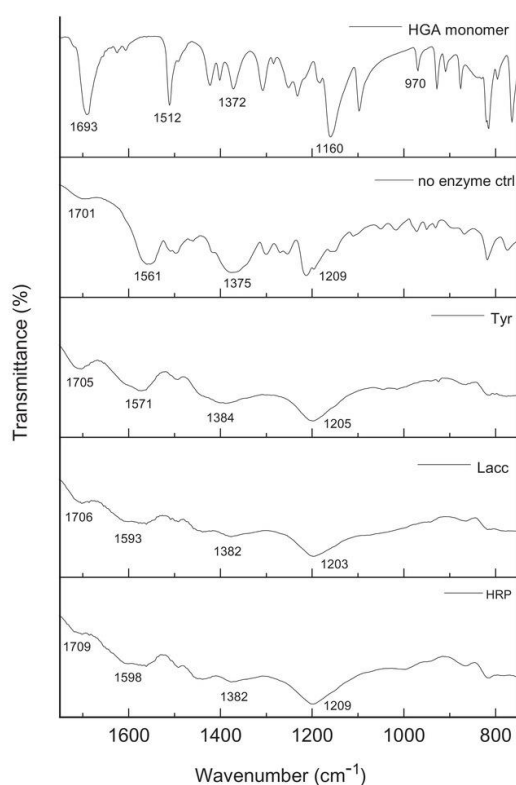
Figure 3.5: XPS O 1s core line spectra A) HGA; B) polyHGA (no enzyme control at pH 5.0); C) polyHGA (no enzyme control at pH 7.4); D) polyHGA (formed in the presence of tyrosinase at pH 5.0); E) polyHGA (formed in the presence of tyrosinase at pH 7.4); F) polyHGA (formed in the presence of laccase at pH 5.0); G) polyHGA (formed in the presence of laccase at pH 7.4); H) polyHGA (formed in the presence of peroxidase at pH 5.0); and I) polyHGA (formed in the presence of peroxidase at pH 7.4).

SEC has previously been used to assess the molecular weight distributions of soluble oligomeric/polymeric melanin derivatives<sup>170, 423</sup> of the polyHGA after dialysis (molecular weight cutoff of 3.5 kDa) showed traces of the low-molecular-weight species and/or oligomeric species; however, higher-molecular-weight species (>3.5 kDa) were not observed due to removal of the aggregates on the guard column of the SEC (**Figure A.1.15, Appendices**). DLS<sup>566</sup> of the same samples showed no higher-molecular-weight species (>3.5 kDa) due to removal of the aggregates during filtration prior to DLS as part of standard sample preparation protocols. SEM was used in combination with EDX spectroscopy to assess the precipitate morphology and the elemental composition of the polyHGAs produced. SEM data show that the precipitates isolated were irregularly shaped with sizes between tens to hundreds of micrometers (**Figures A.1.16-A.1.24, Appendices**). There is no meaningful shape/size correlation as the polyHGAs are produced under unconstrained conditions, whereas the in vivo polyHGA precipitate shapes/sizes would be constrained by the intracellular/extracellular environment in which they are produced. EDX data suggest that all samples are mainly composed of C and O (similar to the XPS data) with additional K and Na from the buffer, Au (sputter coating), Si (substrate), and samples with enzymes also have traces of additional Al, Ca, Mg, and S (**Figures A.1.16-A.1.23, Appendices**).

FTIR spectroscopy was used to analyse the HGA and polyHGAs produced. The FTIR spectrum for the polyHGA (no enzyme control at pH 5) closest to the monomeric HGA is indicative of relatively little polymerisation in line with the mass isolated; however, all other polyHGAs had significantly broader peaks than monomeric HGA, as expected for polymeric species with a variety of chemical environments (**Figure 3.6;**

**Figure A.1.25, Appendices).** A discernible difference in the FTIR spectra of HGA and the polyHGAs was the broadening/diminution of the peak at  $970\text{ cm}^{-1}$  in HGA (from the aromatic hydrogens) suggestive of C-C bond formation, with broadening of bands at  $1500\text{--}1510\text{ cm}^{-1}$  (aromatic C=C bonds) and the weak band at  $1580\text{ cm}^{-1}$  (aromatic C=C). Peaks at  $1200\text{--}1210\text{ cm}^{-1}$  corresponding to phenolic OH and at  $1560\text{--}1570\text{ cm}^{-1}$  corresponding to the C=O bond of the carboxylic acid functional groups are present in all spectra, albeit broader.<sup>552</sup>

pH 5.0



pH 7.4

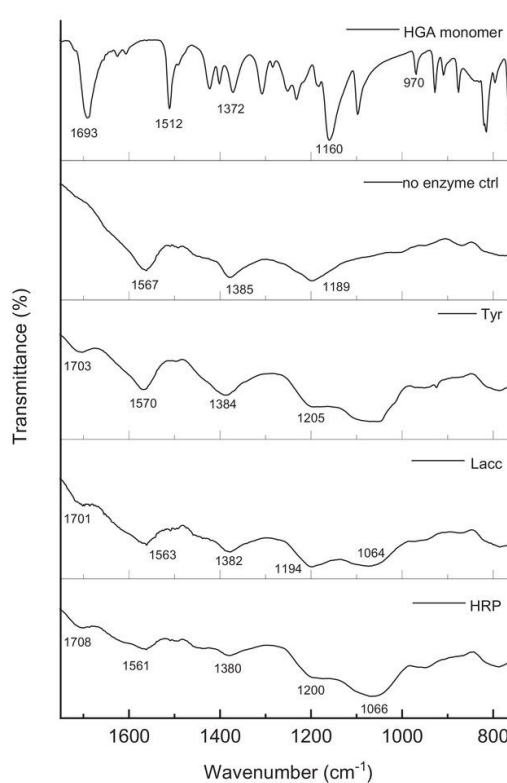


Figure 3.6: FTIR spectra of dialyzed polyHGA isolated after 6 weeks of reaction at pH 5.0 and pH 7.4, generated in the absence of enzyme (no enzyme control) or presence of enzyme (laccase (LACC), peroxidase (HRP), and tyrosinase (TYR)).

EPR spectroscopy was used to study the powders. X-band EPR spectra of all polyHGA powders showed nearly identical spectra (**Figure 3.7**). The spectra had a single peak centered at  $g = 2.0035$ , with a peak-to-peak width of 4 G (the polyHGA generated in the presence of tyrosinase at pH 5.0 gave a slightly broader peak with a peak-to-peak width of 4.6 G). The polyHGA generated in the presence of peroxidase and no enzyme controls gave much more intense peaks than polyHGA generated in the presence of laccase or tyrosinase. This may be related to the extended conjugation length of the different polymers.<sup>567</sup> In general, the EPR peak shape and width were similar to those of eumelanins and consistent with the pyomelanin spectra reported in the literature.<sup>208</sup>

A close inspection of the EPR peak of polyHGA showed a noticeable asymmetry. Spectrum simulation required two components to accurately reproduce the line shape (**Figure 3.8; Figures A.1.26-A.1.28, Appendices**). These components can be assigned to carbon-centered and semiquinone radicals based on their  $g$ -values (2.0034 and 2.0040, respectively). All polyHGA spectra were dominated by the C-centered radical with 2–6% contribution of the semiquinone. This is similar to the precedent for eumelanins, although the contribution of the semiquinone radical in eumelanins is higher.<sup>568</sup>

Recording EPR spectra under saturating conditions (at a high microwave power of up to 200 mW) did not reveal any fast-relaxing organic radical components. In some pyomelanin samples, a clear semiquinone signal was reported in the literature.<sup>552</sup> The absence of this signal in our samples can be explained by the small contribution of the semiquinone radical to the overall EPR signal. The spectra recorded at high power, however, suggested the presence of some EPR-active metals in all enzyme-derived

samples, possibly originating from the traces of residual enzymes (supported by EDX data; see **Figures A.1.16-A.1.23** in the **Appendices**).

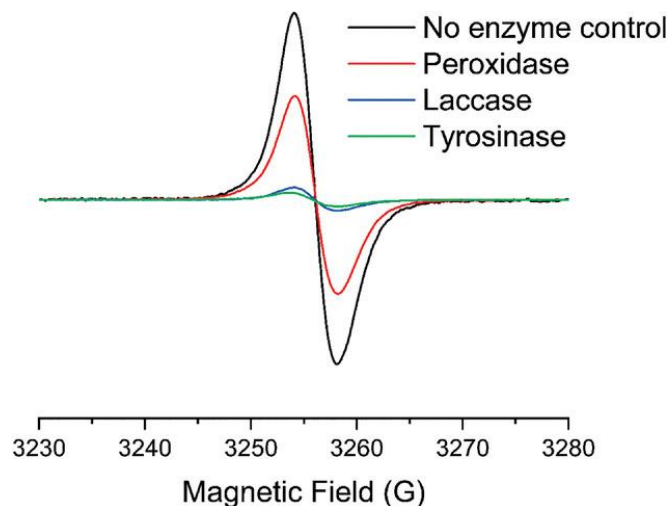


Figure 3.7: band EPR spectra of polyHGA samples generated at pH 7.4 in the absence of enzymes (black), or presence of laccase (blue), peroxidase (red), or tyrosinase (green).

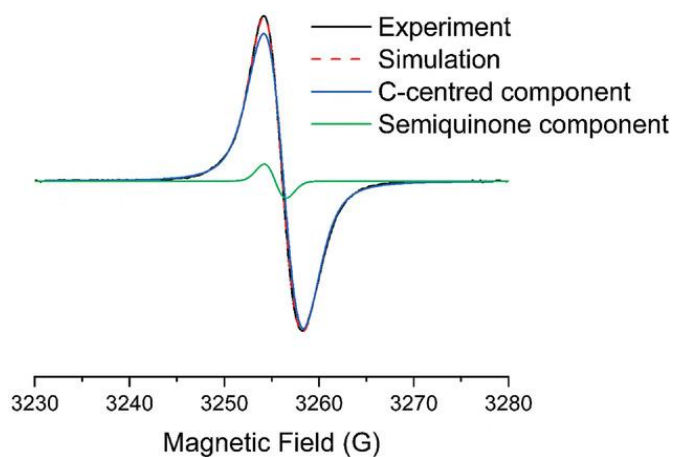


Figure 3.8: Experimental EPR spectrum of polyHGA generated in the presence of peroxidase sample (black) and simulation (red). The simulation included a broad C-centered component ( $g = 2.0034$ , Voigtian line shape with peak-to-peak width 4.2 G, 97.8%) and a sharper semiquinone radical ( $g = 2.004$ , Gaussian line shape with peak-to-peak width 2.2 G, 2.2%).

Cyclic voltammetry has previously been used to study the reduction/oxidation processes and electron-transfer properties of polyphenols analogous to polyHGA. Cyclic voltammetry of HGA shows a clear anodic peak due to the oxidation of HGA to BQA, and a clear cathodic peak due to the reduction of BQA to HGA, the positions of which are solvent and pH dependent.<sup>297, 298</sup> The cyclic voltammograms of the polyHGAs generated in this study at pH 5 (**Figure A.1.29, Appendices**) show an anodic peak at 0.56 V and the corresponding cathodic peak at 0 V versus Ag/AgCl (reference electrode), whereas at pH 7.4 (**Figure A.1.29, Appendices**) the oxidation and reduction peaks were not resolved, i.e., the polyHGAs were electroactive in acidic medium while electro-inactive in neutral medium, confirming the role of protons in the electroactivity of the polyHGA (akin to polycatechol films)<sup>569</sup>. The cyclic voltammograms show that all electrochemical changes are completed after 4 scans, demonstrating their stability under the experimental conditions for the duration of the experiment, and their unsymmetrical cathodic and anodic peaks are attributed to the difference in background current and kinetic limitations.<sup>569</sup>

Conductive tip AFM studies of the powders isolated from polyHGA formation under various conditions showed some to be measurably conductive (the setup is depicted in **Figure A.1.30** in the **Appendices**). The polyHGAs generated by auto-oxidation of HGA at either pH 5 or at pH 7.4 (i.e., no enzyme control) were neither measurably conductive nor were the polyHGAs generated in the presence of tyrosinase at either pH 5 or at pH 7.4, or laccase at pH 5. However, the polyHGAs generated in the presence of laccase at pH 7.4 or peroxidase at either pH 5 or pH 7.4 were measurably conductive (**Figure 3.9**), with average  $\log_{10} G$  values of  $-11.52 \pm 0.28$ ,  $-8.52 \pm 0.24$ , or  $-9.30 \pm 0.32$  S, respectively ( $I$ - $V$  curves are in (**Figures A.1.31-A.1.36** in the **Appendices**), and

a comparison of log  $G$  counter maps is shown in (**Figure A.1.37, Appendices**); i.e., conductivity ( $G$ ) of  $2.9 \times 10^{-3} \pm 1.1 \times 10^{-3}$ ,  $0.58 \pm 0.2$ , or  $3.4 \pm 1.2$  nS, respectively. The differences in the electronic properties of the polymers<sup>567, 570</sup> are likely to be related to the extended conjugation length of the polyHGAs produced by laccase-/peroxidase-mediated polymerisation of HGA, supported by the greater amounts of polyHGAs produced by laccase-/peroxidase-mediated polymerisation of HGA and by EPR data (**Figure 3.7**). The polyHGAs produced have the potential for use in applications as green/sustainable<sup>571</sup> and components of electronic devices,<sup>319, 389, 417, 423, 572-574</sup> or other high value added applications (particularly after optimisation of the synthesis).<sup>27, 571, 575-</sup>

579

The in vitro studies of the polymerisation of HGA to form polyHGA (a simplified version of pyomelanin) described herein, investigated in the absence or presence of enzymes (a laccase, peroxidase, or tyrosinase) at physiologically relevant pH values (either pH 5.0 or 7.4), contribute to our understanding of real-world observations of pyomelanin pigment deposition inside specific tissues in the body (e.g., observed by eye or histological studies), by demonstrating that their presence imparts electrical conductivity to the tissues, and that this may alter the electrophysiology of the tissues and thereby their function.<sup>170, 203, 387, 553</sup>

We note that enzyme activity is affected by various environmental factors (including, but not limited to, pH, salt concentration, and solvent), and the function of enzymes is governed by the primary sequence of the enzyme which is species specific, and systematic studies may offer insight into opportunities for industrial biotechnological approaches to melanin production<sup>579-588</sup>. Recent advances in our analytical capabilities

(e.g., single-cell analysis, and/or single-/multiomics (genomics, metabolomics, proteomics, and transcriptomics) approaches) <sup>589-593</sup> also offer unique insight into biological processes involving melanins in various contexts <sup>570</sup>. In the clinic it is useful to quickly and easily diagnose alkaptonuria using a low-cost spectrophotometric technique for the detection of polyHGA; <sup>555</sup> likewise, one of the potentially exciting applications of polyHGA is as a biocompatible intracellular label for optoacoustic imaging of macrophages with strong optoacoustic contrast to resolve single cells against a strong blood background <sup>594</sup>.

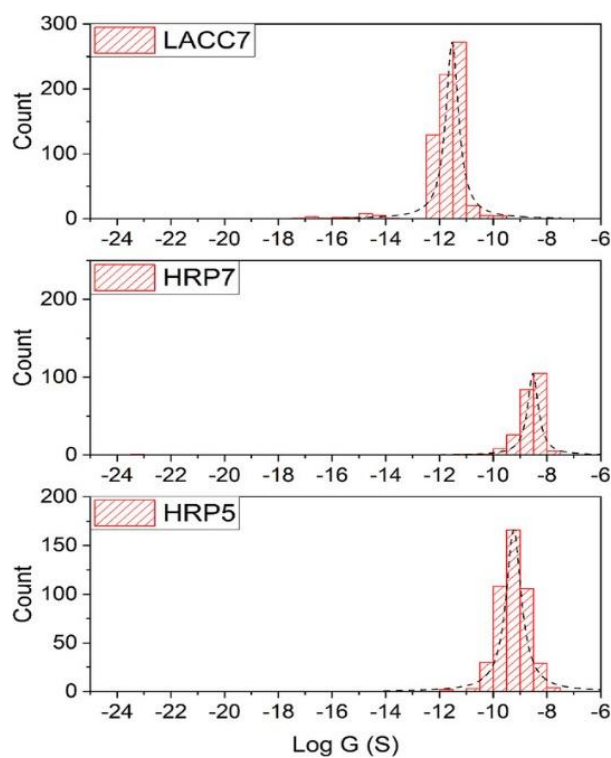


Figure 3.9: Conductive tip AFM data for polyHGAs. comparison of the conductance histograms for polyHGAs generated in the presence of laccase (LACC) at pH 7.4, or peroxidase (HRP) at pH 7.4 or 5.0, respectively.

### **3.4 Conclusion**

Herein polymerisation of HGA to form polyHGA (a simplified version of pyomelanin) was investigated in the absence or presence of enzymes (a laccase, peroxidase, or tyrosinase) at either pH 5.0 or 7.4. A variety of analytical techniques (UV–vis, NMR, XPS, SEC, DLS, SEM, EDX, FTIR, EPR, CV, and C-AFM) were employed to examine the polyHGAs produced under the experimental conditions. The experiments revealed interesting trends in the yields of polyHGAs produced with subtle differences in their properties; notably, C-AFM data for polyHGAs showed that those generated in the presence of LACC at pH 7.4, or HRP at pH 7.4 or 5.0, respectively, displayed measurable conductivity suggesting their potential for application in electronic devices.

# 4 Analysis of phenolic polymers as model melanins

## Overview

Melanins are a class of conjugated biopolymers with varying compositions and functions, which have a variety of potential medical and technical applications. Here we examine the conjugated polymers derived from a variety of phenolic monomers (catechol (CAT), levodopa (DOPA) and homogentisic acid (HGA)), using a selection of different analytical chemistry techniques to compare their properties with a view to understanding structure-function relations. The polymers displayed measurable conductivity, with electronic properties tuned by the functional groups pendant on the polymer backbones (which served as dopants) suggesting their potential for application in electronic devices.

## 4.1 Introduction

Phenolic monomers are common building blocks of melanins (observed in allomelanin, eumelanin, neuromelanin, pheomelanin and pyomelanin),<sup>549</sup> and are known to play important roles in intermolecular/material interactions,<sup>595-597</sup> and here we examine the conjugated polymers derived from a variety of phenolic monomers (catechol (CAT), levodopa (DOPA) and homogentisic acid (HGA)) to understand the role of functional groups pendant on the polymer backbones on their optoelectronic properties<sup>598</sup>. A selection of different analytical techniques are employed for these studies, including: UV-Vis spectroscopy, nuclear magnetic resonance (NMR) spectroscopy, X-ray photoelectron spectroscopy (XPS), zeta potential measurements, transmission electron microscopy (TEM), scanning electron microscopy (SEM), energy dispersive X-ray (EDX) spectroscopy, X-ray diffraction (XRD), Fourier-transform infrared (FTIR) spectroscopy, electron paramagnetic resonance (EPR) spectroscopy, cyclic voltammetry (CV), and conductivity measurements. The properties of the conjugated polymers suggest they may find application in electronic devices.

## 4.2 Experimental Section

### 4.2.1 Synthesis of melanins

300 mg of melanin precursor (catechol (1,2-dihydroxybenzene), CAT; levodopa, DOPA; homogentisic acid, HGA) was dissolved in 50 mL of acetate buffer (50 mM; pH = 6.5) and the reaction was initiated by the addition of 50 mL of Na<sub>2</sub>CO<sub>3</sub> (50 mM). The mixtures were stirred at room temperature and monitored using thin layer chromatography to ensure that the reaction of the melanin precursor compound was complete. In the cases of melanin precursors DOPA and catechol, 10 mL of 0.5 M CaCl<sub>2</sub>

was added to the reaction mixtures; after standing at room temperature overnight a precipitate was observed to have formed, the supernatant was collected after centrifugation (5 mins at 4K rpm) and these were dialyzed against DI water for two days (using dialysis tubes with MWCO of 3.5 kDa) and lyophilized (this is termed the “high solubility fraction”, abbreviated to HS). The precipitates were washed with: a) water, b) 0.1N HCl and c) water, and lyophilized (this is termed the “low solubility fraction”, abbreviated to LS). For CAT and DOPA a high solubility fraction and a low solubility fraction were obtained, polyCAT-HS, polyCAT-LS, polyDOPA-HS and polyDOPA-LS, respectively; whereas in the case of HGA it is important to note that only a soluble fraction was obtained (polyHGA-HS).

### 4.3 Results and Discussion

Various methods of polymerisation of aromatics (e.g., phenols) exist, including enzymatic,<sup>599-604</sup> electrochemical,<sup>605-613</sup> oxidative,<sup>614, 615</sup> etc. and the polymerisation of phenols is the subject of an excellent review from Kobayashi and co-workers,<sup>614, 615</sup> which examined the propensity for C-C or C-O-C bond formation which would be expected to play a role in the conductivity of the resulting polymers (polymers connected via C-C bonds akin to graphene derivatives<sup>616</sup> are expected to have lower electrical conductivity than polymers connected via C-O-C bonds).

In this study, a green approach was applied using a weakly basic aqueous solution of the commercially available monomers CAT, DOPA and HGA (**Figure 4.1**) to polymerise the monomers via autooxidation with a view to understand the potential role of subtle differences in monomer structure and the properties of the resulting conjugated polymers, polyCAT, polyDOPA and polyHGA, respectively.

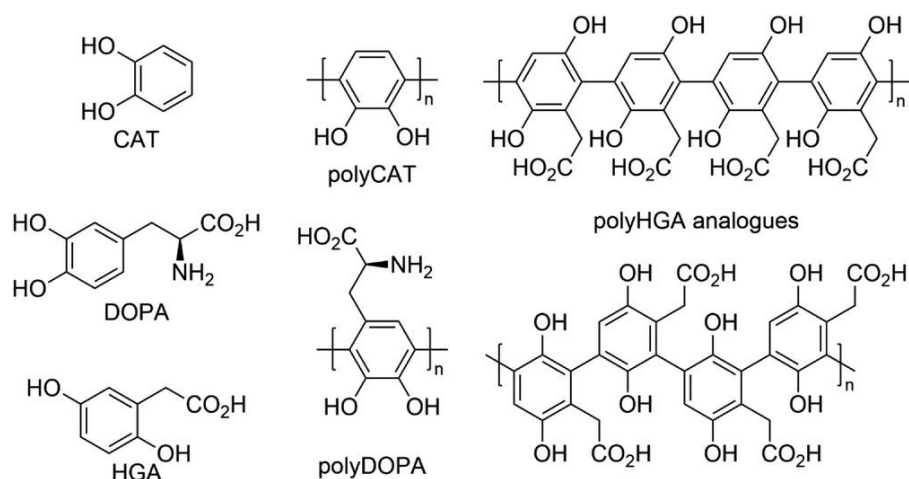


Figure 4.1: A schematic of the polymerization of CAT, DOPA or HGA to form model melanins is important to note that natural melanins may contain other monomers depending on the conditions under which they are formed *in vivo*, and the polymers depicted are therefore simplified version of melanins, polyCAT, polyDOPA or polyHGA, respectively (depicted above), that are studied herein.

The polymerisations of CAT and DOPA resulted in the formation of a colored precipitate (isolated by centrifugation and washing) termed the insoluble or low solubility fraction (polyCAT-LS or polyDOPA-LS, respectively), and supernatant (that was dialyzed against DI water and lyophilized) termed the soluble fraction (polyCAT-HS or polyDOPA-HS, respectively); and under the polymerisation conditions used the polymerisation of HGA resulted in the production of only a soluble fraction (polyHGA-HS). The polymers showed a broadband absorption typical of melanins in the UV-vis spectra (**Figure 4.2**), which are also suggestive of various oxidation states of the

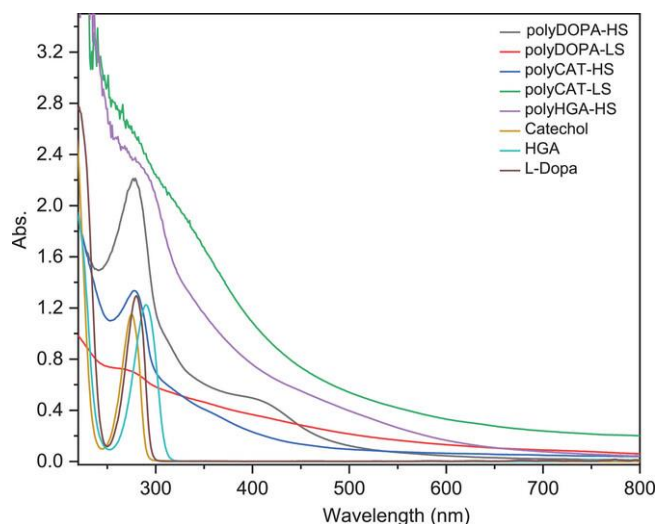


Figure 4.2: UV-vis spectra of the polymers studied herein. (0.0026 mg/mL).

monomeric units constituting the backbone of the polyCAT-HS, polyCAT-LS, polyDOPA-HS, polyDOPA-LS and polyHGA-HS, respectively.

The  $^1\text{H}$  NMR spectra recorded in  $\text{D}_2\text{O}$  of the monomers CAT, DOPA and HGA show sharp peaks characteristic of low molecular weight species (**Figure A.2.1, A.2.2, and A.2.3, Appendices**, respectively), whereas the  $^1\text{H}$  NMR spectra of the polymers (polyCAT-HS, polyCAT-LS, polyDOPA-HS, polyDOPA-LS and polyHGA-HS) are markedly different. The  $^1\text{H}$  NMR spectra of the soluble fractions (polyCAT-HS, polyDOPA-HS, and polyHGA-HS) have some sharp peaks (due to the pendant functional groups) and broad lines characteristic of high molecular weight species, and the  $^1\text{H}$  NMR spectra of the low solubility fractions (polyCAT-LS, polyDOPA-LS) are broader still characteristic of high molecular weight species and/or aggregation of the oligomers/polymers that is characteristic of polyphenols<sup>617</sup> and melanins more generally, leading to relatively featureless solid-like spectra (**Figure A.2.1-A.2.3, Appendices**).

XPS data (**Figure 4.3 and Figure A.2.4, Appendices**) confirmed the polymer powders were predominantly composed of C and O (with traces of N from the NH<sub>2</sub> in polyDOPA-HS and polyDOPA-LS, Na/Ca/F [residual buffer] and Si [potentially from underlying substrate]). The C 1s spectra confirmed the presence of a number of clear peaks, which we correlate to common carbon binding environments (C-C/H, C-N, C-O, C=O, O-C=O). Small peaks towards the higher binding energy side of the C1s spectra may be indicative of  $\pi$ - $\pi^*$  shake-up features. The fluorine signal evident in the wide scan for PolyDOPA-LS may also contribute to the higher energy peaks in the corresponding C 1s spectra. O 1s spectra are fitted with two major peaks which are

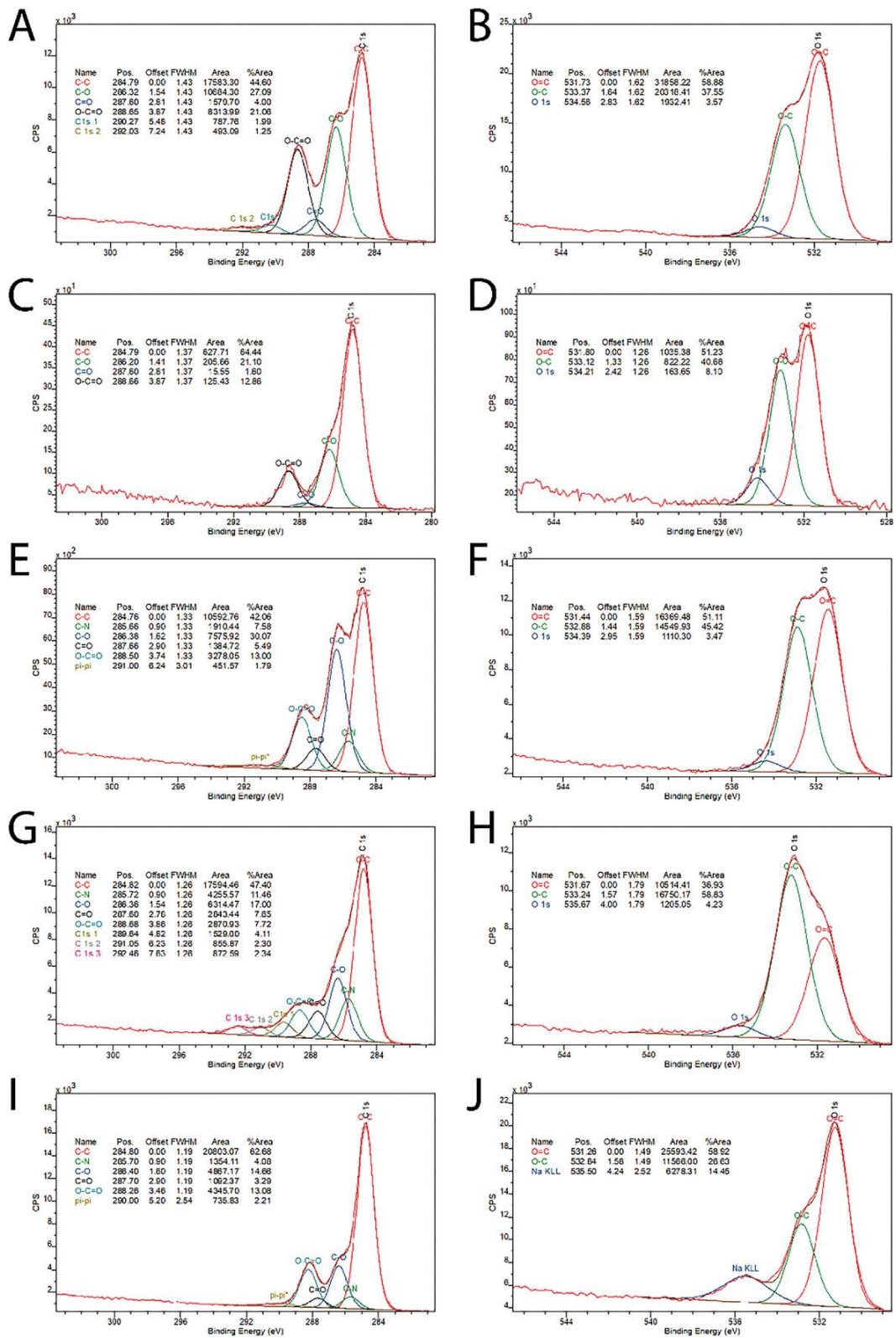


Figure 4.3: X-ray photoelectron spectroscopy (XPS) spectra. A) polyCAT-HS C 1s core line spectra. B) polyCAT-HS O 1s core line spectra. C) polyCAT-LS C 1s core line spectra. D) polyCAT-LS O 1s core line spectra. E) polyDOPA-HS C 1s core line spectra. F) polyDOPA-HS O 1s core line spectra. G) polyDOPA-LS C 1s core line spectra. H) polyDOPA-LS O 1s core line spectra. I) polyHGA-HS C 1s core line spectra. J) polyHGA-LS O 1s core line spectra.

expected to correspond to O=C and O-C bonds in agreement with the C 1s spectra, though some minor peaks are also required to fit the spectra potentially indicating a range of different oxidation states. A Na KLL Auger peak at ~ 536 eV is also evident in the O1s spectra for polyHGA-HS, correlating with the strong Na signal noted in the wide-scan for this polymer. We note that there are clear differences between the polymers, in particular the varying levels of C-O and C=O bonds (plausibly due to both quinones present in all polymers and carboxylic acids in polyDOPA-LS, polyDOPA-HS and polyHGA-HS, respectively) suggestive of differing oxidation states for the monomers incorporated in the backbone of the polymers.

Zeta potential measurements indicate all the polymers/particles are anionic due to deprotonation of phenols and carboxylic acids (polyDOPA-LS, polyDOPA-HS and polyHGA-HS); the zeta potentials for the polyCAT-HS ( $-9.83 \pm 0.84$  mV) and polyCAT-LS ( $-17.83 \pm 0.75$  mV) are somewhat lower than those of phenol, amine and carboxylic acid containing polyDOPA-HS ( $-15.63 \pm 1.25$  mV) and polyDOPA-LS ( $-33.03 \pm 0.12$  mV), and phenol and carboxylic acid containing polyHGA-HS ( $-37.00 \pm 3.30$  mV). The interaction of cationic amines with the anionic phenols and carboxylic acids present in polyDOPA account for the lower zeta potentials for polyDOPA than amine-free polyHGA, and the higher zeta potentials for the LS products than HS products suggest the hydrophobic parts of the polymers are buried within the particles with hydrophilic functional groups clustered on the particles' surfaces as the polymers constituting them assemble/aggregate.<sup>48</sup>

Transmission electron microscopy (TEM), scanning electron microscopy (SEM) and energy dispersive X-ray spectroscopy (EDX) were used to study the morphology and elemental composition of the of the HS and LS polymer fractions produced. TEM of dilute solutions of the polymers deposited on TEM grids showed the presence of nanoscale particles of tens-hundreds of nm characteristic of melanins (the formation of which is proposed to proceed via a nucleation and growth mechanism)<sup>48, 618</sup> (**Figure 4.4**). SEM images of lyophilized solutions of the polymers deposited on SEM stubs shows the particles/precipitates formed were irregularly shaped with sizes between tens to hundreds of micrometers characteristic of melanins (**Figure 4.4**); while the HS particles are generally smaller than the LS precipitates, there is no meaningful correlation between particle/precipitate shapes/sizes as the polymers are produced under unconstrained conditions<sup>604</sup>. By comparison, the shapes/sizes of melanin particles/precipitates in vivo would be constrained by the intracellular/extracellular environment in which they are produced. EDX data suggests that all samples are mainly composed of C and O for all polymers with a trace of N present in the polyDOPA samples (similar to the XPS data), with additional traces of Ca, K and Na from the buffer, Au (sputter coating) and Si (substrate). Interestingly, EDX data shows that the polymers in the highly soluble fractions have higher metal ion contents (measured as relative abundance by EDX) than the low solubility fractions, polyCAT-HS (Ca: 8.9% ± 0.1%. Na: 0.4% ± 0.1%.), polyDOPA-HS (Ca: 8.4% ± 0.1%. Na: 1.6% ± 0.9%.), polyHGA-HS (Ca: 0.3% ± 0.1%. Na: 15.3% ± 0.8%.), by comparison with polyCAT-LS (Ca: 2.1% ± 0.4%. Na: 0.1% ± 0.1%.), and polyDOPA-LS (Ca: 0.2% ± 0.1%. Na: 0.0% ± 0.0%.), confirming the polyphenol's ability to bind metal ions<sup>619, 620</sup>. A putative role for melanins in biology<sup>613, 621</sup> and underpinning their application in energy storage<sup>288, 622-624</sup>. XRD patterns of the samples suggested they were largely amorphous, confirmed

by the very broad peak at  $2\theta$  ca.  $15\text{-}40^\circ$  (**Figure A.2.5, Appendices**), characteristic of natural and synthetic melanins<sup>625-628</sup>.

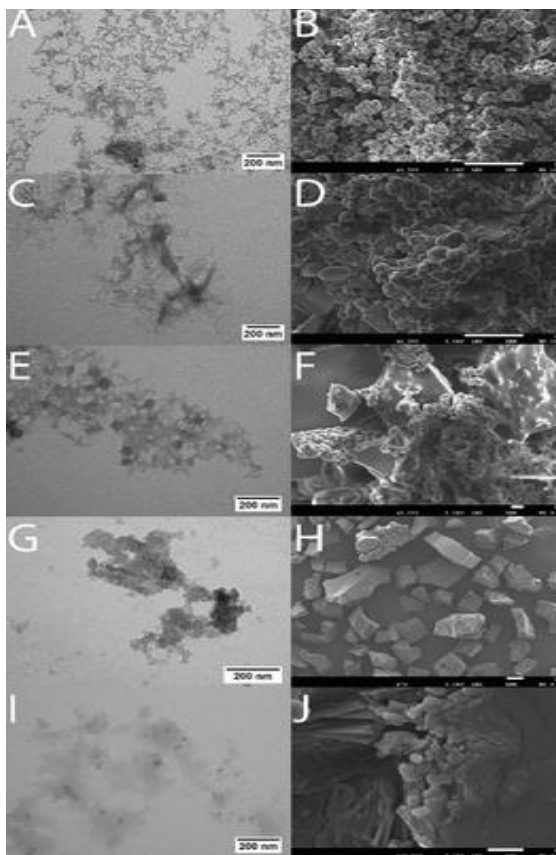


*Figure 4.4: Transmission electron microscopy (TEM) and scanning electron microscopy (SEM) images of samples studied herein. A) polyCAT-HS TEM. B) polyCAT-HS SEM (scale bar represents  $10\ \mu\text{m}$ ). C) polyCAT-LS TEM. D) polyCAT-LS SEM (scale bar represents  $10\ \mu\text{m}$ ). E) polyDOPA-HS TEM. F) polyDOPA-HS SEM (scale bar represents  $1\ \mu\text{m}$ ). G) polyDOPA-LS TEM. H) polyDOPA-LS SEM (scale bar represents  $1\ \mu\text{m}$ ). I) polyHGA-HS TEM. J) polyHGA-HS SEM (scale bar represents  $1\ \mu\text{m}$ ).*

FTIR spectroscopy was used to analyse the polymers produced, all of the peaks were broader than for their constituent monomers as expected for polymeric species with a variety of chemical environments (**Figure 4.5, Figure A.2.6, Appendices**), characteristic of natural and synthetic melanins<sup>629</sup>. A difference in the FTIR spectra of all polymers was the broadening/diminution of peaks at ca.  $970\ \text{cm}^{-1}$  from the aromatic

hydrogens suggestive of C-C bond formation during polymerisation, with broadening of bands at 1500-1520  $\text{cm}^{-1}$  (aromatic C=C bonds) and the weak band at ca. 1580  $\text{cm}^{-1}$  (aromatic C=C). Peaks at ca. 1200-1210  $\text{cm}^{-1}$  corresponding to phenolic OH,<sup>600, 601</sup> and at ca. 1560-1570  $\text{cm}^{-1}$  corresponding to the C=O bond of the carboxylic acid functional groups are present in the spectra of polyDOPAs<sup>630-633</sup> and polyHGA,<sup>604</sup> albeit broader<sup>552</sup>. The broad bands at ca. 3000  $\text{cm}^{-1}$  attributed to aromatic C-H, and at 3400-3200  $\text{cm}^{-1}$  attributed to stretching vibrations of the OH in all polymers and NH<sub>2</sub> in polyDOPAs<sup>630-633</sup>.

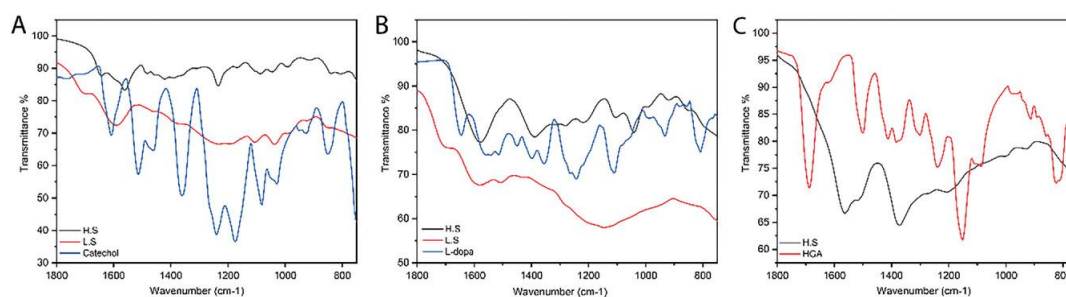


Figure 4.5: Fourier-transform infrared (FTIR) spectra of monomers and polymers. A) Catechol (CAT), polyCAT-HS, and polyCAT-LS. B) levodopa (DOPA), polyDOPA-HS, and polyDOPA-LS. C) Homogentisic acid (HGA) and polyHGA-HS.

Melanins display paramagnetic character due to free radicals in their structures (e.g., semiquinone free radicals) which absorb microwaves under magnetic fields yielding spectra characteristic of the radical species present, consequently EPR spectroscopy was used to study the powders. X-band EPR spectra of all polymer powders showed single peak centred around  $g = 2.0023-2.005$ , with peak-to-peak width ca. 4-5 G, typical of melanin pigments<sup>549</sup> (**Figure 4.6**).

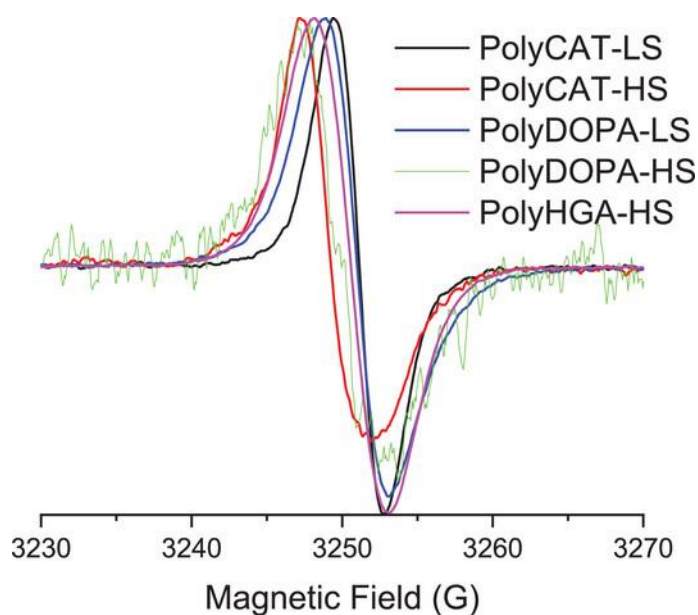


Figure 4.6: -band electron paramagnetic resonance (EPR) spectra of polymers studied herein.

Low solubility fractions polyCAT-LS and polyDOPA-LS were dominated by the signal of a carbon centred radical ( $g = 2.0033$ ), typical of eumelanins. PolyHGA-HS sample also showed a similar spectrum albeit at a slightly higher  $g$  value (2.0036). Interestingly, the two other high-solubility melanins polyCAT-HS and polyDOPA-HS showed clearly asymmetrical spectra with a high contribution of the semiquinone radical (**Figure 4.7**) which is probably due to complexation with  $\text{Ca(II)}$ <sup>549, 634</sup> which is present in these two materials only (see EDX data above).

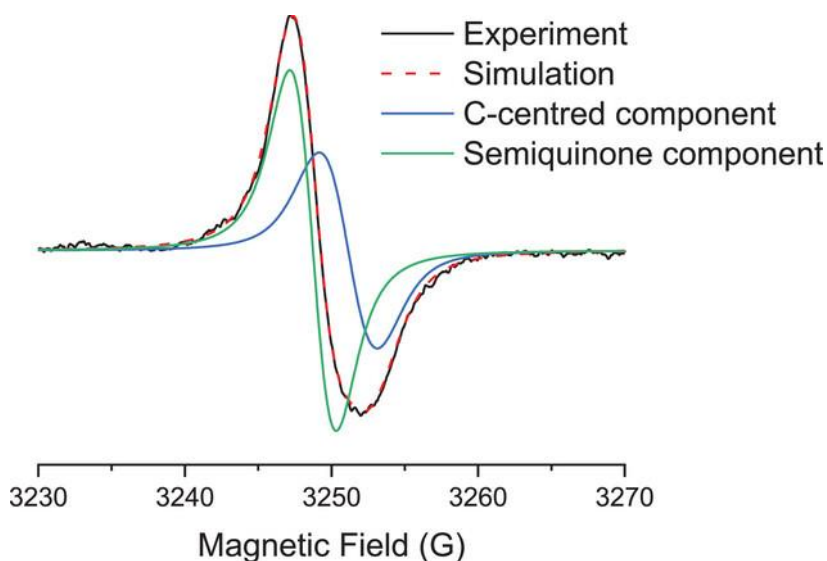


Figure 4.7: Experimental electron paramagnetic resonance (EPR) spectrum of polyCAT-HS (black) and simulation (red). The simulation included a broad C-centered component ( $g = 2.0033$ , 41.6%) and a sharper semiquinone radical ( $g = 2.0048$ , 58.4%).

Cyclic voltammetry can be used to study the reduction/oxidation processes and electron transfer properties of polyphenols such as those studied herein (voltammograms for CAT and polyCATs are shown in **(Figure A.2.7, Appendices)**, for DOPA and polyDOPA in **(Figure A.2.8, Appendices)**, and for HGA and polyHGA in **(Figure A.2.9, Appendices)**). The cyclic voltammograms of the polymers generated in this study at pH 5 typically show anodic peaks at ca. 0.56 V and the corresponding cathodic peak at ca. 0 V vs Ag/AgCl (reference electrode), whereas, at pH 7.4 the oxidation and reduction peaks were less well resolved, i.e., the polymers were electroactive in acidic medium while electroinactive in neutral medium. This is consistent with the literature for polyCATs,<sup>601</sup> polyDOPAs<sup>635</sup> and polyHGAs,<sup>604</sup> and confirms the role of protons in the electroactivity of the polymers<sup>570</sup>. The cyclic voltammograms are consistent after multiple scans demonstrating their stability under the experimental conditions for the duration of the experiment, and their unsymmetrical cathodic and anodic peaks are attributed to the difference in background current and kinetic limitations<sup>570</sup>.

To assess if the electronic properties of the samples studied herein have electronic properties useful for application in electronic devices their conductivity was measured. Interestingly, the powders isolated from lyophilised solutions of the polymers showed them to be measurably conductive (**Figure 4.8**).

The differences in the electronic properties of the polymers<sup>598, 636, 637</sup> are likely to be related to a subtle combination of the extended conjugation length of the LS polymers produced vs. HS polymers (i.e., the longer the conjugation length the higher the conductivity); the hierarchical assembly of the polymers governed by intramolecular and intermolecular interactions (i.e., the greater the levels of pi-stacking interactions the higher the conductivity);<sup>48, 638</sup> and the ability of the anionic component of the polymers to serve as a dopant for the polymers (supported by zeta potential measurements), akin to self-doped conducting polymers<sup>639-642</sup>.

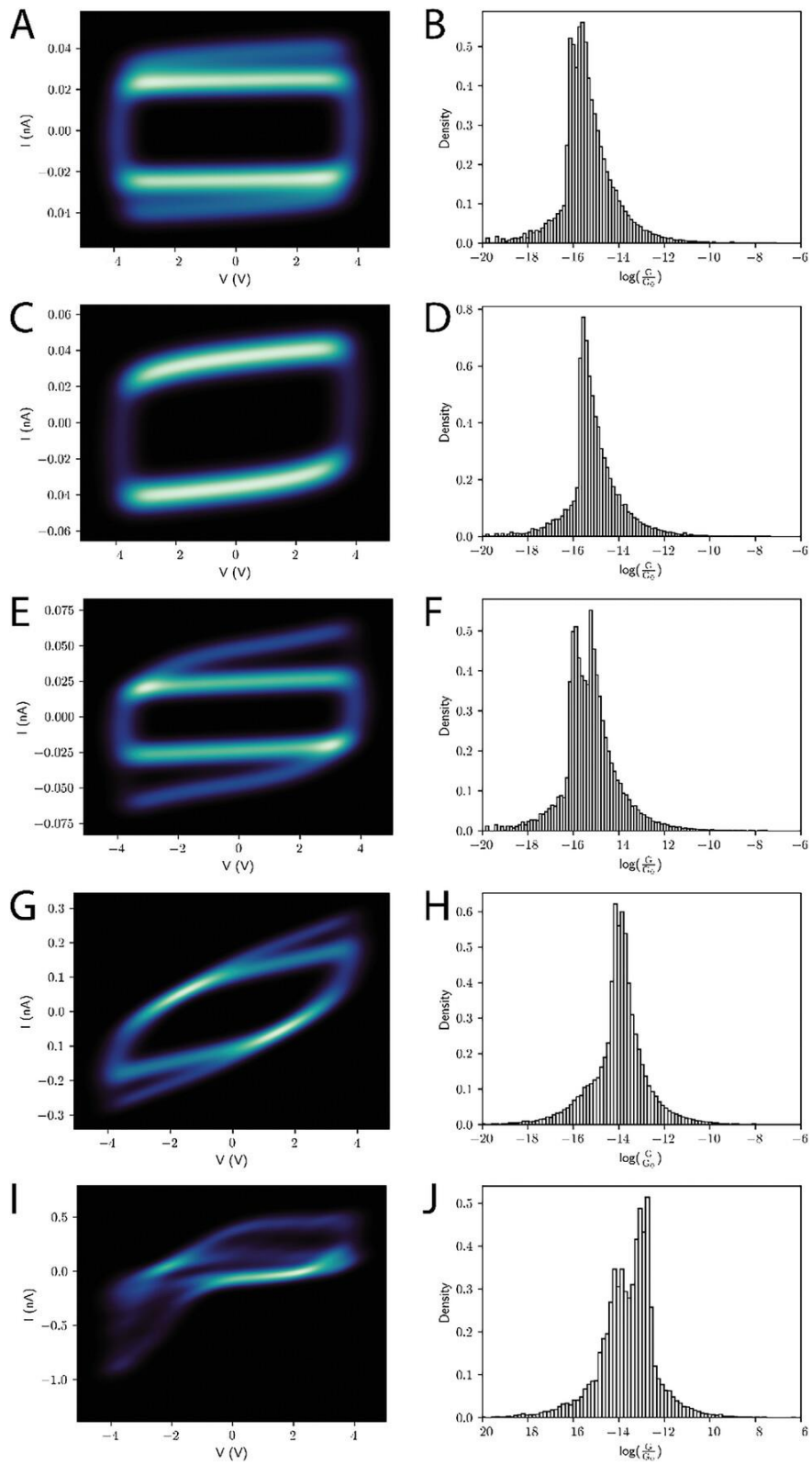


Figure 4.8: Conductance data for polymers studied herein. A) polyCAT-HS I-V curves. B) polyCAT-HS conductance histogram. C) polyCAT-LS I-V curves. D) polyCAT-LS conductance histogram. E) polyDOPA-HS I-V curves. F) polyDOPA-HS conductance histogram. G) polyDOPA-LS I-V curves. H) polyDOPA-LS conductance histogram. I) polyHGA-HS I-V curves. J) polyHGA-HS conductance histogram. Data courtesy of Sam.

## 4.4 Conclusion

Herein polymerisation of a variety of phenolic monomers (CAT, DOPA and HGA), yielded conjugated polymers polyCAT-HS, polyCAT-LS, polyDOPA-HS, polyDOPA-LS or polyHGA-HS, respectively. A variety of analytical techniques (UV-Vis, NMR, XPS, DLS, TEM, SEM, EDX, FTIR, EPR, CV, and conductivity measurements) were employed to examine the polymers produced, the experiments revealed the polymers displayed measurable conductivity, with electronic properties tuned by the functional groups pendant on the polymer backbones (which served as dopants) suggesting their potential for application in electronic devices (e.g. as materials in batteries or capacitors)

551, 643 .

# **5 Analysis of melanin-ECM interactions**

## **Overview**

Melanins are conjugated biopolymers with varying compositions and functions, found in various tissues throughout the body. Here we examine the conjugated polymers derived from levodopa (DOPA) and homogentisic acid (HGA), polyDOPA and polyHGA, respectively, and their interactions with the extracellular matrix (ECM) components chondroitin sulfate A (CSA) and chondroitin sulfate C (CSC), using a selection of different analytical chemistry techniques to understand structure-function relations. The melanin-ECM composites displayed measurable conductivity, with electronic properties tuned by the identity of the model melanin and presence of the ECM component (which served as dopants because of the presence of the carboxylates/sulfates pendant on their backbones).

## 5.1 Introduction

The production of melanin in the body is a result of the conversion of the amino acid tyrosine to a quinone intermediary and then further polymerisation to the pigment polymer melanin. This process is performed by cells which are neural crest in origin; melanocytes.<sup>550</sup> These cells reside in the epidermis of the skin and produce melanin within their intracellular structures; melanosomes. The melanin is donated to nearby keratinocytes which utilise this to protect their nucleus from the sun's UV radiation.<sup>644, 645</sup> In normal and pathological physiological function melanin has little association with collagen or other extracellular matrix proteins. Intermediaries of melanins such as quinones have been shown to bind to collagens, one such example is 1,4-benzoquinone (and others), their interaction with lysine.<sup>646</sup> Lysine accounts for approximately 3-4% of amino acid content in collagen and is key in the cross-linking process.<sup>647</sup> This pathological cross-linking process in the biological milieu alters the mechanical and chemical properties of the collagen resulting in decreased susceptibility to degradation and turnover due to alterations in its conformation.<sup>647, 648</sup> The formation of covalent cross-links between collagen fibers can also result in a decrease in its overall stability. This is the outcome of aggregation of collagen fibers and the formation of dense, fibrous structures, which can cause the ECM to lose its normal function, impairing tissue integrity and leading to pathological conditions like fibrosis.<sup>649</sup>

Here we examine the properties of conjugated polymers derived from phenolic monomers (levodopa (DOPA) and homogentisic acid (HGA)) that were polymerised in the presence of extracellular matrix components (chondroitin sulfate A (CSA) and/or chondroitin sulfate C (CSC)). A selection of different analytical techniques are employed for these studies, including: UV-Vis spectroscopy, zeta potential

measurements, transmission electron microscopy (TEM), X-ray diffraction (XRD), X-ray photoelectron spectroscopy (XPS), zeta potential measurements, Fourier-transform infrared (FTIR) spectroscopy, solid state nuclear magnetic resonance (ssNMR) spectroscopy, cyclic voltammetry (CV), and conductivity measurements. The properties of the materials offer insights into the role of functional groups pendant on the polymer backbones on melanin-ECM interactions using simple model systems.

## **5.2 Experimental Section**

### **5.2.1 Preparation of polyDOPA-CSA:**

1.0 g of ECM component (CSA) and 100 mg precursor (DOPA) were dissolved in 50 mL acetate buffer (50 mM, pH = 6.5) and the reaction was initiated by the addition of 30 mL of Na<sub>2</sub>CO<sub>3</sub> (50 mM). The mixture was gently stirred at room temperature and monitored using chromatography to ensure that the reaction of the melanin precursor compound was complete (about 2 days), after which the reaction mixture was dialyzed against DI water for two days (using dialysis tubes with MWCO of 3.5 kDa), frozen and lyophilized, resulting in production of a brown solid.

### **5.2.2 Preparation of polyDOPA-CSC:**

1.0 g of ECM component (CSC) and 100 mg precursor (DOPA) were dissolved in 50 mL acetate buffer (50 mM, pH = 6.5) and the reaction was initiated by the addition of 30 mL of Na<sub>2</sub>CO<sub>3</sub> (50 mM). The mixture was gently stirred at room temperature and monitored using chromatography to ensure that the reaction of the melanin precursor compound was complete (about 2 days), after which the reaction mixture was dialyzed

against DI water for two days (using dialysis tubes with MWCO of 3.5 kDa), frozen and lyophilized, resulting in production of a brown solid.

### **5.2.3 Preparation of polyDOPA-CSA-CSC:**

1.0 g of ECM components (0.5 g of chondroitin sulfate A and 0.5 g of chondroitin sulfate C) and 100 mg precursor (DOPA) were dissolved in 50 mL acetate buffer (50 mM, pH = 6.5) and the reaction was initiated by the addition of 30 mL of Na<sub>2</sub>CO<sub>3</sub> (50 mM). The mixture was gently stirred at room temperature and monitored using chromatography to ensure that the reaction of the melanin precursor compound was complete (about 2 days), after which the reaction mixture was dialyzed against DI water for two days (using dialysis tubes with MWCO of 3.5 kDa), frozen and lyophilized, resulting in production of a brown solid.

### **5.2.4 Preparation of polyHGA-CSA:**

1.0 g of ECM component (CSA) and 100 mg precursor (HGA) were dissolved in 50mL acetate buffer (50 mM, pH = 6.5) and the reaction was initiated by the addition of 30 mL of Na<sub>2</sub>CO<sub>3</sub> (50 mM). The mixture was gently stirred at room temperature and monitored using chromatography to ensure that the reaction of the melanin precursor compound was complete (about 2 days), after which the reaction mixture was dialyzed against DI water for two days (using dialysis tubes with MWCO of 3.5 kDa), frozen and lyophilized, resulting in production of a brown solid.

### **5.2.5 Preparation of polyHGA-CSC:**

1.0 g of ECM component (CSC) and 100 mg precursor (HGA) were dissolved in 50 mL acetate buffer (50 mM, pH = 6.5) and the reaction was initiated by the addition of 30 mL of Na<sub>2</sub>CO<sub>3</sub> (50 mM). The mixture was gently stirred at room temperature and monitored using chromatography to ensure that the reaction of the melanin precursor compound was complete (about 2 days), after which the reaction mixture was dialyzed against DI water for two days (using dialysis tubes with MWCO of 3.5 kDa), frozen and lyophilized, resulting in production of a brown solid.

### **5.2.6 Preparation of polyHGA-CSA-CSC:**

1.0 g of ECM components (0.5 g of chondroitin sulfate A and 0.5 g of chondroitin sulfate C) and 100 mg precursor (HGA) were dissolved in 50 mL acetate buffer (50 mM, pH = 6.5) and the reaction was initiated by the addition of 30 mL of Na<sub>2</sub>CO<sub>3</sub> (50 mM). The mixture was gently stirred at room temperature and monitored using chromatography to ensure that the reaction of the melanin precursor compound was complete (about 2 days), after which the reaction mixture was dialyzed against DI water for two days (using dialysis tubes with MWCO of 3.5 kDa), frozen and lyophilized, resulting in production of a brown solid.

### 5.3 Results and Discussion

With a view to understand melanin-ECM interactions (e.g., potential role of subtle differences in monomer/ECM structures in the properties of the resulting materials), DOPA or HGA (**Figure 5.1**) were polymerised (via autooxidation) in the presence of the extracellular matrix (ECM) components (**Figure 5.1**) chondroitin sulfate A (CSA) and/or chondroitin sulfate C (CSC), yielding polyDOPA-CSA, polyDOPA-CSC, polyDOPA-CSA-CSC, polyHGA-CSA, polyHGA-CSC and polyHGA-CSA-CSC, respectively.

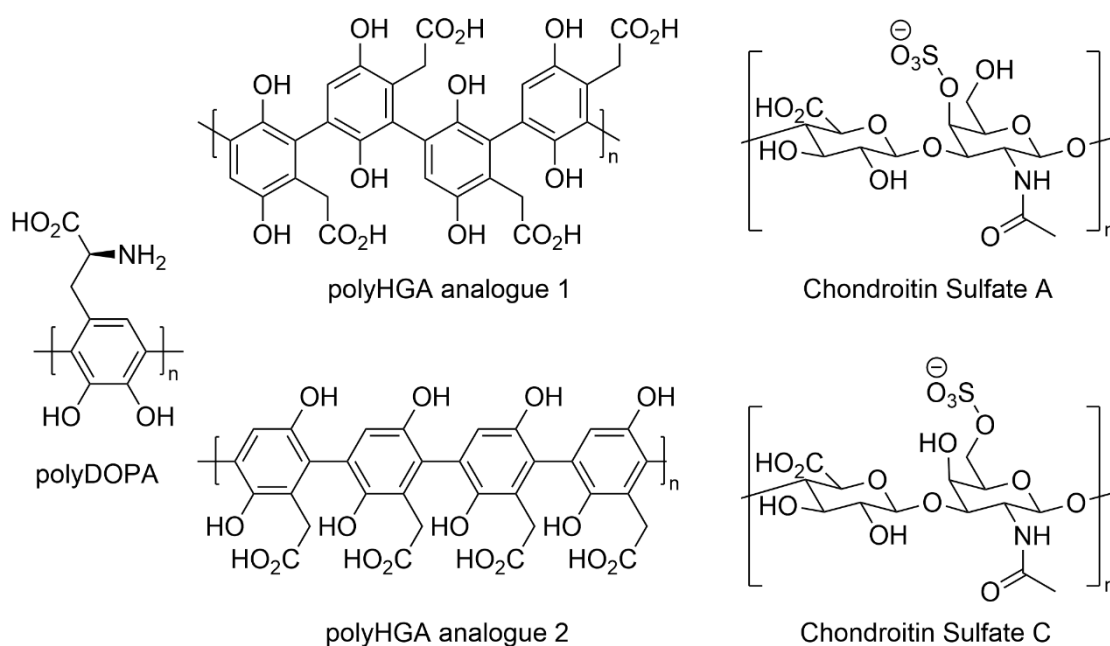


Figure 5.1: Structures of the model melanins (polyDOPA and polyHGA, respectively) and chondroitin sulfate derivatives (CSA and CSC, respectively), that are studied herein.

The polymerisations of DOPA or HGA in the presence of CSA and/or CSC, followed by dialysis and lyophilisation yielded brown solids (polyDOPA-CSA, polyDOPA-CSC, polyDOPA-CSA-CSC, polyHGA-CSA, polyHGA-CSC and polyHGA-CSA-CSC, respectively). The materials showed a broadband absorption typical of melanins in the UV-vis spectra (**Figure 5.2**), which is suggestive of a variety of oxidation states of the monomeric units constituting the backbone of the polyDOPAs and polyHGAs.

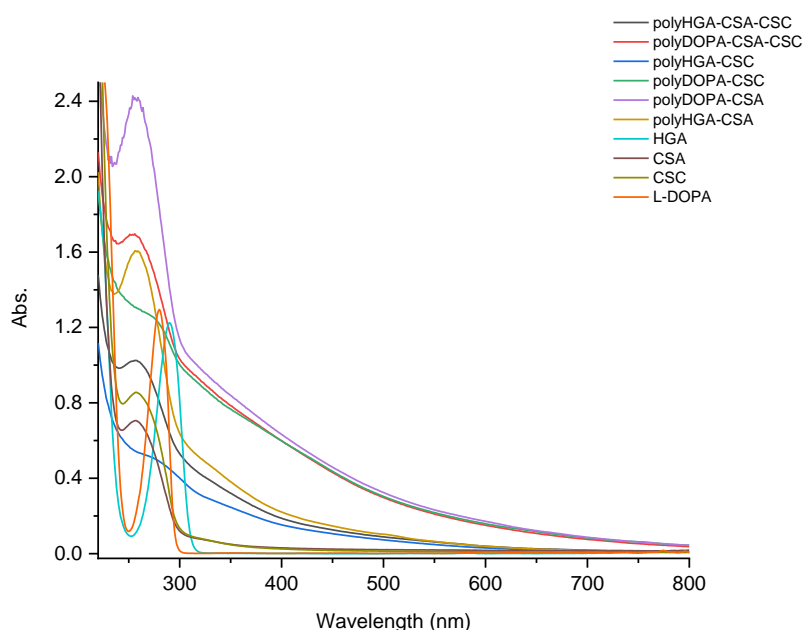


Figure 5.2: UV-vis spectra of the polymers studied herein (0.0208mg/mL)

TEM, zeta potential measurements XRD, and XPS were used study the properties of the materials studied herein. TEM of dilute solutions/suspensions of the materials deposited on TEM grids showed the presence of nanoscale particles of tens-hundreds of nm characteristic of melanins (the formation of which is proposed to proceed via a nucleation and growth mechanism)<sup>48, 618</sup> (**Figure 5.3**). Zeta potential measurements indicate all of the products are anionic due to deprotonation of phenols and carboxylic

acids: polyDOPA-CSA ( $-39.73 \pm 0.76$  mV), polyDOPA-CSC ( $-23.10 \pm 3.30$  mV), polyDOPA-CSA-CSC ( $-35.53 \pm 1.79$  mV), polyHGA-CSA ( $-46.63 \pm 2.60$  mV), polyHGA-CSC ( $-35.43 \pm 7.31$  mV), polyHGA-CSA-CSC ( $-45.57 \pm 4.29$ ). Interestingly, the zeta potentials for melanin-CSA products are more negative than the melanin-CSC products, with the zeta potentials of the melanin-CSA-CSC products containing both CSA and CSC logically observed to be between the products with only CSA or CSC.

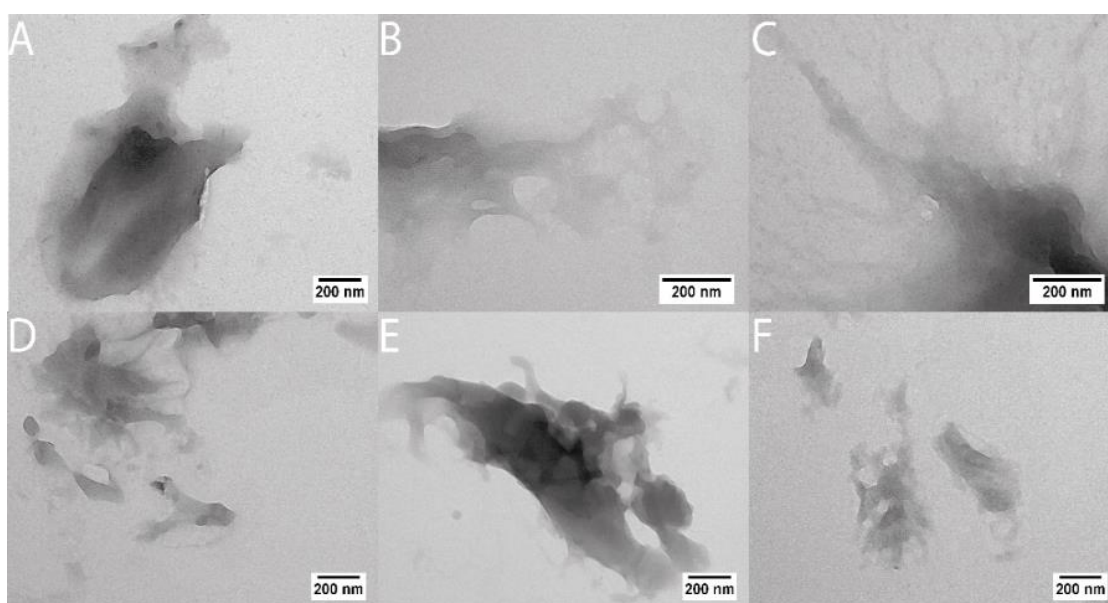


Figure 5.3: TEM. A) polyDOPA-CSA. B) polyDOPA-CSC. C) polyHGA-CSA. D) polyHGA-CSC. E) polyDOPA-CSA-CSC. F) polyHGA-CSA-CSC.

XRD patterns of the samples suggested they were amorphous (**Figure A.3.1, Appendices**), characteristic of natural and synthetic melanins<sup>625-628</sup>. XPS data (**Figures 5.4 and Figures 5.5**) confirmed the polymers were predominantly composed of C and O (with N from the  $\text{NH}_2$  in polyDOPA and  $\text{NHCOCH}_3$  in CSA/CSC, Na/Cl [residual buffer] and Si [substrate]). The C 1s spectra confirmed the presence of C-C, C-O, C=O,

O-C=O, and  $\pi$ - $\pi$  bonds; and the O 1s spectra confirmed the presence of C=O and C-O bonds, and a Na KLL Auger peak which overlaps the O1s envelope at  $\sim 536\text{eV}$ ; we also note the varying levels of C=O bonds (plausibly due to both quinones present in all polymers and carboxylic acids in polyDOPA and polyHGA-HS, respectively) are suggestive of differing oxidation states for the monomers incorporated in the backbone of the polymers.

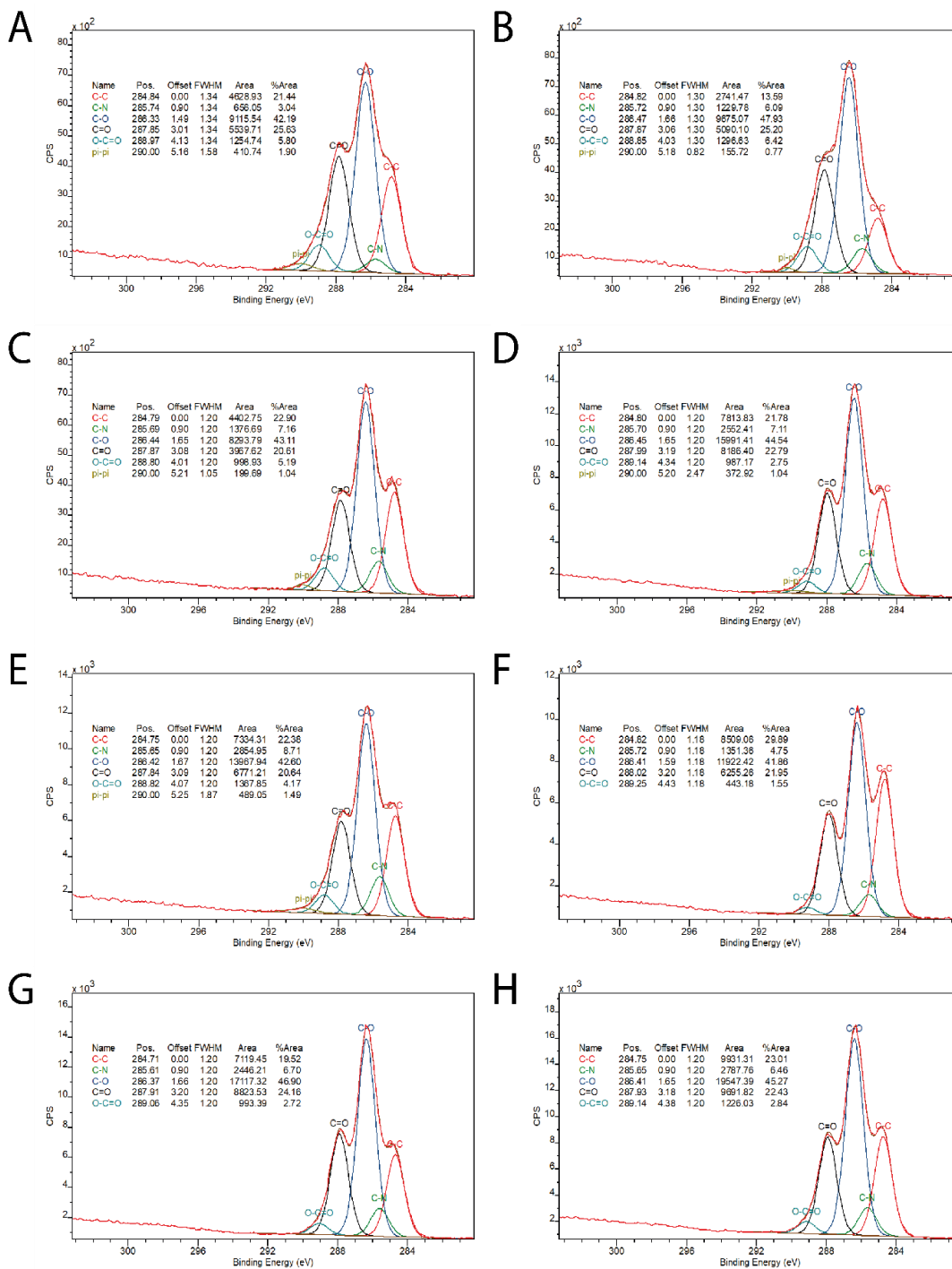


Figure 5.4: XPS spectra (C 1s core line spectra). A) CSA. B) CSC. C) polyDOPA-CSA. D) polyDOPA-CSC. E) polyDOPA-CSA-CSC. F) polyHGA-CSA. G) polyHGA-CSC. H) polyHGA-CSA-CSC.

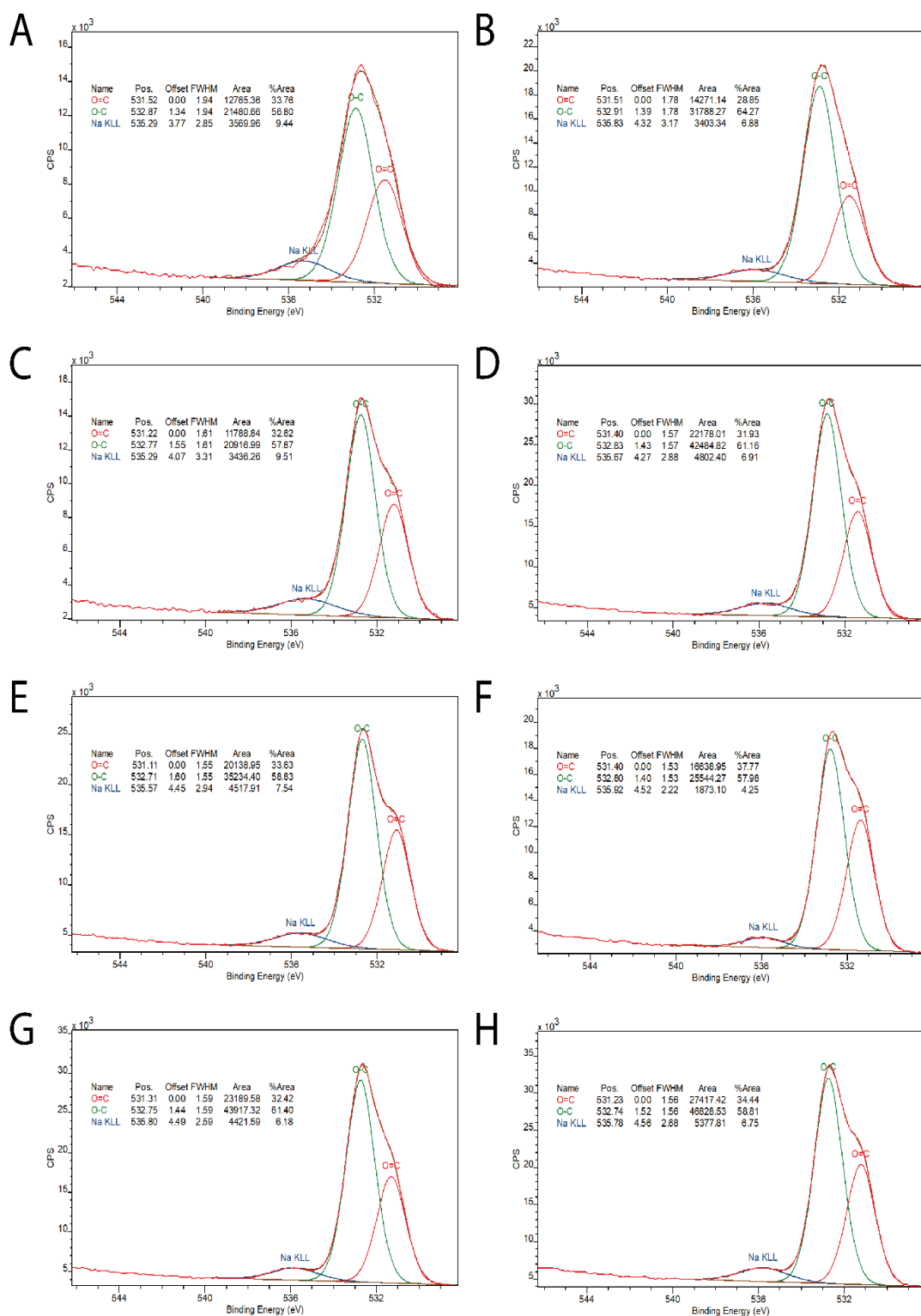


Figure 5.5: XPS spectra ( $O\ 1s$  core line spectra). A) CSA. B) CSC. C) polyDOPA-CSA. D) polyDOPA-CSC. E) polyDOPA-CSA-CSC. F) polyHGA-CSA. G) polyHGA-CSC. H) polyHGA-CSA-CSC.

FTIR spectroscopy was used to analyse the materials studied herein, which were complex due to the variety of chemical environments (**Figure 5.6** and **Figure A.3.2, Appendices**); samples including the polyDOPA or polyHGA contained peaks/shoulders broader than for their constituent monomers (DOPA or HGA, respectively) as expected for polymeric species, characteristic of natural and synthetic melanins<sup>629</sup>. The FTIR spectra of HGA has a peak at 970 cm<sup>-1</sup> (C-H in plane/out of plane bending mode), a broad peak at 1210 cm<sup>-1</sup> (phenolic OH), at 1421 cm<sup>-1</sup> (bending of -CH<sub>2</sub>), and 1512 cm<sup>-1</sup> to (C=O of the carboxylic acid)<sup>604, 650</sup>. The FTIR spectra of CSA and CSC are very similar, with peaks between 800-860 cm<sup>-1</sup> (C-O-S) the exact location of which differentiates the CSA from the CSC (peaks at roughly 855 cm<sup>-1</sup> correspond to CSA, whereas peaks at 823 cm<sup>-1</sup> correspond to CSC)<sup>651, 652</sup>. In CSA the peaks at 1077 cm<sup>-1</sup> and 1130 cm<sup>-1</sup> correspond to C-C vibrations, whereas in CSC the peaks are observed at 1070 cm<sup>-1</sup> and 1128 cm<sup>-1</sup><sup>653</sup>. The peaks at 1228 cm<sup>-1</sup> and 1220 cm<sup>-1</sup> in CSA and CSC, respectively, correspond to the asymmetrical vibration of (-SO<sub>3</sub><sup>-</sup>)<sup>654, 655</sup>. Peaks in the range in the range of 1375 cm<sup>-1</sup> and 1420 cm<sup>-1</sup> correspond to C-H and OH bonds<sup>650, 653</sup>. The peaks between 1610-1628 cm<sup>-1</sup> correspond to the amide I band in CSA/CSC, and the peaks between 1550-1558 cm<sup>-1</sup> correspond to the amide II band in CSA/CSC<sup>655</sup>. A discernible difference in the FTIR spectra of the materials was the broadening/diminution of peaks at ca. 970 cm<sup>-1</sup> from the aromatic hydrogens suggestive of C-C bond formation during polymerisation, with broadening of bands at 1500-1520 cm<sup>-1</sup> (aromatic C=C bonds) and the weak band at ca. 1580 cm<sup>-1</sup> (aromatic C=C). Peaks at ca. 1200-1210 cm<sup>-1</sup> corresponding to phenolic OH,<sup>600, 601</sup> and at ca. 1560-1570 cm<sup>-1</sup> corresponding to the C=O bond of the carboxylic acid functional groups are present in the spectra of polyDOPAs<sup>630-633</sup> and polyHGA,<sup>604</sup> albeit broader

<sup>552</sup>. The broad bands at ca. 3000 cm<sup>-1</sup> attributed to aromatic C-H, and at 3400-3200 cm<sup>-1</sup> attributed to stretching vibrations of the OH in all polymers and NH<sub>2</sub> in polyDOPAs (confirming that the particles are composed of model melanin and biopolymer dopants).

630-633

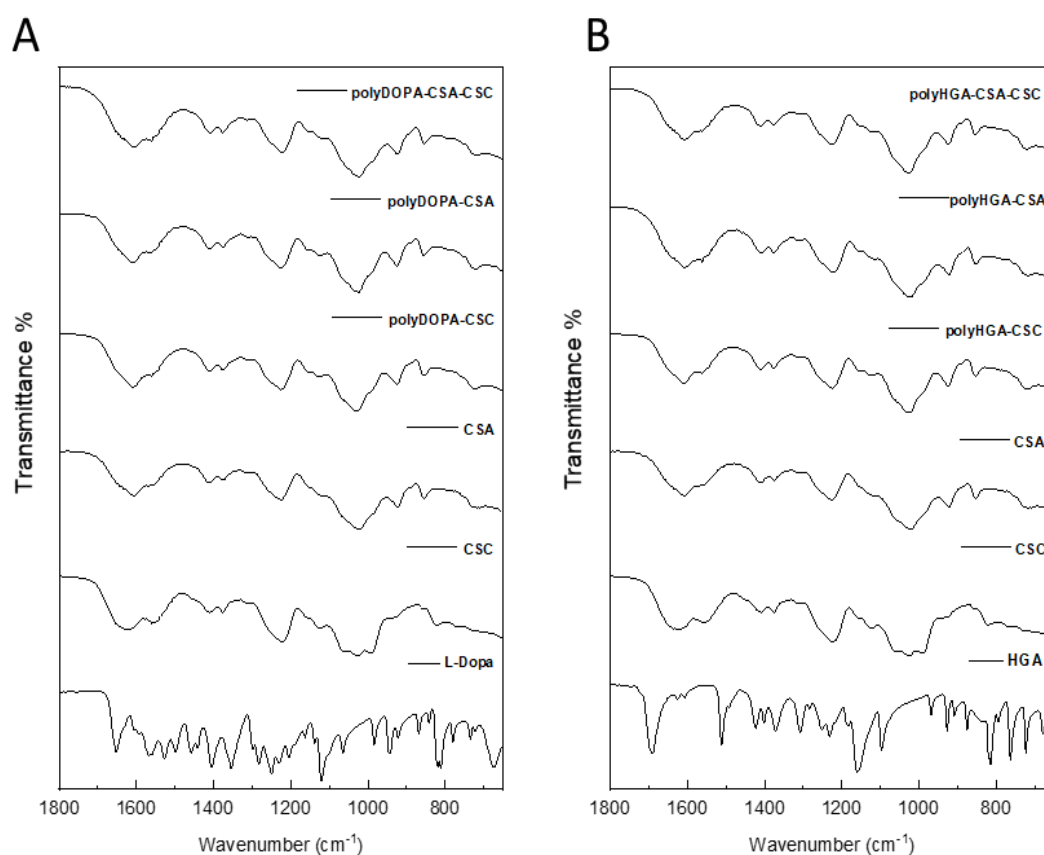


Figure 5.6: FTIR spectra of monomers and polymers studied herein.

NMR is routinely used to study biomolecules including melanins and the ECM<sup>656</sup>, with ssNMR data for CSA and CSC<sup>657</sup>, polyDOPA<sup>658</sup> and cartilage containing pyomelanin (naturally occurring polyHGA which is likely to contain other aromatic species in the polymer backbone)<sup>203</sup> reported in the literature. The <sup>13</sup>C ssNMR spectra recorded of the ECM components (CSA and CSC) shown in (Figure 5.7) are in line with the literature

<sup>657</sup>. The ssNMR spectra of CSA shows peaks for the acetamidodeoxyhexose at 24.0 ppm (CH<sub>3</sub>), 53.0 ppm (carbon A-2), 62.5 ppm (carbon A-6), 76.0 ppm (carbon A-5), 77.0 ppm (carbon A-4), 81.9 ppm (carbon A-3), 101.2 ppm (carbon A-1), and 176.4 ppm (Ac); and of D-glucosyluronic acid at 73.8 ppm (carbon U-2), 75.1 ppm (carbon U-3), 78.1 ppm (carbon U-4 and carbon U-5), 105.0 ppm (carbon U-1) and 175.7 ppm (carbon U-6). The ssNMR spectra of CSC shows peaks for the acetamidodeoxyhexose at 24.0 ppm (CH<sub>3</sub>), 52.4 ppm (carbon A-2), 69.0 ppm (carbon A-4 and carbon A-6), 75.4 ppm (carbon A-5), 81.3 ppm (carbon A-3), 102.7 ppm (carbon A-1), 176.3 ppm (Ac); and D-glucosyluronic acid at 74.1 ppm (carbon U-2 and carbon U-3), 78.0 ppm (carbon U-5), 82.5 ppm (carbon U-4), 105.4 ppm (carbon U-1) and 175.4 ppm (carbon U-6). The reason the peaks are broad in the NMR spectra is because of the disordered nature of the polymer structure which results in a distribution of local structural environments for any particular chemical group and therefore a distribution in the chemical shift (line broadening), which is an inherent limitation on the resolution when looking at polymers. The <sup>13</sup>C ssNMR spectra of the polyDOPA-CSA, polyDOPA-CSC, polyDOPA-CSA-CSC, polyHGA-CSA, polyHGA-CSC and polyHGA-CSA-CSC, show relatively minor changes in peak shapes/widths etc. to the spectra of the constituent CSA/CSC because of the small quantity of polyDOPA or polyHGA present in the materials studied herein, and moreover, the unpaired electrons in the melanins will wipe out the signal from anything in the vicinity so that it cannot be observed (i.e., the NMR spectrum is not representative of the structure near any radicals, metal ions); so what we are observing in the ssNMR is the portion of CSA/CSC that is not interacting strongly with the melanins owing to the large excess of CSA/CSC used during the synthesis (10:1 mass ratio of CSA/CSC:melanin precursor).

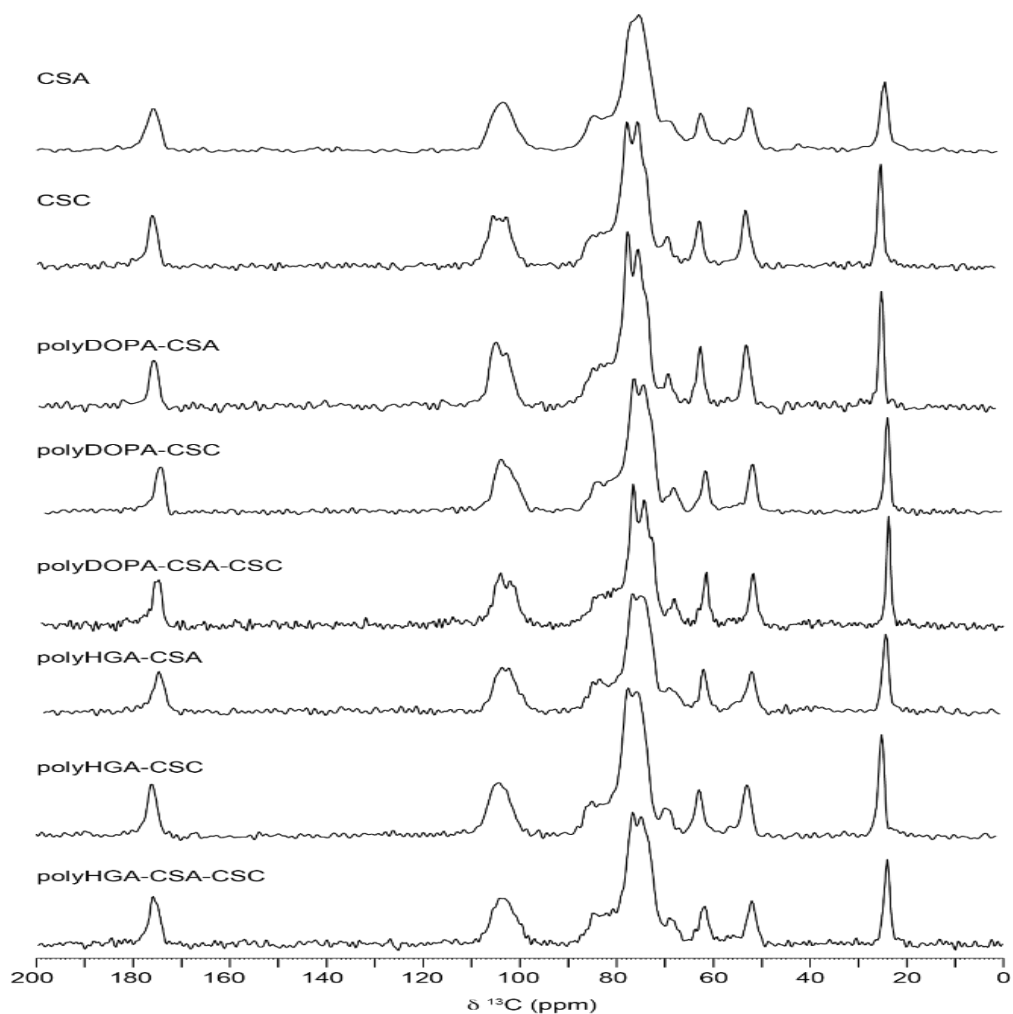


Figure 5.7:  $^{13}\text{C}$  ssNMR spectra of the materials studied herein.

Cyclic voltammetry can be used to study the reduction/oxidation processes and electron transfer properties of polyphenols such as those studied herein (voltammograms for DOPA, HGA, CSA and CSC at pH 5 and 7.4 are shown in **(Figure A.3.3, Appendices)**, for polyDOPA-CSA, polyDOPA-CSC and polyDOPA-CSA-CSC at pH 5 and 7.4 are shown in **(Figure A.3.4, Appendices)**, and for polyHGA-CSA, polyHGA-CSC and polyHGA-CSA-CSC at pH 5 and 7.4 are shown in **(Figure A.3.5, Appendices)**). The cyclic voltammograms of the polymers generated in this study at pH 5 typically show anodic peaks at ca. 0.56 V and the corresponding cathodic peak at ca. 0 V vs Ag/AgCl

(reference electrode), whereas, at pH 7.4 the oxidation and reduction peaks were less well resolved, i.e., the polymers were electroactive in acidic medium, yet less clear electroactive responses in neutral medium (not defined peaks). This is consistent with the literature for polyDOPAs<sup>635</sup> and polyHGAs,<sup>604</sup> and confirms the role of protons in the electroactivity of the polymers<sup>570</sup>. The cyclic voltammograms are consistent after multiple scans demonstrating their stability under the experimental conditions for the duration of the experiment, and their unsymmetrical cathodic and anodic peaks are attributed to the difference in background current and kinetic limitations.<sup>570</sup>

The electronic properties of the samples studied herein were assessed using conductive tip AFM (**Figure A.3.6, Appendices**) to understand if their conductivity was measurable (potentially contributing to the electrophysiology of tissues or indeed useful for application in electronic devices). Interestingly, the products were measurably conductive (**Figures 5.8**). The differences in the electronic properties of the polymers<sup>598, 636, 637</sup> are likely to be related to a subtle combination of the extended conjugation length of the polyDOPAs and polyHGAs produced; their hierarchical assembly with the ECM components CSA and/or CSC (governed by intramolecular and intermolecular interactions);<sup>48, 638</sup> and the ability of the anionic component of the polymers to serve as a dopant for the polymers (supported by zeta potential measurements), akin to self-doped conducting polymers.<sup>639-642</sup>

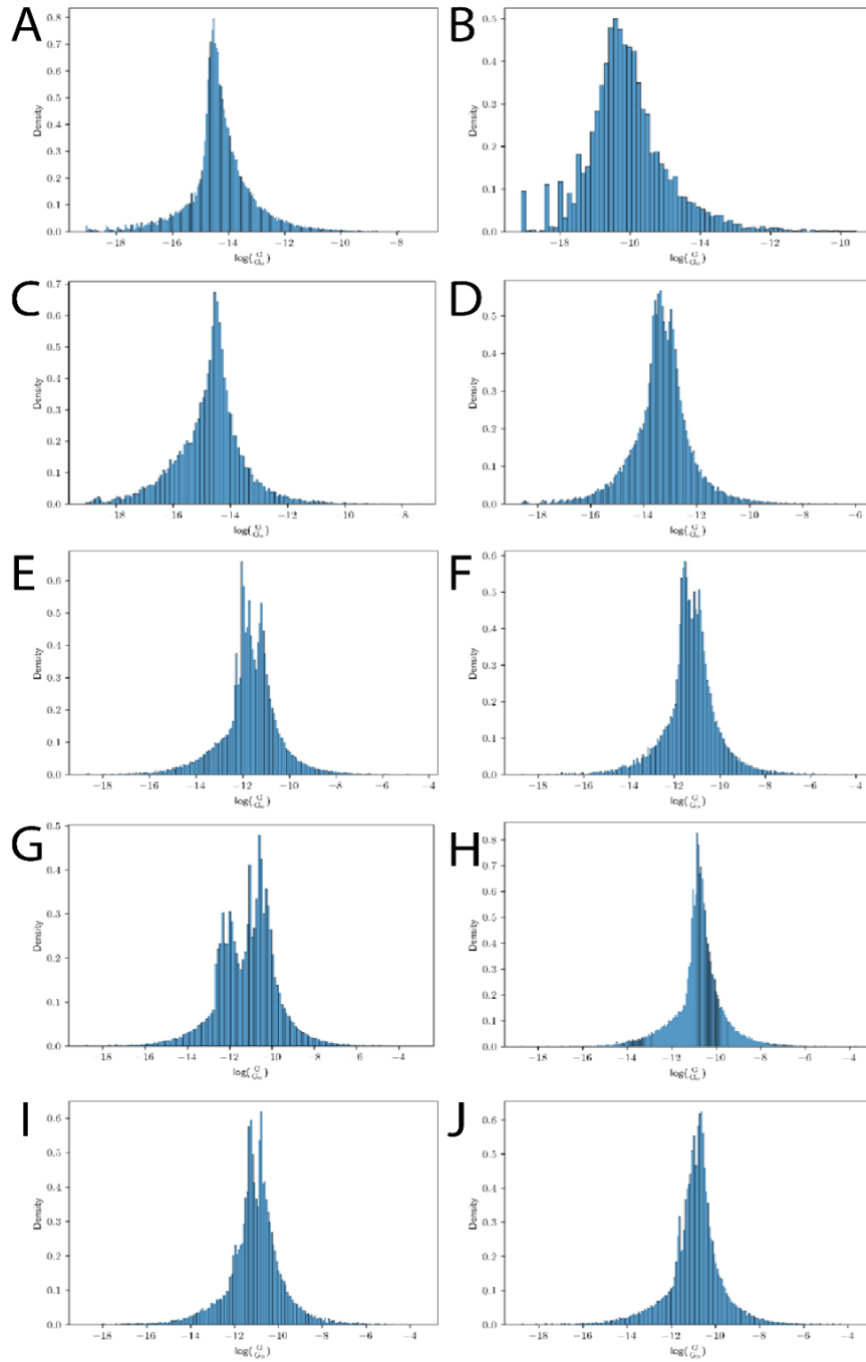


Figure 5.8: I-V measurements for materials studied herein. A) DOPA. B) HGA. C) CSA. D) CSC. E) polyDOPA-CSA. F) polyDOPA-CSC. G) polyDOPA-CSA-CSC. H) polyHGA-CSA. I) polyHGA-CSC. J) polyHGA-CSA-CSC. Data courtesy of Sam

## 5.4 Conclusion

Herein polymerisation of a variety of phenolic monomers (DOPA or HGA) in the presence of ECM components (CSA and/or CSC), yielded conjugated polymer-based materials polyDOPA-CSA, polyDOPA-CSC, polyDOPA-CSA-CSC, polyHGA-CSA, polyHGA-CSC or polyHGA-CSA-CSC, respectively. A variety of analytical techniques (UV-Vis, zeta potential, ssNMR, XPS, TEM, XRD, FTIR, CV, and conductivity measurements) were employed to examine the polymers produced, which showed evidence of ionic interactions between the model melanins and ECM component. The experiments revealed interesting trends in the properties of the polymers, notably conductivity measurement data for the polymers confirmed they displayed measurable conductivity, with electronic properties tuned by the functional groups pendant on the polymer backbones (which served as dopants) suggesting their potential for changing the electronic properties of tissues and in degradable electronic devices<sup>551, 643</sup>.

# 6 Pyomelanin-ECM interactions

## Overview

Melanins are conjugated biopolymers with varying compositions and functions, found in various tissues throughout the body. Here we examine the conjugated polymers derived from homogentisic acid (HGA), polyHGA (a simplified model of pyomelanin), formed in an ex vivo tendon model with a view to understanding interactions between melanins and the extracellular matrix (ECM) using a selection of different analytical techniques, including spectroscopy (energy dispersive X-ray, infrared and Raman), X-ray diffraction and microscopy (electron, optical and scanning electrochemical). The combination of techniques facilitated an understanding of subtle differences in the composition and distribution of ECM component, hydroxyapatite and melanin in the tendons for the first time.

## 6.1 Introduction

Melanin in healthy tissues is typically found in specialised cells or areas of the body, such as melanocytes of the skin or the substantia nigra in the brain. Melanin is normally not associated with ECM proteins, although a melanin like polymer, polyHGA, has been shown to associate with ECM proteins such as collagen and GAGs of the ECM in AKU<sup>387, 659</sup>. Whilst melanin is not typically found in the extracellular matrix of healthy tissues, its precursor – tyrosine (TYR) and the intermediate dopaquinone, as well as other polyphenol and quinones have shown the ability to bind collagen and stiffen it<sup>660</sup>. Whilst stiffer collagen is beneficial in some instances, it is a challenge to get the level of stiffness correct, given that overly stiff collagen alters mechanical loading through the tissue(s), often pathologically through stress shielding in tendons and bone<sup>339, 661</sup>, as well as through fibrosis in lung tissues<sup>662</sup>.

Phenolic monomers are common building blocks of melanins (observed in allomelanin, eumelanin, neuromelanin, pheomelanin and pyromelanin),<sup>656</sup> and are known to play important roles in intermolecular/material interactions.<sup>595-597</sup> Here we examine the properties of conjugated polymers derived from phenolic monomer homogentisic acid (HGA) polymerised in the presence of ECM components from Turkey tendon *ex vivo*. A selection of different analytical techniques was employed for these studies, including: Raman spectroscopy, X-ray diffraction (XRD), Fourier-transform infrared (FTIR) spectroscopy, scanning electron microscopy (SEM), energy dispersive X-ray (EDX) spectroscopy, and scanning electrochemical microscopy (SECM). The properties of the materials offer insights into the role of functional groups pendant on the polymer

backbones on melanin-ECM interactions using simple model systems (polyHGA-tendon in this case).

## **6.2 Experimental Section**

### **6.2.1 Preparation of samples:**

Two turkeys, aged 20 weeks, were purchased from a farm, and killed in accordance with UK food and farming standards. Prior to dissection the turkeys were stored at -20°C. *M. flexor hallucis longus* and *M. flexor digitorum* were targeted for removal from each leg, as they are the longest tendons present in the leg of the turkey. The tendons were placed in solutions of 0.33 $\mu$ M or 0.33 mM of HGA in PBS or in a control solution of PBS, and incubated at 37°C for 7 days.

### **6.2.2 Raman Spectroscopy:**

Raman spectra were acquired from the tendons using an InVia Raman microspectrometer (Renishaw Ltd), equipped with a 785 nm laser. Spectra were acquired at 100% laser power (2 mW at sample) at 30 seconds and 2 accumulations. Prior to spectral acquisition tendons were thawed at ambient temperature. Data was collected from the tendons in the same orientation, acquiring spectra from the distal to proximal end. An origin was set 1 cm superior to the bifurcation point (distal end) of the tendon. Spectra were collected along the length of each tendon at 10 mm intervals, with the spectra labelled as belonging to the proximal, middle or distal thirds for subsequent analysis. All spectra were baseline corrected using polynomial order 7, and vector normalized. Principal component analysis (PCA) was performed, which is an unsupervised technique that forms linear components, and considers the data as a set,

with classes color coded after analysis. Visualisation of the scores plot reveals any patterns in the data, where the closer two points are the more similar they are spectrally, and therefore biochemically, and vice versa. Univariate analysis of 1/full width and half height of the phosphate peak was performed to determine the crystallinity of the phosphate peaks.

### 6.3 Results and Discussion

With a view to understand pyomelanin-ECM interactions (e.g., potential role of the ECM in controlling the distribution of melanin in tissues), HGA (**Figure 6.1**) was polymerised (via autooxidation) in the presence of the extracellular matrix (ECM) components (ex vivo Turkey tendon model). The polymerisation of HGA in the tendon resulted in the coloration of the tendon due to the formation of ochronotic pigment due to the presence of nanoscale particles of tens-hundreds of nm composed of conjugated polymers (the formation of which is proposed to proceed via a nucleation and growth mechanism)<sup>48</sup> that may further aggregate to larger structures<sup>618</sup>.

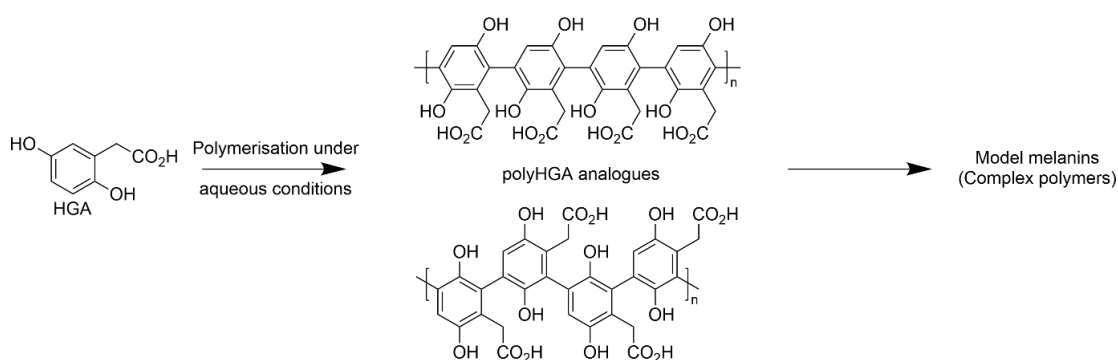


Figure 6.1: Schematic of the polymerization of homogentisic acid (HGA) to form polyHGA, a simplified model of pyomelanin studied herein. It is important to note that natural pyomelanin samples may contain other monomers depending on the conditions under which they are formed in vivo.

The average Raman spectra from the untreated (control) tendons indicate that, although the turkeys were 20 weeks old the mineralisation status of the distal ends of the tendons are incomplete. Specifically, from 12 to 18 weeks of age the tendons mineralise at the proximal and then distal ends, leaving the central third non-mineralised. The spectra in **(Figure 6.2.A)** have a clear phosphate peak ( $960\text{ cm}^{-1}$ ) in the proximal spectra, no phosphate peak in the central third, and a developing peak in the distal third; likewise, the XRD patterns **(Figure A.4.1, Appendices)** for the untreated control tendons show peaks between  $2\theta\ 31\text{-}33^\circ$  characteristic of hydroxyapatite for the proximal and distal samples, but not the mid-point. Interestingly, non-mineralised collagen (evident from the proline peak at  $920\text{ cm}^{-1}$  in the Raman spectra) is more distinct in the distal compared to the proximal spectra; furthermore, the relative amount of collagen present is higher in the central third, compared to either end. PCA analysis of the untreated compared to the two HGA treated groups reveals that the high concentration is more distinct and separate from the lower concentration and untreated groups. As is demonstrated from the spectra in **(Figure 6.2.C and D)**, the presence of high concentration HGA led to the collection of very noisy spectra, with none being able to be collected from the treated distal tendon. At the point of spectral collection, the high concentration treated tendons resulted in a saturated detector i.e., a large amount of light flooding the detector, meaning that no measurements could be acquired. A comparison of what is happening at each of the three areas of the tendon shows that the effect of the lower concentration HGA on the distal tendon decreases the mineral content relatively. This is also demonstrated in the proximal third of the tendons, to a higher extent. In the central third, which did not contain collagen, there was less of an affect, with the spectra visually comparable. Due to the number of samples, further multivariate analysis was not possible. However, a comparison of  $1/\text{FWHM}$  revealed that the untreated proximal and

distal spectra were more mature i.e., had a higher degree of crystallinity, compared to the tendons treated with a low concentration of HGA (data available on request). This observation is supported by XRD data, noting that XRD patterns of the samples (**Figure A.4.1, Appendices**) suggested that with the exception of hydroxyapatite the samples were largely amorphous at the microscale (i.e., molecular lattice, unit cell dimension symmetry), characteristic of collagen and natural/synthetic melanins<sup>625-628, 663, 664</sup>. Overall, the treatment of high concentration of HGA was disruptive to the tendons to the point where measurements could not be equally acquired from all tendons. A comparison of untreated to low concentration HGA treatment shows, that in areas of the tendons that are mineralised the mineral components are reduced and less mature, potentially due to the HGA either blocking the mineral or disrupting it (supported by XRD data). In the central region there was less of an effect, however, this warrants further investigation with more samples, as it is known that naturally non-mineralised collagen is affected in AKU, the condition where people have an excess of HGA.

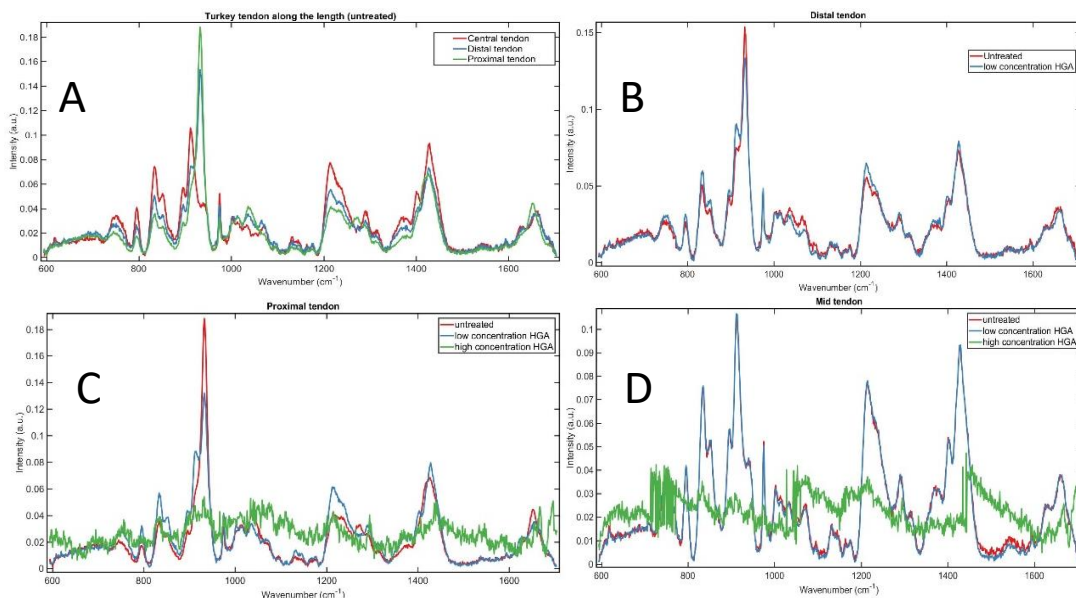


Figure 6.2: Raman spectra of tendons studied herein. A) Turkey tendon along the length (untreated). B) Distal section of tendon. C) Proximal of tendon. D) Mid-point section of tendon.

FTIR spectroscopy was used to analyse the samples studied herein which were complex due to the variety of chemical environments (**Figure 6.3, Figure A.4.2, Appendices**). The spectra for all samples showed peaks characteristic of the ECM components in tendon, particularly the amide I (1620-1680  $\text{cm}^{-1}$ ), amide II (1510-1560  $\text{cm}^{-1}$ ), amide III (1190-1320  $\text{cm}^{-1}$ ), amide A (3305  $\text{cm}^{-1}$ ) and amide B (2936  $\text{cm}^{-1}$ ) bands from the proteinaceous content, and peaks characteristic of arginine (a strong absorption between 1688–1695 $\text{cm}^{-1}$  from  $\nu_{\text{as}}(\text{CN}_3\text{H}_5^+)$ , and a weaker absorption at 1576–1577 $\text{cm}^{-1}$  from  $\nu_{\text{s}}(\text{CN}_3\text{H}_5^+)$ ), however, these may overlap with amide I and II peaks; peaks characteristic of proline (at 1456  $\text{cm}^{-1}$  from  $\delta\text{CH}_2$ , and at 1400-1454  $\text{cm}^{-1}$  from  $\nu\text{CN}$ ); and peaks characteristic of aspartic acid (at 1729  $\text{cm}^{-1}$  from  $\nu(\text{C}=\text{O})$  of the carboxylic acid, at 1570  $\text{cm}^{-1}$  from  $\nu_{\text{as}}(\text{COO}^-)$ ). While it is plausible the peak between 850-890  $\text{cm}^{-1}$  corresponds to the  $\nu_2$  carbonate region (particularly at 884  $\text{cm}^{-1}$ ), and the peak between 900-1180  $\text{cm}^{-1}$  corresponds to the  $\nu_1, \nu_3$  phosphate region of apatite (particularly at 978  $\text{cm}^{-1}$  and 1030  $\text{cm}^{-1}$ ), it is possible the peaks are from other functional groups in the samples (e.g., aromatic C-H bonds). While it is easy to visually assess the presence of polyHGA in samples due to their coloration (i.e., tendon incubated with low and high concentrations of HGA) the spectra are convoluted due to overlapping peaks in the region corresponding to phenolic OH, C=O bond of the carboxylic acid functional and aromatic C=C bonds, at 1200-1210  $\text{cm}^{-1}$ , 1560-1570  $\text{cm}^{-1}$  and 1500-1510  $\text{cm}^{-1}$ , respectively.

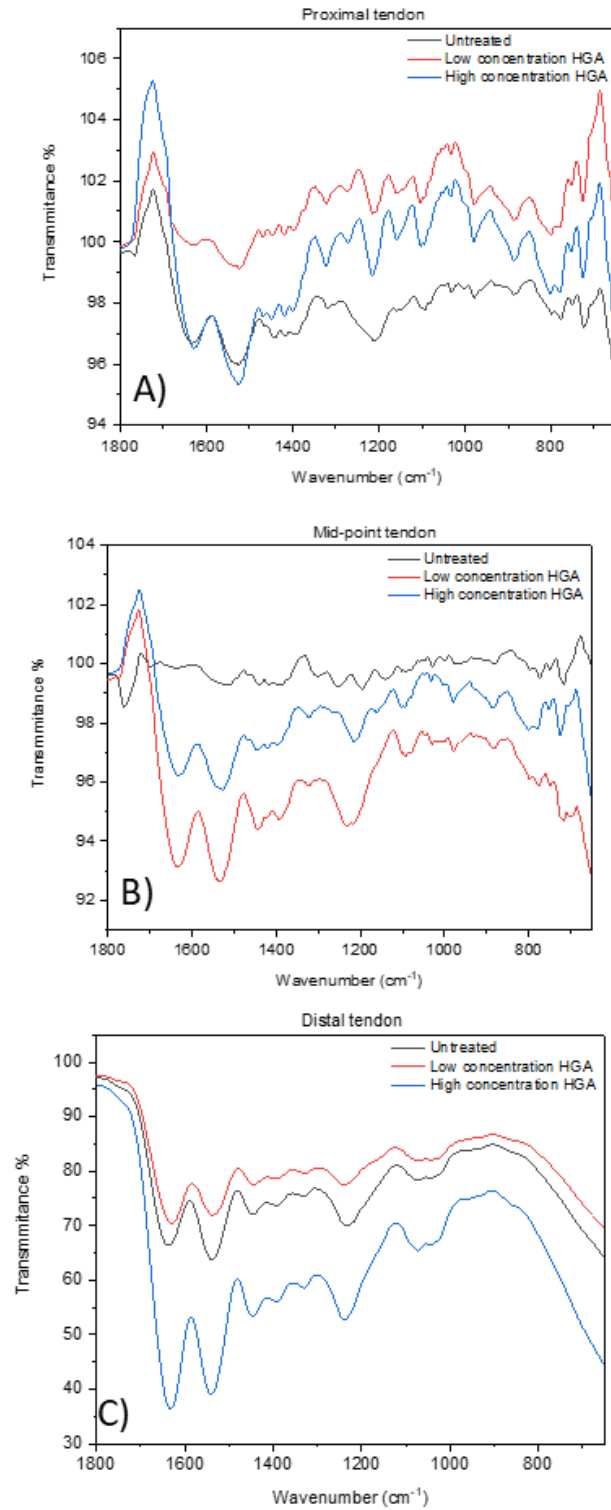
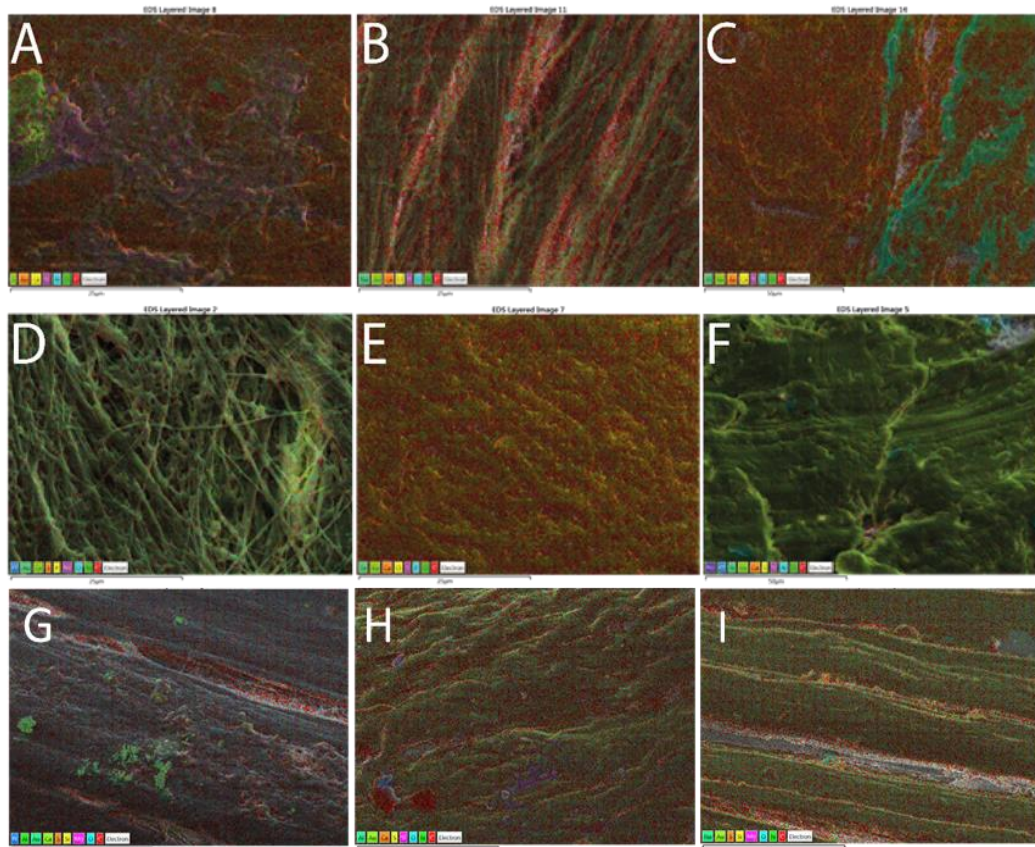


Figure 6.3: FTIR spectra of tendons studied herein. A) Proximal section of tendon. B) Mid-point of tendon. C) Distal section of tendon.

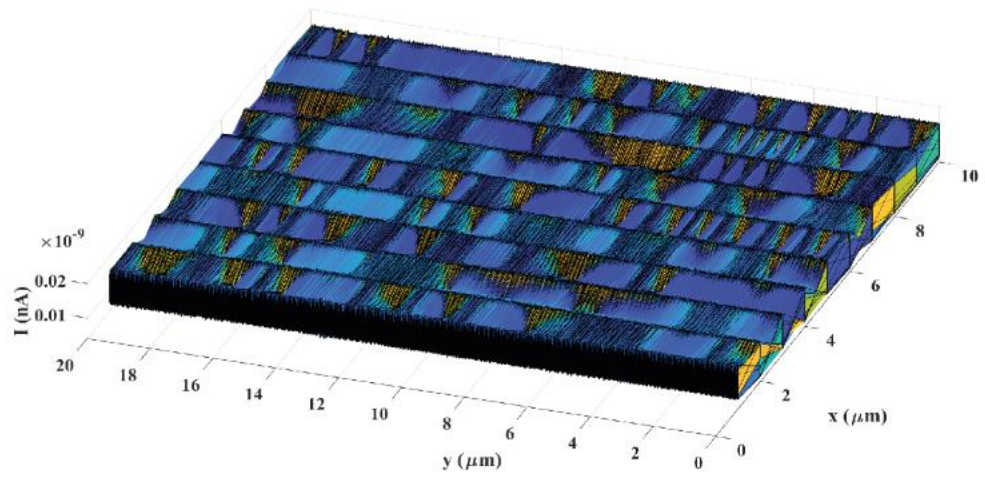
SEM images of the samples (**Figure 6.4**) shows a degree of organisation of the collagen fibrils characteristic of tendon tissue, and exposure to high concentrations of HGA and concomitant polyHGA deposition disrupts this organisation. EDX data suggests that all samples are mainly composed of C, N, O, P and S characteristic of proteins and other biomolecules, with additional traces of Cl, K, Na, P from the buffer, however, quantitative comparison not possible.



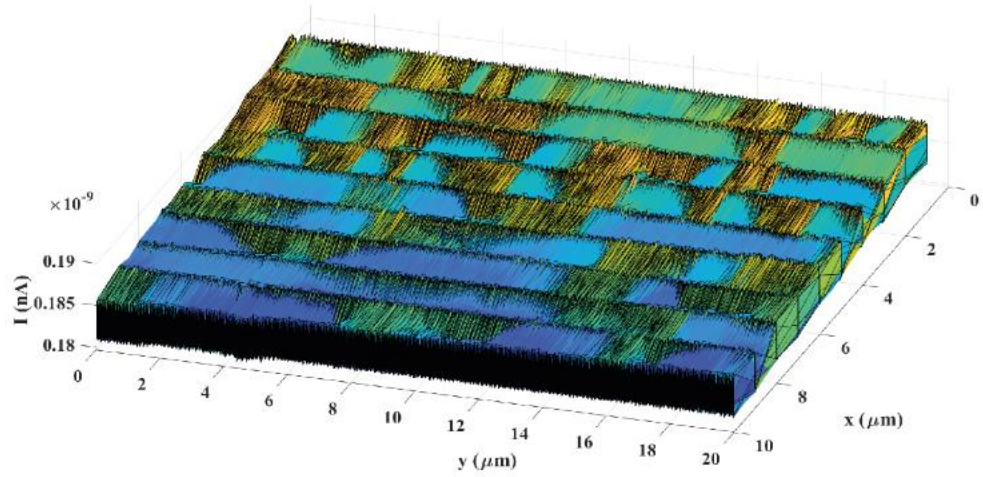
*Figure 6.4: SEM. A) Proximal section of tendon (control). B) Proximal section of tendon (low [HGA]). C) Proximal section of tendon (high [HGA]). D) Mid-point section of tendon (control). E) Mid-point section of tendon (low [HGA]). F) Mid-point section of tendon (high [HGA]). G) Distal section of tendon (control). H) Distal section of tendon (low [HGA]). I) Distal section of tendon (high [HGA]).*

Scanning probe microscopy uses various probes to analyse the surface of samples enabling examination of a multitude of properties, and scanning electrochemical microscopy (SECM) enables studies of electrochemical processes on a variety of surfaces including for biological samples<sup>521, 665-668</sup>. SECM (recorded in the laboratory of Jane Stockman in Canada) shows differences in conductivity between the samples (**Figures 6.5, 6.6 and 6.7**). All samples have low background measurable conductivity in the nA regime, and those samples prepared with a biomimetic concentration of HGA (low), or higher concentration of HGA (high) used for accelerated studies, have a small number of features (spikes) that are discernibly more conductive which we ascribe to the presence of polyHGA particles embedded in the tendons.

A



B



C

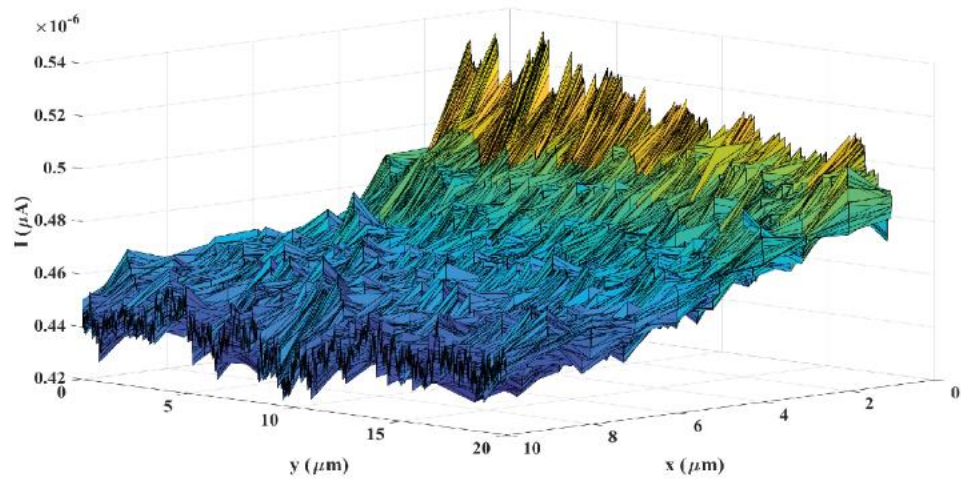


Figure 6.5: SECM. A) proximal section of tendon (control). B) proximal section of tendon low [HGA]. C) proximal section of tendon (high [HGA])

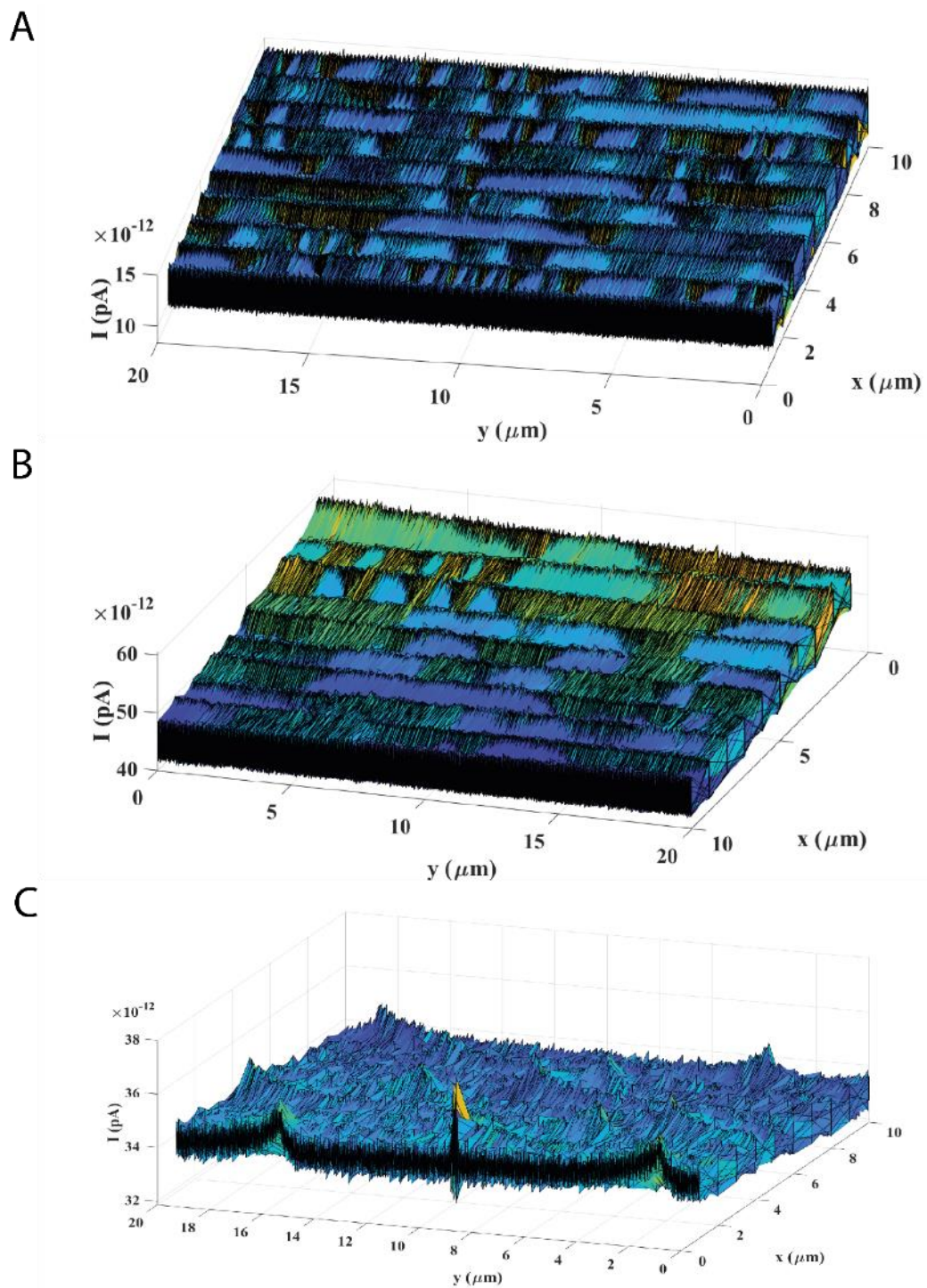


Figure 6.6: SECM. A) Mid section of tendon (control). B) Mid section of tendon low [HGA]. C) Mid section of tendon (high [HGA])

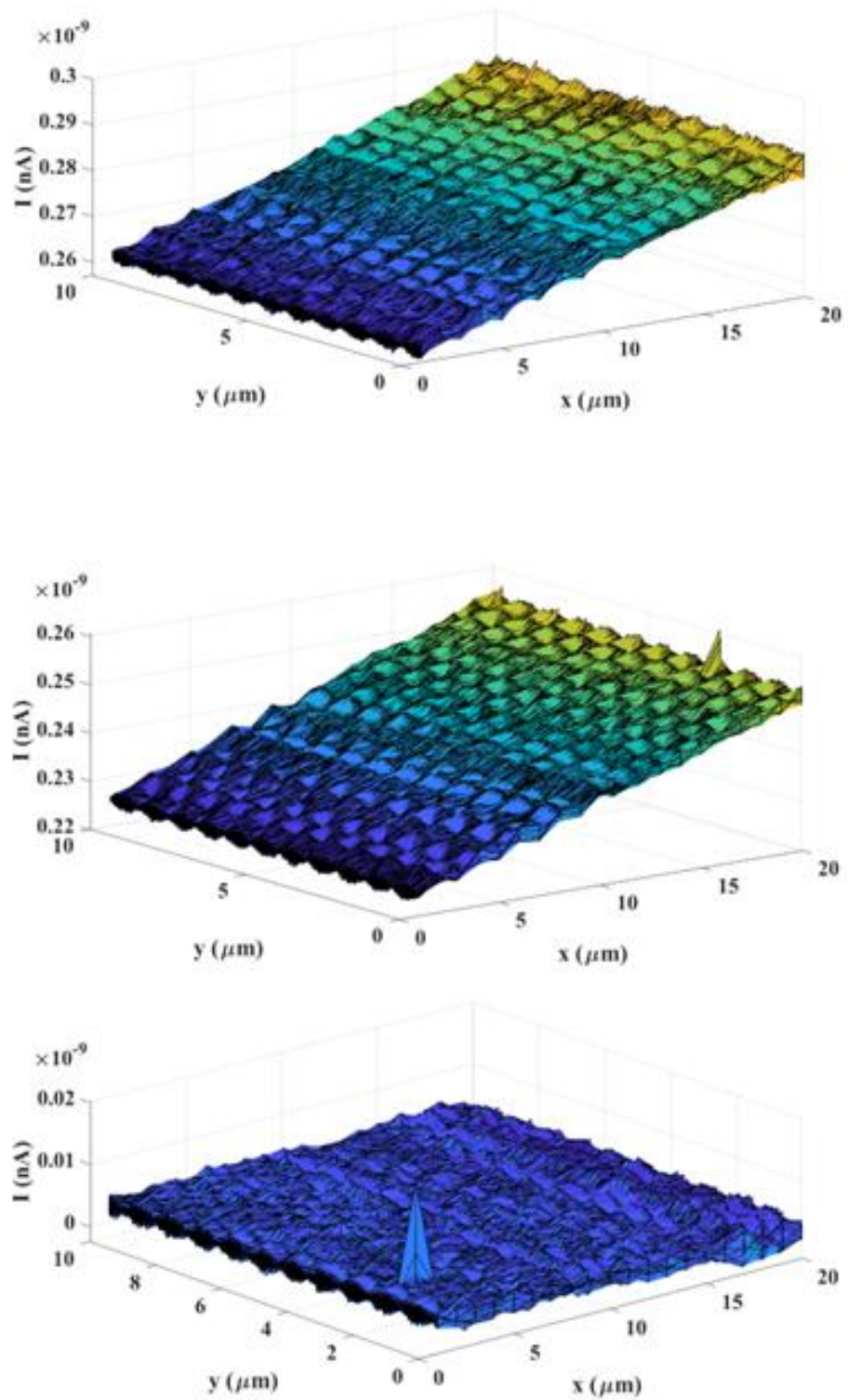


Figure 6.7: SECM. A) Distal section of tendon (control). B) Distal section of tendon low [HGA]. C) Distal section of tendon (high [HGA])

## 6.4 Conclusion

Herein polymerisation of a HGA in the presence of ECM components (an ex vivo turkey tendon model), yielded conjugated polymer-based materials polyHGA in ECM. A variety of analytical techniques (Raman, XRD, FTIR, SEM-EDX, and SECM) were employed to examine the composites produced. The experiments revealed interesting trends in the distribution of ECM/hydroxyapatite/melanin at different points in the tendons, with SECM offering insights into the conductivity of the tissues which may play a role in their electrophysiology and therefore their function. Importantly what we have learned is the complex biological processes underpinning alkaptonuria affect the physicochemical properties of tissues.

# 7 Conclusion & Future Work

## 7.1 Conclusion

The aim of this PhD was to investigate melanin formation/deposition using a variety of analytical techniques which may enhance our understanding of the deposition of pyomelanin *in vivo*. This involved a detailed review of the literature describing the application of analytical techniques to study melanins which helped identify open questions and opportunities for research.

The first results chapter in the thesis analysed the polymerisation of homogentisic acid (HGA) *in vitro* to help understand if the (bio)chemical environment (e.g., pH and enzymes) play a role in the polymerisation of HGA, as this will play a role in where AKU deposits are formed in the body. We observed some enzymes were better than others at polymerising the HGA (peroxidase  $\geq$  laccase  $>$  tyrosinase  $\approx$  no enzyme control), with subtle variations in yields at pH 5 or 7.4. The oxidation and reduction peaks were not well resolved, i.e., the polyHGAs were electroactive in acidic medium while electro-inactive in neutral medium, confirming the role of protons in the electroactivity of the polyHGA (akin to polycatechol films, and the polyHGAs generated in the presence of laccase at pH 7.4 or peroxidase at either pH 5 or pH 7.4 were measurably conductive).

The second results chapter in the thesis analysed the polymerisation of similar phenols (catechol and levodopa) *in vitro* to understand if the (bio)chemical environment (e.g., monomers available) played a role in the structure of the melanins formed, and their properties. The polymers displayed measurable conductivity, with electronic properties

tuned by the functional groups pendant on the polymer backbones (which served as dopants) suggesting their potential for application in electronic devices.

The third results chapter in the thesis analysed the polymerisation of HGA and DOPA in the presence of components of the extracellular matrix (ECM) *in vitro* to understand if the (bio)chemical environment (e.g., ECM available – exemplified with chondroitin sulfate A and C) may play a role in the structure of the melanins formed, and their properties. The melanin-ECM composites displayed measurable conductivity, with electronic properties tuned by the functional groups pendant on the polymer backbones (which served as dopants).

The fourth results chapter in the thesis analysed polymerisation of HGA in an *ex vivo* tendon model with a view to understanding interactions between melanins and the extracellular matrix (ECM) observing subtle differences in the composition and distribution of ECM component, hydroxyapatite and melanin in the tendons.

## **7.2 Future work**

The thesis offers insights into melanin formation in various contexts and opens the door for a significant amount of future work at the interface of different disciplines. It is widely recognised that for people with alkaptonuria, over many years homogentisic acid slowly builds up in tissues throughout the body. The build up can happen almost everywhere in the body, including the blood vessels, bones, cartilage, ears, eyes, heart, nails, tendons, etc., resulting in discoloration of the tissues (typically much darker than normal), causing a wide range of problems. Logical extrapolations in future experiments

from this thesis include working with biologists to understand any correlation between the biochemical microenvironment in tissues and AKU deposits formed in the body.

The first results chapter focused on the polymerization of HGA to form polyHGA (a simplified version of pyomelanin) in the absence or presence of enzymes (a laccase, peroxidase, or tyrosinase) at either pH 5.0 or 7.4. A variety of analytical techniques were employed to examine the polyHGAs produced under the experimental conditions. The experiments revealed interesting trends in the yields of polyHGAs produced with subtle differences in their properties; notably, C-AFM data for polyHGAs showed that those generated in the presence of LACC at pH 7.4, or HRP at pH 7.4 or 5.0, respectively, displayed measurable conductivity. Examples of specific experiments arising from this chapter include (but are not limited to) further studies that seek to mimic the natural ECM environment, i.e., systematic variation of the ECM components, enzymes (type, concentration) and/or other biochemical conditions in different tissue niches in which it is possible to deposit pigments.

The second results chapter focused on the polymerization of a variety of phenolic monomers (CAT, DOPA, and HGA), yielding conjugated polymers polyCAT-HS, polyCAT-LS, polyDOPA-HS, polyDOPA-LS, or polyHGA-HS, respectively. A variety of analytical techniques were employed to examine the polymers produced. TEM and SEM images reported here show the structure of the polyHGA particles that have similarities to those of polyDOPA formed in geometrically unconstrained conditions. The significance of our findings on HGA and poly-HGA is important for the field of Alkaptonuria, where it has long been discussed that the polymeric material that is accumulated from HGA is a polymer derived from benzoquinone acetic acid. This has appeared in the literature regarding the disease for many decades, with recent interest

and advances in understanding the pathophysiological processes shedding new light on the chemical behavior of HGA in tissues and cells. Examples of specific experiments arising from this chapter include (but are not limited to) further studies that seek to mimic the natural ECM environment, i.e., systematic variation of the ECM components, monomers (a wider selection of monomer types, mixtures of monomers, concentrations, etc.) and/or other biochemical conditions in different tissue niches in which it is possible to deposit pigments. This might help explain why some tissues are more likely to be pigmented than others.

The third results chapter focused on the polymerization of a variety of phenolic monomers (DOPA or HGA) in the presence of ECM components (CSA and/or CSC), yielding conjugated polymer-based materials polyDOPA-CSA, polyDOPA-CSC, polyDOPA-CSA-CSC, polyHGA-CSA, polyHGA-CSC or polyHGA-CSA-CSC, respectively. A variety of analytical techniques were employed to examine the polymers produced. The experiments revealed interesting trends in the properties of the polymers, notably conductivity measurement data showed the electronic properties tuned by the functional groups pendant on the backbones of both the polyDOPA/polyHGA/CSA/CSC (which served as dopants). Examples of specific experiments arising from this chapter include (but are not limited to) further studies that seek to mimic the natural ECM environment, i.e., systematic variation of the ECM components (variation of the structures of the ECM biopolymers, i.e., polysaccharides, proteins, etc.), monomers, and/or other biochemical conditions in different tissue niches in which it is possible to deposit pigments. The presence of other biopolymeric components of the ECM (e.g., proteins such

as collagen, polysaccharides such as hyaluronic acid, proteoglycans, etc.) in vitro is expected to help us to understand if/how the biopolymers tune the properties of the materials.

The fourth results chapter focused on the polymerization of a HGA in the presence of ECM components (an ex vivo turkey tendon model), yielding conjugated polymer-based materials (polyHGA in ECM) that were studied by a variety of analytical techniques. The experiments revealed interesting trends in the distribution of ECM/hydroxyapatite/polyHGA at different points in the tendons, with SECM offering insights into the conductivity of the tissues which may play a role in their electrophysiology. The conductivity of polyHGA is a novel finding in this study and raises questions about the involvement it may have in neurological role(s) in AKU. There is currently no evidence of significant differences in nerve conduction speeds in patients with AKU compared to normal/control subjects, this could partly be due to the limited number of AKU patients able to participate due to the rarity of the condition, but likely warrants further investigation. AKU patients have been detailed with Parkinson's Disease in the medical literature, it is not clear whether this is above the presence in the wider non-AKU population. There is also a growing body of literature around the presence of ochronotic pigment in neurological tissues and those that surround them, raising the question of whether there is any role of HGA or polyHGA in the nervous system and presentation of multiple neurological symptoms that AKU patients present with clinically. Examples of specific experiments arising from this chapter include (but are not limited to) further studies that seek to study the deposition of polyHGA in other ex vivo models to help elucidate the role of the natural ECM environment on pigment deposition; furthermore, electrophysiology studies of

diseased/healthy tissues to help us to understand if/how the melanins may be playing a role in neurological disorders or other conditions associated with ageing.

## REFERENCES

1. K. J. J. o. C. P. A. Arikawa, 2003, **189**, 791-800.
2. T. W. Cronin and N. J. Marshall, *Nature*, 1989, **339**, 137-140.
3. L. de Andres-Bragado and S. G. Sprecher, *Curr Opin Insect Sci*, 2019, **36**, 25-32.
4. D. Osorio and M. Vorobyev, *Vision Research*, 2008, **48**, 2042-2051.
5. B. C. Regan, C. Julliot, B. Simmen, F. Viénot, P. Charles-Dominique and J. D. Mollon, *Philosophical transactions of the Royal Society of London. Series B, Biological sciences*, 2001, **356**, 229-283.
6. J. Marshall, K. L. Carleton and T. Cronin, *Curr Opin Neurobiol*, 2015, **34**, 86-94.
7. S. Tadepalli, J. M. Slocik, M. K. Gupta, R. R. Naik and S. Singamaneni, *Chemical Reviews*, 2017, **117**, 12705-12763.
8. J. Ren, Y. Wang, Y. Yao, Y. Wang, X. Fei, P. Qi, S. Lin, D. L. Kaplan, M. J. Buehler and S. Ling, *Chemical Reviews*, 2019, **119**, 12279-12336.
9. A. Gürses, M. Açıkıldız, K. Güneş and M. S. Gürses, in *Dyes and Pigments*, Springer, 2016, pp. 13-29.
10. D. I. Speiser, Y. L. Gagnon, R. K. Chhetri, A. L. Oldenburg and S. Johnsen, *Integrative and Comparative Biology*, 2016, **56**, 796-808.
11. S. T. Williams, *Biological Reviews*, 2017, **92**, 1039-1058.
12. S. Williams, S. Ito, K. Wakamatsu, T. Goral, N. Edwards, R. Wogelius, T. Henkel, L. de Oliveira, L. Maia and S. Strekopytov, *PLoS One*, 2016, **11**, e0156664.
13. K. J. McGraw, *Pigment Cell & Melanoma Research*, 2008, **21**, 133-138.
14. R. K. Hari, T. R. Patel and A. M. Martin, *Food Reviews International*, 1994, **10**, 49-70.
15. G. Hendry, in *Natural food colorants*, Springer, 1996, pp. 1-39.
16. F. Delgado-Vargas, A. R. Jiménez and O. Paredes-López, *Critical reviews in food science and nutrition*, 2000, **40**, 173-289.
17. N. B. Roberts, S. A. Curtis, A. M. Milan and L. R. Ranganath, in *JIMD Reports, Volume 24*, Springer, 2015, pp. 51-66.
18. G. Britton, *The biochemistry of natural pigments*, Cambridge University Press, 1983.
19. F. Solano, *New Journal of Science*, 2014, **2014**.
20. G.-E. Costin and V. J. J. T. F. j. Hearing, 2007, **21**, 976-994.
21. R. Meys, *Medicine*, 2017, **45**, 438-443.
22. P. J. T. i. j. o. b. Riley and c. biology, 1997, **29**, 1235-1239.
23. B. Larsson and H. Tjälve, *Biochemical pharmacology*, 1979, **28**, 1181-1187.
24. A.-F. Aubry, *Journal of Chromatography B*, 2002, **768**, 67-74.
25. O. Karlsson and N. G. Lindquist, *Archives of toxicology*, 2016, **90**, 1883-1891.
26. J. M. Menter, *Polymer International*, 2016, **65**, 1300-1305.
27. M. d'Ischia, K. Wakamatsu, F. Cicoira, E. Di Mauro, J. C. Garcia-Borron, S. Commo, I. Galván, G. Ghanem, K. Kenzo, P. J. P. c. Meredith and m. research, 2015, **28**, 520-544.
28. P. Meredith, C. J. Bettinger, M. Irimia-Vladu, A. B. Mostert and P. E. Schwenn, *Reports on Progress in Physics*, 2013, **76**, 034501.

29. M. Abbas, F. D'Amico, L. Morresi, N. Pinto, M. Ficcadenti, R. Natali, L. Ottaviano, M. Passacantando, M. Cuccioloni and M. Angeletti, *The European Physical Journal E*, 2009, **28**, 285-291.
30. M. Xiao, M. D. Shawkey and A. Dhinojwala, *Advanced Optical Materials*, 2020, 2000932.
31. Y. Pan, L. Hu and T. Zhao, *National Science Review*, 2019, **6**, 1040-1053.
32. A. D. Schweitzer, E. Revskaya, P. Chu, V. Pazo, M. Friedman, J. D. Nosanchuk, S. Cahill, S. Frases, A. Casadevall and E. Dadachova, *International Journal of Radiation Oncology\*Biology\*Physics*, 2010, **78**, 1494-1502.
33. K.-Y. Ju, J. W. Lee, G. H. Im, S. Lee, J. Pyo, S. B. Park, J. H. Lee and J.-K. J. B. Lee, 2013, **14**, 3491-3497.
34. C. Ninh, M. Cramer and C. J. J. B. s. Bettinger, 2014, **2**, 766-774.
35. M. Araújo, R. Viveiros, T. R. Correia, I. J. Correia, V. D. Bonifácio, T. Casimiro and A. J. I. j. o. p. Aguiar-Ricardo, 2014, **469**, 140-145.
36. M. Mohorčić, J. Friedrich, I. Renimel, P. André, D. Mandin, J.-P. J. B. Chaumont and B. Engineering, 2007, **12**, 200-206.
37. S. Ito and K. Wakamatsu, *Pigment cell research*, 2003, **16**, 523-531.
38. D. Sulzer, C. Cassidy, G. Horga, U. J. Kang, S. Fahn, L. Casella, G. Pezzoli, J. Langley, X. P. Hu and F. A. Zucca, *NPJ Parkinson's disease*, 2018, **4**, 1-13.
39. R. L. Haining and C. Achat-Mendes, *Neural regeneration research*, 2017, **12**, 372.
40. A. Mejía-Caballero, R. de Anda, G. Hernández-Chávez, S. Rogg, A. Martinez, F. Bolívar, V. M. Castaño and G. Gosset, *Microbial Cell Factories*, 2016, **15**, 161.
41. Q. Ye, F. Zhou and W. Liu, *Chemical Society Reviews*, 2011, **40**, 4244-4258.
42. M. Sugumaran and H. Barek, *International journal of molecular sciences*, 2016, **17**, 1753.
43. X. Chen, D. Xiao, X. Du, X. Guo, F. Zhang, N. Desneux, L. Zang and S. Wang, *Frontiers in Physiology*, 2019, **10**.
44. M. J. Beltrán-García, F. M. Prado, M. S. Oliveira, D. Ortiz-Mendoza, A. C. Scalfio, A. Pessoa Jr, M. H. Medeiros, J. F. White and P. Di Mascio, *PloS one*, 2014, **9**, e91616.
45. J. D. Simon, M. R. Goldsmith, L. Hong, V. R. Kempf, L. E. McGuckin, T. Ye and G. Zuber, *Photochemistry and photobiology*, 2006, **82**, 318-323.
46. L. Huang, M. Liu, H. Huang, Y. Wen, X. Zhang and Y. Wei, *Biomacromolecules*, 2018, **19**, 1858-1868.
47. A. A. R. Watt, J. P. Bothma and P. Meredith, *Soft Matter*, 2009, **5**, 3754-3760.
48. A. Büngeler, B. Hämisch and O. I. Strube, *International Journal of Molecular Sciences*, 2017, **18**, 1901.
49. H. Claus and H. Decker, *Systematic and Applied Microbiology*, 2006, **29**, 3-14.
50. P. Manivasagan, J. Venkatesan, K. Sivakumar and S.-K. Kim, *World Journal of Microbiology and Biotechnology*, 2013, **29**, 1737-1750.
51. M. Butler and A. J. C. J. o. M. Day, 1998, **44**, 1115-1136.
52. T. A. Belozerskaya, N. N. Gessler and A. A. Aver'yanov, *Fungal Metabolites*, 2017, **2017**, 263-291.
53. J. D. Nosanchuk, R. E. Stark and A. Casadevall, *Frontiers in microbiology*, 2015, **6**, 1463.

54. V. M. Sava, S.-M. Yang, M.-Y. Hong, P.-C. Yang and G. S. Huang, *Food Chemistry*, 2001, **73**, 177-184.
55. Y. Zou, C. Xie, G. Fan, Z. Gu and Y. Han, *Innovative Food Science & Emerging Technologies*, 2010, **11**, 611-615.
56. C. Agius, in *Fish immunology*, Elsevier, 1985, pp. 85-105.
57. R. L. Schroeder, K. L. Double and J. P. Gerber, *Journal of Chemical Neuroanatomy*, 2015, **64-65**, 20-32.
58. M. T. H. Khan, *Pure and Applied Chemistry*, 2007, **79**, 2277-2295.
59. E. Dadachova and A. Casadevall, *Current opinion in microbiology*, 2008, **11**, 525-531.
60. N. V. Mironenko, I. A. Alekhina, N. N. Zhdanova and S. A. Bulat, *Ecotoxicology and environmental safety*, 2000, **45**, 177-187.
61. A. Saadawi, A. Ayad and V. Maltsev, *Journal of hygiene, epidemiology, microbiology, and immunology*, 1991, **35**, 241-249.
62. N. N. Zhdanova, T. Tugay, J. Dighton, V. Zheltonozhsky and P. Mcdermott, *Mycological research*, 2004, **108**, 1089-1096.
63. T. Alekhova, A. Aleksandrova, T. Y. Novozhilova, L. Lysak, N. Zagustina and A. Bezborodov, *Applied Biochemistry and Microbiology*, 2005, **41**, 382-389.
64. V. Baranov, N. Polikarpov, N. Novikova, E. Deshevaia, S. Poddubko, I. Svistunova and V. Tsetlin, *Aviakosmicheskaiia i ekologicheskaiia meditsina= Aerospace and environmental medicine*, 2006, **40**, 3-9.
65. L. H. Lin, J. Hall, J. Lippmann-Pipke, J. A. Ward, B. Sherwood Lollar, M. DeFlaun, R. Rothmel, D. Moser, T. M. Gihring and B. Mislowack, *Geochemistry, Geophysics, Geosystems*, 2005, **6**.
66. L.-H. Lin, P.-L. Wang, D. Rumble, J. Lippmann-Pipke, E. Boice, L. M. Pratt, B. S. Lollar, E. L. Brodie, T. C. Hazen and G. L. Andersen, *Science*, 2006, **314**, 479-482.
67. D. Chivian, E. L. Brodie, E. J. Alm, D. E. Culley, P. S. Dehal, T. Z. DeSantis, T. M. Gihring, A. Lapidus, L.-H. Lin and S. R. Lowry, *Science*, 2008, **322**, 275-278.
68. E. Dadachova, R. A. Bryan, X. Huang, T. Moadel, A. D. Schweitzer, P. Aisen, J. D. Nosanchuk and A. Casadevall, *PloS one*, 2007, **2**, e457.
69. V. B. Yerger and R. E. Malone, *Nicotine & Tobacco Research*, 2006, **8**, 487-498.
70. M. Bakhshi, S. Rahmani and A. J. L. i. m. s. Rahmani, 2015, **30**, 2195-2203.
71. J. Lindgren, A. Moyer, M. H. Schweitzer, P. Sjövall, P. Uvdal, D. E. Nilsson, J. Heimdal, A. Engdahl, J. A. Gren and B. P. J. P. o. t. R. S. B. B. S. Schultz, 2015, **282**, 20150614.
72. D. Braconi, L. Millucci, G. Bernardini and A. Santucci, *Free Radical Biology and Medicine*, 2015, **88**, 70-80.
73. C. E. Turick, A. S. Knox, J. M. Becnel, A. A. Ekechukwu and C. E. Milliken, in *Biopolymers*, IntechOpen, 2010, ch. 23.
74. J. D. Simon, D. Peles, K. Wakamatsu and S. Ito, *Pigment cell & melanoma research*, 2009, **22**, 563-579.
75. G. Prota, *Pigment Cell Research*, 2000, **13**, 283-293.
76. E. S. Jacobson, *Clinical microbiology reviews*, 2000, **13**, 708-717.
77. L. Panzella, A. Ebato, A. Napolitano and K. Koike, *International journal of molecular sciences*, 2018, **19**, 1753.
78. Z. Jin and H. Fan, *Polymer International*, 2016, **65**, 1258-1266.

79. R. Mrówczyński, R. Markiewicz and J. Liebscher, *Polymer International*, 2016, **65**, 1288-1299.
80. F. Solano, *International journal of molecular sciences*, 2017, **18**, 1561.
81. J. D. Simon, L. Hong and D. N. Peles, *The Journal of Physical Chemistry B*, 2008, **112**, 13201-13217.
82. N. J. Pazdernik and D. P. Clark, *Biotechnology*, Academic Press, 2015.
83. T. T. Pandian and D. Kandavel, *Textbook of biotechnology*, I.K. International Pub., India, 2008.
84. O. N. Kanwugu, M. N. Ivantsova and K. D. Chidumaga, 2018.
85. H. Vieira, M. C. Leal and R. Calado, *Trends in Biotechnology*, 2020.
86. S. La Barre and S. S. Bates, *Blue biotechnology: production and use of marine molecules*, John Wiley & Sons, 2018.
87. Ecorys, *Study in support of Impact Assessment work on Blue Biotechnology*, 2014.
88. M. Gavrilescu and Y. Chisti, *Biotechnology advances*, 2005, **23**, 471-499.
89. S. Riedel, 2004.
90. V. Barras and G. Greub, *Clinical Microbiology and Infection*, 2014, **20**, 497-502.
91. J. Park, H. Moon and S. Hong, *Biomaterials Research*, 2019, **23**, 24.
92. A. S. ElObeid, A. Kamal-Eldin, M. A. K. Abdelhalim and A. M. Haseeb, *Basic & Clinical Pharmacology & Toxicology*, 2017, **120**, 515-522.
93. D. J. A. Harvey and b. chemistry, 2011, **399**, 149-152.
94. D. A. Skoog, F. J. Holler and S. R. Crouch, *Principles of instrumental analysis*, Cengage learning, 2017.
95. D. Harvey, *Modern analytical chemistry*, McGraw-Hill, 2000.
96. I.-E. Pralea, R.-C. Moldovan, A.-M. Petrache, M. Ilieș, S.-C. Hegheș, I. Ielciu, R. Nicoară, M. Moldovan, M. Ene and M. Radu, *International journal of molecular sciences*, 2019, **20**, 3943.
97. in *HPLC*, 2007, DOI: 10.1002/9780470079096.ch16, ch. 16, pp. 195-199.
98. M. W. Dong, *HPLC and UHPLC for Practicing Scientists*, John Wiley & Sons, 2019.
99. Y. V. Kazakevich and R. Lobrutto, *HPLC for pharmaceutical scientists*, John Wiley & Sons, 2007.
100. Y. Kazakevich, in *Separation Science and Technology*, Elsevier, 2007, vol. 8, pp. 13-44.
101. A. Strigel, W. Yau, J. Kirkland and D. Bly, *Journal*, 2009.
102. D. Held and P. Kilz, *Monitoring Polymerization Reactions*, 2014, 171.
103. P. Mielczarek and J. Silberring, *Mass Spectrometry: An Applied Approach*, 2019, 209.
104. J. T. Watson and O. D. Sparkman, *Introduction to mass spectrometry: instrumentation, applications, and strategies for data interpretation*, John Wiley & Sons, 2007.
105. C. Dass, *Fundamentals of contemporary mass spectrometry*, John Wiley & Sons, 2007.
106. in *Handbook of Spectroscopy*, 2014, DOI: 10.1002/9783527654703.ch35, pp. 1287-1312.

107. N. E. Jacobsen, *NMR spectroscopy explained: simplified theory, applications and examples for organic chemistry and structural biology*, John Wiley & Sons, 2007.
108. G. Gauglitz and D. S. Moore, *Handbook of spectroscopy*, Wiley-VCH Weinheim, Germany, 2014.
109. M. Kaupp, V. Malkin and M. Bühl, *Journal*, 2004.
110. P. Blumer, P. Blumler, B. Blunich and R. E. Botto, *Journal*, 1999.
111. M. E. P. Resonance, *Journal*, 2011.
112. in *Handbook of Spectroscopy*, 2003, DOI: 10.1002/3527602305.ch12, ch. 12, pp. 421-496.
113. N. Ramanujam, *Encyclopedia of Analytical Chemistry: Applications, Theory and Instrumentation*, 2006.
114. L. P. d. Silva, *A Comprehensive Guide to Chemiluminescence*, Nova Science Publishers Inc, 15 Oct 2019.
115. Sun, in *Physical Chemistry of Macromolecules*, 2004, DOI: 10.1002/0471623571.ch17, ch. 17, pp. 399-435.
116. G. Turrell, in *Encyclopedia of Analytical Chemistry*, 2006, DOI: 10.1002/9780470027318.a5607.
117. F. B. Waanders, *MLOSSBAUER SPECTROSCOPY*, 2013, 576.
118. S. Morton, *Handbook of Spectroscopy*, 2014.
119. S. E. B. N. G. C. A. M. A. Proskurnin, in *Photothermal Spectroscopy Methods*, 2019, DOI: 10.1002/9781119279105.ch5, pp. 219-284.
120. A. M. Kelley, in *Condensed-Phase Molecular Spectroscopy and Photophysics*, 2012, DOI: 10.1002/9781118493052.ch11, pp. 215-237.
121. W. W. Parson, *Modern optical spectroscopy*, Springer, 2007.
122. E. Smith and G. Dent, 2005.
123. J.-L. Coutaz, F. Garet and V. P. Wallace, *Principles of Terahertz time-domain spectroscopy: an introductory textbook*, CRC Press, 2018.
124. J. S. J. A. Zeitler, in *Disordered Pharmaceutical Materials*, 2016, DOI: 10.1002/9783527652693.ch13, pp. 393-426.
125. M. Theuer, S. S. Harsha, D. Molter, G. Torosyan and R. Beigang, *ChemPhysChem*, 2011, **12**, 2695-2705.
126. J. D. F. Ramsay, in *Handbook of Porous Solids*, 2002, DOI: 10.1002/9783527618286.ch6, pp. 135-181.
127. P. Staron, A. Schreyer, H. Clemens and S. Mayer, *Neutrons and synchrotron radiation in engineering materials science: From fundamentals to applications*, John Wiley & Sons, 2017.
128. in *Physical Chemistry of Macromolecules*, 2004, DOI: 10.1002/0471623571.ch16, pp. 371-398.
129. R. Richardson, in *Colloid Science*, 2005, DOI: 10.1002/9781444305395.ch12, pp. 228-254.
130. H. G. Elias, in *Macromolecules*, 2008, DOI: 10.1002/9783527627233.ch5, pp. 139-171.
131. D. Donatella, C. Silvestre, S. Cimmino, A. Marra and M. Pezzuto, *Polymer Morphology: Principles, Characterization, and Processing*, 2016, 374-396.
132. P. D. I. A. C. M. B. E. Fazio, in *Industrial Crystallization Process Monitoring and Control*, 2012, DOI: 10.1002/9783527645206.ch6, pp. 51-57.
133. E. Zolotoyabko, *Basic concepts of X-ray diffraction*, John Wiley & Sons, 2014.

134. V. S. Urban, in *Characterization of Materials*, 2012, DOI: 10.1002/0471266965.com113, pp. 1-16.
135. J. Lindner, R. Meckenstock and M. Farle, *Journal*, 2012.
136. H.-G. Elias, *Macromolecules, Volume 3: Physical Structures and Properties*, Wiley-VCH, 2008.
137. J. Menzel and R. Prime, *Journal*, 2009.
138. Y. Leng, *Materials characterization: introduction to microscopic and spectroscopic methods*, John Wiley & Sons, 2009.
139. P. Gabbott, *Principles and applications of thermal analysis*, John Wiley & Sons, 2008.
140. Q. Guo, *Polymer morphology: principles, characterization, and processing*, John Wiley & Sons, 2016.
141. L. R. Faulkner and A. J. Bard, *Electrochemical methods: fundamentals and applications*, John Wiley and Sons, 2002.
142. T. M. Nahir, *Journal*, 2005.
143. M. Hoppert, *Microscopic techniques in biotechnology*, John Wiley & Sons, 2006.
144. R. S. Khandpur, *Compendium of Biomedical Instrumentation*, John Wiley & Sons, Ltd., 2019.
145. G. H. M. W. Lebek, in *Polymer Morphology*, 2016, DOI: 10.1002/9781118892756.ch3, pp. 37-53.
146. M. Hoppert, in *Microscopic Techniques in Biotechnology*, 2003, DOI: 10.1002/3527602615.ch2, pp. 147-286.
147. I. S. Gilmore and J. C. Vickerman, *Surface analysis: the principal techniques*, John Wiley & Sons, 2009.
148. V. V. Tsukruk and S. Singamaneni, *Scanning probe microscopy of soft matter: fundamentals and practices*, John Wiley & Sons, 2012.
149. M. R. M. Zacharias, in *Biomolecular and Bioanalytical Techniques*, 2019, DOI: 10.1002/9781119483977.ch19, pp. 501-535.
150. D. Sholl and J. A. Steckel, *Density functional theory: a practical introduction*, John Wiley & Sons, 2011.
151. A. Varnek and I. I. Baskin, *Molecular Informatics*, 2011, **30**, 20-32.
152. G. Alterovitz and M. Ramoni, *Knowledge-based bioinformatics: from analysis to interpretation*, John Wiley & Sons, 2011.
153. H. de Matthew and S. Petoukhov, *Journal*, 2011.
154. B. A. J. R. F. A. K. Nandi, in *Integrative Cluster Analysis in Bioinformatics*, 2015, DOI: 10.1002/9781118906545.ch1, pp. 1-8.
155. R. B. A. J. M. Dugan, in *Structural Bioinformatics*, 2003, DOI: 10.1002/0471721204.ch1, pp. 1-14.
156. K. Wakamatsu and S. Ito, 2002, **15**, 174-183.
157. W. Yang, L. Ruan, J. Tao, D. Peng, J. Zheng and M. Sun, *Frontiers in microbiology*, 2018, **9**, 2242.
158. K. E. Keith, L. Killip, P. He, G. R. Moran and M. A. Valvano, *Journal of bacteriology*, 2007, **189**, 9057-9065.
159. H. Wang, Y. Qiao, B. Chai, C. Qiu and X. Chen, *PLoS One*, 2015, **10**, e0120923.
160. C. E. Turick, F. Caccavo and L. S. Tisa, *Canadian journal of microbiology*, 2008, **54**, 334-339.

161. S. I. Kotob, S. L. Coon, E. J. Quintero and R. M. Weiner, *Appl. Environ. Microbiol.*, 1995, **61**, 1620-1622.
162. L. P. Mekala, M. Mohammed, S. Chinthalapati and V. R. Chinthalapati, *International journal of biological macromolecules*, 2019, **126**, 755-764.
163. J. Dai, H. Xia, C. Yang and X. Chen, *Frontiers in Microbiology*, 2021, **12**, 601963.
164. G. A. Greenblatt and M. H. Wheeler, *Journal of Liquid Chromatography*, 1986, **9**, 971-981.
165. G. Jacomelli, V. Micheli, G. Bernardini, L. Millucci and A. Santucci, in *JIMD Reports, Volume 31*, Springer, 2016, pp. 51-56.
166. R. Simoni, L. Gomes, M. Faria, J. B. Neto and M. J. J. o. i. m. d. Costa de Oliveira, 1994, **17**, 632-633.
167. C. Bory, R. Boulieu, C. Chantin and M. Mathieu, *Clinical chemistry*, 1989, **35**, 321-322.
168. S. Ito and K. Jimbow, *Journal of Investigative Dermatology*, 1983, **80**, 268-272.
169. A. Napolitano, P. Di Donato and G. Prota, *The Journal of organic chemistry*, 2001, **66**, 6958-6966.
170. A. M. Taylor and K. P. Vercruysee, in *JIMD Reports, Volume 35*, Springer, 2017, pp. 79-85.
171. K. Vercruysee and M. M. Whalen, 2018.
172. K. Vercruysee, S. Russell, J. Knight, N. Stewart, N. Wilson and N. Richardson, 2017.
173. K. P. Vercruysee, A. M. Clark, P. A. Bello and M. J. J. o. C. B. Alhumaidi, 2017, **1061**, 11-16.
174. G. Frazzetto, *EMBO reports*, 2003, **4**, 835-837.
175. D. Byrom, *Trends in biotechnology*, 1987, **5**, 246-250.
176. S. Shoda, A. Kobayashi and S. Kobayashi, in *White Biotechnology for Sustainable Chemistry*, 2015, pp. 274-309.
177. S. Jemli, D. Ayadi-Zouari, H. B. Hlima and S. Bejar, *Critical reviews in biotechnology*, 2016, **36**, 246-258.
178. S. Heux, I. Meynial-Salles, M. O'Donohue and C. Dumon, *Biotechnology advances*, 2015, **33**, 1653-1670.
179. C. David, A. Daro, E. Szalai, T. Atarhouch and M. Mergeay, *European polymer journal*, 1996, **32**, 669-679.
180. T. Fujii, K. Ikeda, M. J. B. Saito, *biotechnology, and biochemistry*, 2011, **75**, 489-495.
181. R. Hou, X. Liu, J. Yan, K. Xiang, X. Wu, W. Lin, G. Chen, M. Zheng, J. J. F. Fu and function, 2019, **10**, 1017-1027.
182. L. Ffolkes, D. Brull, S. Krywawych, M. Hayward and S. J. J. o. c. p. Hughes, 2007, **60**, 92-93.
183. S. A. Al-Sarayreh, I. N. Al-Tarawneh, M. S. Al-Sbou, E. M. Albatayneh, J. M. Al-Shuneigat and Y. M. J. J. J. o. B. S. Al-Sarairah, 2014, **147**, 1-4.
184. M. Thapa, J. Yu, W. Lee, M. F. Islam and H.-R. Yoon, *분석과학*, 2015, **28**, 323-330.
185. Y. Tokuhara, K. Shukuya, M. Tanaka, K. Sogabe, Y. Ejima, S. Hosokawa, H. Ohsaki, T. Morinishi, E. Hirakawa, Y. Yatomi and T. Shimosawa, *Scientific Reports*, 2018, **8**, 11364.

186. D. Braconi, L. Millucci, A. Bernini, O. Spiga, P. Lupetti, B. Marzocchi, N. Niccolai, G. Bernardini and A. J. B. e. B. A.-G. S. Santucci, 2017, **1861**, 135-146.
187. R. P. McGlinchey, F. Shewmaker, P. McPhie, B. Monterroso, K. Thurber and R. B. Wickner, *Proceedings of the National Academy of Sciences*, 2009, **106**, 13731-13736.
188. J. N. Pedersen, Z. Jiang, G. Christiansen, J. C. Lee, J. S. Pedersen and D. E. Otzen, *Biochimica et Biophysica Acta (BBA)-Proteins and Proteomics*, 2019, **1867**, 519-528.
189. A. Hughes, A. Milan, P. Christensen, G. Ross, A. Davison, J. Gallagher, J. Dutton and L. Ranganath, *Journal of Chromatography B*, 2014, **963**, 106-112.
190. W.-Y. Hsu, C.-M. Chen, F.-J. Tsai and C.-C. J. C. C. A. Lai, 2013, **420**, 140-145.
191. B. P. Norman, A. S. Davison, G. A. Ross, A. M. Milan, A. T. Hughes, H. Sutherland, J. C. Jarvis, N. B. Roberts, J. A. Gallagher and L. R. J. C. c. Ranganath, 2019, **65**, 530-539.
192. C. E. Turick, A. S. Beliaev, B. A. Zakrajsek, C. L. Reardon, D. A. Lowy, T. E. Poppy, A. Maloney and A. A. Ekechukwu, *FEMS microbiology ecology*, 2009, **68**, 223-235.
193. C. Colleary, A. Dolocan, J. Gardner, S. Singh, M. Wuttke, R. Rabenstein, J. Habersetzer, S. Schaal, M. Feseha and M. Clemens, *Proceedings of the National Academy of Sciences*, 2015, **112**, 12592-12597.
194. J. Vinther, *BioEssays*, 2015, **37**, 643-656.
195. M. L. Tran, B. J. Powell and P. Meredith, *Biophysical journal*, 2006, **90**, 743-752.
196. S. Aime, M. FASANO, E. Terreno and C. J. GROOMBRIDGE, *Pigment cell research*, 1991, **4**, 216-221.
197. A. Carreira, L. M. Ferreira and V. Loureiro, *Journal of applied microbiology*, 2001, **90**, 372-379.
198. M. Engelen, R. Vanna, C. Bellei, F. A. Zucca, K. Wakamatsu, E. Monzani, S. Ito, L. Casella and L. Zecca, *PLoS One*, 2012, **7**.
199. K. Double, L. Zecca, P. Costi, M. Mauer, C. Griesinger, S. Ito, D. Ben-Shachar, G. Bringmann, R. Fariello and P. Riederer, *Journal of neurochemistry*, 2000, **75**, 2583-2589.
200. E. Camacho, R. Viji, C. Chrissian, R. Prados-Rosales, D. Gil, R. N. O'Meally, R. J. Cordero, R. N. Cole, J. M. McCaffery and R. E. Stark, *Journal of Biological Chemistry*, 2019, **294**, 10471-10489.
201. B. B. Adhyaru, N. G. Akhmedov, A. R. Katritzky and C. R. Bowers, *Magnetic Resonance in Chemistry*, 2003, **41**, 466-474.
202. S. Ghiani, S. Baroni, D. Burgio, G. Digilio, M. Fukuhara, P. Martino, K. Monda, C. Nervi, A. Kiyomine and S. Aime, *Magnetic Resonance in Chemistry*, 2008, **46**, 471-479.
203. W. Y. Chow, A. M. Taylor, D. G. Reid, J. A. Gallagher and M. J. Duer, *Journal of inherited metabolic disease*, 2011, **34**, 1137-1140.
204. R. C. Sealy, W. Puzyna, B. Kalyanaraman and C. C. Felix, *Biochimica et Biophysica Acta (BBA)-General Subjects*, 1984, **800**, 269-276.
205. M. Blois, A. Zahlan and J. Maling, *Biophysical Journal*, 1964, **4**, 471-490.

206. L. Chauffe, J. Windle and M. Friedman, *Biophysical journal*, 1975, **15**, 565-572.
207. B. Pilawa, M. Zdybel and E. Chodurek, *Melanin*, 2017.
208. I. A. Menon, S. D. Persad, H. F. Haberman, P. K. Basu, J. F. Norfray, C. C. Felix and B. Kalyanaraman, *Biochemistry and cell biology*, 1991, **69**, 269-273.
209. S.-S. Chio, J. S. Hyde, R. C. J. A. o. b. Sealy and biophysics, 1982, **215**, 100-106.
210. M. Pasenkiewicz-Gierula and R. J. B. e. B. A.-G. S. Sealy, 1986, **884**, 510-516.
211. Z. Wang, T. Tschirhart, Z. Schultzhaus, E. E. Kelly, A. Chen, E. Oh, O. Nag, E. R. Glaser, E. Kim and P. F. Lloyd, *Applied and Environmental Microbiology*, 2020, **86**.
212. M. Al Khatib, M. Harir, J. Costa, M. C. Baratto, I. Schiavo, L. Trabalzini, S. Pollini, G. M. Rossolini, R. Basosi and R. Pogni, *Molecules*, 2018, **23**, 1916.
213. R. Hou, X. Liu, K. Xiang, L. Chen, X. Wu, W. Lin, M. Zheng and J. Fu, *Food chemistry*, 2019, **277**, 533-542.
214. N. Ushakova, A. Dontsov, N. Sakina, A. Bastrakov and M. Ostrovsky, *Biomolecules*, 2019, **9**, 408.
215. N. Ushakova, A. Dontsov, A. Bastrakov, N. Y. Garmash and D. Pavlov, 2017.
216. E. Kim, M. Kang, T. Tschirhart, M. Malo, E. Dadachova, G. Cao, J.-J. Yin, W. E. Bentley, Z. Wang and G. F. Payne, *Biomacromolecules*, 2017, **18**, 4084-4098.
217. K. Glass, S. Ito, P. R. Wilby, T. Sota, A. Nakamura, C. R. Bowers, J. Vinther, S. Dutta, R. Summons and D. E. J. P. o. t. N. A. o. S. Briggs, 2012, **109**, 10218-10223.
218. T. Shima, T. Sarna, H. M. Swartz, A. Stroppolo, R. Gerbasi, L. J. F. R. B. Zecca and Medicine, 1997, **23**, 110-119.
219. A. Zadlo, G. Szewczyk, M. Sarna, A. Kozinska, A. Pilat, P. Kaczara and T. Sarna, *Free Radical Biology and Medicine*, 2016, **97**, 320-329.
220. M. Okazaki, K. Kuwata, Y. Miki, S. Shiga and T. Shiga, *Archives of biochemistry and biophysics*, 1985, **242**, 197-205.
221. K. Nakagawa, S. Minakawa and D. Sawamura, *Analytical Sciences*, 2018, **34**, 837-840.
222. P. M. Plonka, *Experimental dermatology*, 2009, **18**, 472-484.
223. M. Müller and B. Keßler, *Langmuir*, 2011, **27**, 12499-12505.
224. R. A. Zangmeister, T. A. Morris and M. J. Tarlov, *Langmuir*, 2013, **29**, 8619-8628.
225. A. Zadlo, G. Szewczyk, M. Sarna, T. G. Camenisch, J. W. Sidabras, S. Ito, K. Wakamatsu, F. Sagan, M. Mitoraj and T. Sarna, *Pigment cell & melanoma research*, 2019, **32**, 359-372.
226. X. Zhou, N. C. McCallum, Z. Hu, W. Cao, K. Gnanasekaran, Y. Feng, J. F. Stoddart, Z. Wang and N. C. Gianneschi, *ACS nano*, 2019, **13**, 10980-10990.
227. R. A. Milch, *Arthritis & Rheumatism*, 1965, **8**, 1002-1005.
228. K. Tarangini and S. Mishra, *Research Journal of Engineering Sciences ISSN*, 2013, **2278**, 9472.
229. V. Manirethan, K. Raval, R. Rajan, H. Thaira and R. M. J. D. i. b. Balakrishnan, 2018, **20**, 178-189.
230. W. Lyu, Y. Shi and Y. J. J. o. F. R. Zheng, 2019, **30**, 739-743.
231. M. Apte, G. Girme, A. Bankar, A. RaviKumar and S. J. J. o. n. Zinjarde, 2013, **11**, 2.
232. A. Mboniryivuze, B. Mwakikunga, S. M. Dhlamini and M. Maaza, 2015.

233. S. A. Centeno and J. Shamir, *Journal of Molecular Structure*, 2008, **873**, 149-159.
234. F. Wolff, I. Biauou, C. Koopmansch, M. B. Vanden, A. Pozdzik, T. Roumeguere and F. Cotton, *Clinical nephrology*, 2015, **84**, 339-342.
235. F. F. Stenn, J. W. Milgram, S. L. Lee, R. J. Weigand and A. Veis, *Science*, 1977, **197**, 566.
236. A. V. Kalueff, J. W. Aldridge, J. L. LaPorte, D. L. Murphy and P. Tuohimaa, *Nature protocols*, 2007, **2**, 2538.
237. F. R. Kohl, C. Grieco and B. Kohler, *Chemical Science*, 2020.
238. M. L. Roldán, S. A. Centeno and A. J. J. o. R. S. Rizzo, 2014, **45**, 1160-1171.
239. I. Galván, C. Araujo-Andrade, M. Marro, P. Loza-Alvarez, K. J. P. c. Wakamatsu and m. research, 2018, **31**, 673-682.
240. I. Galván, A. Jorge and M. J. I. B. García-Gil, 2017, **9**, 751-761.
241. I. Galván, J. Cerezo, A. Jorge and K. Wakamatsu, *Integrative Biology*, 2018, **10**, 464-473.
242. B.-K. Hsiung, T. A. Blackledge and M. D. J. J. o. E. B. Shawkey, 2015, **218**, 3632-3635.
243. A. Culka, J. Jehlička, C. Ascaso, O. Artieda, C. M. Casero and J. J. J. o. R. S. Wierzchos, 2017, **48**, 1487-1493.
244. T. C. Lei, D. A. Ammar, O. Masihzadeh, E. A. Gibson and M. Y. Kahook, *Molecular vision*, 2011, **17**, 2628.
245. J. R. Beattie, S. Finnegan, R. W. Hamilton, M. Ali, C. F. Inglehearn, A. W. Stitt, J. J. McGarvey, P. M. Hocking and W. J. Curry, *Investigative ophthalmology & visual science*, 2012, **53**, 413-420.
246. Z. Huang, H. Lui, M. X. Chen, A. Alajlan, D. I. McLean and H. Zeng, *Journal of biomedical optics*, 2004, **9**, 1198-1206.
247. B. Moncada, L. K. Sahagún-Sánchez, B. Torres-Álvarez, J. P. Castanedo-Cázares, J. D. Martínez-Ramírez and F. J. González, *Photodermatology, Photoimmunology & Photomedicine*, 2009, **25**, 159-160.
248. B. Moncada, C. Castillo-Martínez, E. Arenas, F. León-Bejarano, M. Ramírez-Elías and F. González, *Skin Research and Technology*, 2016, **22**, 170-173.
249. S.-i. Morita, S. Takanezawa, S. Watanabe and Y. Sako, *Journal of Spectroscopy*, 2013, **2013**.
250. E. Brauchle and K. Schenke-Layland, *Biotechnology journal*, 2013, **8**, 288-297.
251. B. Bodanese, F. L. Silveira, R. A. Zângaro, M. T. T. Pacheco, C. A. Pasqualucci and L. Silveira Jr, *Photomedicine and laser surgery*, 2012, **30**, 381-387.
252. X. Feng, A. J. Moy, H. T. Nguyen, J. Zhang, M. C. Fox, K. R. Sebastian, J. S. Reichenberg, M. K. Markey and J. W. Tunnell, *Biomedical optics express*, 2017, **8**, 2835-2850.
253. L. Silveira, F. L. Silveira, R. A. Zângaro, M. T. Pacheco and B. Bodanese, *Journal of biomedical optics*, 2012, **17**, 077003.
254. R. A. Milch, E. D. Titus and T. L. Loo, *Science*, 1957, **126**, 209-210.
255. Y. Tokuhara, K. Shukuya, M. Tanaka, M. Mouri, R. Ohkawa, M. Fujishiro, T. Takahashi, S. Okubo, H. Yokota and M. Kurano, *PLoS One*, 2014, **9**, e86606.
256. R. Consden, H. Forbes, L. Glynn and W. M. J. B. J. Stanier, 1951, **50**, 274.
257. L. Lahuerta Zamora and M. Pérez-Gracia, *Journal of The Royal Society Interface*, 2012, **9**, 1892-1897.

258. Y. Kitano and F. Hu, *Journal of Investigative Dermatology*, 1970, **55**, 444-451.
259. P. F. Hall, *General and Comparative Endocrinology*, 1969, **2**, 451-458.
260. M. W. Colley, *American Journal of Botany*, 1931, 266-287.
261. S. Hoti and K. Balaraman, *Microbiology*, 1993, **139**, 2365-2369.
262. X. Wang, Z. Chen, P. Yang, J. Hu, Z. Wang and Y. Li, *Polymer Chemistry*, 2019, **10**, 4194-4200.
263. M. G. Bridelli, *Biophysical chemistry*, 1998, **73**, 227-239.
264. A. I. El-Batal and M. S. Al Tamie, *Der Pharmacia Lettre*, 2016, **8**, 315-333.
265. R. R. Ansari, *Journal of biomedical optics*, 2004, **9**, 22-38.
266. K. Tarangini and S. Mishra, *Journal*, 2014.
267. S. S. Sajjan, O. Anjaneya, B. K. Guruprasad, S. N. Anand, B. M. Suresh and T. Karegoudar, *Korean J Microbiol Biotechnol*, 2013, **41**, 60-69.
268. C. Ganesh Kumar, N. Sahu, G. Narender Reddy, R. B. N. Prasad, N. Nagesh and A. Kamal, *Letters in applied microbiology*, 2013, **57**, 295-302.
269. A. Casadevall, A. Nakouzi, P. R. Crippa and M. Eisner, *PloS one*, 2012, **7**.
270. V. Capozzi, G. Perna, P. Carmone, A. Gallone, M. Lastella, E. Mezzenga, G. Quartucci, M. Ambrico, V. Augelli and P. J. T. S. F. Biagi, 2006, **511**, 362-366.
271. A. Mbonyiryivuze, I. Omollo, B. D. Ngom, B. Mwakikunga, S. M. Dhlamini, E. Park and M. Maaza, *Physics and Materials Chemistry*, 2015, **3**, 1-6.
272. L. Zecca, F. A. Zucca, H. Wilms and D. Sulzer, *Trends in neurosciences*, 2003, **26**, 578-580.
273. R. Lagier and S. Sit'Aj, *Annals of the rheumatic diseases*, 1974, **33**, 86.
274. J. Li, A. Jiao, S. Chen, Z. Wu, E. Xu and Z. Jin, *Journal of Molecular Structure*, 2018, **1165**, 391-400.
275. J. Cheng, S. C. MOSS, M. EISNER and P. ZSCHACK, *Pigment cell research*, 1994, **7**, 255-262.
276. J. Cheng, S. C. MOSS and M. EISNER, *Pigment Cell Research*, 1994, **7**, 263-273.
277. K. C. Littrell, J. M. Gallas, G. W. Zajac, P. J. P. Thiyagarajan and photobiology, 2003, **77**, 115-120.
278. J. Gallas, K. Littrell, S. Seifert, G. Zajac and P. J. B. J. Thiyagarajan, 1999, **77**, 1135-1142.
279. X. Ma, C. Shi, X. Huang, Y. Liu and Y. Wei, *Polymer Journal*, 2019, **51**, 547-558.
280. A. Coroaba, A. E. Chiriac, L. Sacarescu, T. Pinteala, B. Minea, S.-A. Ibanescu, M. Perteau, A. Moraru, I. Esanu and S. S. Maier, *PeerJ*, 2020, **8**, e8376.
281. M. Arzillo, G. Mangiapia, A. Pezzella, R. K. Heenan, A. Radulescu, L. Paduano and M. d'Ischia, *Biomacromolecules*, 2012, **13**, 2379-2390.
282. N. F. della Vecchia, P. Cerruti, G. Gentile, M. E. Errico, V. Ambrogi, G. D'Errico, S. Longobardi, A. Napolitano, L. Paduano and C. Carfagna, *Biomacromolecules*, 2014, **15**, 3811-3816.
283. J. Yao, Y. Liu, T. Z. Wang, J. B. Liu, P. Liu and Z. N. Yu, *Chinese Chemical Letters*, 2003, **14**, 619-622.
284. J. Geng, P. Yuan, C. Shao, S.-B. Yu, B. Zhou, P. Zhou and X.-D. Chen, *Archives of microbiology*, 2010, **192**, 321-329.
285. W. D. Bush and J. D. Simon, *Pigment cell research*, 2007, **20**, 134-139.
286. J. Ribera, G. Panzarasa, A. Stobbe, A. Osypova, P. Rupper, D. Kloese and F. W. Schwarze, *Journal of agricultural and food chemistry*, 2018, **67**, 132-139.
287. L.-F. Wang and J.-W. Rhim, *LWT*, 2019, **99**, 17-23.

288. Y. J. Kim, W. Wu, S.-E. Chun, J. F. Whitacre and C. J. Bettinger, *Proceedings of the National Academy of Sciences*, 2013, **110**, 20912-20917.
289. B. Simonovic and T. Wilczok, *JOURNAL-SERBIAN CHEMICAL SOCIETY*, 1995, **60**, 981-981.
290. G. S. Kiran, S. A. Jackson, S. Priyadharsini, A. D. Dobson and J. J. S. r. Selvin, 2017, **7**, 9167.
291. Ł. Łopusiewicz, F. Jędra and M. Mizielińska, *Polymers*, 2018, **10**, 386.
292. G. Panzarasa, A. Osypova, G. Consolati, F. Quasso, G. Soliveri, J. Ribera and F. W. Schwarze, *Nanomaterials*, 2018, **8**, 54.
293. G. Bernardini, G. Leone, L. Millucci, M. Consumi, D. Braconi, O. Spiga, S. Galderisi, B. Marzocchi, C. Viti and G. Giorgetti, *Journal of cellular physiology*, 2019, **234**, 6696-6708.
294. M. Eslami, H. R. Zare and M. J. T. J. o. P. C. B. Namazian, 2012, **116**, 12552-12557.
295. I. G. Kim, H. J. Nam, H. J. Ahn and D.-Y. J. E. A. Jung, 2011, **56**, 2954-2959.
296. H. R. Zare, M. Namazian and M. L. J. E. A. Coote, 2009, **54**, 5353-5357.
297. M. Eslami, M. Namazian and H. R. Zare, *The Journal of Physical Chemistry B*, 2013, **117**, 2757-2763.
298. M. Eslami, H. R. Zare and M. Namazian, *Journal of Electroanalytical Chemistry*, 2014, **720**, 76-83.
299. R. Xu, C. Santato and F. Soavi, *Frontiers in bioengineering and biotechnology*, 2019, **7**, 227.
300. R. Xu, C. T. Prontera, E. Di Mauro, A. Pezzella, F. Soavi and C. Santato, *APL Materials*, 2017, **5**, 126108.
301. S. Gidanian and P. J. Farmer, *Journal of inorganic biochemistry*, 2002, **89**, 54-60.
302. S. Su, E. Amba, R. Boissy, A. Greatens and W. Heineman, *Microbiology*, 2013, **159**, 1736-1747.
303. S. Bravina, P. Lutsyk, A. Verbitsky and N. Morozovsky, *Materials Research Bulletin*, 2016, **80**, 230-236.
304. E. S. Jacobson and J. D. Hong, *Journal of bacteriology*, 1997, **179**, 5340-5346.
305. N. Madkhali, H. R. Alqahtani, S. Alterary, H. A. Albrithen, A. Laref and A. Hassib, *Arabian Journal of Chemistry*, 2020.
306. E. Kim, L. Panzella, R. Micillo, W. E. Bentley, A. Napolitano and G. F. Payne, *Scientific reports*, 2015, **5**, 18447.
307. M. Jastrzebska, A. Kocot, J. Vij, J. Zalewska-Rejda and T. Witecki, *Journal of molecular structure*, 2002, **606**, 205-210.
308. M. Sheliakina, A. B. Mostert and P. Meredith, *Advanced Functional Materials*, 2018, **28**, 1805514.
309. K. Motovilov, V. Grinenko, M. Savinov, Z. Gagkaeva, L. Kadyrov, A. Pronin, Z. Bedran, E. Zhukova, A. Mostert and B. Gorshunov, *RSC advances*, 2019, **9**, 3857-3867.
310. F. De Marchi, G. Galeotti, M. Simenas, P. Ji, L. Chi, E. Tornau, A. Pezzella, J. MacLeod, M. Ebrahimi and F. Rosei, *Nanoscale*, 2019, **11**, 5422-5428.
311. F. De Marchi, G. Galeotti, M. Simenas, E. Tornau, A. Pezzella, J. MacLeod, M. Ebrahimi and F. Rosei, *Nanoscale*, 2018, **10**, 16721-16729.

312. A. G. Orive, A. H. Creus, P. Carro and R. C. Salvarezza, *Organic Electronics*, 2012, **13**, 1844-1852.
313. A. Antidormi, G. Aprile, G. Cappellini, E. Cara, R. Cardia, L. Colombo, R. Farris, M. d'Ischia, M. Mehrabian and C. Melis, *The Journal of Physical Chemistry C*, 2018, **122**, 28405-28415.
314. M. d'Ischia, A. Napolitano, V. Ball, C.-T. Chen and M. J. Buehler, *Accounts of chemical research*, 2014, **47**, 3541-3550.
315. B. Oetzel, F. Ortmann, L. Matthes, F. Tandetzky, F. Bechstedt and K. Hannewald, *Physical Review B*, 2012, **86**, 195407.
316. M. Kang, E. Kim, Z. I. Temoçin, J. Li, E. Dadachova, Z. Wang, L. Panzella, A. Napolitano, W. E. Bentley and G. F. Payne, *Chemistry of Materials*, 2018, **30**, 5814-5826.
317. M. Ambrico, P. F. Ambrico, T. Ligonzo, A. Cardone, S. R. Cicco, M. d'Ischia and G. M. Farinola, *Journal of Materials Chemistry C*, 2015, **3**, 6413-6423.
318. R. Kautz, D. D. Ordinario, V. Tyagi, P. Patel, T. N. Nguyen and A. A. Gorodetsky, *Advanced Materials*, 2018, **30**, 1704917.
319. E. Vahidzadeh, A. P. Kalra and K. Shankar, *Biosensors and Bioelectronics*, 2018, **122**, 127-139.
320. L. D'Alba, C. Van Hemert, K. Spencer, B. Heidinger, L. Gill, N. Evans, P. Monaghan, C. Handel and M. ShawNey, *Integrative and Comparative Biology*, 2014, **54**, 633-644.
321. O. A. Alajoulin, M. S. Alsbou, O. Somayya and H. M. Kalbouneh, *Saudi medical journal*, 2015, **36**, 1486.
322. M. Al-Essa, L. Al-Shamsan, M. Rashed and P. Ozand, *Annals of Saudi medicine*, 1998, **18**, 442-444.
323. F. H. Craide, J. S. B. M. d. Fonseca, P. C. Mariano, N. M. Fernandez, C. G. C. d. Castro and Y. d. S. L. Mene, *Anais brasileiros de dermatologia*, 2014, **89**, 799-801.
324. N. Damarla, P. Linga, M. Goyal, S. R. Tadisina, G. S. Reddy and H. Bommisetti, *Indian journal of ophthalmology*, 2017, **65**, 518.
325. A. Wilke and D. Steverding, *Journal of medical case reports*, 2009, **3**, 9302.
326. A. G. Dumanli and T. Savin, *Chemical Society Reviews*, 2016, **45**, 6698-6724.
327. Y. Fu, C. A. Tippets, E. U. Donev and R. Lopez, *Wiley Interdisciplinary Reviews: Nanomedicine and Nanobiotechnology*, 2016, **8**, 758-775.
328. A. Seago, P. Brady, J. Vigneron and T. Schultz, *S165–S184*, 2009.
329. Q. He and R. Wang, *Biomedical Optics Express*, 2020, **11**, 895-910.
330. T. Ha, H. Javedan, K. Waterston, L. Naysmith and J. L. Rees, *Pigment cell research*, 2003, **16**, 477-479.
331. A. R. Matias, M. Ferreira, P. Costa and P. Neto, *Skin Research and Technology*, 2015, **21**, 346-362.
332. P. Bhargava, C. Prakash, S. Tiwari and R. Lakhani, *Pigment International*, 2016, **3**, 72.
333. M. van der Wal, M. Bloemen, P. Verhaegen, W. Tuinebreijer, H. de Vet, P. van Zuijlen and E. Middelkoop, *Journal of Burn Care & Research*, 2013, **34**, e187-e194.
334. C. Y. Wright, A. E. Karsten, M. Wilkes, A. Singh, J. Du Plessis, P. N. Albers and P. A. Karsten, *Photochemistry and photobiology*, 2016, **92**, 632-636.
335. W. Verkruysse, L. O. Svaasand, W. Franco and J. S. Nelson, *Journal of biomedical optics*, 2009, **14**, 014005.

336. C. Ash, G. Town, P. Bjerring and S. Webster, *Photonics & Lasers in Medicine*, 2015, **4**, 177-186.
337. L. Tinti, A. M. Taylor, A. Santucci, B. Wlodarski, P. J. Wilson, J. C. Jarvis, W. D. Fraser, J. S. Davidson, L. R. Ranganath and J. A. J. R. Gallagher, 2010, **50**, 271-277.
338. L. R. Ranganath, J. C. Jarvis and J. A. Gallagher, *Journal of clinical pathology*, 2013, **66**, 367-373.
339. A. Taylor, A. Boyde, P. J. Wilson, J. C. Jarvis, J. S. Davidson, J. Hunt, L. Ranganath and J. A. Gallagher, *Arthritis & Rheumatism*, 2011, **63**, 3887-3896.
340. L. Tinti, A. Spreafico, F. Chellini, M. Galeazzi and A. Santucci, *Clinical and Experimental Rheumatology-Incl Supplements*, 2011, **29**, 693.
341. D. Fu, T. Ye, T. E. Matthews, G. Yurtsever and W. S. Warren, *Journal of biomedical optics*, 2007, **12**, 054004.
342. T. Taubitz, Y. Fang, A. Biesemeier, S. Julien-Schraermeyer and U. Schraermeyer, *EBioMedicine*, 2019, **48**, 592-604.
343. E. Betzig, J. K. Trautman, T. Harris, J. Weiner and R. Kostelak, *Science*, 1991, **251**, 1468-1470.
344. S. G. Stanciu, D. E. Tranca, R. Hristu and G. A. Stanciu, *Biomedical optics express*, 2017, **8**, 5374-5383.
345. H. Hirayama and S. Nakamura, *Journal of Biomedical Optics*, 2015, **20**, 076014.
346. S. Jiao, M. Jiang, J. Hu, A. Fawzi, Q. Zhou, K. K. Shung, C. A. Puliafito and H. F. Zhang, *Optics express*, 2010, **18**, 3967-3972.
347. M. Liu, B. Maurer, B. Hermann, B. Zabihian, M. G. Sandrian, A. Unterhuber, B. Baumann, E. Z. Zhang, P. C. Beard and W. J. Weninger, *Biomedical optics express*, 2014, **5**, 3150-3159.
348. X. Shu, H. Li, B. Dong, C. Sun and H. F. Zhang, *Biomedical optics express*, 2017, **8**, 2851-2865.
349. M. Lapierre-Landry, A. L. Huckenpahler, B. A. Link, R. F. Collery, J. Carroll and M. C. Skala, *Translational vision science & technology*, 2018, **7**, 4-4.
350. M. Pircher, C. K. Hitzenberger and U. Schmidt-Erfurth, *Progress in retinal and eye research*, 2011, **30**, 431-451.
351. M. Miura, S. Makita, S. Sugiyama, Y.-J. Hong, Y. Yasuno, A. E. Elsner, S. Tamiya, R. Tsukahara, T. Iwasaki and H. Goto, *Scientific reports*, 2017, **7**, 1-12.
352. E. Götzinger, M. Pircher, W. Geitzenauer, C. Ahlers, B. Baumann, S. Michels, U. Schmidt-Erfurth and C. K. Hitzenberger, *Optics express*, 2008, **16**, 16410-16422.
353. H. S. Nam and H. Yoo, *Applied Spectroscopy Reviews*, 2018, **53**, 91-111.
354. D. J. Harper, T. Konegger, M. Augustin, K. Schützenberger, P. Eugui, A. Lichtenegger, C. W. Merkle, C. K. Hitzenberger, M. Glösmann and B. Baumann, *Journal of biophotonics*, 2019, **12**, e201900153.
355. H. Lin, Y. Dong, D. Markl, Z. Zhang, Y. Shen and J. A. Zeitler, *Journal of Pharmaceutical Sciences*, 2017, **106**, 3171-3176.
356. H. Lin, Z. Zhang, D. Markl, J. A. Zeitler and Y. Shen, *Applied Sciences*, 2018, **8**, 2700.
357. R. B. Saager, A. N. Dang, S. S. Huang, K. M. Kelly and A. J. Durkin, *Review of Scientific Instruments*, 2017, **88**, 094302.

358. D. K. Sardar, M. L. Mayo and R. D. Glickman, *Journal of biomedical optics*, 2001, **6**, 404-412.
359. R. B. Saager, A. Sharif, K. M. Kelly and A. J. Durkin, *Journal of biomedical optics*, 2016, **21**, 057001.
360. A. E. Karsten and J. E. Smit, *Photochemistry and photobiology*, 2012, **88**, 469-474.
361. C. Regan, C. Hayakawa and B. Choi, *Biomedical optics express*, 2017, **8**, 5708-5723.
362. I. V. Meglinski, 2003.
363. R. Hennessy, M. K. Markey and J. W. Tunnell, *Journal of biomedical optics*, 2015, **20**, 027001.
364. B. Simon and C. A. DiMarzio, *Journal of biomedical optics*, 2007, **12**, 064020.
365. B. Simon and C. A. DiMarzio, 2008.
366. S. Vyas, A. Banerjee, L. Garza, S. Kang and P. Burlina, 2013.
367. S. Vyas, A. Banerjee and P. Burlina, *Journal of biomedical optics*, 2013, **18**, 057008.
368. M. Strauss, P. A. Amendt, R. A. London, D. J. Maitland, M. E. Glinsky, C. P. Lin and M. W. Kelly, 1997.
369. C. Sramek, Y. M. Paulus, H. Nomoto, P. Huie, J. Brown and D. V. Palanker, *Journal of biomedical optics*, 2009, **14**, 034007.
370. C. Sramek, Y. M. Paulus, H. Nomoto, P. Huie and D. Palanker, 2009.
371. C. Sramek, Y. M. Paulus, H. Nomoto, P. Huie and D. Palanker, 2009.
372. M. Pihet, P. Vandeputte, G. Tronchin, G. Renier, P. Saulnier, S. Georgeault, R. Mallet, D. Chabasse, F. Symoens and J.-P. Bouchara, *BMC microbiology*, 2009, **9**, 177.
373. A. Mboniyirivuze, Z. Nuru, B. D. Ngom, B. Mwakikunga, S. M. Dhlamini, E. Park and M. Maaza, 2015.
374. D. Gur, J. D. Nicolas, V. Brumfeld, O. Bar-Elli, D. Oron and G. Levkowitz, *Advanced Science*, 2018, **5**, 1800338.
375. W. Meyer, N. Correa, C. Covarrubias, G. Hermosilla, F. Magne, V. Olate, P. Rodas, C. Tapia and C. Valdes, 2017.
376. Y. Liu, L. Hong, K. Wakamatsu, S. Ito, B. B. Adhyaru, C. Y. Cheng, C. R. Bowers and J. D. Simon, *Photochemistry and Photobiology*, 2005, **81**, 510-516.
377. J. Lindgren, P. Uvdal, P. Sjövall, D. E. Nilsson, A. Engdahl, B. P. Schultz and V. Thiel, *Nature communications*, 2012, **3**, 1-7.
378. W. D. Bush, J. Garguilo, F. A. Zucca, A. Albertini, L. Zecca, G. S. Edwards, R. J. Nemanich and J. D. Simon, *Proceedings of the National Academy of Sciences*, 2006, **103**, 14785-14789.
379. F. J. Contreras-Moreno, J. Muñoz-Dorado, N. I. García-Tomsig, G. Martínez-Navajas, J. Pérez and A. Moraleda-Muñoz, *Frontiers in microbiology*, 2020, **11**, 94.
380. G. Lucotte and T. Thomasset, *Archaeological Discovery*, 2016, **5**, 1-21.
381. L. Millucci, L. Ghezzi, E. Paccagnini, G. Giorgetti, C. Viti, D. Braconi, M. Laschi, M. Geminiani, P. Soldani and P. Lupetti, *Mediators of inflammation*, 2014, **2014**.
382. L. Millucci, G. Bernardini, A. Spreafico, M. Orlandini, D. Braconi, M. Laschi, M. Geminiani, P. Lupetti, G. Giorgetti, C. Viti, B. Frediani, B. Marzocchi and A. Santucci, *Calcified Tissue International*, 2017, **101**, 50-64.

383. L. Millucci, G. Giorgetti, C. Viti, L. Ghezzi, S. Gambassi, D. Braconi, B. Marzocchi, A. Paffetti, P. Lupetti and G. J. J. o. c. p. Bernardini, 2015, **230**, 1148-1157.
384. S. Alaluf, A. Heath, N. Carter, D. Atkins, H. Mahalingam, K. Barrett, R. Kolb and N. J. P. c. r. Smit, 2001, **14**, 337-347.
385. T. Caesar-Tonthat, K. F. Van Ommen, G. G. Geesey and J. M. Henson, *Appl. Environ. Microbiol.*, 1995, **61**, 1968-1975.
386. E. Mitri, L. Millucci, L. Merolle, G. Bernardini, L. Vaccari, A. Gianoncelli and A. Santucci, *Biochimica et Biophysica Acta (BBA)-General Subjects*, 2017, **1861**, 1000-1008.
387. A. M. Taylor, B. Wlodarski, I. A. Prior, P. J. Wilson, J. C. Jarvis, L. R. Ranganath and J. A. Gallagher, *Rheumatology*, 2010, **49**, 1412-1414.
388. A. Biesemeier, O. Eibl, S. Eswara, J.-N. Audinot, T. Wirtz and U. Schraermeyer, *Metallomics*, 2018, **10**, 296-308.
389. L. Migliaccio, P. Manini, D. Altamura, C. Giannini, P. Tassini, M. G. Maglione, C. Minarini and A. Pezzella, *Frontiers in chemistry*, 2019, **7**, 162.
390. M. Ambrico, P. F. Ambrico, A. Cardone, S. R. Cicco, F. Palumbo, T. Ligonzo, R. Di Mundo, V. Petta, V. Augelli and P. Favia, *Journal of Materials Chemistry C*, 2014, **2**, 573-582.
391. C. J. Bettinger, J. P. Bruggeman, A. Misra, J. T. Borenstein and R. Langer, *Biomaterials*, 2009, **30**, 3050-3057.
392. A. M. Moore and P. S. Weiss, *Annual Review of Analytical Chemistry*, 2008, **1**, 857-882.
393. G. Zajac, J. Gallas and A. Alvarado-Swaisgood, *Journal of Vacuum Science & Technology B: Microelectronics and Nanometer Structures Processing, Measurement, and Phenomena*, 1994, **12**, 1512-1516.
394. J. M. GALLAS, G. W. ZAJAC, T. SARNA and P. L. STOTTER, *Pigment cell research*, 2000, **13**, 99-108.
395. G. Zajac, J. Gallas, J. Cheng, M. Eisner, S. Moss and A. Alvarado-Swaisgood, *Biochimica et Biophysica Acta (BBA)-General Subjects*, 1994, **1199**, 271-278.
396. P. Díaz, Y. Gimeno, P. Carro, S. González, P. L. Schilardi, G. Benítez, R. C. Salvarezza and A. H. Creus, *Langmuir*, 2005, **21**, 5924-5930.
397. A. González Orive, P. Dip, Y. Gimeno, P. Díaz, P. Carro, A. Hernandez Creus, G. Benítez, P. L. Schilardi, L. Andrini and F. Requejo, *Chemistry—A European Journal*, 2007, **13**, 473-482.
398. Y. Liu and J. D. Simon, *Pigment cell research*, 2005, **18**, 42-48.
399. E. Di Mauro, O. Carpentier, S. Y. Sánchez, N. I. Ignoumba, M. Lalancette-Jean, J. Lefebvre, S. Zhang, C. F. Graeff, F. Cicoira and C. Santato, *Journal of Materials Chemistry C*, 2016, **4**, 9544-9553.
400. N. Jalili and K. Laxminarayana, *Mechatronics*, 2004, **14**, 907-945.
401. A. Büngeler, B. Hämisch, K. Huber, W. Bremser and O. I. Strube, *Langmuir*, 2017, **33**, 6895-6901.
402. G. Perna, M. Lasalvia, P. D'Antonio, A. Mallardi, G. Palazzo, D. Fiocco, A. Gallone, R. Cicero and V. Capozzi, *Micron*, 2014, **64**, 28-33.
403. J. Wünsche, F. Cicoira, C. F. Graeff and C. Santato, *Journal of Materials Chemistry B*, 2013, **1**, 3836-3842.

404. A. Zadlo, A. Pilat, M. Sarna, A. Pawlak and T. Sarna, *Cell biochemistry and biophysics*, 2017, **75**, 319-333.
405. G. Sun, F. Zu, N. Koch, J. Rappich and K. Hinrichs, *physica status solidi (b)*, 2019, **256**, 1800308.
406. M. Salomäki, M. Tupala, T. Parviainen, J. Leiro, M. Karonen and J. Lukkari, *Langmuir*, 2016, **32**, 4103-4112.
407. L. G. Albano, E. Di Mauro, P. Kumar, F. Cicoira, C. F. Graeff and C. Santato, *Polymer International*, 2016, **65**, 1315-1322.
408. J. Wünsche, L. Cardenas, F. Rosei, F. Cicoira, R. Gauvin, C. F. Graeff, S. Poulin, A. Pezzella and C. Santato, *Advanced Functional Materials*, 2013, **23**, 5591-5598.
409. J. Bayry, A. Beaussart, Y. F. Dufrêne, M. Sharma, K. Bansal, O. Kniemeyer, V. Aimanianda, A. A. Brakhage, S. V. Kaveri and K. J. Kwon-Chung, *Infection and immunity*, 2014, **82**, 3141-3153.
410. C. M. Clancy and J. D. Simon, *Biochemistry*, 2001, **40**, 13353-13360.
411. M. Xiao, W. Chen, W. Li, J. Zhao, Y.-l. Hong, Y. Nishiyama, T. Miyoshi, M. D. Shawkey and A. Dhinojwala, *Journal of The Royal Society Interface*, 2018, **15**, 20180045.
412. Y. Sun, L. Tian, J. Wen, J. Zhao, W. Zhang, C. Xie, M. Zhou, X. Qiu and D. Chen, *Journal of Ocean University of China*, 2017, **16**, 461-467.
413. D. N. Peles, L. Hong, D.-N. Hu, S. Ito, R. J. Nemanich and J. D. Simon, *The Journal of Physical Chemistry B*, 2009, **113**, 11346-11351.
414. Y. Liu, L. Hong, K. Wakamatsu, S. Ito, B. Adhyaru, C. Y. Cheng, C. R. Bowers and J. D. Simon, *Photochemistry and Photobiology*, 2005, **81**, 135-144.
415. T. Terlier, J. Lee and Y. Lee, *Journal of Vacuum Science & Technology B, Nanotechnology and Microelectronics: Materials, Processing, Measurement, and Phenomena*, 2018, **36**, 03F131.
416. S. Guo, L. Hong, B. B. Akhremitchev and J. D. Simon, *Photochemistry and photobiology*, 2008, **84**, 671-678.
417. M. Da Silva, S. Deziderio, J. Gonzalez, C. Graeff and M. Cotta, *Journal of applied physics*, 2004, **96**, 5803-5807.
418. F. P. Guengerich and F. K. Yoshimoto, *Chemical Reviews*, 2018, **118**, 6573-6655.
419. T.-S. Chang, *International journal of molecular sciences*, 2009, **10**, 2440-2475.
420. V. Zannoni, N. Lomtevas and S. J. B. e. B. A.-G. S. Goldfinger, 1969, **177**, 94-105.
421. J. R. Stone, in *Cardiovascular pathology*, Elsevier, 2022, pp. 307-351.
422. M. Ghoul and L. Chebil, in *Enzymatic polymerization of phenolic compounds by oxidoreductases*, Springer, 2012, pp. 1-46.
423. H. A. Galeb, E. L. Wilkinson, A. F. Stowell, H. Lin, S. T. Murphy, P. L. Martin-Hirsch, R. L. Mort, A. M. Taylor and J. G. Hardy, *Global Challenges*, 2021, **5**, 2000102.
424. N. NicDaéid, in *Encyclopedia of Analytical Science (Third Edition)*, eds. P. Worsfold, C. Poole, A. Townshend and M. Miró, Academic Press, Oxford, 2019, DOI: <https://doi.org/10.1016/B978-0-12-409547-2.14457-9>, pp. 75-80.
425. J. Tom, UV-Vis spectroscopy: Principles, strengths, and limitations and applications, <https://www.technologynetworks.com/analysis/articles/uv-vis-spectroscopy-principle-strengths-and-limitations-and-applications-349865>, (accessed July 2022).

426. J. Q. Brown, K. Vishwanath, G. M. Palmer and N. Ramanujam, *Current opinion in biotechnology*, 2009, **20**, 119-131.
427. J. L. Aleixandre-Tudo, A. Buica, H. Nieuwoudt, J. L. Aleixandre and W. du Toit, *Journal of agricultural and food chemistry*, 2017, **65**, 4009-4026.
428. J. Bates, *Science*, 1976, **191**, 31-37.
429. P. M. Shameer and P. M. Nishath, in *Advanced biofuels*, Elsevier, 2019, pp. 181-213.
430. R. Sindhu, P. Binod and A. Pandey, in *Industrial Biorefineries & White Biotechnology*, eds. A. Pandey, R. Höfer, M. Taherzadeh, K. M. Nampoothiri and C. Larroche, Elsevier, Amsterdam, 2015, DOI: <https://doi.org/10.1016/B978-0-444-63453-5.00019-7>, pp. 575-605.
431. F. Van de Voort, *Food Research International*, 1992, **25**, 397-403.
432. N. Jaggi and D. R. Vij, 2007, DOI: 10.1007/0-387-37590-2\_9, pp. 411-450.
433. M. Rani, Keshu and U. Shanker, in *Green Functionalized Nanomaterials for Environmental Applications*, eds. U. Shanker, C. M. Hussain and M. Rani, Elsevier, 2022, DOI: <https://doi.org/10.1016/B978-0-12-823137-1.00026-9>, pp. 43-80.
434. Z. Bacsik, J. Mink and G. Keresztury, *Applied Spectroscopy Reviews*, 2004, **39**, 295-363.
435. N. Vlachos, Y. Skopelitis, M. Psaroudaki, V. Konstantinidou, A. Chatzilazarou and E. Tegou, *Analytica chimica acta*, 2006, **573**, 459-465.
436. D. Titus, E. J. J. Samuel and S. M. Roopan, in *Green synthesis, characterization and applications of nanoparticles*, Elsevier, 2019, pp. 303-319.
437. M. Kaliva and M. Vamvakaki, in *Polymer science and nanotechnology*, Elsevier, 2020, pp. 401-433.
438. M. A. Mohamed, Z. A. Mohd Hir, W. N. A. Wan Mokhtar and N. S. Osman, in *Colloidal Metal Oxide Nanoparticles*, eds. S. Thomas, A. Tresa Sunny and P. Velayudhan, Elsevier, 2020, DOI: <https://doi.org/10.1016/B978-0-12-813357-6.00008-5>, pp. 83-122.
439. J. H. F. Bothwell and J. L. Griffin, *Biological Reviews*, 2011, **86**, 493-510.
440. M. K. Singh and A. Singh, *Characterization of Polymers and Fibres*, Elsevier, 2021.
441. R. Brüscheiler and F. Zhang, *The Journal of Chemical Physics*, 2004, **120**, 5253-5260.
442. K. Cheng, in *Natural Polyphenols from Wood*, eds. K. Cheng and C. Hagiopol, Elsevier, 2021, DOI: <https://doi.org/10.1016/B978-0-12-822205-8.00007-4>, pp. 147-182.
443. I. Fleming and D. H. Williams, *Spectroscopic methods in organic chemistry*, Springer, 1966.
444. H. E. Gottlieb, V. Kotlyar and A. Nudelman, *The Journal of Organic Chemistry*, 1997, **62**, 7512-7515.
445. R. F. Ilmasani, *Mechanism of the Passive NO<sub>x</sub> Adsorption Process on Zeolite Supported Pd in Controlling Cold Start Emissions*, Chalmers University of Technology, 2022.
446. B. Reif, S. E. Ashbrook, L. Emsley and M. Hong, *Nature Reviews Methods Primers*, 2021, **1**, 2.

447. K. C. Bynum, in *Separation Science and Technology*, Elsevier, 2011, vol. 10, pp. 361-396.
448. B. E. Lucier and Y. Huang, *Annual Reports on NMR Spectroscopy*, 2015, **84**, 233-289.
449. D. Massiot, F. Fayon, M. Capron, I. King, S. Le Calvé, B. Alonso, J. O. Durand, B. Bujoli, Z. Gan and G. Hoatson, *Magnetic resonance in chemistry*, 2002, **40**, 70-76.
450. M. Leskes, in *Encyclopedia of Analytical Science*, Elsevier, 2019, pp. 403-413.
451. M. Geppi, G. Mollica, S. Borsacchi and C. A. Veracini, *Applied Spectroscopy Reviews*, 2008, **43**, 202-302.
452. K. H. Mroue, A. Viswan, N. Sinha and A. Ramamoorthy, *Annual Reports on NMR Spectroscopy*, 2017, **92**, 365-413.
453. M. H. Cardoso, K. G. Oshiro, S. B. Rezende, E. S. Cândido and O. L. Franco, *Advances in protein chemistry and structural biology*, 2018, **112**, 359-384.
454. J. M. Hollander and W. L. Jolly, *Accounts of chemical research*, 1970, **3**, 193-200.
455. F. A. Stevie and C. L. Donley, *Journal of Vacuum Science & Technology A: Vacuum, Surfaces, and Films*, 2020, **38**, 063204.
456. R. R. Mather, in *Surface Modification of Textiles*, ed. Q. Wei, Woodhead Publishing, 2009, DOI: <https://doi.org/10.1533/9781845696689.296>, pp. 296-317.
457. H. Huang, Y. Qiao, Y. Yuan and J. Zhang, in *Reference Module in Materials Science and Materials Engineering*, Elsevier, 2022, DOI: <https://doi.org/10.1016/B978-0-12-822425-0.00073-7>.
458. T. L. Barr, *Journal of Vacuum Science & Technology A: Vacuum, Surfaces, and Films*, 1991, **9**, 1793-1805.
459. D. Frost, A. Ishitani and C. McDowell, *Molecular Physics*, 1972, **24**, 861-877.
460. C. S. Fadley, *Journal of Electron Spectroscopy and Related Phenomena*, 2010, **178**, 2-32.
461. D. Briggs and G. Beamson, *Analytical Chemistry*, 1992, **64**, 1729-1736.
462. J. F. Moulder, W. F. Stickle, P. E. Sobol and K. D. Bomben, *Perkin-Elmer Corp., Eden Prairie, MN*, 1992.
463. H. G. Barth, B. E. Boyes and C. Jackson, *ANALYTICAL CHEMISTRY-WASHINGTON DC-*, 1998, **70**, 251 R-278 R.
464. L. K. Kostanski, D. M. Keller and A. E. Hamielec, *Journal of biochemical and biophysical methods*, 2004, **58**, 159-186.
465. K. Nagy and K. VÉKey, in *Medical Applications of Mass Spectrometry*, eds. K. Vékey, A. Telekes and A. Vertes, Elsevier, Amsterdam, 2008, DOI: <https://doi.org/10.1016/B978-044451980-1.50007-0>, pp. 61-92.
466. P. K. Deb, S. F. Kokaz, S. N. Abed, A. Paradkar and R. K. Tekade, in *Basic Fundamentals of Drug Delivery*, ed. R. K. Tekade, Academic Press, 2019, DOI: <https://doi.org/10.1016/B978-0-12-817909-3.00006-6>, pp. 203-267.
467. K. Štulík, V. Pacáková and M. Tichá, *Journal of Biochemical and Biophysical Methods*, 2003, **56**, 1-13.
468. M. Rosado, R. Silva, M. G. Bexiga, J. G. Jones, B. Manadas and S. I. Anjo, in *Advances in Clinical Chemistry*, ed. G. S. Makowski, Elsevier, 2019, vol. 92, pp. 141-199.
469. J. Stetefeld, S. A. McKenna and T. R. Patel, *Biophysical reviews*, 2016, **8**, 409-427.

470. W. I. Goldberg, *American Journal of Physics*, 1999, **67**, 1152-1160.
471. M. Kaszuba, D. McKnight, M. T. Connah, F. K. McNeil-Watson and U. Nobbmann, *Journal of nanoparticle research*, 2008, **10**, 823-829.
472. N. Raval, R. Maheshwari, D. Kalyane, S. R. Youngren-Ortiz, M. B. Chougule and R. K. Tekade, in *Basic Fundamentals of Drug Delivery*, ed. R. K. Tekade, Academic Press, 2019, DOI: <https://doi.org/10.1016/B978-0-12-817909-3.00010-8>, pp. 369-400.
473. V. N. Uversky and A. K. Dunker, in *Comprehensive Biophysics*, ed. E. H. Egelman, Elsevier, Amsterdam, 2012, DOI: <https://doi.org/10.1016/B978-0-12-374920-8.00312-X>, pp. 170-211.
474. M. I. Szykowska, in *Encyclopedia of Analytical Science (Second Edition)*, eds. P. Worsfold, A. Townshend and C. Poole, Elsevier, Oxford, 2005, DOI: <https://doi.org/10.1016/B0-12-369397-7/00385-X>, pp. 134-143.
475. K. Vernon-Parry, *III-Vs Review*, 2000, **13**, 40-44.
476. N. Altawell, in *Introduction to Machine Olfaction Devices*, ed. N. Altawell, Academic Press, 2022, DOI: <https://doi.org/10.1016/B978-0-12-822420-5.00008-8>, pp. 139-157.
477. S. Lewis, K. Agg, S. Gutowski and P. Ross, in *In Encyclopedia of Analytical Science*, Second Edition edn., 2005, pp. 430-360.
478. O. D. Neikov and N. A. Yefimov, in *Handbook of Non-Ferrous Metal Powders (Second Edition)*, eds. O. D. Neikov, S. S. Naboychenko and N. A. Yefimov, Elsevier, Oxford, 2019, DOI: <https://doi.org/10.1016/B978-0-08-100543-9.00001-4>, pp. 3-62.
479. S. Ebnesajjad, in *Surface Treatment of Materials for Adhesive Bonding (Second Edition)*, ed. S. Ebnesajjad, William Andrew Publishing, Oxford, 2014, DOI: <https://doi.org/10.1016/B978-0-323-26435-8.00004-6>, pp. 39-75.
480. K. He, in *Encyclopedia of Energy Storage*, ed. L. F. Cabeza, Elsevier, Oxford, 2022, DOI: <https://doi.org/10.1016/B978-0-12-819723-3.00084-6>, pp. 256-264.
481. T. Lovejoy, Q. Ramasse, M. Falke, A. Kaepfel, R. Terborg, R. Zan, N. Dellby and O. Krivanek, *Applied Physics Letters*, 2012, **100**, 154101.
482. A. F. Ismail, K. C. Khulbe and T. Matsuura, in *Reverse Osmosis*, eds. A. F. Ismail, K. C. Khulbe and T. Matsuura, Elsevier, 2019, DOI: <https://doi.org/10.1016/B978-0-12-811468-1.00003-7>, pp. 57-90.
483. M. Nasrollahzadeh, M. Atarod, M. Sajjadi, S. M. Sajadi and Z. Issaabadi, in *Interface Science and Technology*, eds. M. Nasrollahzadeh, S. M. Sajadi, M. Sajjadi, Z. Issaabadi and M. Atarod, Elsevier, 2019, vol. 28, pp. 199-322.
484. J. Bergström, in *Mechanics of Solid Polymers*, ed. J. Bergström, William Andrew Publishing, 2015, DOI: <https://doi.org/10.1016/B978-0-323-31150-2.00002-9>, pp. 19-114.
485. I. Prencipe, D. Dellasega, A. Zani, D. Rizzo and M. Passoni, *Science and technology of advanced materials*, 2015.
486. S. Padhi and A. Behera, in *Agri-Waste and Microbes for Production of Sustainable Nanomaterials*, eds. K. A. Abd-Elsalam, R. Periakaruppan and S. Rajeshkumar, Elsevier, 2022, DOI: <https://doi.org/10.1016/B978-0-12-823575-1.00008-1>, pp. 397-440.

487. S. R. Spurgeon, C. Ophus, L. Jones, A. Petford-Long, S. V. Kalinin, M. J. Olszta, R. E. Dunin-Borkowski, N. Salmon, K. Hattar and W.-C. D. Yang, *Nature materials*, 2021, **20**, 274-279.
488. T. A. Sonia and C. P. Sharma, in *Oral Delivery of Insulin*, eds. T. A. Sonia and C. P. Sharma, Woodhead Publishing, 2014, DOI: <https://doi.org/10.1533/9781908818683.169>, pp. 169-217.
489. M. Jonasz and G. R. Fournier, in *Light Scattering by Particles in Water*, eds. M. Jonasz and G. R. Fournier, Academic Press, Amsterdam, 2007, DOI: <https://doi.org/10.1016/B978-012388751-1/50005-3>, pp. 267-445.
490. B. Misof, P. Roschger and P. Fratzl, in *Comprehensive Biomaterials*, ed. P. Ducheyne, Elsevier, Oxford, 2011, DOI: <https://doi.org/10.1016/B978-0-08-055294-1.00112-4>, pp. 407-426.
491. P. Sciau, in *Advances in Imaging and Electron Physics*, ed. P. W. Hawkes, Elsevier, 2016, vol. 198, pp. 43-67.
492. H. Rostamabadi, S. R. Falsafi and S. M. Jafari, in *Characterization of Nanoencapsulated Food Ingredients*, ed. S. M. Jafari, Academic Press, 2020, vol. 4, pp. 53-82.
493. N. Hogg, *Free Radical Biology and Medicine*, 2010, **49**, 122-129.
494. J. T. Klopogge, in *Developments in Clay Science*, eds. P. Yuan, A. Thill and F. Bergaya, Elsevier, 2016, vol. 7, pp. 115-136.
495. J. G. Speight, in *Environmental Inorganic Chemistry for Engineers*, ed. J. G. Speight, Butterworth-Heinemann, 2017, DOI: <https://doi.org/10.1016/B978-0-12-849891-0.00005-9>, pp. 231-282.
496. E. Mateos-Diaz, S. Amara, A. Roussel, S. Longhi, C. Cambillau and F. Carrière, in *Methods in Enzymology*, ed. M. H. Gelb, Academic Press, 2017, vol. 583, pp. 279-307.
497. B. A. Goodman and C. Yeretzyan, in *Processing and Impact on Active Components in Food*, ed. V. Preedy, Academic Press, San Diego, 2015, DOI: <https://doi.org/10.1016/B978-0-12-404699-3.00067-6>, pp. 559-566.
498. A.-F. Miller and G. W. Brudvig, *Biochimica et Biophysica Acta (BBA) - Bioenergetics*, 1991, **1056**, 1-18.
499. G. Jeschke, *Macromolecular rapid communications*, 2002, **23**, 227-246.
500. N. Senesi and G. S. Senesi, in *Encyclopedia of Soils in the Environment*, ed. D. Hillel, Elsevier, Oxford, 2005, DOI: <https://doi.org/10.1016/B0-12-348530-4/00209-5>, pp. 426-437.
501. *Nature Reviews Methods Primers*, 2021, **1**, 34.
502. S. Chevion, M. A. Roberts and M. Chevion, *Free radical biology and medicine*, 2000, **28**, 860-870.
503. F. Marken, A. Neudeck and A. M. Bond, in *Electroanalytical Methods: Guide to Experiments and Applications*, eds. F. Scholz, A. M. Bond, R. G. Compton, D. A. Fiedler, G. Inzelt, H. Kahlert, Š. Komorsky-Lovrić, H. Lohse, M. Lovrić, F. Marken, A. Neudeck, U. Retter, F. Scholz and Z. Stojek, Springer Berlin Heidelberg, Berlin, Heidelberg, 2010, DOI: 10.1007/978-3-642-02915-8\_4, pp. 57-106.
504. A. W. Bott, *Current Separations*, 1997, **16**, 23-26.
505. J. F. Rusling and S. L. Suib, *Advanced Materials*, 1994, **6**, 922-930.
506. J. Zhang, J. Wu, H. Zhang and J. Zhang, *PEM fuel cell testing and diagnosis*, Newnes, 2013.

507. P. T. Kissinger and W. R. Heineman, *Journal of chemical education*, 1983, **60**, 702.
508. S. Goel, M. Munjal, R. K. Sharma and G. Singh, in *Applications of Advanced Green Materials*, ed. S. Ahmed, Woodhead Publishing, 2021, DOI: <https://doi.org/10.1016/B978-0-12-820484-9.00014-3>, pp. 339-371.
509. H. Si, S. Zhang, S. Ma, Z. Xiong, A. Kausar, Q. Liao, Z. Zhang, A. Sattar, Z. Kang and Y. Zhang, *Advanced Energy Materials*, 2020, **10**, 1903922.
510. J. Alvarez, I. Ngo, M.-E. Gueunier-Farret, J.-P. Kleider, L. Yu, P. R. Cabarrocas, S. Perraud, E. Rouvière, C. Celle and C. Mouchet, *Nanoscale research letters*, 2011, **6**, 1-9.
511. S. Kwon, S. J. Lee, S. M. Kim, Y. Lee, H. Song and J. Y. Park, *Nanoscale*, 2015, **7**, 12297-12301.
512. in *Fundamentals and Applications of Nano Silicon in Plasmonics and Fullerenes*, ed. M. Nayfeh, Elsevier, 2018, DOI: <https://doi.org/10.1016/B978-0-323-48057-4.00005-0>, pp. 89-137.
513. Y. Zhu, T.-R. Kuo, Y.-H. Li, M.-Y. Qi, G. Chen, J. Wang, Y.-J. Xu and H. M. Chen, *Energy & Environmental Science*, 2021, **14**, 1928-1958.
514. P. M. A. Sherwood, in *Encyclopedia of Materials: Science and Technology*, eds. K. H. J. Buschow, R. W. Cahn, M. C. Flemings, B. Ilschner, E. J. Kramer, S. Mahajan and P. Veyssièrè, Elsevier, Oxford, 2001, DOI: <https://doi.org/10.1016/B0-08-043152-6/00183-2>, pp. 985-995.
515. T. Tamiri and S. Zitrin, in *Encyclopedia of Forensic Sciences (Second Edition)*, eds. J. A. Siegel, P. J. Saukko and M. M. Houck, Academic Press, Waltham, 2013, DOI: <https://doi.org/10.1016/B978-0-12-382165-2.00083-0>, pp. 64-84.
516. T. M. G. Selva, J. S. G. Selva and R. B. Prata, in *Reference Module in Biomedical Sciences*, Elsevier, 2021, DOI: <https://doi.org/10.1016/B978-0-12-822548-6.00081-9>.
517. M. Gumustas, C. T. Sengel-Turk, A. Gumustas, S. A. Ozkan and B. Uslu, in *Multifunctional Systems for Combined Delivery, Biosensing and Diagnostics*, ed. A. M. Grumezescu, Elsevier, 2017, DOI: <https://doi.org/10.1016/B978-0-323-52725-5.00005-8>, pp. 67-108.
518. O. O. Sonibare, T. Haeger and S. F. Foley, *Energy*, 2010, **35**, 5347-5353.
519. A. J. Bard, F. R. F. Fan, J. Kwak and O. Lev, *Analytical Chemistry*, 1989, **61**, 132-138.
520. A. J. Bard, G. Denuault, C. Lee, D. Mandler and D. O. Wipf, *Accounts of Chemical Research*, 1990, **23**, 357-363.
521. P. Sun, F. O. Laforge and M. V. Mirkin, *Physical Chemistry Chemical Physics*, 2007, **9**, 802-823.
522. T. Kai, C. G. Zoski and A. J. Bard, *Chemical communications*, 2018, **54** **16**, 1934-1947.
523. S. Amemiya, A. J. Bard, F.-R. F. Fan, M. V. Mirkin and P. R. Unwin, *Annual Review of Analytical Chemistry*, 2008, **1**, 95-131.
524. D. Polcari, P. Dauphin-Ducharme and J. Mauzeroll, *Chemical reviews*, 2016, **116** **22**, 13234-13278.
525. N. Kallay, D. Kovačević and S. Žalac, in *Interface Science and Technology*, ed. J. Lützenkirchen, Elsevier, 2006, vol. 11, pp. 133-170.

526. P. Moulin and H. Roques, *Journal of colloid and interface science*, 2003, **261** **1**, 115-126.
527. B. Salopek, D. Krsić and S. Filipović, 1992.
528. B. J. Kirby and E. F. Hasselbrink Jr., *ELECTROPHORESIS*, 2004, **25**, 187-202.
529. B. B. Weiner, W. W. Tscharnuter and D. Fairhurst, 1993.
530. Y. Yamashita and K. Sakamoto, *Cosmetic Science and Technology. Amsterdam: Elsevier*, 2017, 635-655.
531. S. Samimi, N. Maghsoudnia, R. B. Eftekhari and F. Dorkoosh, in *Characterization and Biology of Nanomaterials for Drug Delivery*, eds. S. S. Mohapatra, S. Ranjan, N. Dasgupta, R. K. Mishra and S. Thomas, Elsevier, 2019, DOI: <https://doi.org/10.1016/B978-0-12-814031-4.00003-9>, pp. 47-76.
532. G. V. Lowry, R. J. Hill, S. Harper, A. F. Rawle, C. O. Hendren, F. Klaessig, U. Nobbmann, P. Sayre and J. Rumble, *Environmental Science: Nano*, 2016, **3**, 953-965.
533. E. Joseph and G. Singhvi, *Nanomaterials for drug delivery and therapy*, 2019, 91-116.
534. S. Bhattacharjee, *Journal of controlled release*, 2016, **235**, 337-351.
535. J. D. Clogston and A. K. Patri, in *Zeta potential measurement: Characterization of Nanoparticles Intended for Drug Delivery*, ed. S. E. In McNeil, 2011, DOI: 10.1007/978-1-60327-198-1\_6, ch. 6, pp. 63-70.
536. C. N. Lunardi, A. J. Gomes, F. S. Rocha, J. de Tommaso and G. S. Patience, *Canadian Journal of Chemical Engineering*, 2020.
537. G. W. Lu and P. Gao, in *Handbook of Non-Invasive Drug Delivery Systems*, ed. V. S. Kulkarni, William Andrew Publishing, Boston, 2010, DOI: <https://doi.org/10.1016/B978-0-8155-2025-2.10003-4>, pp. 59-94.
538. C. V. Kumar and A. Pattammattel, in *Introduction to Graphene*, eds. C. V. Kumar and A. Pattammattel, Elsevier, 2017, DOI: <https://doi.org/10.1016/B978-0-12-813182-4.00008-8>, pp. 155-186.
539. J. Zschocke, K. M. Gibson, G. Brown, E. Morava and V. Peters, *JIMD reports*, Springer, 2015.
540. M. Xiao, M. D. Shawkey and A. Dhinojwala, *Advanced Optical Materials*, 2020, **8**, 2000932.
541. S. Ito and K. J. P. c. r. Wakamatsu, 2003, **16**, 523-531.
542. X. Chen, D. Xiao, X. Du, X. Guo, F. Zhang, N. Desneux, L. Zang and S. Wang, *Frontiers in physiology*, 2019, **10**, 1066.
543. M. J. Beltrán-García, F. M. Prado, M. S. Oliveira, D. Ortiz-Mendoza, A. C. Scalfio, A. Pessoa Jr, M. H. Medeiros, J. F. White and P. J. P. o. Di Mascio, 2014, **9**, e91616.
544. B. Roulier, B. Pérès and R. Haudecoeur, *Journal of Medicinal Chemistry*, 2020, **63**, 13428-13443.
545. A. Büngeler, B. Hämisch and O. J. I. j. o. m. s. Strube, 2017, **18**, 1901.
546. R. L. Schroeder, K. L. Double and J. P. J. J. o. c. n. Gerber, 2015, **64**, 20-32.
547. V. B. Yerger, R. E. J. N. Malone and t. research, 2006, **8**, 487-498.
548. F. J. I. j. o. m. s. Solano, 2017, **18**, 1561.
549. W. Cao, X. Zhou, N. C. McCallum, Z. Hu, Q. Z. Ni, U. Kapoor, C. M. Heil, K. S. Cay, T. Zand and A. J. Mantanona, *Journal of the American Chemical Society*, 2021, **143**, 2622-2637.
550. R. L. Mort, I. J. Jackson and E. E. Patton, *Development*, 2015, **142**, 620-632.

551. M. d'Ischia, A. Napolitano, A. Pezzella, P. Meredith and M. Buehler, *Angewandte Chemie International Edition*, 2020, **59**, 11196-11205.
552. M. Al Khatib, J. Costa, D. Spinelli, E. Capecchi, R. Saladino, M. C. Baratto and R. Pogni, *International journal of molecular sciences*, 2021, **22**, 1739.
553. L. Ranganath, A. M. Taylor, A. Shenkin, W. D. Fraser, J. Jarvis, J. A. Gallagher and N. Sireau, *Journal of inherited metabolic disease*, 2011, **34**, 723-730.
554. F. Lorquin, F. Ziarelli, A. Amouric, C. Di Giorgio, M. Robin, P. Piccerelle and J. Lorquin, *Scientific reports*, 2021, **11**, 1-16.
555. Y. Tokuhara, K. Shukuya, M. Tanaka, K. Sogabe, Y. Ejima, S. Hosokawa, H. Ohsaki, T. Morinishi, E. Hirakawa and Y. Yatomi, *Scientific reports*, 2018, **8**, 11364.
556. S. Castro-Sowinski, G. Martinez-Drets and Y. Okon, *FEMS Microbiology Letters*, 2002, **209**, 119-125.
557. G. Bayramoğlu and M. Y. Arica, *Journal of hazardous materials*, 2008, **156**, 148-155.
558. M. Masuda, A. Sakurai and M. Sakakibara, *World Journal of Microbiology and Biotechnology*, 2002, **18**, 739-743.
559. K. Ikehata and J. A. Nicell, *Bioresource Technology*, 2000, **74**, 191-199.
560. M. d'Ischia, A. Napolitano and G. Prota, *Biochimica et Biophysica Acta (BBA) - General Subjects*, 1991, **1073**, 423-430.
561. S. Kobayashi and H. J. P. i. P. S. Higashimura, 2003, **28**, 1015-1048.
562. J. López, J. M. Hernández-Alcántara, P. Roquero, C. Montiel, K. Shirai, M. Gimeno and E. Bárzana, *Journal of Molecular Catalysis B: Enzymatic*, 2013, **97**, 100-105.
563. M. Sánchez-Mundo, V. Escobedo-Crisantes, S. Mendoza-Arvizu and M. Jaramillo-Flores, *CyTA-Journal of Food*, 2016, **14**, 594-603.
564. A. C. Ferrari, F. Bonaccorso, V. Fal'Ko, K. S. Novoselov, S. Roche, P. Bøggild, S. Borini, F. H. Koppens, V. Palermo and N. Pugno, *Nanoscale*, 2015, **7**, 4598-4810.
565. Y. Topal, S. Tapan, E. Gokturk and E. Sahmetlioglu, *Journal of Saudi Chemical Society*, 2017, **21**, 731-740.
566. J. B. Max, P. J. Mons, J. C. Tom and F. H. Schacher, *Macromolecular Chemistry and Physics*, 2020, **221**, 1900383.
567. J. C. Alves and J. A. Freire, *Macromolecular Theory and Simulations*, 2018, **27**, 1800020.
568. A. B. Mostert, G. R. Hanson, T. Sarna, I. R. Gentle, B. J. Powell and P. Meredith, *The Journal of Physical Chemistry B*, 2013, **117**, 4965-4972.
569. S. Dubey, D. Singh, R. J. E. Misra and m. technology, 1998, **23**, 432-437.
570. P. Meredith and T. Sarna, *Pigment Cell Research*, 2006, **19**, 572-594.
571. M. A. Dubé and S. Salehpour, *Macromolecular Reaction Engineering*, 2014, **8**, 7-28.
572. T. Eom, K. Woo, W. Cho, J. E. Heo, D. Jang, J. I. Shin, D. C. Martin, J. J. Wie and B. S. Shim, *Biomacromolecules*, 2017, **18**, 1908-1917.
573. J. Paulin, A. Coleone, A. Batagin-Neto, G. Burwell, P. Meredith, C. Graeff and A. Mostert, *Journal of Materials Chemistry C*, 2021, **9**, 8345-8358.
574. J. P. Bothma, J. de Boor, U. Divakar, P. E. Schwenn and P. Meredith, *Advanced Materials*, 2008, **20**, 3539-3542.

575. P. Zheng, B. Ding and G. Li, *Macromolecular Bioscience*, 2020, 2000228.
576. S. Wang, Q. Liu, L. Li and M. W. Urban, *Macromolecular Rapid Communications*, 2021, **42**, 2100054.
577. D. Cui, C. Xie and K. Pu, *Macromolecular rapid communications*, 2017, **38**, 1700125.
578. J. H. Ryu, P. B. Messersmith and H. Lee, *ACS Applied Materials & Interfaces*, 2018, **10**, 7523-7540.
579. D. R. Amin, C. Sugnaux, K. H. A. Lau and P. B. Messersmith, *Biomimetics*, 2017, **2**, 17.
580. A. Banerjee and S. Ray, *Gene*, 2016, **592**, 99-109.
581. C. Olivares and F. Solano, *Pigment Cell & Melanoma Research*, 2009, **22**, 750-760.
582. S. V. S. Kumar, P. S. Phale, S. Durani and P. P. Wangikar, *Biotechnology and Bioengineering*, 2003, **83**, 386-394.
583. Y.-T. Chien and S.-W. Huang, *PloS one*, 2012, **7**, e47951.
584. A. J. M. Ribeiro, J. D. Tyzack, N. Borkakoti, G. L. Holliday and J. M. Thornton, *Journal of Biological Chemistry*, 2020, **295**, 314-324.
585. T. Zhang, H. Zhang, K. Chen, S. Shen, J. Ruan and L. Kurgan, *Bioinformatics*, 2008, **24**, 2329-2338.
586. K. CHOI and S. KIM, *Journal of Bioinformatics and Computational Biology*, 2011, **09**, 597-611.
587. I. Shah and L. Hunter, *Proceedings. International Conference on Intelligent Systems for Molecular Biology*, 1997, **5**, 276-283.
588. M. Gauden, A. Pezzella, L. Panzella, M. Neves-Petersen, E. Skovsen, S. B. Petersen, K. Mullen, A. Napolitano, M. d'Ischia and V. Sundstrom, *Journal of the American Chemical Society*, 2008, **130**, 17038-17043.
589. T. H. P. Atlas, <https://www.proteinatlas.org/ENSG00000179630-LACC1/tissue>, (accessed August 2022).
590. T. H. P. Atlas, <https://www.proteinatlas.org/ENSG00000077498-TYR/tissue>, (accessed August 2022).
591. M. A. Durante, D. A. Rodriguez, S. Kurtenbach, J. N. Kuznetsov, M. I. Sanchez, C. L. Decatur, H. Snyder, L. G. Feun, A. S. Livingstone and J. W. Harbour, *Nature communications*, 2020, **11**, 1-10.
592. R. L. Belote, D. Le, A. Maynard, U. E. Lang, A. Sinclair, B. K. Lohman, V. Planells-Palop, L. Baskin, A. D. Tward and S. Darmanis, *Nature Cell Biology*, 2021, **23**, 1035-1047.
593. Z. ABATTYANI, L. Xerri, J. Hassoun, J. J. BONERANDI and J. J. GROB, *Pigment cell research*, 1993, **6**, 400-405.
594. I. Weidenfeld, C. Zakian, P. Duewell, A. Chmyrov, U. Klemm, J. Aguirre, V. Ntziachristos and A. C. Stiel, *Nature communications*, 2019, **10**, 1-12.
595. A. A. Putnam and J. J. Wilker, *Soft Matter*, 2021, **17**, 1999-2009.
596. M. Dunbar and S. Ketten, *Macromolecules*, 2020, **53**, 9397-9405.
597. X. Hu, Z. Li, Z. Yang, F. Zhu, W. Zhao, G. Duan and Y. Li, *ACS Macro Letters*, 2022, **11**, 251-256.
598. A. Moliton and R. C. Hiorns, *Polymer International*, 2004, **53**, 1397-1412.
599. S. Kobayashi, *Journal of Polymer Science Part A: Polymer Chemistry*, 1999, **37**, 3041-3056.
600. N. Aktaş, N. Şahiner, Ö. Kantoğlu, B. Salih and A. Tanyolaç, *Journal of Polymers and the Environment*, 2003, **11**, 123-128.

601. S. Dubey, D. Singh and R. A. Misra, *Enzyme and Microbial Technology*, 1998, **23**, 432-437.
602. N. Li, H.-B. Wang, L. Thia, J.-Y. Wang and X. Wang, *Analyst*, 2015, **140**, 449-455.
603. F. Li, Y. Yu, Q. Wang, J. Yuan, P. Wang and X. Fan, *Enzyme and Microbial Technology*, 2018, **119**, 58-64.
604. H. A. Galeb, A. Lamantia, A. Robson, K. König, J. Eichhorn, S. J. Baldock, M. D. Ashton, J. V. Baum, R. L. Mort, B. J. Robinson, F. H. Schacher, V. Chechik, A. M. Taylor and J. G. Hardy, *Macromolecular Chemistry and Physics*, 2022, **223**, 2100489.
605. R. J. Waltman and J. Bargon, *Canadian Journal of Chemistry*, 1986, **64**, 76-95.
606. H. Ma, Y. Chen, X. Li and B. Li, *Advanced Functional Materials*, 2021, **31**, 2101861.
607. M. R. J. Scherer, in *Double-Gyroid-Structured Functional Materials: Synthesis and Applications*, ed. M. R. J. Scherer, Springer International Publishing, Heidelberg, 2013, DOI: 10.1007/978-3-319-00354-2\_7, pp. 135-156.
608. Q. Zhang, H. Dong and W. Hu, *Journal of Materials Chemistry C*, 2018, **6**, 10672-10686.
609. R. Pourghobadi, D. Nematollahi, M. R. Baezzat, S. Alizadeh and H. Goljani, *Journal of Electroanalytical Chemistry*, 2020, **866**, 114180.
610. E. Voisin and V. E. Williams, *Macromolecules*, 2008, **41**, 2994-2997.
611. K. Yong and M. Shao-Lin, *Chinese Journal of Chemistry*, 2003, **21**, 630-637.
612. S. Li, H. Wang, M. Young, F. Xu, G. Cheng and H. Cong, *Langmuir*, 2019, **35**, 1119-1125.
613. F. Lorquin, P. Piccerelle, C. Orneto, M. Robin and J. Lorquin, *Journal of Industrial Microbiology and Biotechnology*, 2022, **49**.
614. S. Kobayashi and H. Higashimura, *Progress in Polymer Science*, 2003, **28**, 1015-1048.
615. S. Kobayashi, S.-i. Shoda and H. Uyama, in *Polymer Synthesis/Polymer Engineering*, Springer Berlin Heidelberg, Berlin, Heidelberg, 1995, DOI: 10.1007/BFb0018577, pp. 1-30.
616. A. C. Ferrari, F. Bonaccorso, V. Fal'ko, K. S. Novoselov, S. Roche, P. Bøggild, S. Borini, F. H. L. Koppens, V. Palermo, N. Pugno, J. A. Garrido, R. Sordan, A. Bianco, L. Ballerini, M. Prato, E. Lidorikis, J. Kivioja, C. Marinelli, T. Ryhänen, A. Morpurgo, J. N. Coleman, V. Nicolosi, L. Colombo, A. Fert, M. Garcia-Hernandez, A. Bachtold, G. F. Schneider, F. Guinea, C. Dekker, M. Barbone, Z. Sun, C. Galiotis, A. N. Grigorenko, G. Konstantatos, A. Kis, M. Katsnelson, L. Vandersypen, A. Loiseau, V. Morandi, D. Neumaier, E. Treossi, V. Pellegrini, M. Polini, A. Tredicucci, G. M. Williams, B. Hee Hong, J.-H. Ahn, J. Min Kim, H. Zirath, B. J. van Wees, H. van der Zant, L. Occhipinti, A. Di Matteo, I. A. Kinloch, T. Seyller, E. Quesnel, X. Feng, K. Teo, N. Rupesinghe, P. Hakonen, S. R. T. Neil, Q. Tannock, T. Löfwander and J. Kinaret, *Nanoscale*, 2015, **7**, 4598-4810.
617. L. W. Flanagan, C. L. McAdams, W. D. Hinsberg, I. C. Sanchez and C. G. Willson, *Macromolecules*, 1999, **32**, 5337-5343.

618. H. A. Galeb, E. L. Wilkinson, A. F. Stowell, H. Lin, S. T. Murphy, P. L. Martin-Hirsch, R. L. Mort, A. M. Taylor and J. G. Hardy, *Global Challenges*, 2021, **5**, 2000102.
619. X. Ma, Z. Sun, W. Su, Z. Yi, X. Cui, B. Guo and X. Li, *Journal of Materials Chemistry B*, 2018, **6**, 3811-3819.
620. L. Klosterman and C. J. Bettinger, *International Journal of Molecular Sciences*, 2017, **18**, 14.
621. L. Hong and J. D. Simon, *The Journal of Physical Chemistry B*, 2007, **111**, 7938-7947.
622. P. Kumar, E. Di Mauro, S. Zhang, A. Pezzella, F. Soavi, C. Santato and F. Cicoira, *Journal of Materials Chemistry C*, 2016, **4**, 9516-9525.
623. L. Yang, X. Guo, Z. Jin, W. Guo, G. Duan, X. Liu and Y. Li, *Nano Today*, 2021, **37**, 101075.
624. A. Gouda, A. Masson, M. Hoseinizadeh, F. Soavi and C. Santato, *Communications Chemistry*, 2022, **5**, 98.
625. M. Nicolai, G. Gonçalves, F. Natalio and M. Humanes, *Journal of Inorganic Biochemistry*, 2011, **105**, 887-893.
626. S. N. Dezidério, C. A. Brunello, M. I. N. da Silva, M. A. Cotta and C. F. O. Graeff, *Journal of Non-Crystalline Solids*, 2004, **338-340**, 634-638.
627. V. Capozzi, G. Perna, P. Carmone, A. Gallone, M. Lastella, E. Mezzenga, G. Quartucci, M. Ambrico, V. Augelli, P. F. Biagi, T. Ligonzo, A. Minafra, L. Schiavulli, M. Pallara and R. Cicero, *Thin Solid Films*, 2006, **511-512**, 362-366.
628. G. Khouqeer, M. Alghrably, N. Madkhali, M. Dhahri, M. Jaremko and A.-H. Emwas, *Nano Select*, 2022, **3**, 1598-1608.
629. B. Bilińska, *Spectrochimica Acta Part A: Molecular and Biomolecular Spectroscopy*, 1996, **52**, 1157-1162.
630. H. Wei, J. Ren, B. Han, L. Xu, L. Han and L. Jia, *Colloids and Surfaces B: Biointerfaces*, 2013, **110**, 22-28.
631. Z.-Y. Xi, Y.-Y. Xu, L.-P. Zhu, Y. Wang and B.-K. Zhu, *Journal of Membrane Science*, 2009, **327**, 244-253.
632. J. Stainsack, A. S. Mangrich, C. M. B. F. Maia, V. G. Machado, J. C. P. dos Santos and S. Nakagaki, *Inorganica Chimica Acta*, 2003, **356**, 243-248.
633. S. Paim, L. F. Linhares, A. S. Mangrich and J. P. Martin, *Biology and Fertility of Soils*, 1990, **10**, 72-76.
634. T. Sarna, H. M. Swartz and A. Zadlo, *Applied Magnetic Resonance*, 2022, **53**, 105-121.
635. J. Szewczyk, D. Aguilar-Ferrer and E. Coy, *European Polymer Journal*, 2022, **174**, 111346.
636. K. Namsheer and C. S. Rout, *RSC advances*, 2021, **11**, 5659-5697.
637. M. Bajpai, R. Srivastava, R. Dhar and R. Tiwari, *Indian Journal of Materials Science*, 2016, **2016**.
638. W. Han, M. He, M. Byun, B. Li and Z. Lin, *Angewandte Chemie International Edition*, 2013, **52**, 2564-2568.
639. A. O. Patil, Y. Ikenoue, N. Basescu, N. Colaneri, J. Chen, F. Wudl and A. J. Heeger, *Synthetic Metals*, 1987, **20**, 151-159.
640. D. A. Lukyanov, A. A. Vereshchagin, A. V. Soloviova, O. V. Grigorova, P. S. Vlasov and O. V. Levin, *ACS Applied Energy Materials*, 2021, **4**, 5070-5078.

641. C. Beaumont, J. Turgeon, M. Idir, D. Neusser, R. Lapointe, S. Caron, W. Dupont, D. D'Astous, S. Shamsuddin, S. Hamza, É. Landry, S. Ludwigs and M. Leclerc, *Macromolecules*, 2021, **54**, 5464-5472.
642. I. Imae and K. Krukiewicz, *Bioelectrochemistry*, 2022, **146**, 108127.
643. M. d'Ischia, A. Napolitano, A. Pezzella, P. Meredith and T. Sarna, *Angewandte Chemie International Edition*, 2009, **48**, 3914-3921.
644. S. Benito-Martínez, L. Salavessa, G. Raposo, M. S. Marks and C. Delevoeye, *Integrative and Comparative Biology*, 2021, **61**, 1546-1555.
645. A. Slominski, D. J. Tobin, S. Shibahara and J. Wortsman, *Physiological reviews*, 2004, **84**, 1155-1228.
646. A. A. Fisher, M. T. Labenski, S. Malladi, J. D. Chapman, S. B. Bratton, T. J. Monks and S. S. Lau, *Toxicological Sciences*, 2011, **122**, 64-72.
647. M. Yamauchi and M. Sricholpech, *Essays in biochemistry*, 2012, **52**, 113-133.
648. J. G. Snedeker and A. Gautieri, *Muscles, ligaments and tendons journal*, 2014, **4**, 303.
649. K. M. Mak, C. Y. M. Png and D. J. Lee, *The Anatomical Record*, 2016, **299**, 613-629.
650. E. Saylam, Y. Akkaya, E. Ilhan, S. Cesur, E. Guler, A. Sahin, M. E. Cam, N. Ekren, F. N. Oktar and O. Gunduz, *Applied Sciences*, 2021, **11**, 10727.
651. W. Garnjanagoonchorn, L. Wongekalak and A. Engkagul, *Chemical Engineering and Processing: Process Intensification*, 2007, **46**, 465-471.
652. S. HONDA, H. YUKI and K. TAKIURA, *The Journal of Biochemistry*, 1974, **76**, 209-211.
653. M. Foot and M. Mulholland, *Journal of Pharmaceutical and Biomedical Analysis*, 2005, **38**, 397-407.
654. F. Cabassi, B. Casu and A. S. Perlin, *Carbohydrate Research*, 1978, **63**, 1-11.
655. R. Servaty, J. Schiller, H. Binder and K. Arnold, *International Journal of Biological Macromolecules*, 2001, **28**, 121-127.
656. W. Cao, X. Zhou, N. C. McCallum, Z. Hu, Q. Z. Ni, U. Kapoor, C. M. Heil, K. S. Cay, T. Zand, A. J. Mantanona, A. Jayaraman, A. Dhinojwala, D. D. Deheyn, M. D. Shawkey, M. D. Burkart, J. D. Rinehart and N. C. Gianneschi, *Journal of the American Chemical Society*, 2021, **143**, 2622-2637.
657. G. K. Hamer and A. S. Perlin, *Carbohydrate Research*, 1976, **49**, 37-48.
658. M. Cîrcu and C. Filip, *Polymer Chemistry*, 2018, **9**, 3379-3387.
659. A. M. Taylor, M.-F. Hsueh, L. R. Ranganath, J. A. Gallagher, J. P. Dillon, J. L. Huebner, J. B. Catterall and V. B. Kraus, *Rheumatology*, 2017, **56**, 156-164.
660. L. Wu, H. Shao, Z. Fang, Y. Zhao, C. Y. Cao and Q. Li, *ACS Biomaterials Science & Engineering*, 2019, **5**, 4272-4284.
661. E. Yamamoto, K. Hayashi and N. Yamamoto, *Clinical Biomechanics*, 1999, **14**, 418-425.
662. R. G. Wells, *Elife*, 2022, **11**, e77041.
663. A. K. Maurya, A. Parrilli, T. Kochetkova, J. Schwiedrzik, A. Dommann and A. Neels, *Acta Biomaterialia*, 2021, **129**, 169-177.
664. A. Spilotros, A. Gruzinov and D. I. Svergun, in *Encyclopedia of Analytical Chemistry*, DOI: <https://doi.org/10.1002/9780470027318.a9447.pub2>, pp. 1-39.
665. L. Huang, Z. Li, Y. Lou, F. Cao, D. Zhang and X. Li, *Materials*, 2018, **11**, 1389.

666. F. Conzuelo, A. Schulte and W. Schuhmann, *Proceedings of the Royal Society A: Mathematical, Physical and Engineering Sciences*, 2018, **474**, 20180409.
667. I. Beaulieu, S. Kuss, J. Mauzeroll and M. Geissler, *Analytical Chemistry*, 2011, **83**, 1485-1492.
668. T.-E. Lin, F. Cortés-Salazar, A. Lesch, L. Qiao, A. Bondarenko and H. H. Girault, *Electrochimica Acta*, 2015, **179**, 57-64.

# 8 Appendices

## 8.1 Appendix

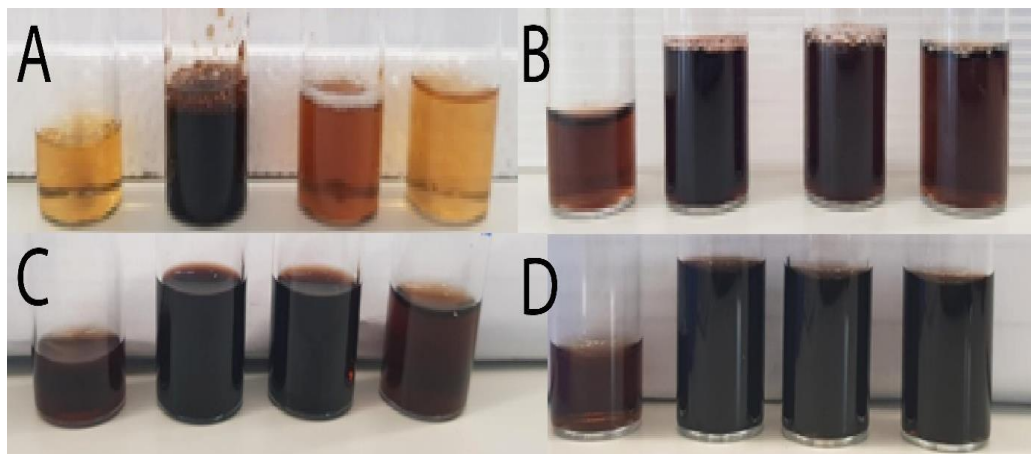


*Figure A.1.1: Photographs of reaction mixtures. In each case from left to right: no enzyme control, with peroxidase, with laccase, with tyrosinase. A) After 24 hours at pH 5. B) After 24 hours at pH 7.4. C) After 6 weeks at pH 5. D) After 6 weeks at pH 7.4.*

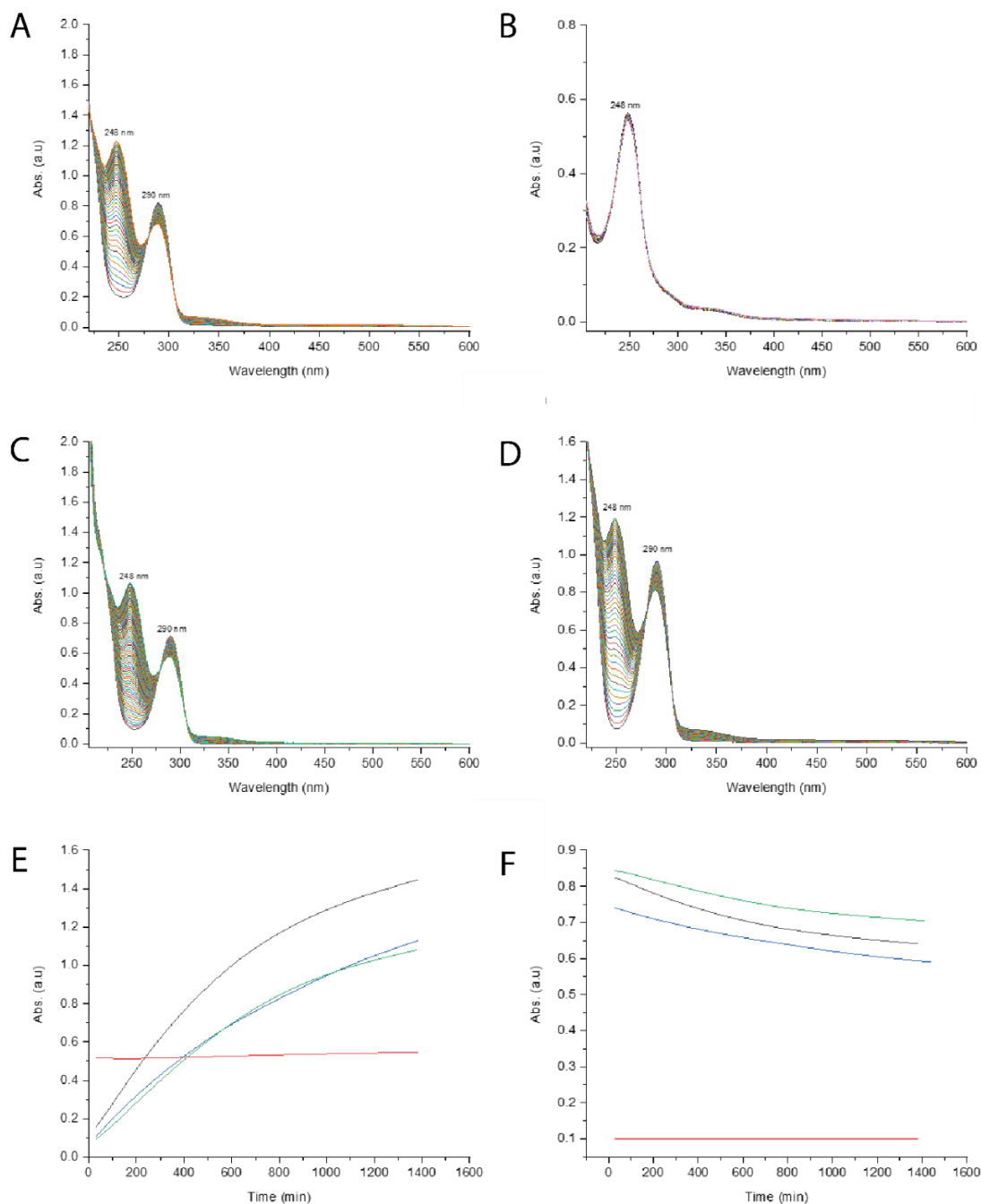


Figure A.1.2: UV-vis spectra of reaction mixtures over a period of 24 hours at pH 7.4. **A)** no enzyme control. **B)** with peroxidase. **C)** with laccase. **D)** with tyrosinase. **E and F)** Average peak intensity over 24 hours at 248 and 290 nm, respectively: no enzyme control (black line), with peroxidase (red line), with laccase (blue line), with tyrosinase (green line). For the no enzyme control, reaction in the presence of laccase or tyrosinase, the peak intensity at 290 nm characteristic of HGA decreases in intensity over 24 hours, and the peak intensity at 248 nm characteristic of BQA increases in intensity; by comparison for the reaction in the presence of peroxidase the oxidation of HGA to BQA is very fast, as is the onset of polymerization (broad band absorption > 300 nm).

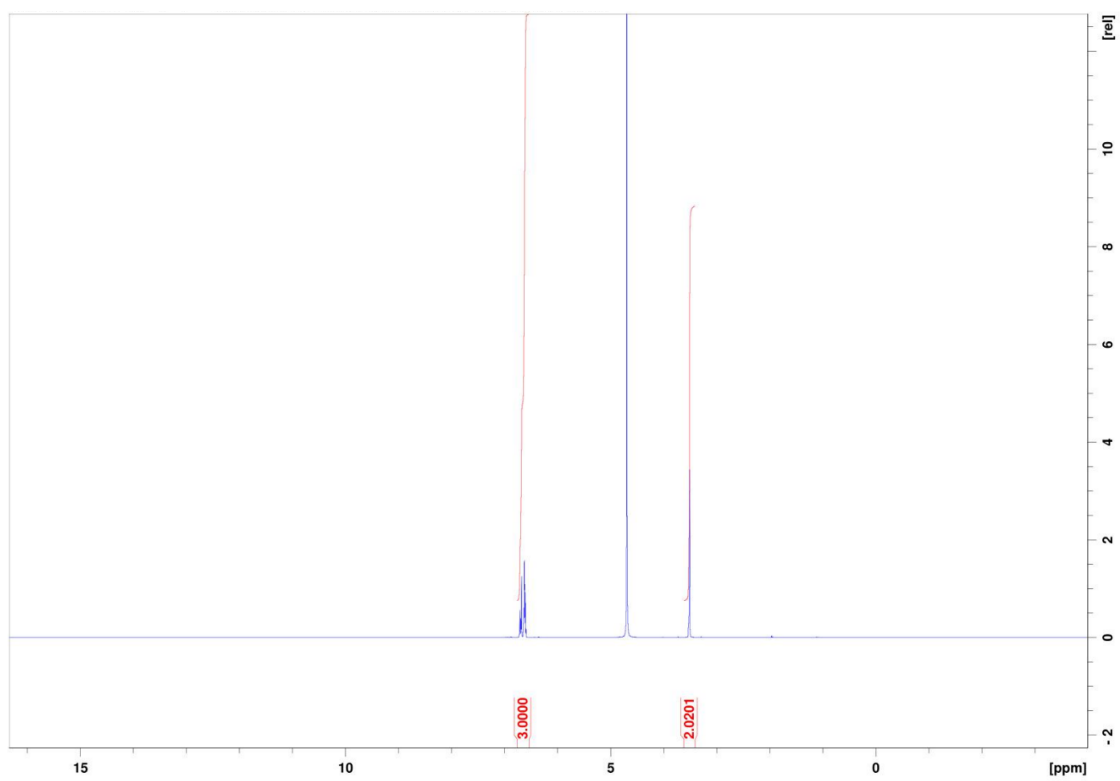


Figure A.1.3:  $^1\text{H}$  NMR of HGA in  $\text{D}_2\text{O}$ .

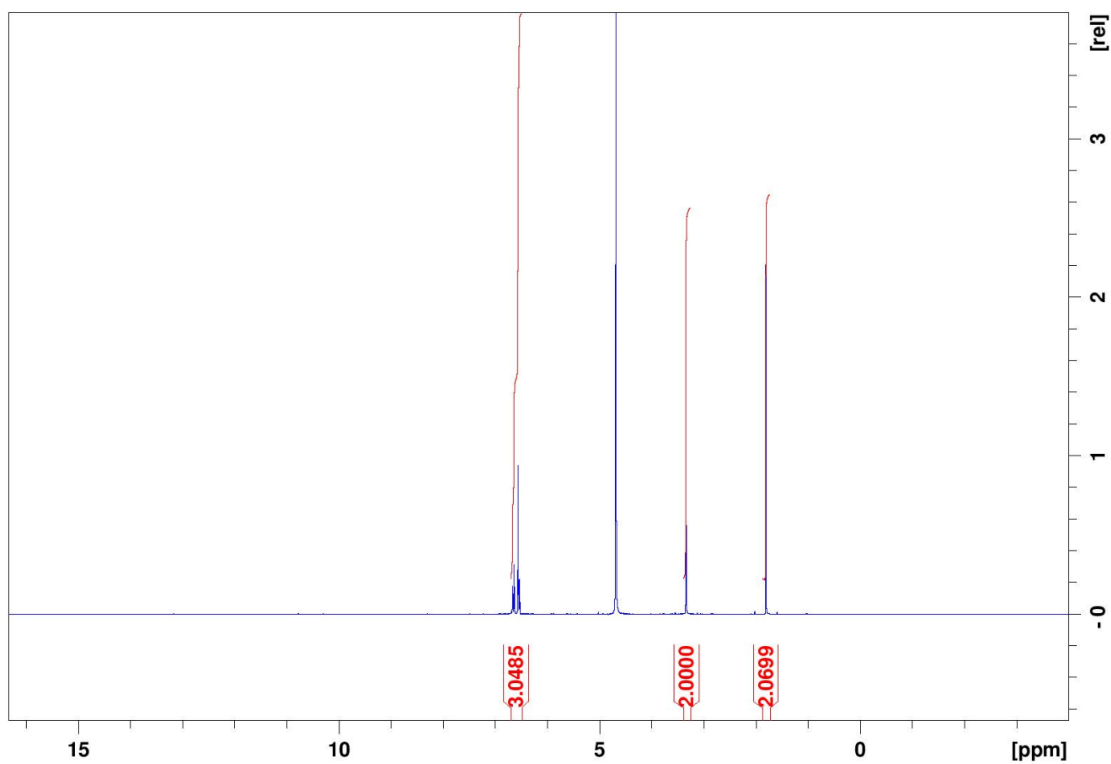


Figure A.1.4:  $^1\text{H}$  NMR of polyHGA in  $\text{D}_2\text{O}$  (no enzyme control at pH 5.0); includes trace of acetone.

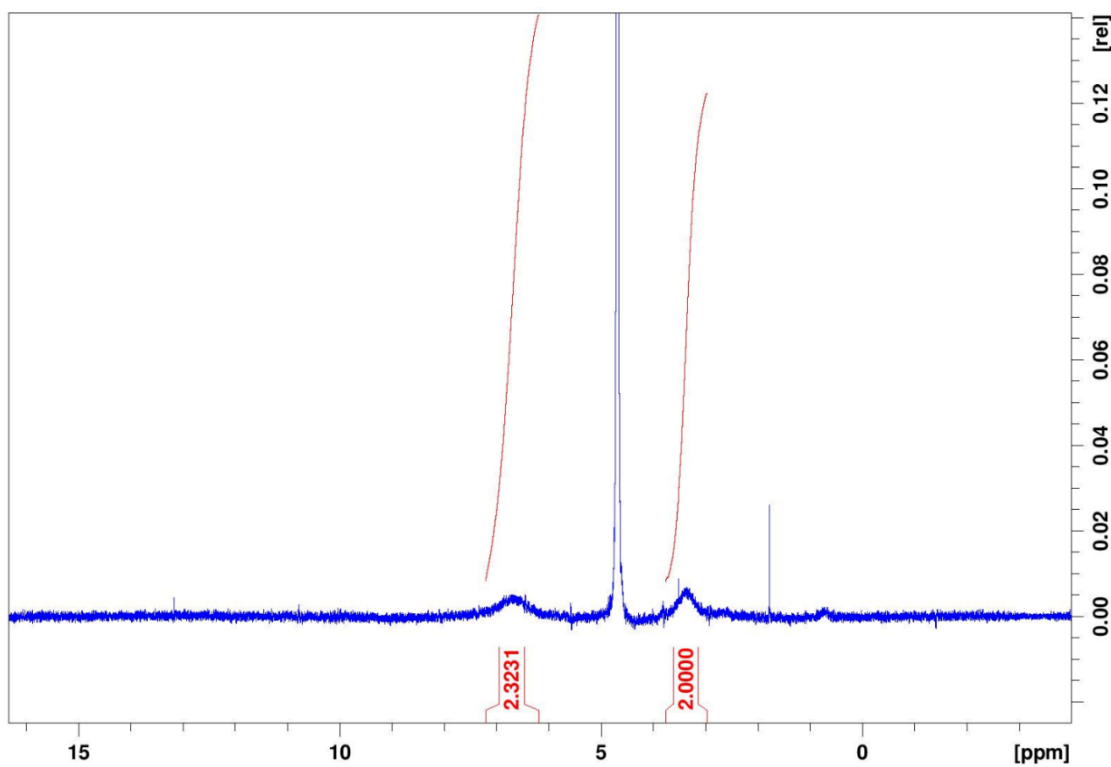


Figure A.1.5:  $^1\text{H}$  NMR of polyHGA in  $\text{D}_2\text{O}$  (no enzyme control at pH 7.4).

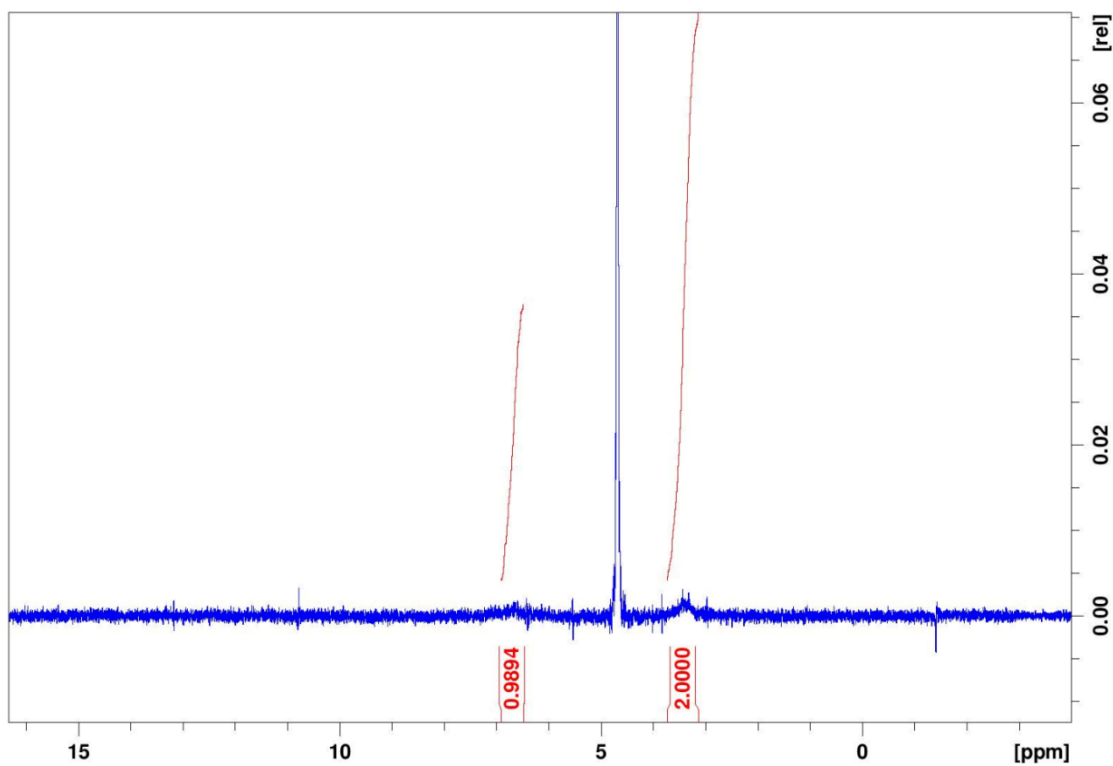


Figure A.1.6:  $^1\text{H}$  NMR of polyHGA in  $\text{D}_2\text{O}$  (formed in the presence of tyrosinase at pH 5.0).

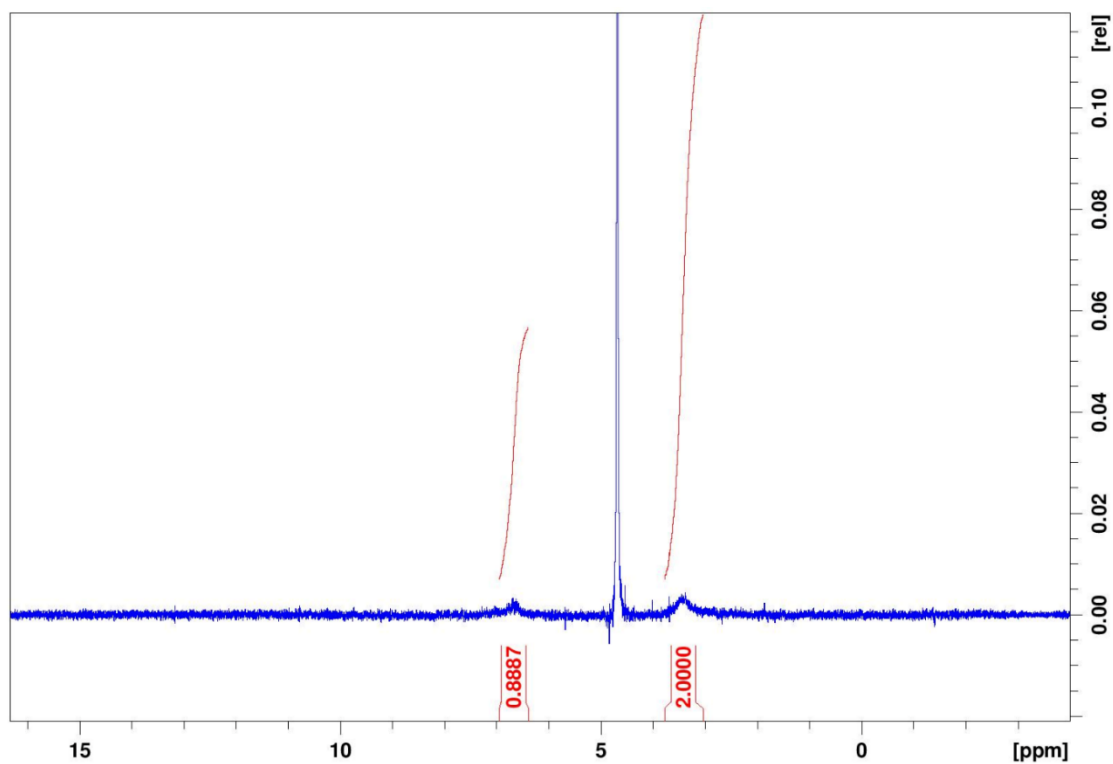


Figure A.1.7:  $^1\text{H}$  NMR of polyHGA in  $\text{D}_2\text{O}$  (formed in the presence of tyrosinase at pH 7.4).

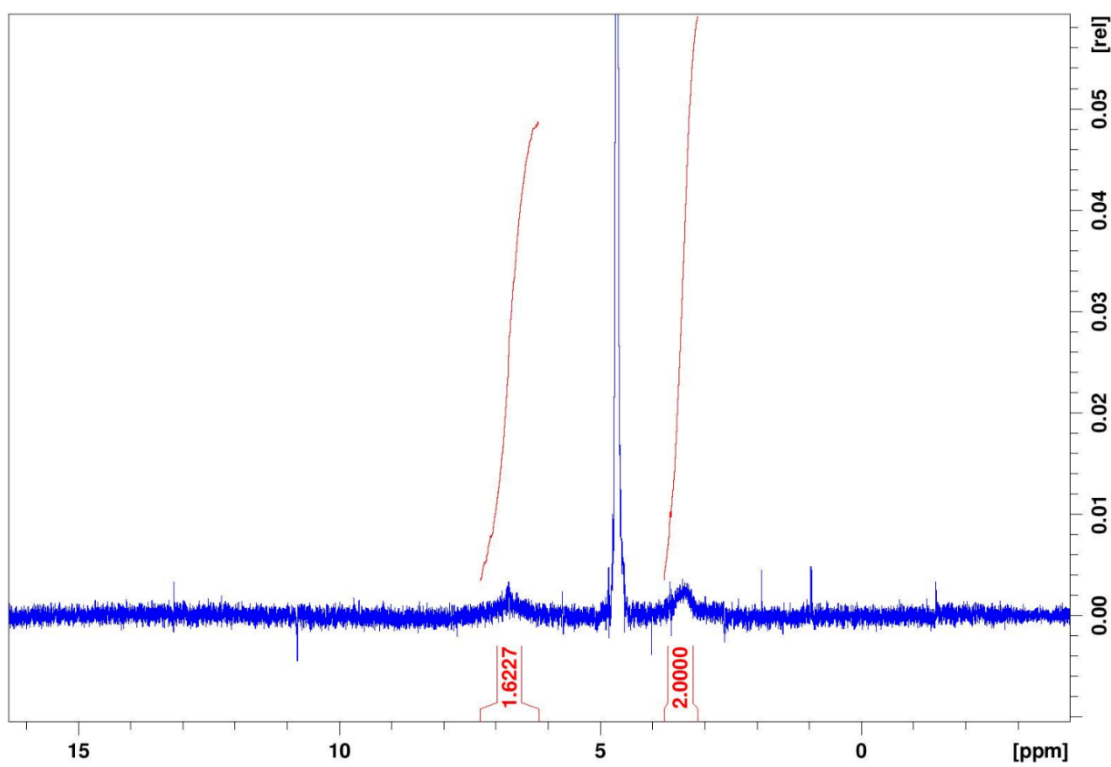


Figure A.1.8:  $^1\text{H}$  NMR of polyHGA in  $\text{D}_2\text{O}$  (formed in the presence of laccase at pH 5.0).

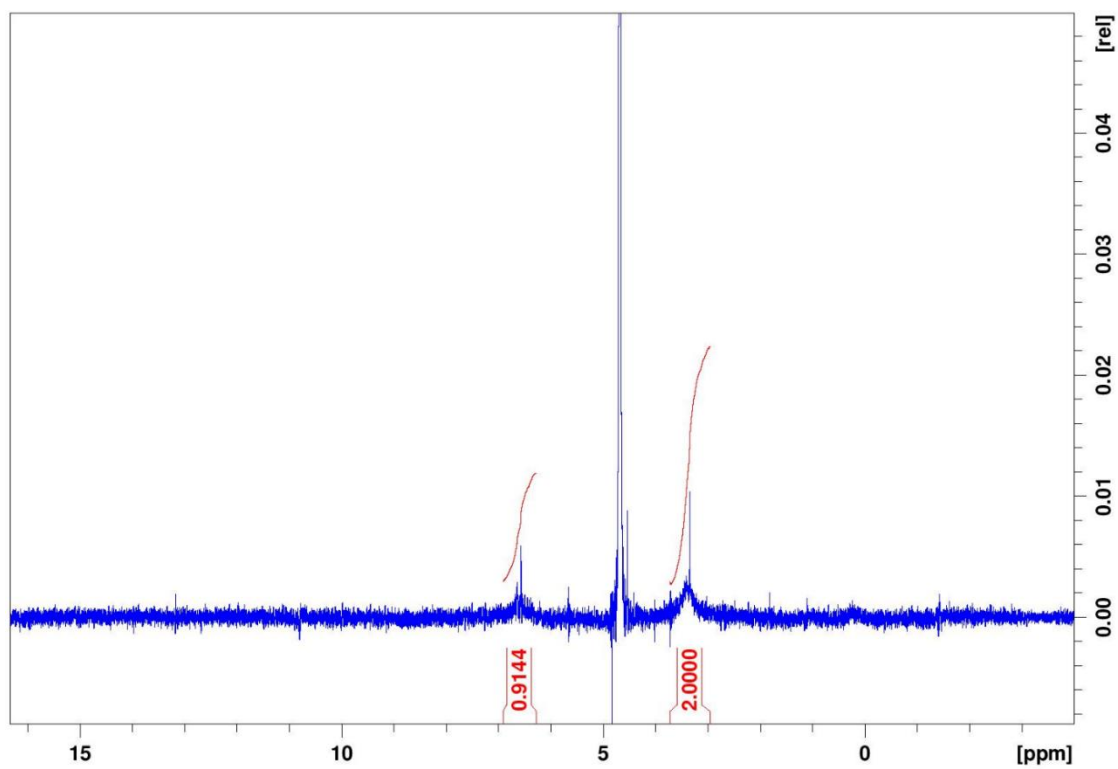


Figure A.1.9:  $^1\text{H}$  NMR of polyHGA in  $\text{D}_2\text{O}$  (formed in the presence of laccase at pH 7.4).

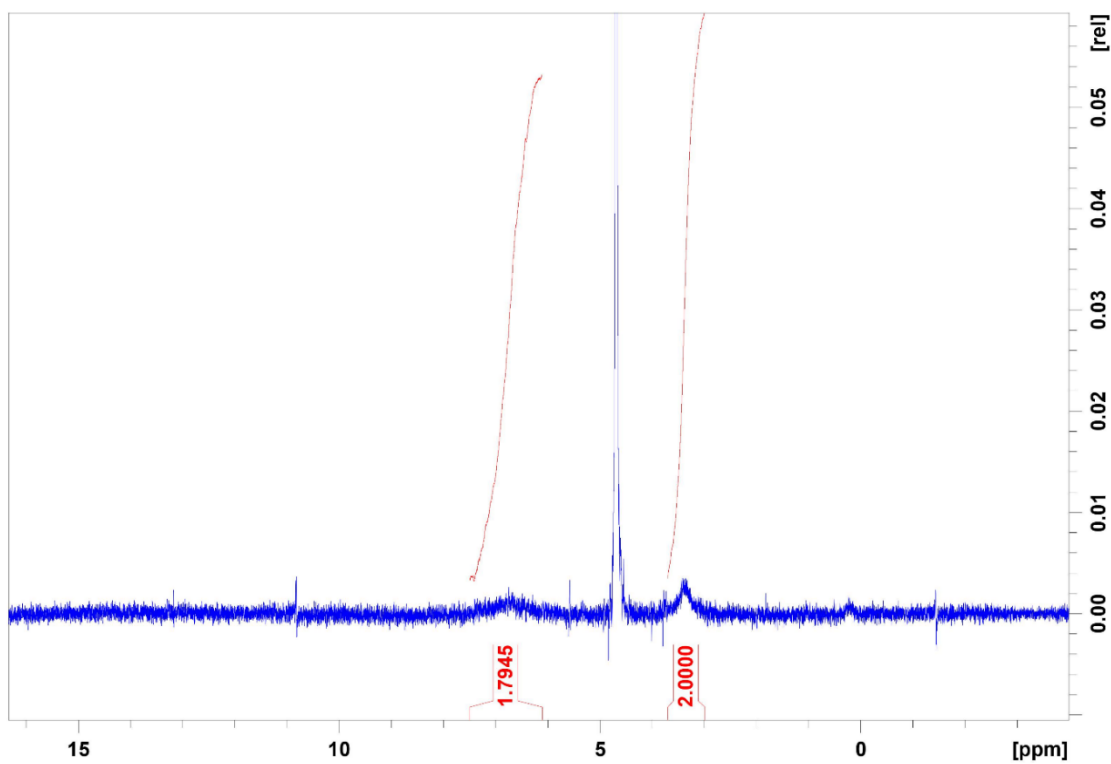


Figure A.1.10:  $^1\text{H}$  NMR of polyHGA in  $\text{D}_2\text{O}$  (formed in the presence of peroxidase at pH 5.0).

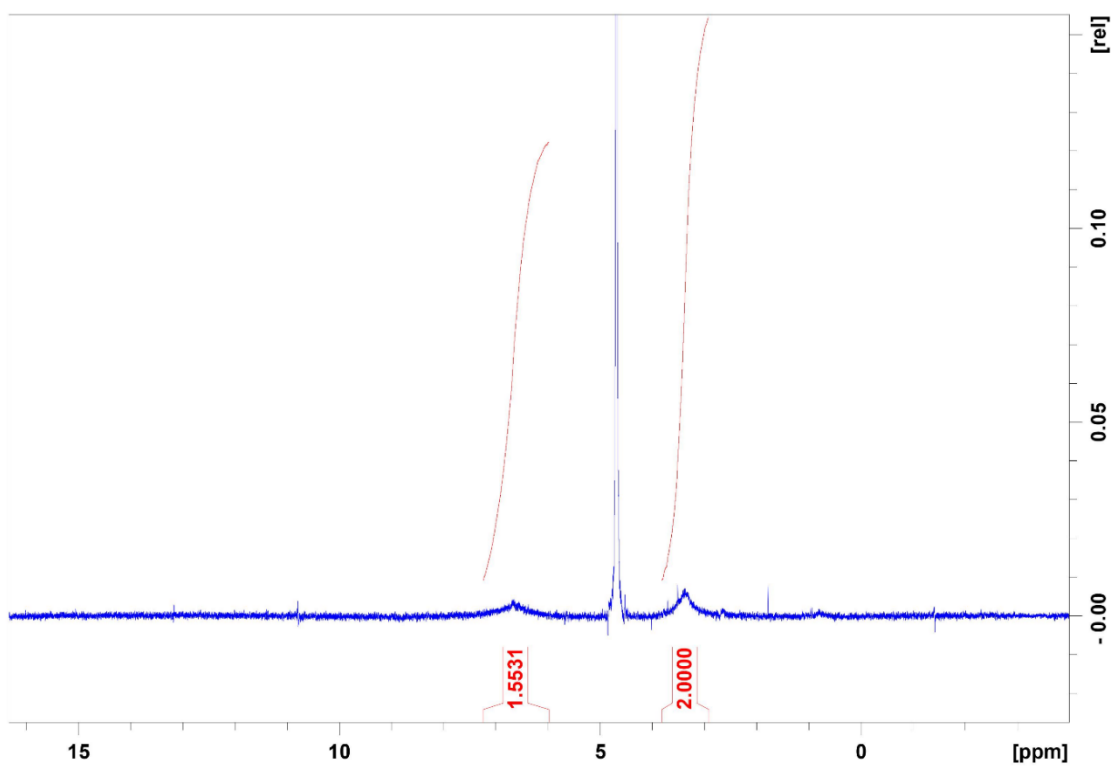


Figure A.1.11:  $^1\text{H}$  NMR of polyHGA in  $\text{D}_2\text{O}$  (formed in the presence of peroxidase at pH 7.4).

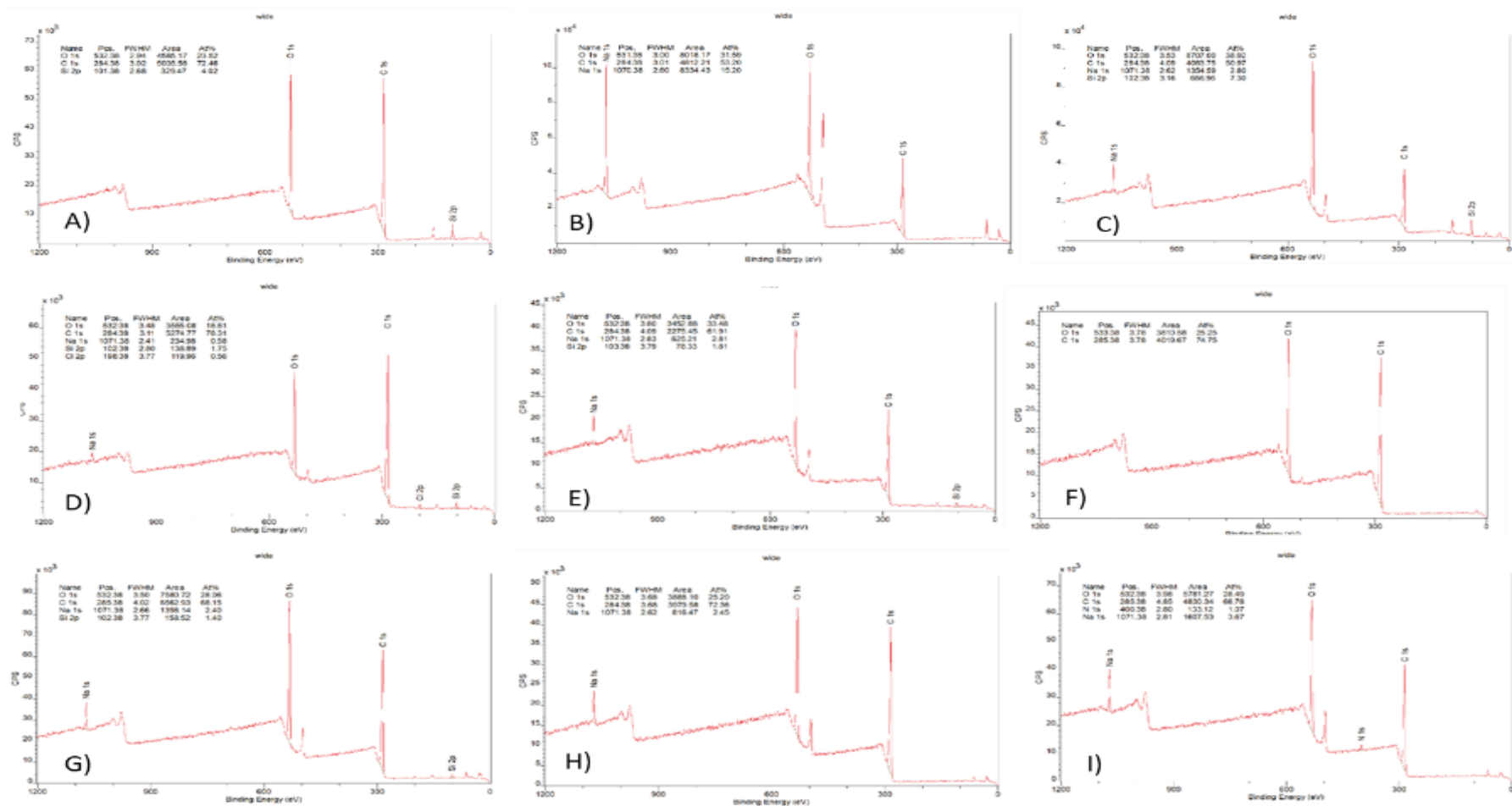


Figure A.1.12: XPS wide scans: A) HGA; B) polyHGA (no enzyme control at pH 5.0); C) polyHGA (no enzyme control at pH 7.4); D) polyHGA (formed in the presence of tyrosinase at pH 5.0); E) polyHGA (formed in the presence of tyrosinase at pH 7.4); F) polyHGA (formed in the presence of laccase at pH 5.0); G) polyHGA (formed in the presence of laccase at pH 7.4); H) polyHGA (formed in the presence of peroxidase at pH 5.0); I) polyHGA (formed in the presence of peroxidase at pH 7.4).

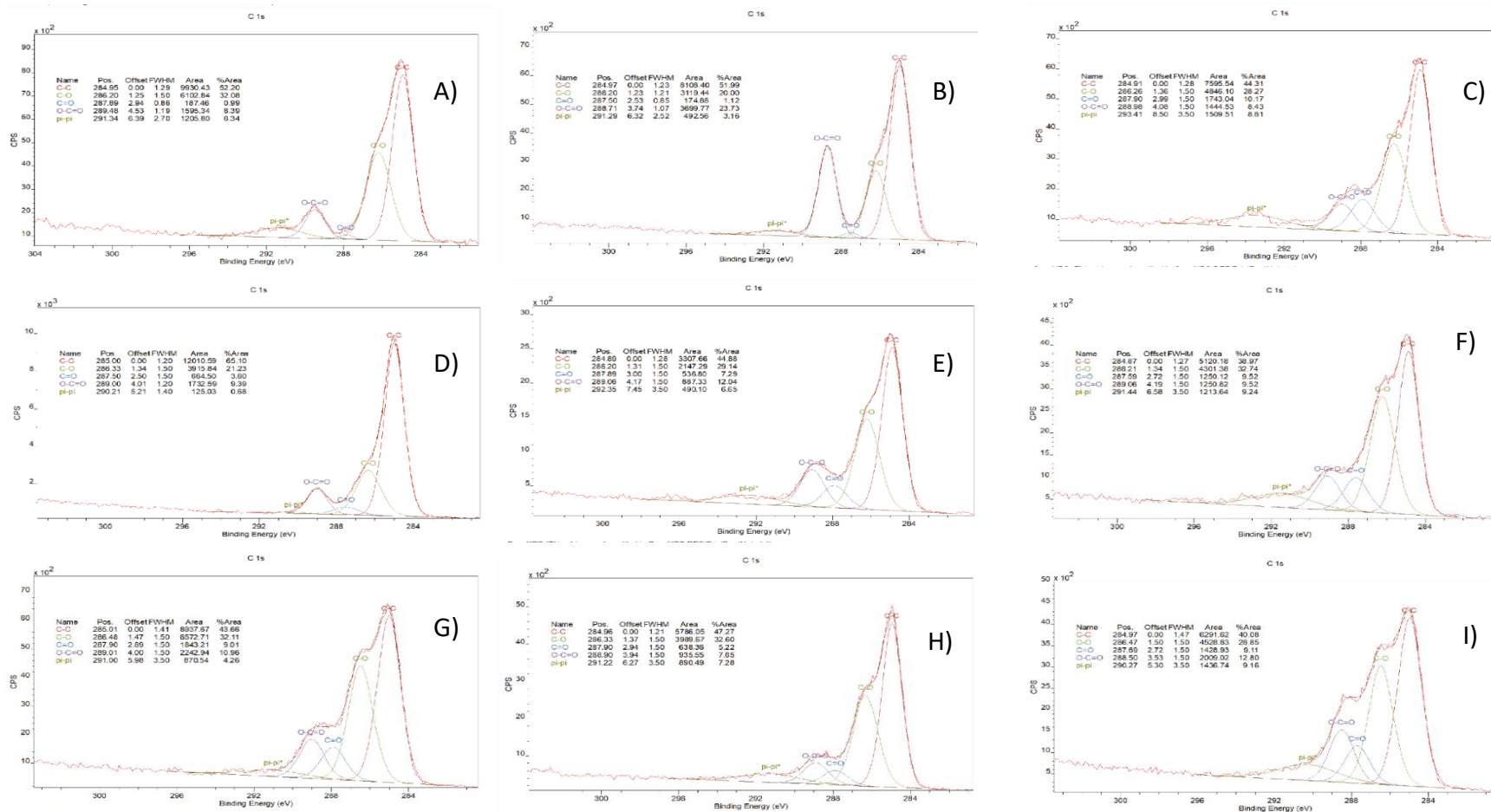


Figure A.1.13: XPS C 1s core line spectra: A) HGA; B) polyHGA (no enzyme control at pH 5.0); C) polyHGA (no enzyme control at pH 7.4); D) polyHGA (formed in the presence of tyrosinase at pH 5.0); E) polyHGA (formed in the presence of tyrosinase at pH 7.4); F) polyHGA (formed in the presence of laccase at pH 5.0); G) polyHGA (formed in the presence of laccase at pH 7.4); H) polyHGA (formed in the presence of peroxidase at pH 5.0); I) polyHGA (formed in the presence of peroxidase at pH 7.4).

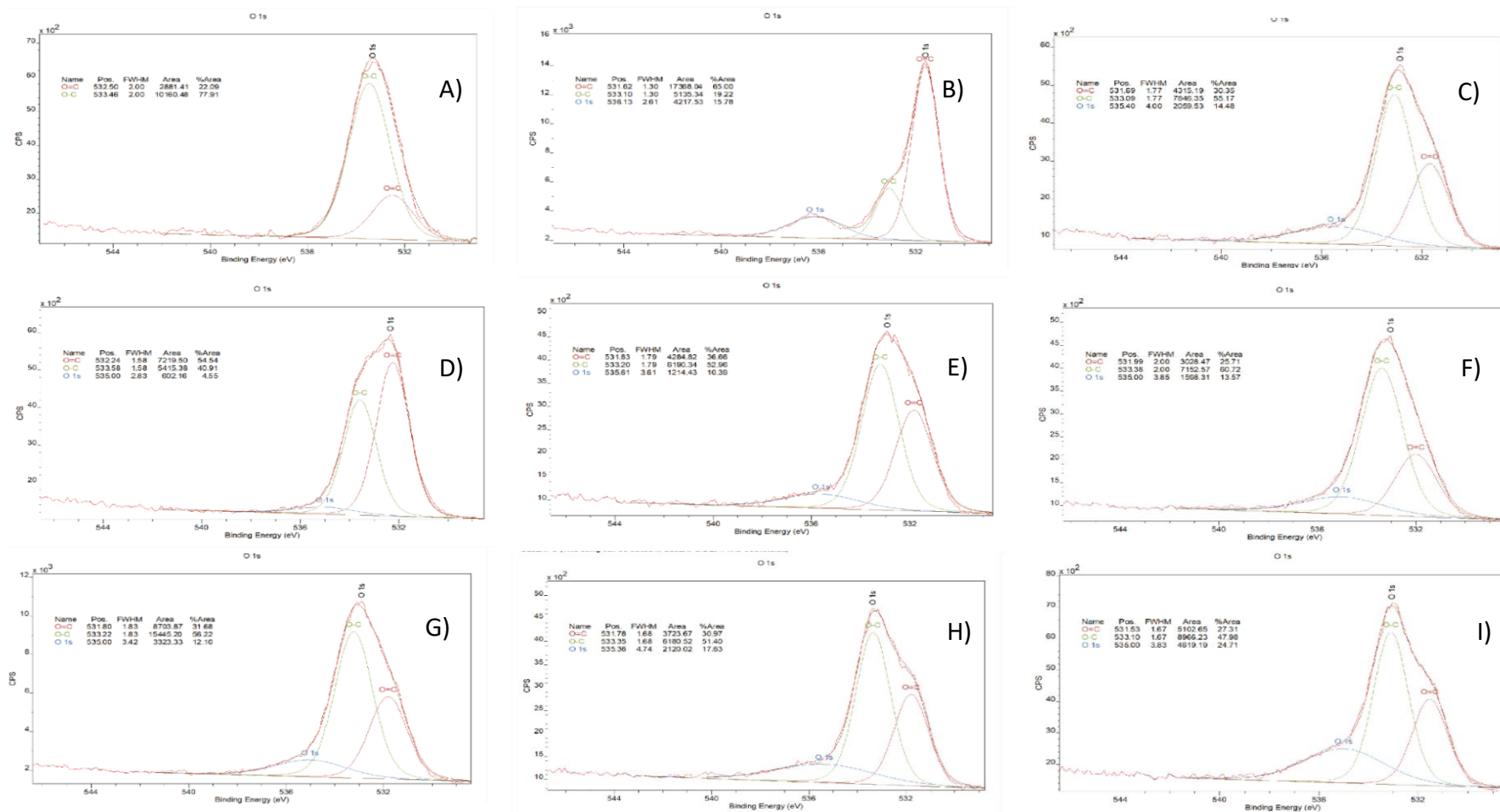


Figure A.1.14: XPS O 1s core line spectra: A) HGA; B) polyHGA (no enzyme control at pH 5.0); C) polyHGA (no enzyme control at pH 7.4); D) polyHGA (formed in the presence of tyrosinase at pH 5.0); E) polyHGA (formed in the presence of tyrosinase at pH 7.4); F) polyHGA (formed in the presence of laccase at pH 5.0); G) polyHGA (formed in the presence of laccase at pH 7.4); H) polyHGA (formed in the presence of peroxidase at pH 5.0); I) polyHGA (formed in the presence of peroxidase at pH 7.4).

Table A.1.1: Summary of XPS data (C 1s and O 1s) for HGA.

| Functionality | Average<br>[%]<br>Content<br>Measured<br>for<br>HGA | Normalized<br>% Content:<br>normalized<br>to O-C=O<br>for C 1s,<br>and to O=C<br>for O 1s. |
|---------------|---|--|
| C 1s) C-C     | 52.24 ± 0.96  | 2.23   |
| C 1s) C-O     | 20.44 ± 0.64  | 0.87   |
| C 1s) C=O     | 1.00 ± 0.95   | 0.04   |
| C 1s) O-C=O   | 23.40 ± 1.90  | 1.00   |
| C 1s) pi-pi   | 2.92 ± 0.57   | 0.12   |
| O 1s) O=C     | 65.74 ± 0.66  | 1.00   |
| O 1s) O-C     | 18.00 ± 1.50  | 0.27   |
| O 1s) Na KLL  | 16.27 ± 1.29  | 0.25   |

Table A.1.2: Summary of XPS data (C 1s and O 1s) for polyHGA (no enzyme control)

| Functionality | Average<br>[%]<br>Content<br>Measured<br>for<br>PolyHGA<br>formed at<br>pH 5.0. | Normalized<br>% Content:<br>normalized<br>to O-C=O<br>for C 1s,<br>and to O=C<br>for O 1s. | Average<br>[%]<br>Content<br>Measured<br>for<br>PolyHGA<br>formed at<br>pH 7.4. | Normalized<br>% Content:<br>normalized<br>to O-C=O<br>for C 1s,<br>and to O=C<br>for O 1s. |
|---------------|---|--|---|--|
| C 1s) C-C     | 52.24 ± 0.96  | 2.23   | 43.98 ± 2.11  | 4.98   |
| C 1s) C-O     | 20.44 ± 0.64  | 0.87   | 29.11 ± 1.17  | 3.30   |
| C 1s) C=O     | 1.00 ± 0.95   | 0.04   | 9.55 ± 0.57   | 1.08   |
| C 1s) O-C=O   | 23.40 ± 1.90  | 1.00   | 8.83 ± 0.64   | 1.00   |
| C 1s) pi-pi   | 2.92 ± 0.57   | 0.12   | 8.53 ± 0.51   | 0.97   |
| O 1s) O=C     | 65.74 ± 0.66  | 1.00   | 32.71 ± 8.40  | 1.00   |
| O 1s) O-C     | 18.00 ± 1.50  | 0.27   | 56.96 ± 9.25  | 1.74   |
| O 1s) Na KLL  | 16.27 ± 1.29  | 0.25   | 10.33 ± 0.54  | 0.32   |

Table A.1.3: Summary of XPS data (C 1s and O 1s) for polyHGA formed in the presence of tyrosinase.

| Functionality | Average<br>[%]<br>Content<br>Measured<br>for<br>PolyHGA<br>formed at<br>pH 5.0. | Normalized<br>% Content:<br>normalized<br>to O-C=O<br>for C 1s,<br>and to O=C<br>for O 1s. | Average<br>[%]<br>Content<br>Measured<br>for<br>PolyHGA<br>formed at<br>pH 7.4. | Normalized<br>% Content:<br>normalized<br>to O-C=O<br>for C 1s,<br>and to O=C<br>for O 1s. |
|---------------|---|--|---|--|
| C 1s) C-C     | 64.25 ± 3.12  | 6.62   | 48.96 ± 5.62  | 4.24   |
| C 1s) C-O     | 21.08 ± 1.21  | 2.17   | 27.17 ± 2.22  | 2.36   |
| C 1s) C=O     | 4.45 ± 2.33   | 0.46   | 6.83 ± 0.81   | 0.59   |
| C 1s) O-C=O   | 9.71 ± 0.85   | 1.00   | 11.53 ± 0.68  | 1.00   |
| C 1s) pi-pi   | 0.51 ± 0.45   | 0.05   | 5.51 ± 1.98   | 0.48   |
| O 1s) O=C     | 56.76 ± 2.78  | 1.00   | 40.60 ± 5.51  | 1.00   |
| O 1s) O-C     | 40.18 ± 1.77  | 0.71   | 53.52 ± 2.72  | 1.32   |
| O 1s) Na KLL  | 3.39 ± 0.84   | 0.06   | 5.88 ± 3.15   | 0.14   |

Table A.1.4: Summary of XPS data (C 1s and O 1s) for polyHGA formed in the presence of laccase.

| Functionality | Average<br>[%]<br>Content<br>Measured<br>for<br>PolyHGA<br>formed at<br>pH 5.0. | Normalized<br>% Content:<br>normalized<br>to O-C=O<br>for C 1s,<br>and to O=C<br>for O 1s. | Average<br>[%]<br>Content<br>Measured<br>for<br>PolyHGA<br>formed at<br>pH 7.4. | Normalized<br>% Content:<br>normalized<br>to O-C=O<br>for C 1s,<br>and to O=C<br>for O 1s. |
|---------------|---|--|---|--|
| C 1s) C-C     | 38.58 ± 1.61  | 4.08   | 43.68 ± 0.77  | 3.89   |
| C 1s) C-O     | 32.30 ± 0.15  | 3.41   | 32.00 ± 2.19  | 2.85   |
| C 1s) C=O     | 9.89 ± 0.34   | 1.05   | 8.31 ± 1.23   | 0.74   |
| C 1s) O-C=O   | 9.46 ± 0.07   | 1.00   | 11.23 ± 0.92  | 1.00   |
| C 1s) pi-pi   | 9.68 ± 1.71   | 1.02   | 4.79 ± 1.33   | 0.43   |
| O 1s) O=C     | 28.49 ± 1.21  | 1.00   | 33.47 ± 5.51  | 1.00   |
| O 1s) O-C     | 61.37 ± 2.22  | 2.15   | 57.91 ± 6.61  | 1.73   |
| O 1s) Na KLL  | 10.15 ± 1.03  | 0.36   | 8.62 ± 1.37   | 0.26   |

| Functionality | Average<br>[%] | Normalized<br>% Content: | Average<br>[%] | Normalized<br>% Content: |
|---------------|----------------|--------------------------|----------------|--------------------------|
|---------------|----------------|--------------------------|----------------|--------------------------|

Table

|              | Content<br>Measured<br>for<br>PolyHGA<br>formed at<br>pH 5.0. | normalized<br>to O-C=O<br>for C 1s,<br>and to O=C<br>for O 1s. | Content<br>Measured<br>for<br>PolyHGA<br>formed at<br>pH 7.4. | normalized<br>to O-C=O<br>for C 1s,<br>and to O=C<br>for O 1s. |
|--------------|---|--|---|--|
| C 1s) C-C    | 47.48 ± 1.49  | 6.06   | 37.36 ± 5.72  | 4.08   |
| C 1s) C-O    | 28.94 ± 4.63  | 3.69   | 29.09 ± 0.46  | 3.18   |
| C 1s) C=O    | 4.90 ± 0.52   | 0.63   | 14.89 ± 5.54  | 1.63   |
| C 1s) O-C=O  | 7.83 ± 0.51   | 1.00   | 9.16 ± 3.19   | 1.00   |
| C 1s) pi-pi  | 7.86 ± 0.61   | 1.00   | 9.49 ± 2.77   | 1.04   |
| O 1s) O=C    | 32.64 ± 0.69  | 1.00   | 29.59 ± 0.92  | 1.00   |
| O 1s) O-C    | 55.53 ± 0.39  | 1.70   | 52.26 ± 4.18  | 1.77   |
| O 1s) Na KLL | 11.83 ± 0.97  | 0.36   | 18.15 ± 3.48  | 0.61   |

A.1.5: Summary of XPS data (C 1s and O 1s) for polyHGA formed in the presence of peroxidase.

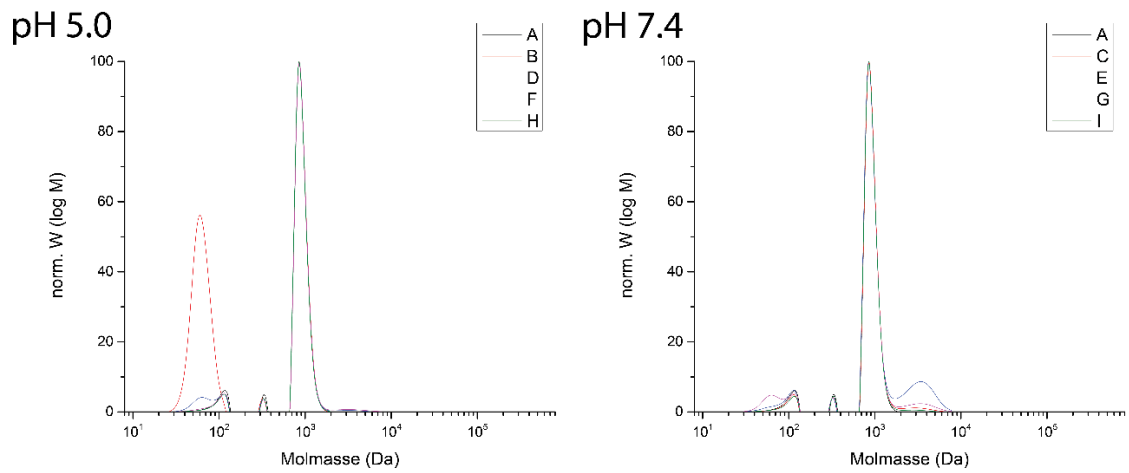


Figure A.1.15: SEC data for various samples. A) Blank control. B) PolyHGA (no enzyme control at pH 5.0). C) PolyHGA (no enzyme control at pH 7.4). D) PolyHGA (formed in the presence of tyrosinase at pH 5.0). E) PolyHGA (formed in the presence of tyrosinase at pH 7.4). F) PolyHGA (formed in the presence of laccase at pH 5.0). G) PolyHGA (formed in the presence of laccase at pH 7.4). H) PolyHGA (formed in the presence of peroxidase at pH 5.0). I) PolyHGA (formed in the presence of peroxidase at pH 7.4).

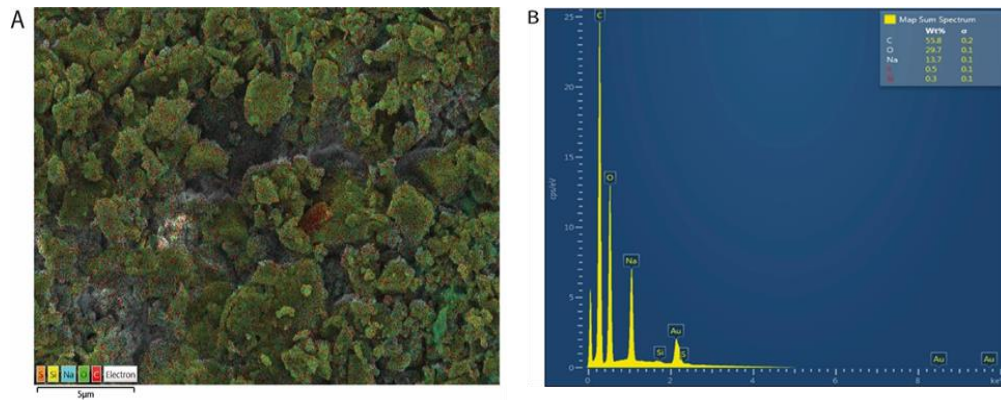


Figure A.1.16: SEM and EDX data for polyHGA (no enzyme control at pH 5.0). A) SEM-EDX layered image (scale bar represents 25  $\mu\text{m}$ ). B) EDX spectrum.

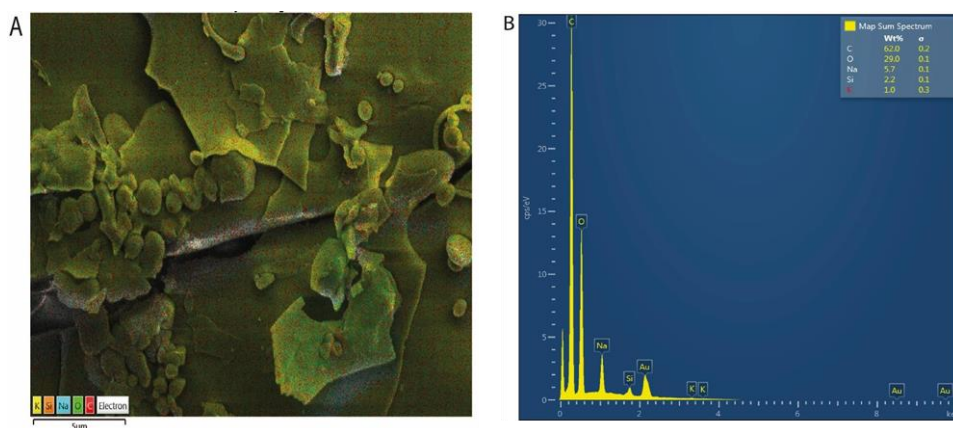


Figure A.1.17: SEM and EDX data for polyHGA (no enzyme control at pH 7.4). A) SEM-EDX layered image (scale bar represents 25 μm). B) EDX spectrum.

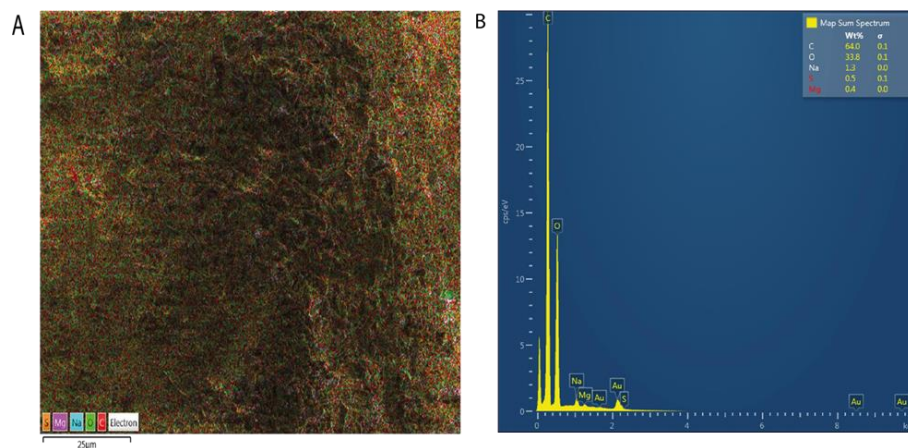


Figure A.1.18: SEM and EDX data for polyHGA formed in the presence of tyrosinase at pH 5.0.

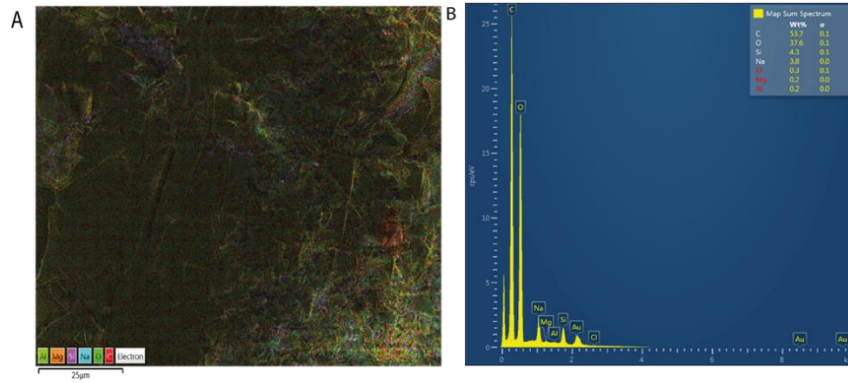


Figure A.1.19: SEM and EDX data for polyHGA formed in the presence of tyrosinase at pH 7.4.

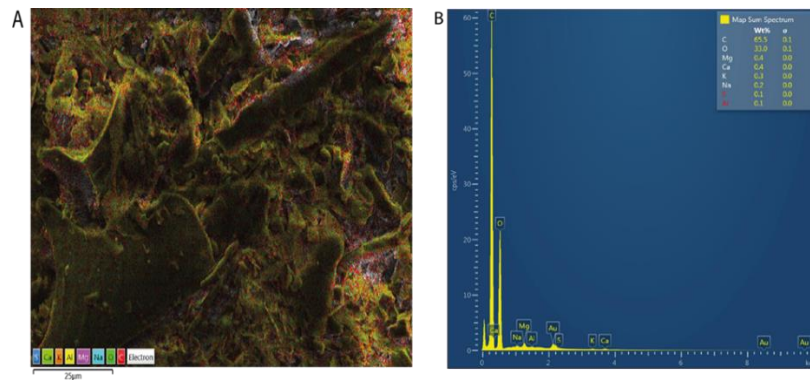


Figure A.1.20: SEM and EDX data for polyHGA formed in the presence of laccase at pH 5.0.

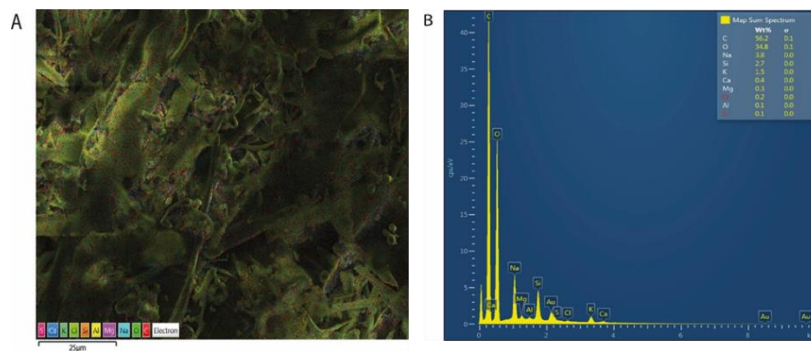


Figure A.1.21: SEM and EDX data for polyHGA formed in the presence of laccase at pH 7.4. A) SEM-EDX layered image (scale bar represents 25 µm). B) EDX spectrum.

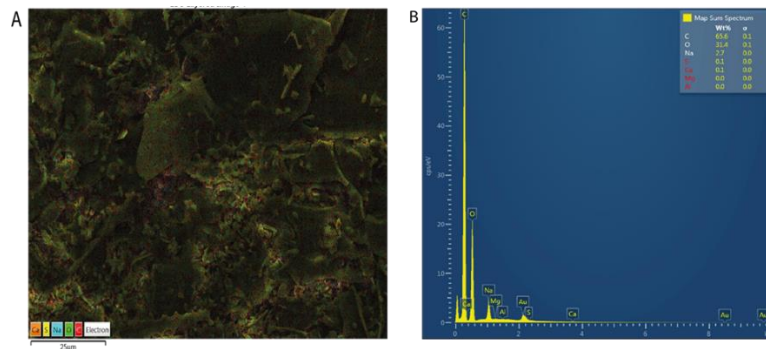


Figure A.1 22: SEM and EDX data for polyHGA formed in the presence of peroxidase at pH5.0. A) SEM-EDX layered image (scale bar represents 25  $\mu$ m). B) EDX spectrum.

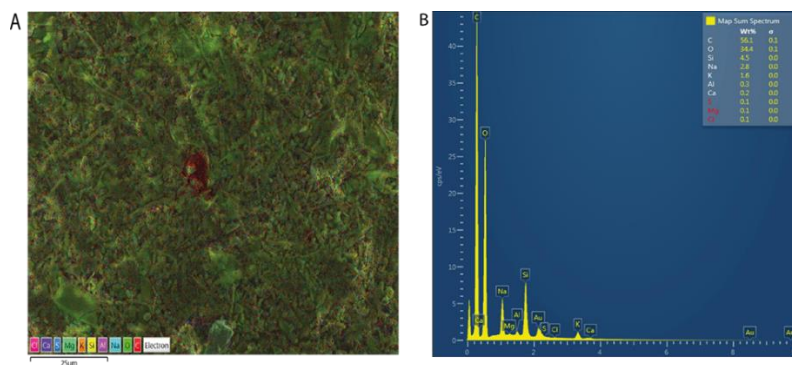


Figure A.1.23: SEM and EDX data for polyHGA formed in the presence of peroxidase at pH7.4. A) SEM-EDX layered image (scale bar represents 25  $\mu$ m). B) EDX spectrum.

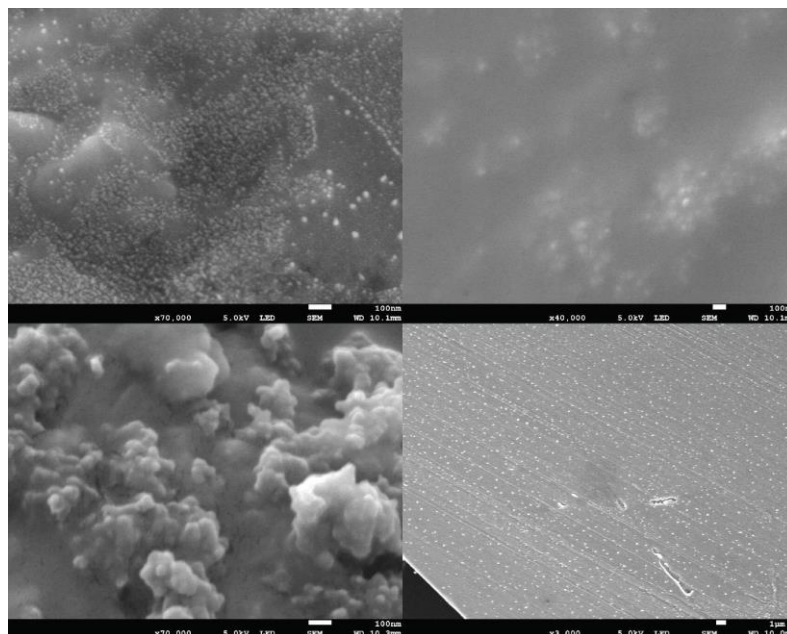


Figure A.1.24: High magnification SEM images. A) polyHGA, no enzyme control at pH 7.4 (scale bar represents 100 nm). B) polyHGA formed in the presence of tyrosinase at pH 7.4 (scale bar represents 100 nm). C) polyHGA formed in the presence of laccase at pH 7.4 (scale bar represents 100 nm). D) polyHGA formed in the presence of peroxidase at pH 7.4 (scale bar represents 1  $\mu$ m). Figure A.1.26. Experimental EPR spectrum of polyHGA generated in the absence of enzymes at pH 7.4, (black) and simulation (red). The simulation included a broad C-centered component ( $g = 2.0034$ , Voigtian line shape with peak-to-peak width 4.3 G, 93.8%) and a sharper semiquinone radical ( $g = 2.0039$ , Gaussian line shape with peak-to-peak width 2.7 G, 6.2%).

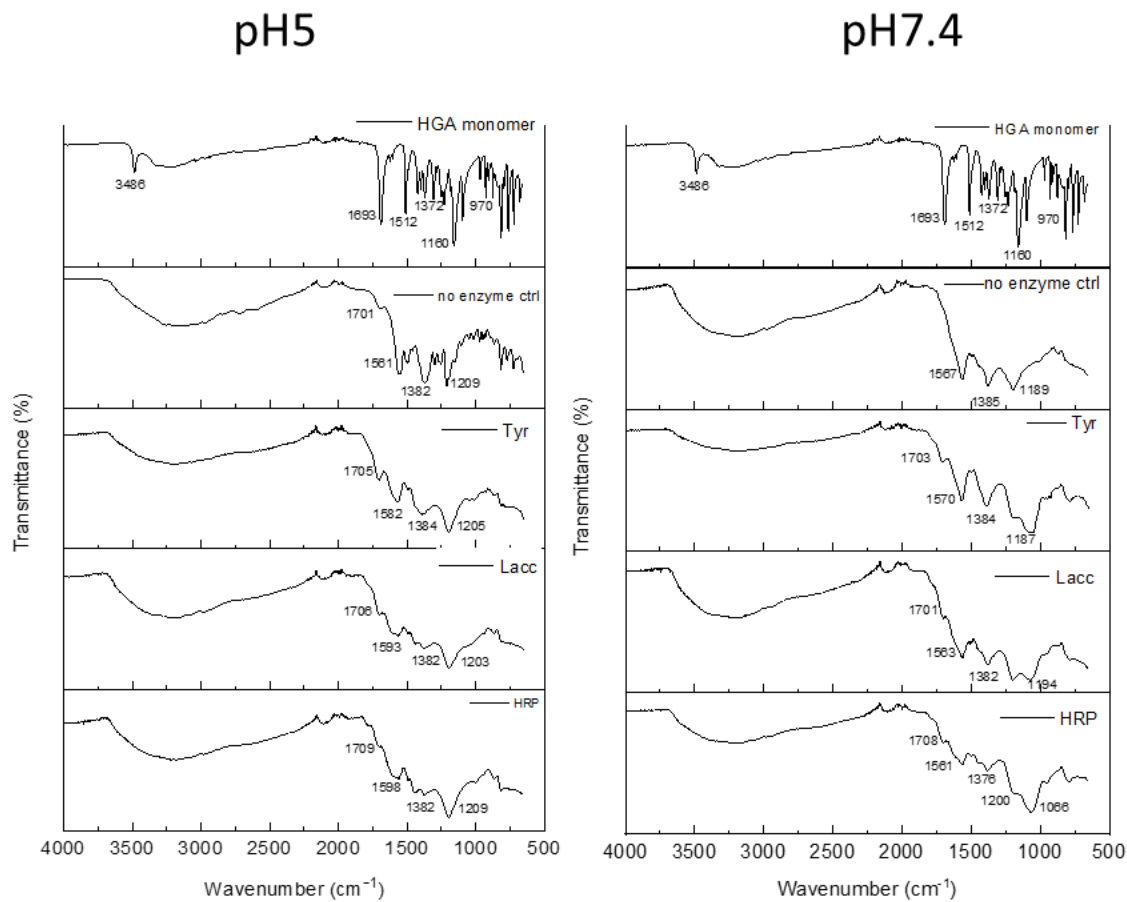


Figure A.1.25: FTIR spectra of dialyzed polyHGA isolated after 6 weeks of reaction at pH 5.0 and pH 7.4, generated in the absence of enzyme (no enzyme control) or presence of enzyme (laccase [Lacc], peroxidase [HRP], tyrosinase [Tyr]).

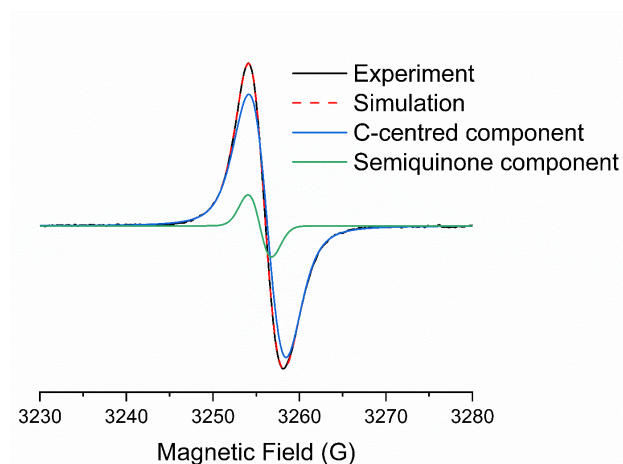


Figure A.1.26: Experimental EPR spectrum of polyHGA generated in the absence of enzymes at pH 7.4, (black) and simulation (red). The simulation included a broad C-centered component ( $g = 2.0034$ , Voigtian line shape with peak-to-peak width 4.3 G, 93.8%) and a sharper semiquinone radical ( $g = 2.0039$ , Gaussian line shape with peak-to-peak width 2.7 G, 6.2%).

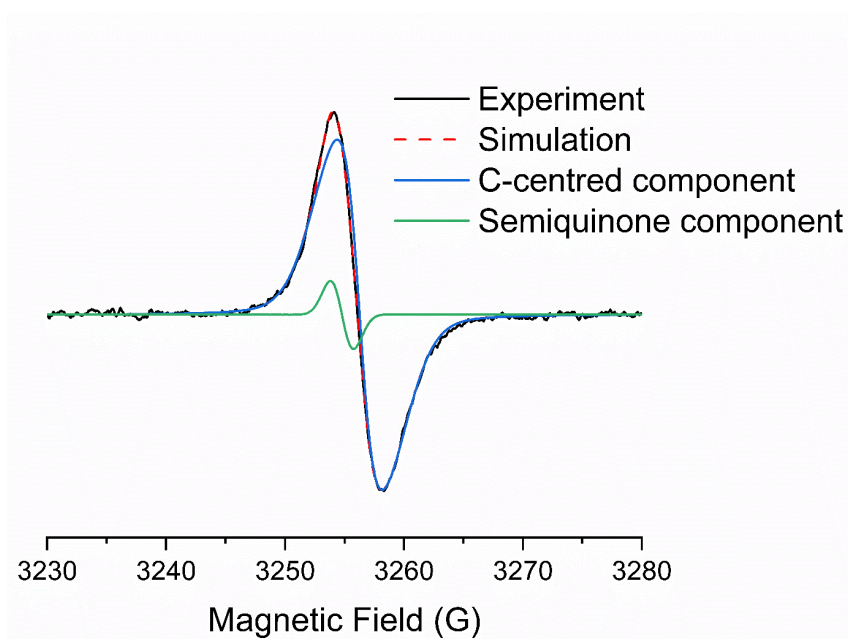


Figure A.1.27: Experimental EPR spectrum of polyHGA generated in the presence of laccase at pH 7.4, sample (black) and simulation (red). The simulation included a broad C-centered radical component ( $g = 2.0034$ , Voigtian line shape with peak-to-peak width 4.5 G, 95.2%) and a sharper semiquinone radical ( $g = 2.0039$ , Gaussian line shape with peak-to-peak width 2.7 G, 4.8%).

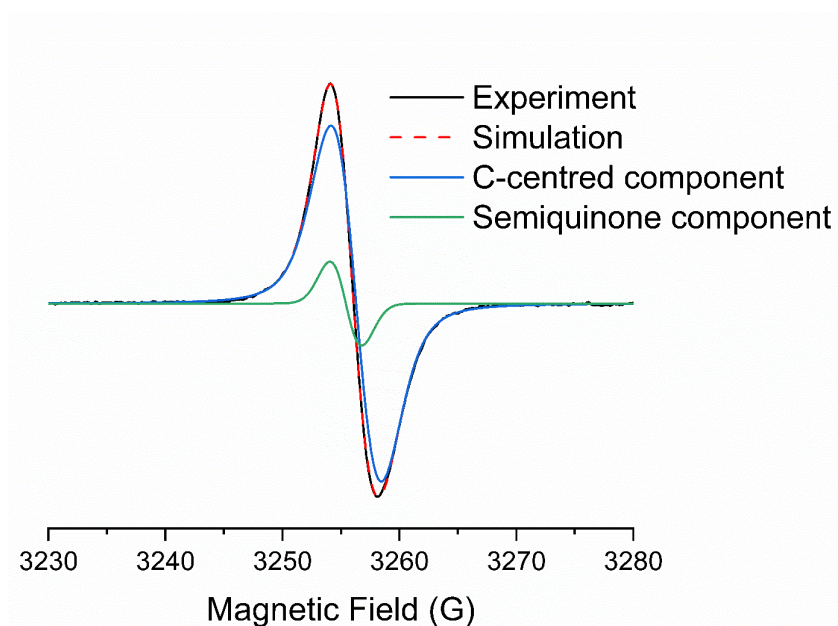


Figure A.1.28: Experimental EPR spectrum of polyHGA generated in the presence of tyrosinase at pH 7.4, sample (black) and simulation (red). The simulation included a broad C-centered component ( $g = 2.0036$ , Voigtian line shape with peak-to-peak width 4.4 G, 96.1%) and a sharper semiquinone radical ( $g = 2.0039$ , Gaussian line shape with peak-to-peak width 3.0 G, 3.9%).

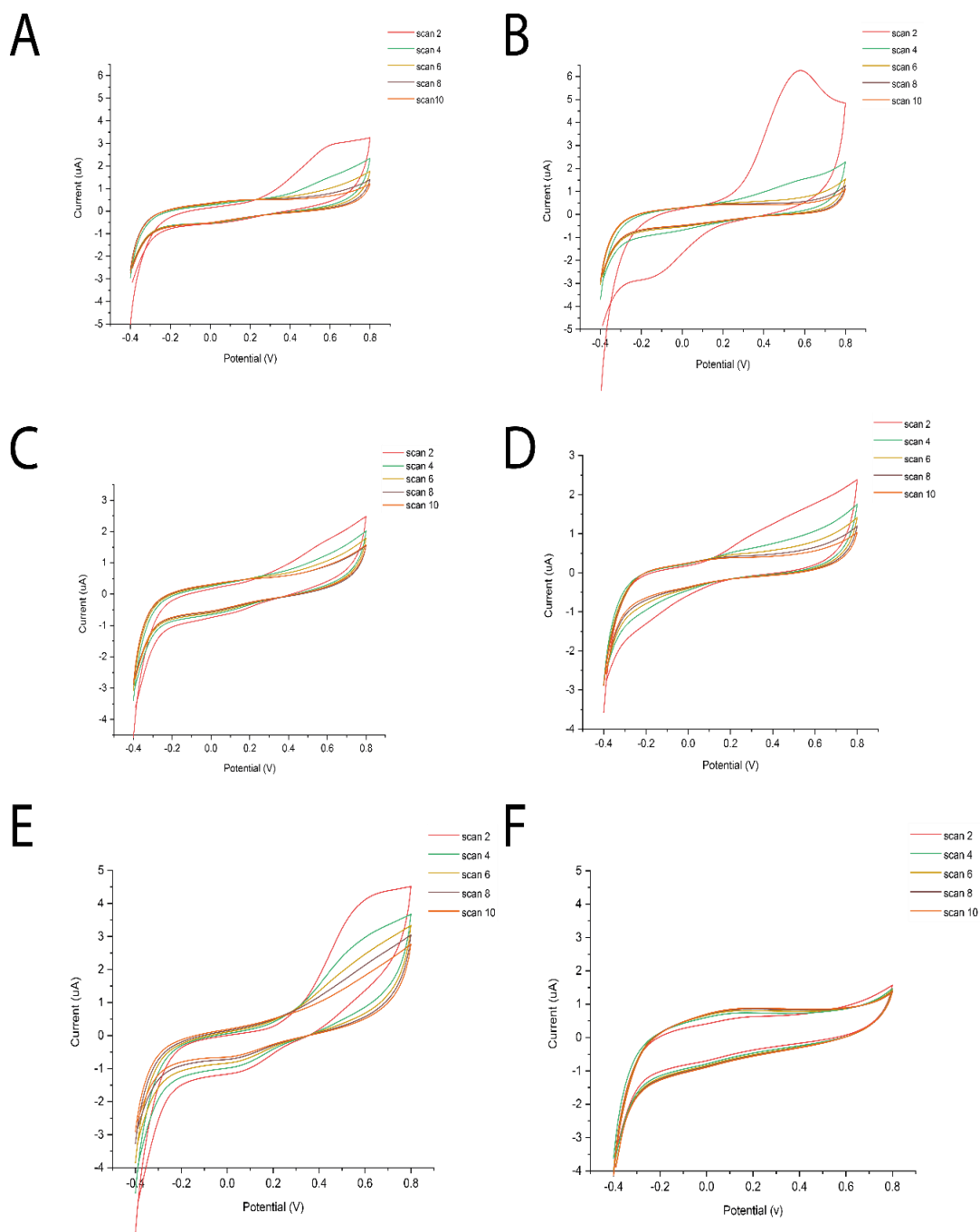


Figure A.1.29: Cyclic voltammograms of polyHGAs. A) PolyHGA (prepared in the presence of tyrosinase at pH 5.0) at pH 5.0. B) PolyHGA (prepared in the presence of tyrosinase at pH 7.4) at pH 7.4. C) PolyHGA (prepared in the presence of laccase at pH 5.0) at pH 5.0. D) PolyHGA (prepared in the presence of laccase at pH 7.4) at pH 7.4. E) PolyHGA (prepared in the presence of peroxidase at pH 5.0) at pH 5.0. F) PolyHGA (prepared in the presence of peroxidase at pH 7.4) at pH 7.4.

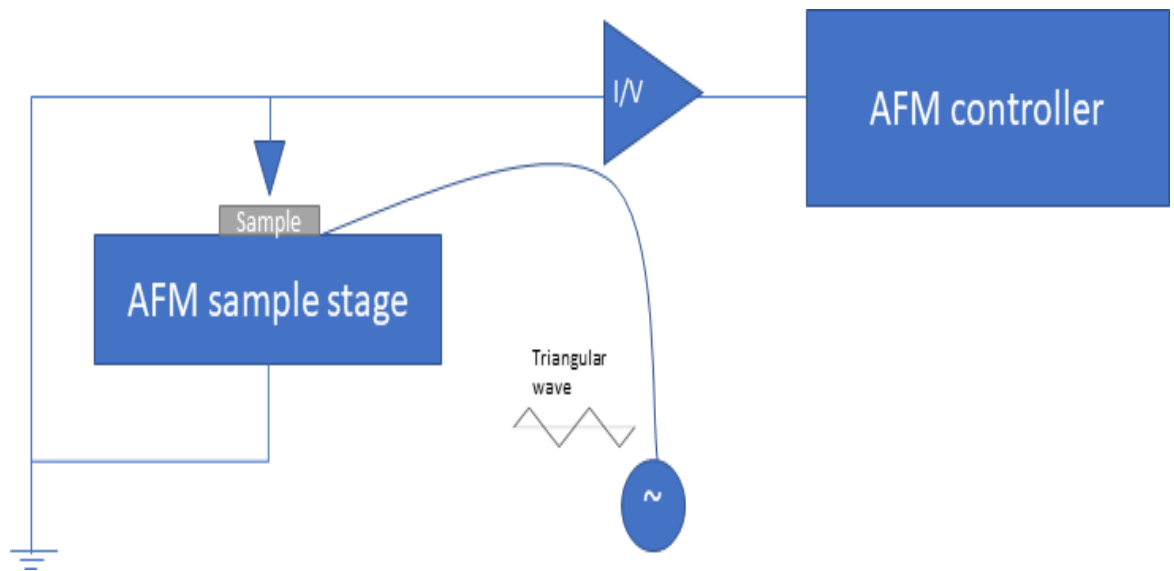


Figure A.1.30: Conductive probe AFM setup.

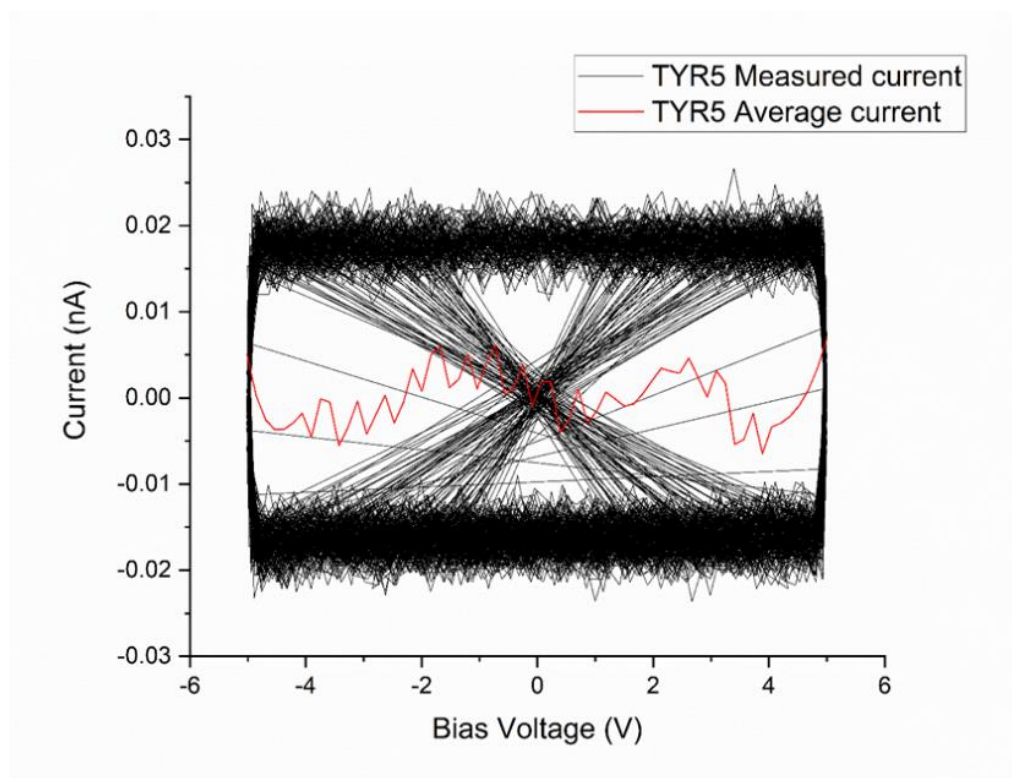
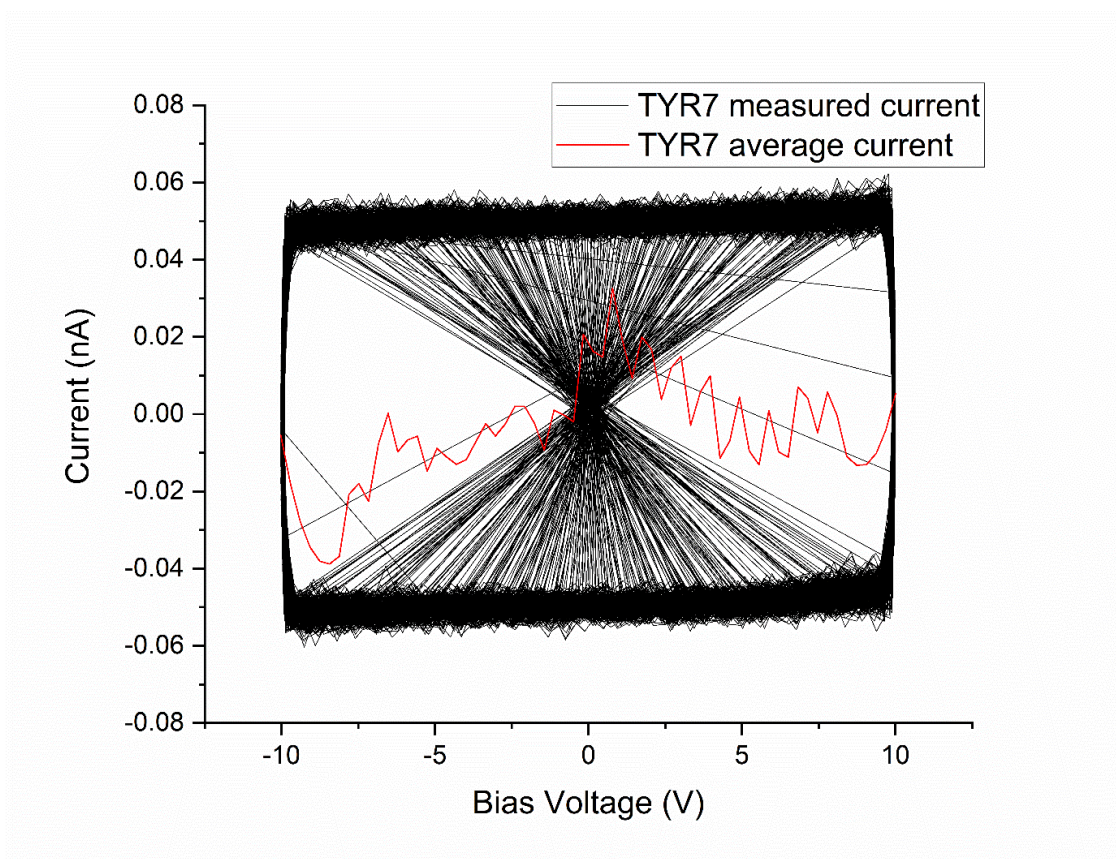


Figure A.1.31: I-V curves for the polyHGA generated in the presence of tyrosinase at pH 5.0. Data courtesy of Angelo.



*Figure A.1.32: I-V curves for the polyHGA generated in the presence of tyrosinase at pH 7.4*

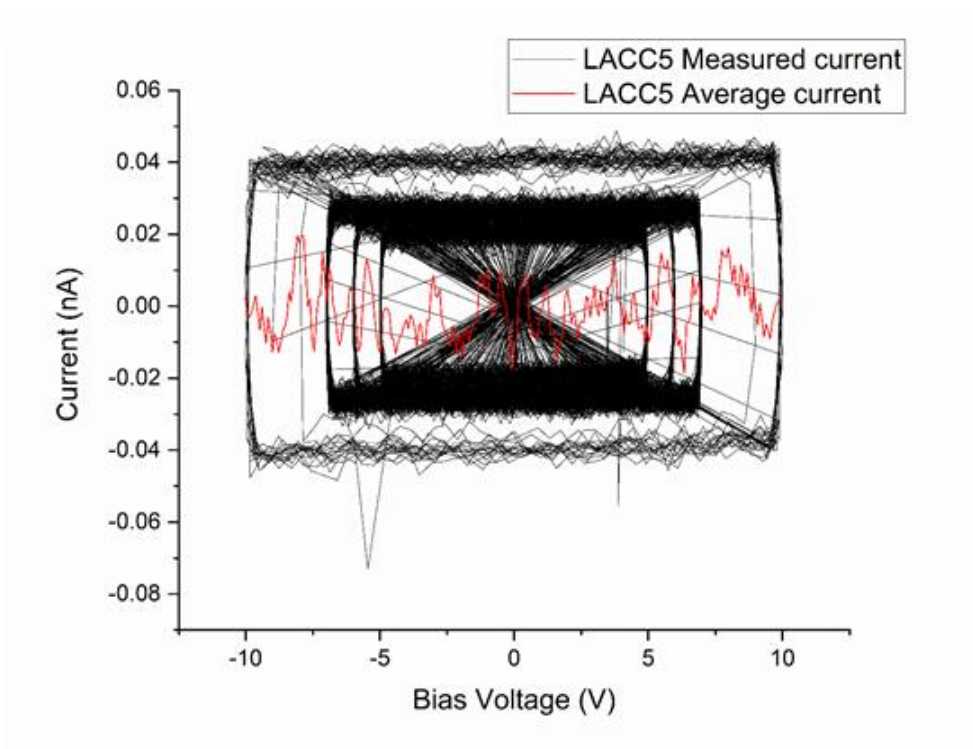


Figure A.1.33: I-V curves for the polyHGA generated in the presence of laccase (LACC) at pH 5.0.

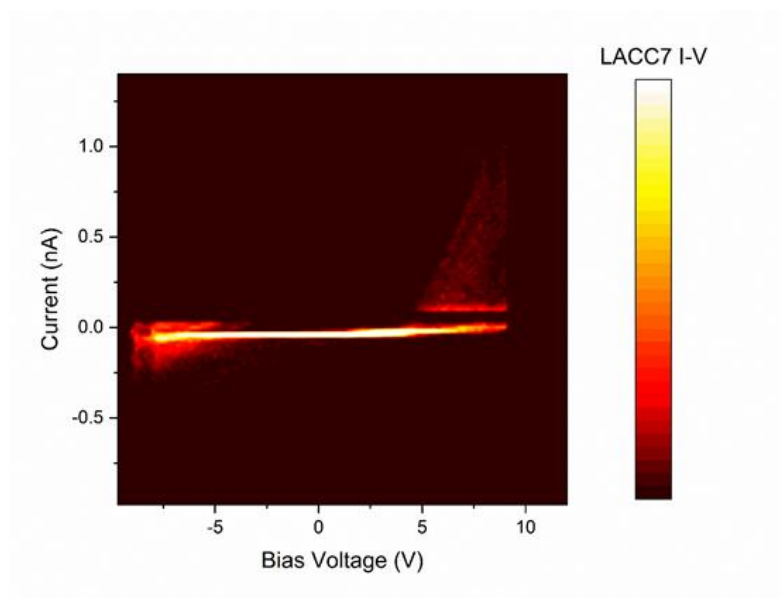


Figure A.1.34: I-V curve for the polyHGA generated in the presence of laccase (LACC) at pH 7.4.

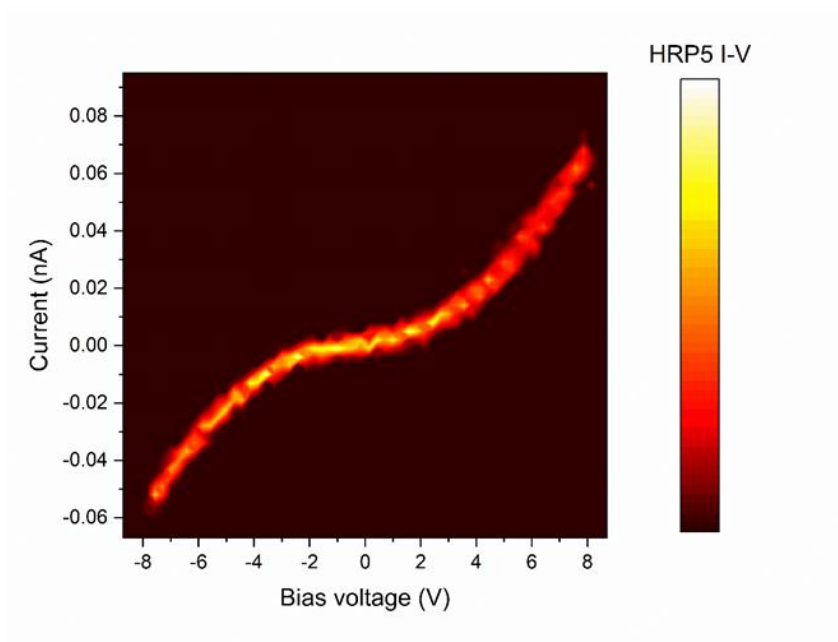


Figure A.1.35: I-V curve for the polyHGA generated in the presence of peroxidase (HRP) at pH 5.0.

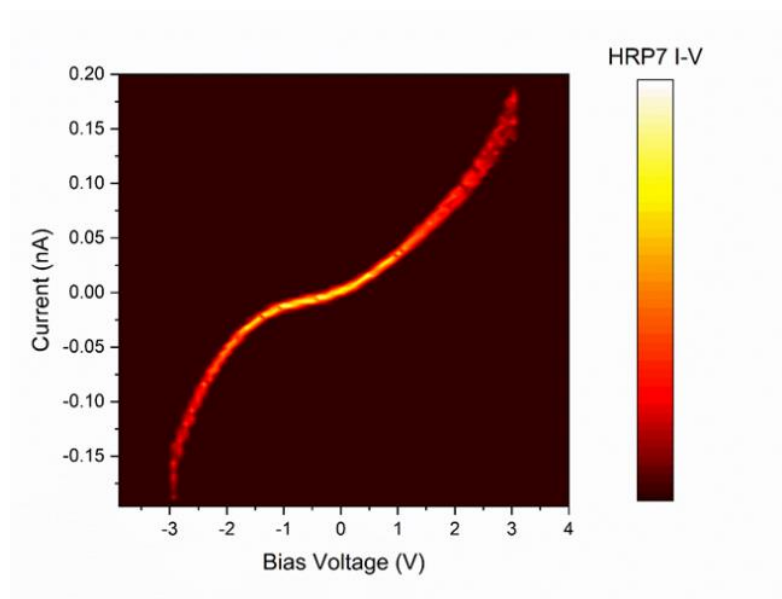
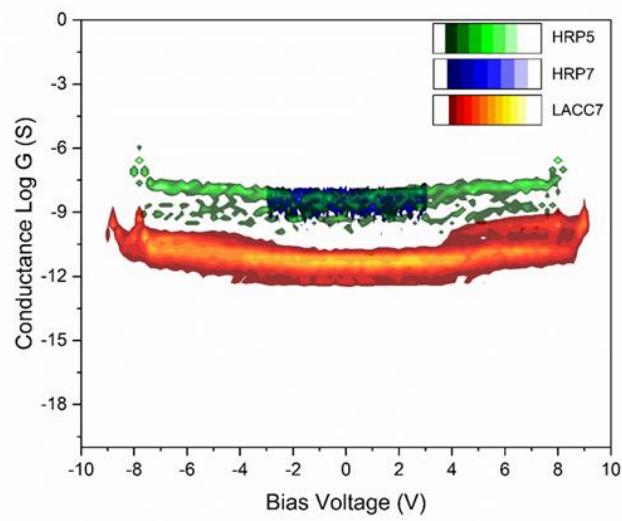


Figure A.1.36: I-V curve for the polyHGA generated in the presence of peroxidase (HRP) at pH 7.4.



Figure

*G* counter  
 polyHGAs  
 presence of laccase (LACC) at pH 7.4, or peroxidase (HRP) at pH 7.4 or 5.0, respectively.

A.1.37:  
 Comparison of Log  
 maps for the  
 generated in the

## 8.2 Appendix

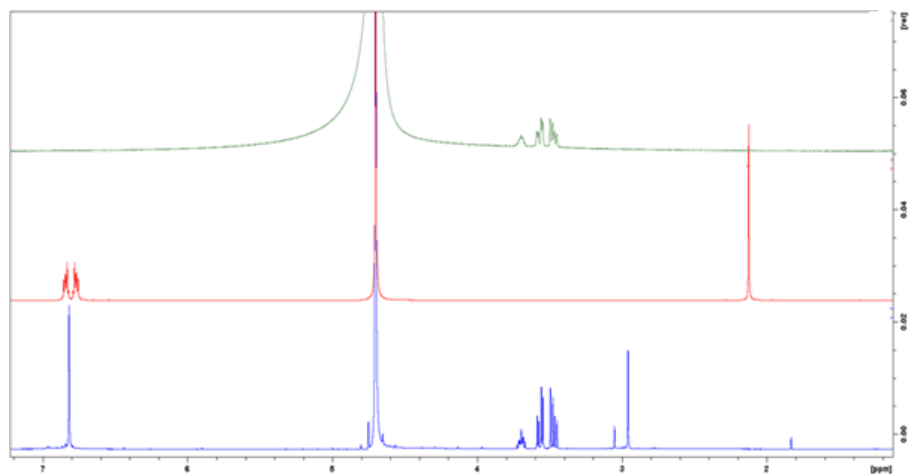


Figure A.2.1:  $^1\text{H}$  NMR of CAT (red, includes trace of acetone), polyCAT-HS (blue) and polyCAT-LS (green) in  $\text{D}_2\text{O}$ .

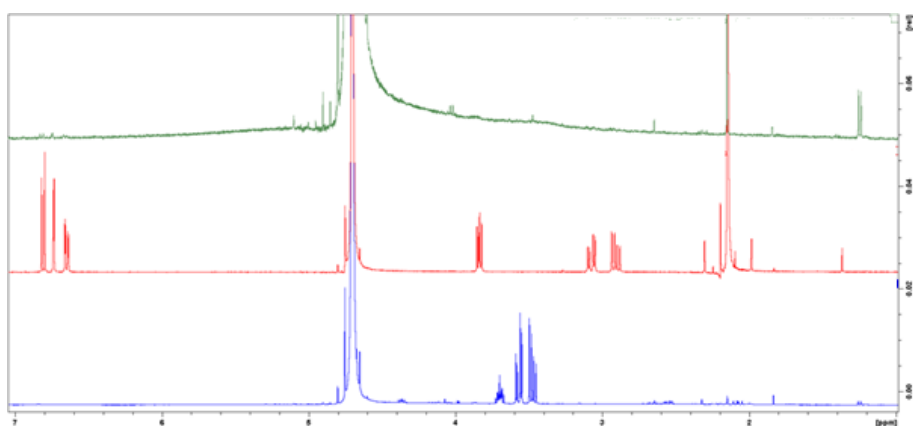


Figure A.2.2:  $^1\text{H}$  NMR of L-DOPA (red), polyLDOPA-HS (blue) and polyLDOPA-LS (green) in  $\text{D}_2\text{O}$ .

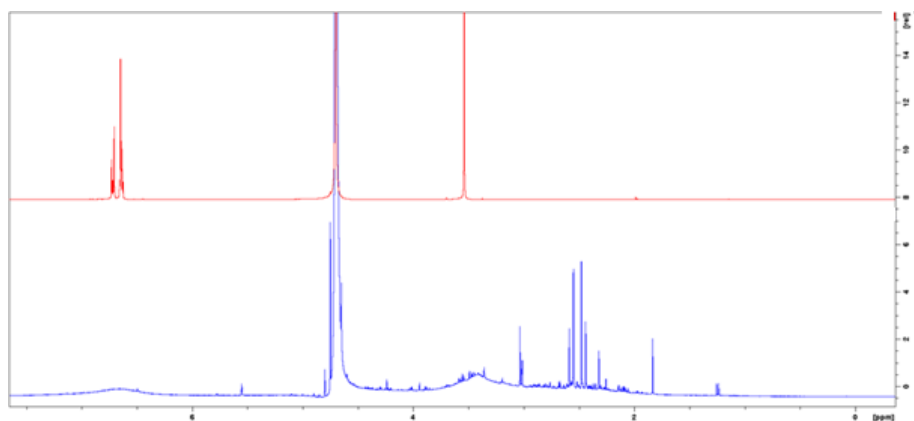


Figure A.2.3:  $^1\text{H}$  NMR of HGA (red) and polyHGA-HS (blue) in  $\text{D}_2\text{O}$ .

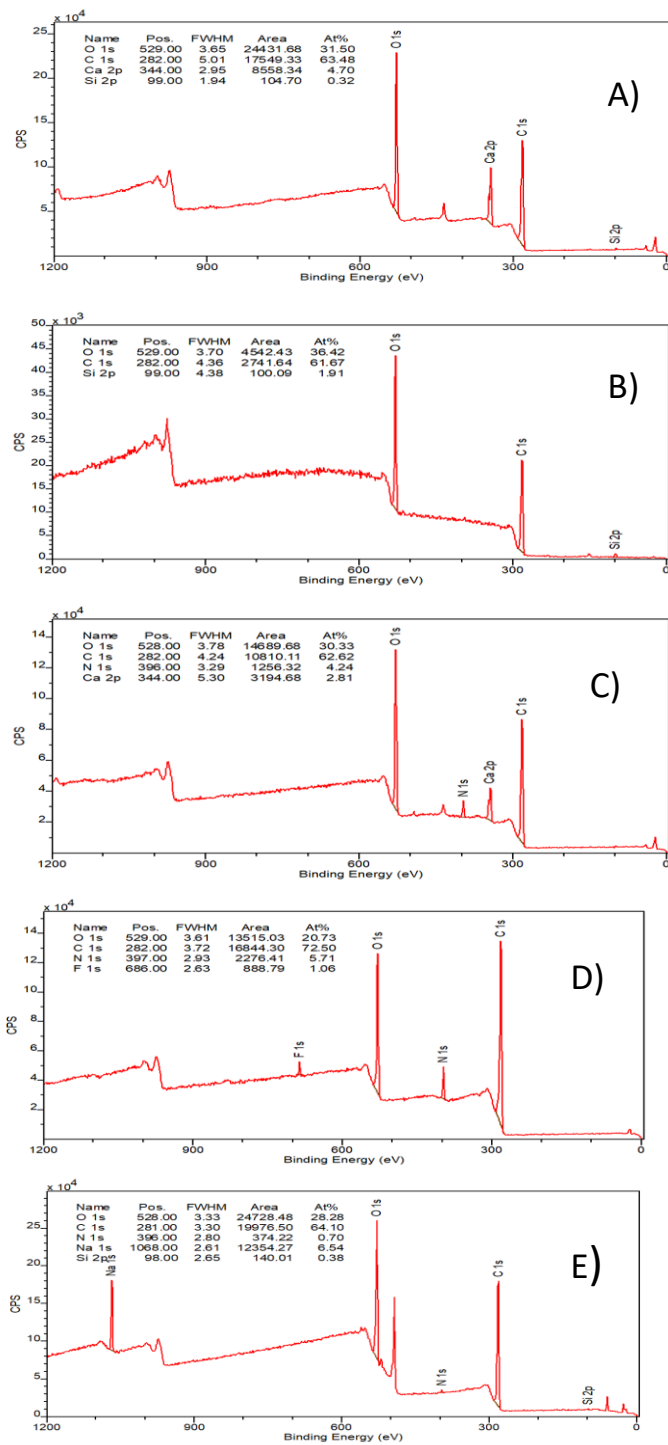


Figure A.2.4: XPS spectra. A) polyCAT-HS wide scan. B) polyCAT-LS wide scan. C) polyDOPA-HS wide scan. D) polyDOPA-LS wide scan. E) polyHGA-HS wide scan.

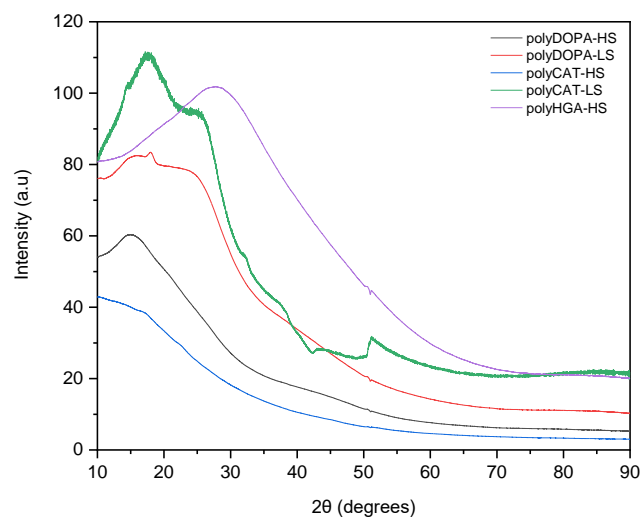


Figure A.2.5: X-ray diffractograms of samples studied herein.

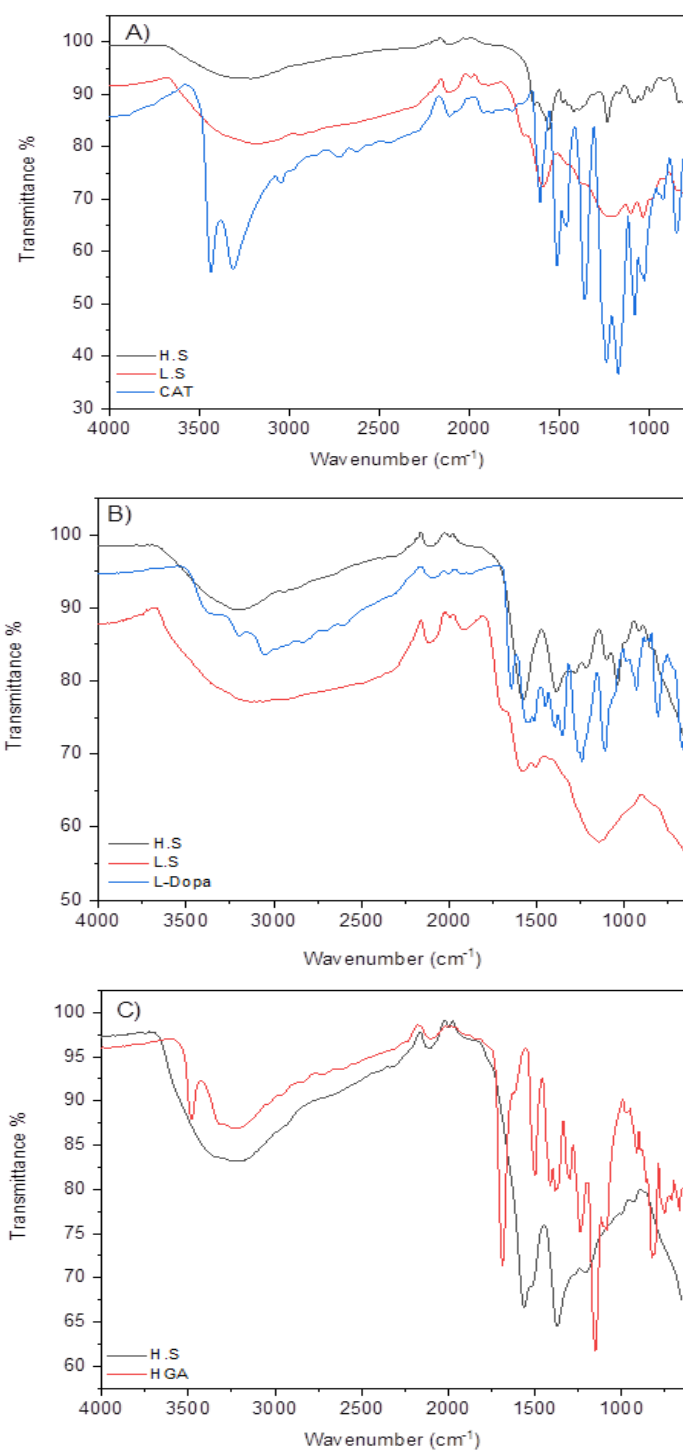


Figure A.2.6: FTIR spectra of monomers and polymers. A) CAT, polyCAT-HS and polyCAT-LS. B) DOPA, polyDOPA-HS and polyDOPA-LS. C) HGA and polyHGA-HS.

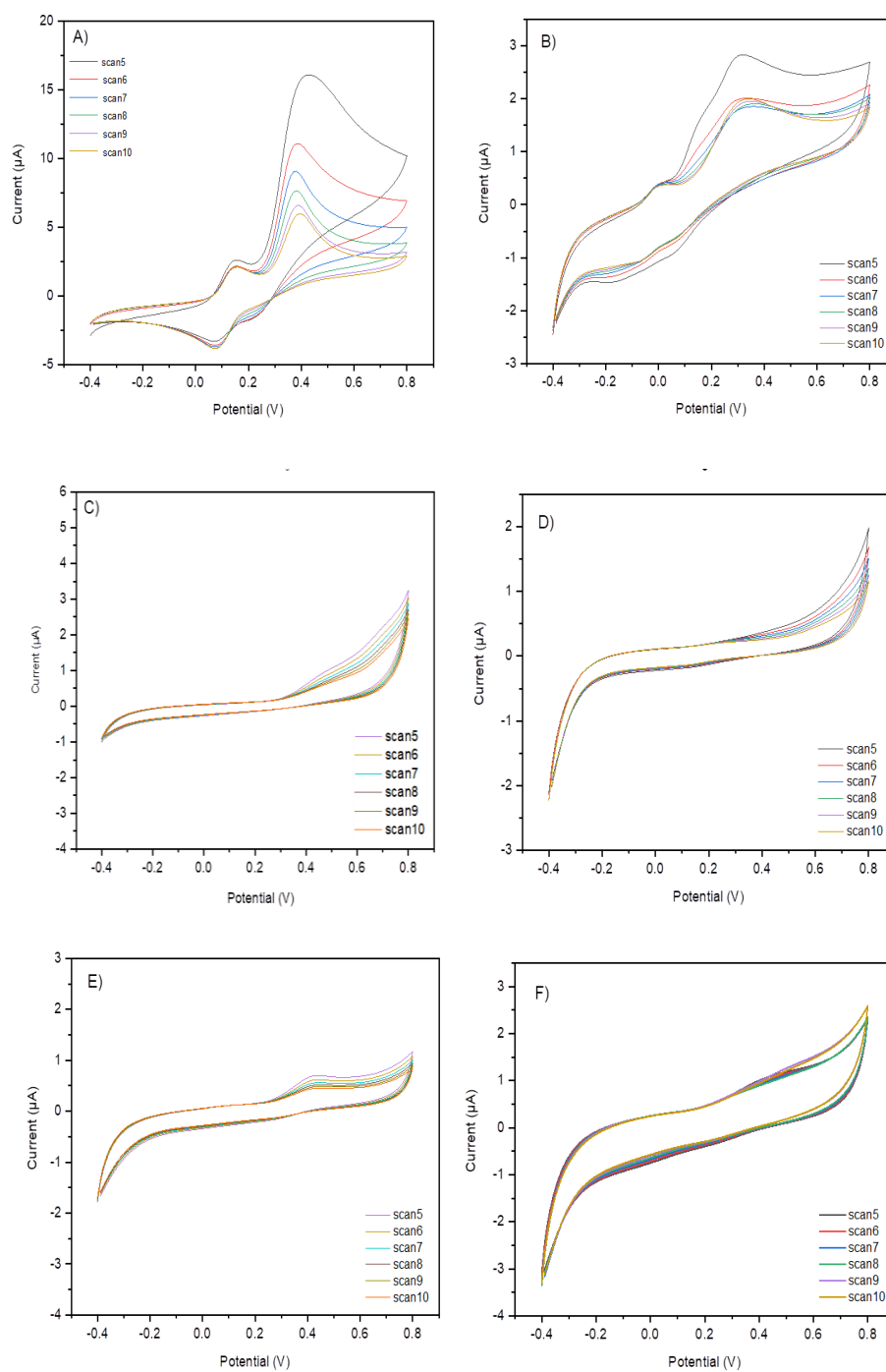


Figure A.2.7: Cyclic voltammograms of monomers and polymers studied herein. A) CAT pH5. B) CAT pH 7.4. C) polyCAT-HS pH 5. D) polyCAT-HS pH 7.4. E) polyCAT-LS pH 5. F) polyCAT-LS pH 7.4

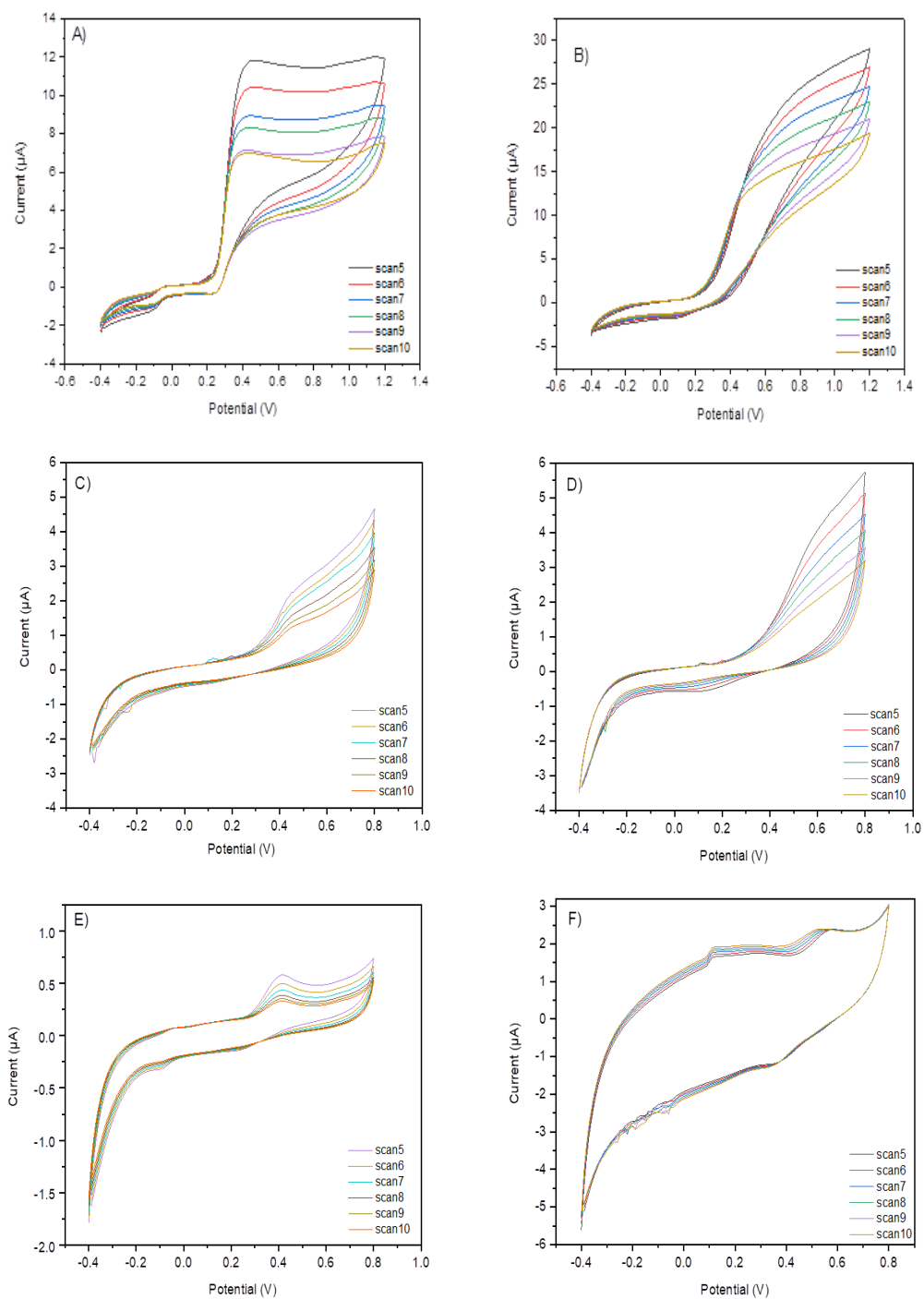


Figure A.2.8: Cyclic voltammograms of monomers and polymers studied herein. A) DOPA pH 5. B) DOPA pH 7.4. C) polyDOPA-HS pH 5. D) polyDOPA-HS pH 7.4. E) polyDOPA-LS pH 5. F) polyDOPA-LS pH 7.4.

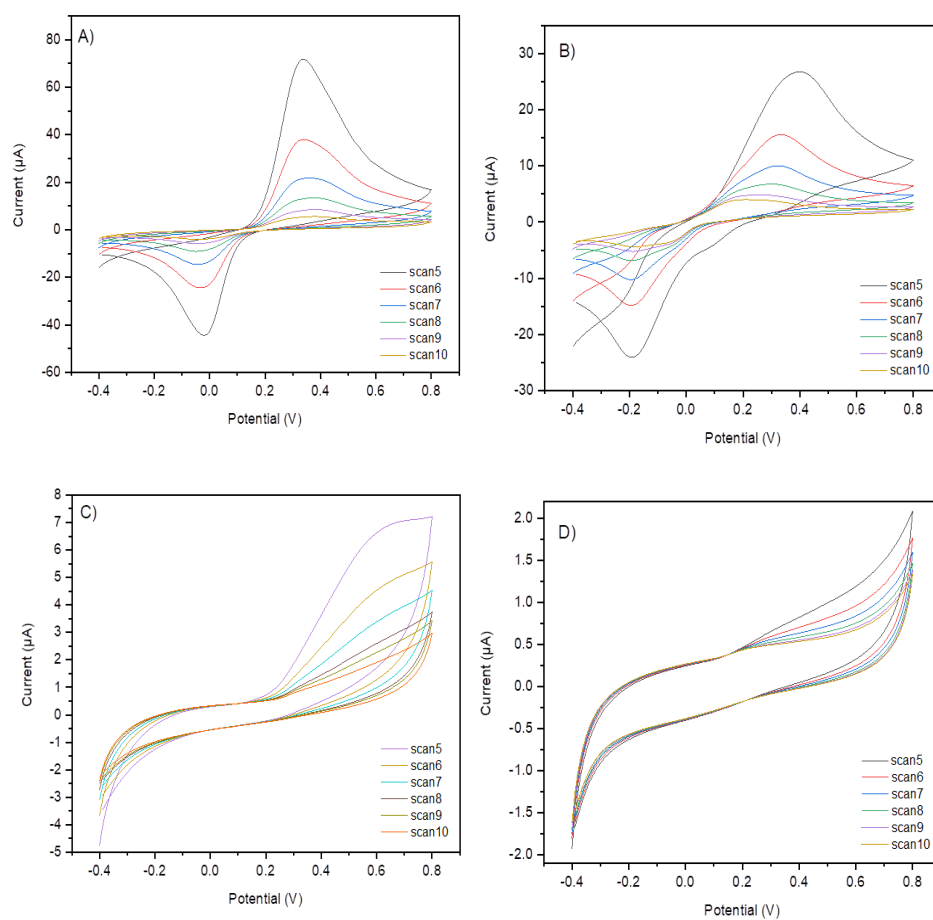


Figure A.2.9: Cyclic voltammograms of monomers and polymers studied herein. A) HGA pH 5. B) HGA pH 7.4. C) polyHGA-HS pH 5. D) polyHGA-HS pH 7.4.

### 8.3 Appendix

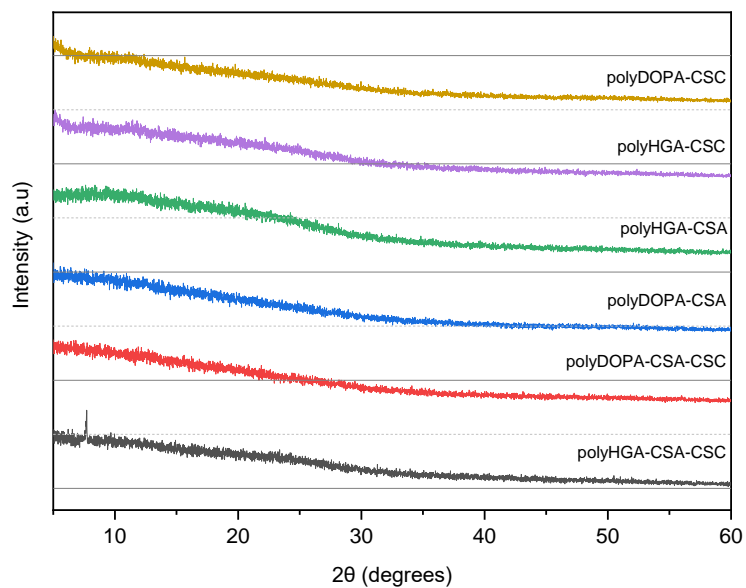


Figure A.3.1: X-ray diffractograms of samples studied herein.

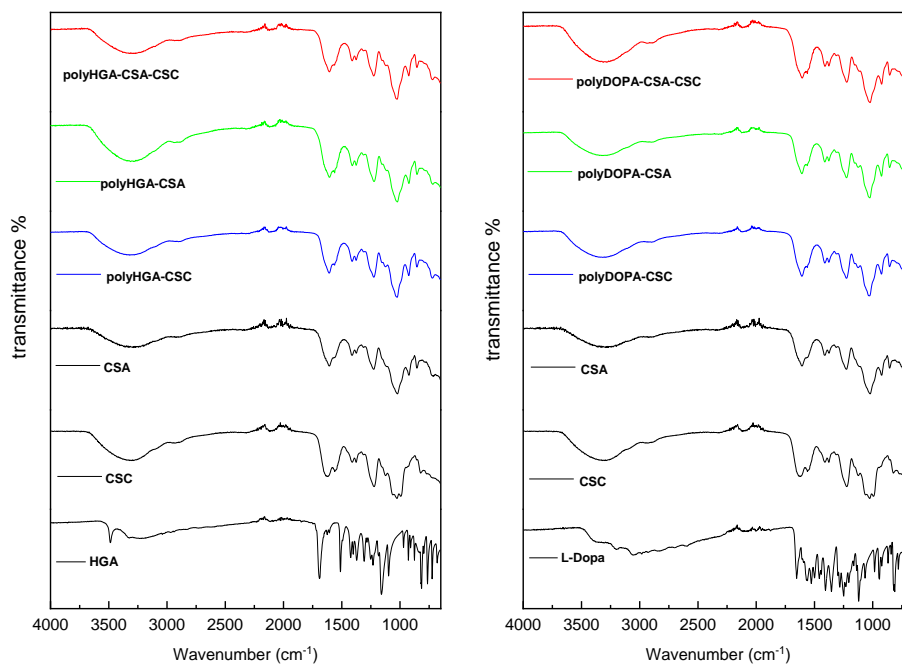


Figure A.3.2: FTIR spectra of monomers and polymers studied herein (full spectrum).

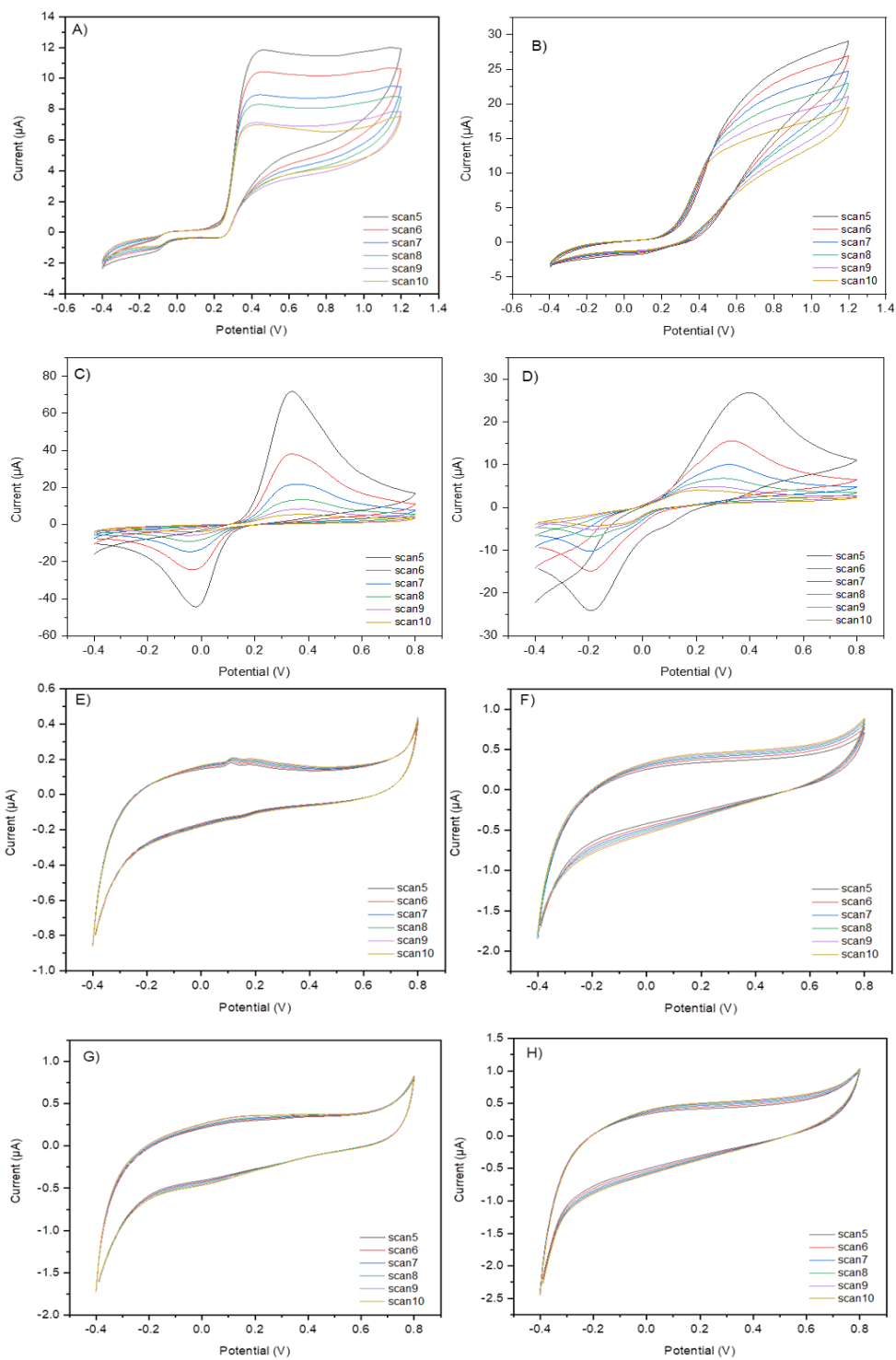


Figure A.3.3: Cyclic voltammograms of monomers. A) DOPA pH 5. B) DOPA pH 7.4. C) HGA pH 5. D) HGA pH 7.4. E) CSA pH 5. F) CSA pH 7.4. G) CSC pH 5. H) CSC pH 7.

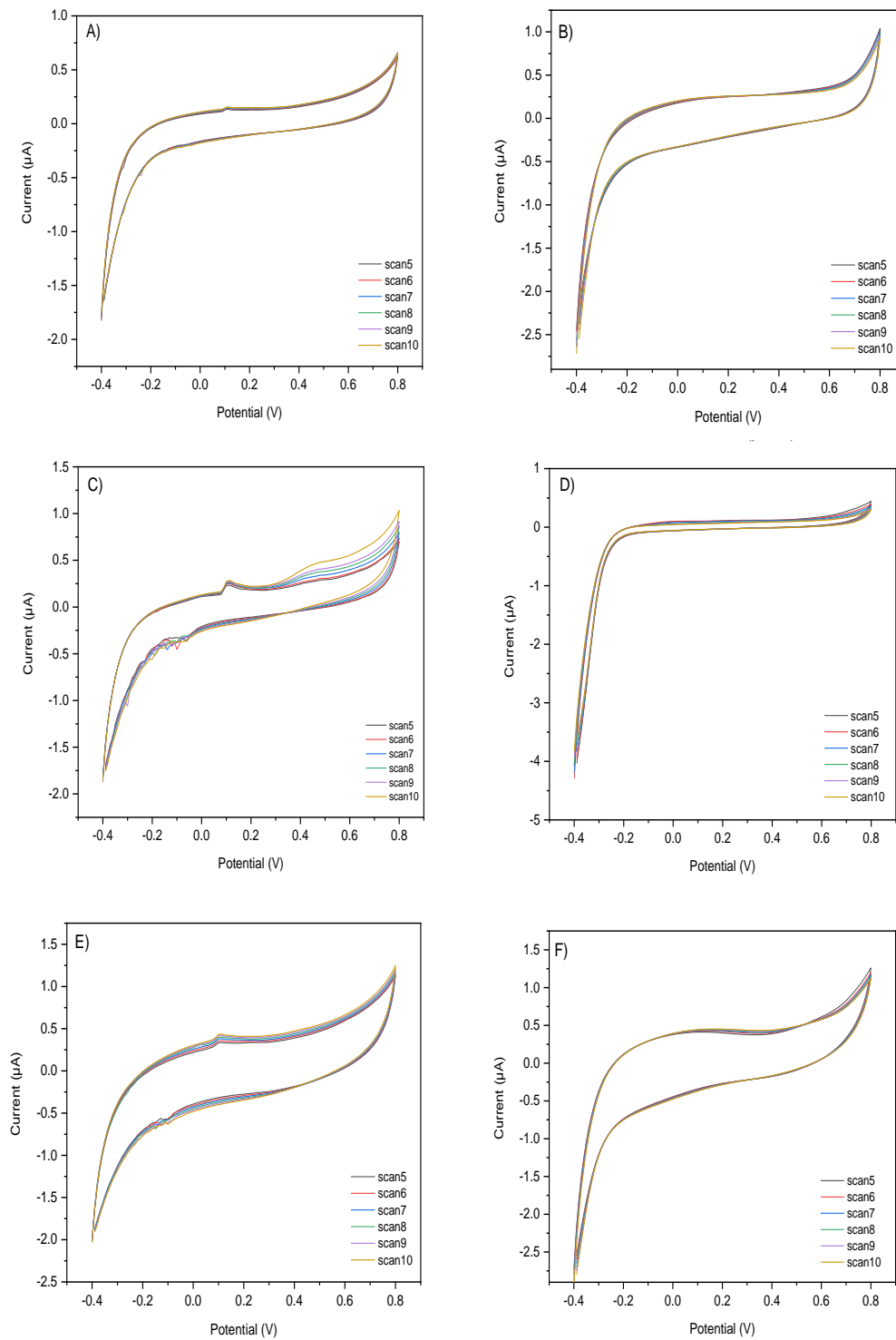


Figure A.3.4: Cyclic voltammograms of polymers studied herein. A) polyDOPA-CSA pH 5. B) polyDOPA-CSA pH 7.4. C) polyDOPA-CSC pH 5. D) polyDOPA-CSC pH 7.4. E) polyDOPA-CSA-CSC pH 5. F) polyDOPA-CSA-CSC pH 7.4.

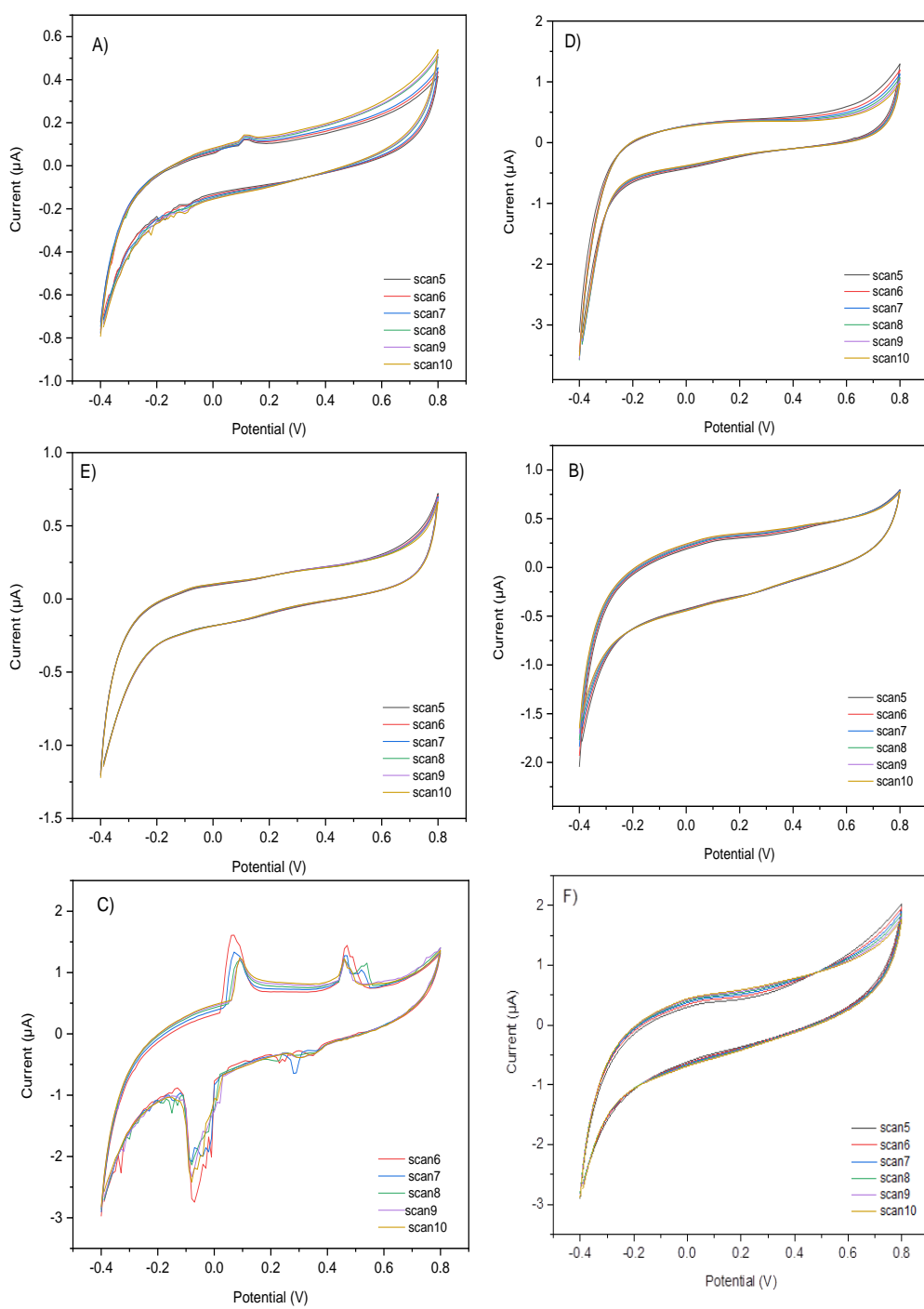


Figure A.3.5: Cyclic voltammograms of polymers studied herein. A) polyHGA-CSA pH 5. B) polyHGA-CSA pH 7.4. C) polyHGA-CSC pH 5. D) polyHGA-CSC pH 7.4. E) polyHGA-CSA-CSC pH 5. F) polyHGA-CSA-CSC pH 7.4.

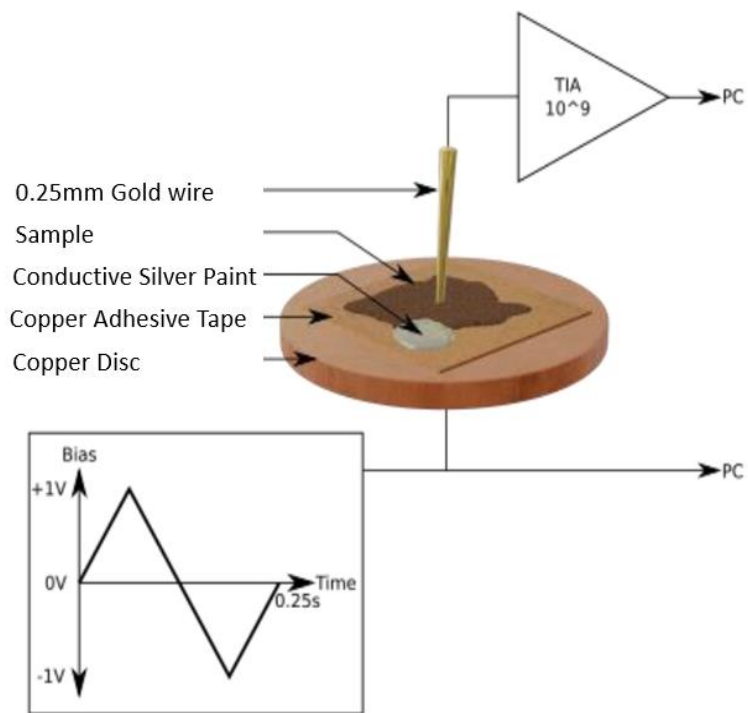


Figure A.3.6: Set up for electronic measurement.

## 8.4 Appendix

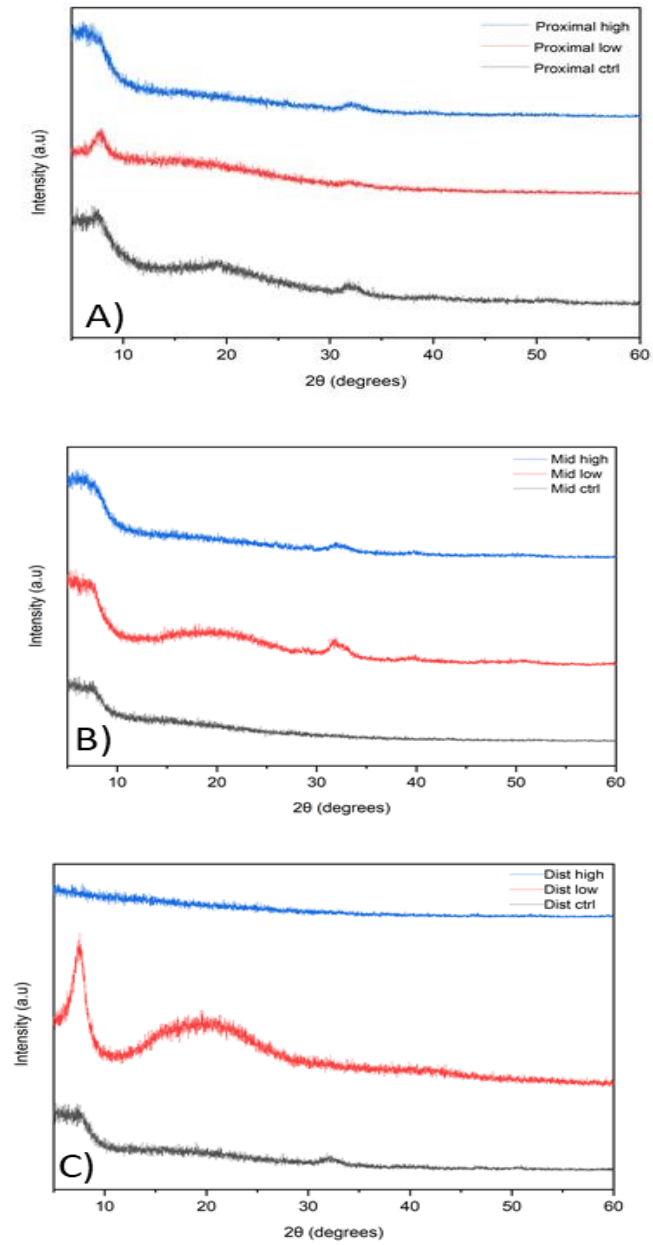


Figure A.4.1: X-ray diffractograms of samples studied herein. A) Proximal section of tendon. B) Mid-point of tendon. C) Distal section of tendon.

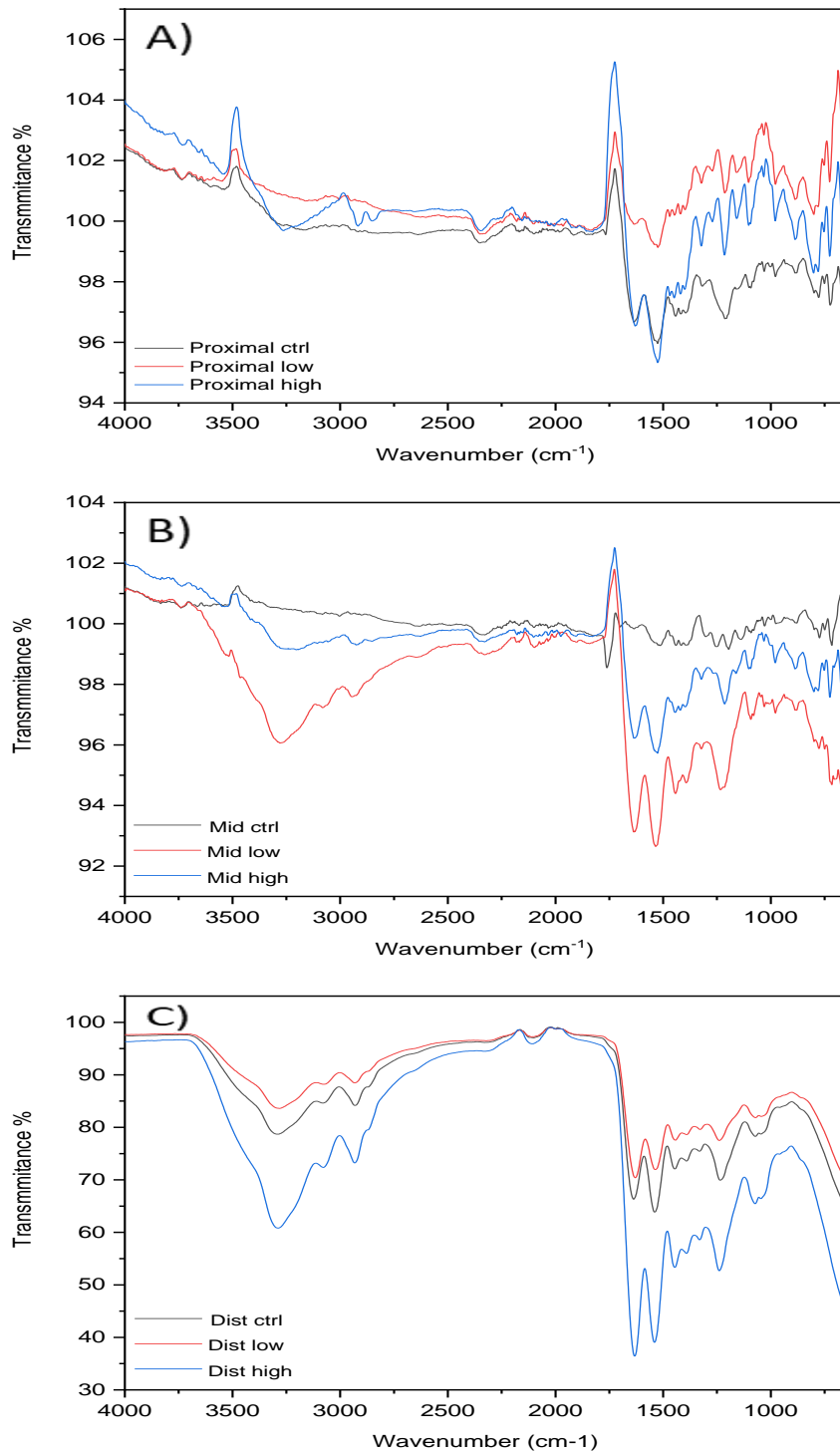


Figure A.4.2: FTIR spectra of tendons studied herein. A) Proximal section of tendon. B) Mid-point of tendon. C) Distal section of tendon.